AD-A043 357 NEW MEXICO UNIV ALBUQUERQUE ERIC H WANG CIVIL ENGINE--ETC F/G 11/2
BEHAVIOR OF REINFORCED CONCRETE BEAMS UNDER COMBINED AXIAL AND --ETC(U)
MAY 77 G E LANE F29601-76-C-0015
UNCLASSIFIED CERF-SSR-8 AFWL-TR-76-130 NL

1 OF 2
ADA
043357

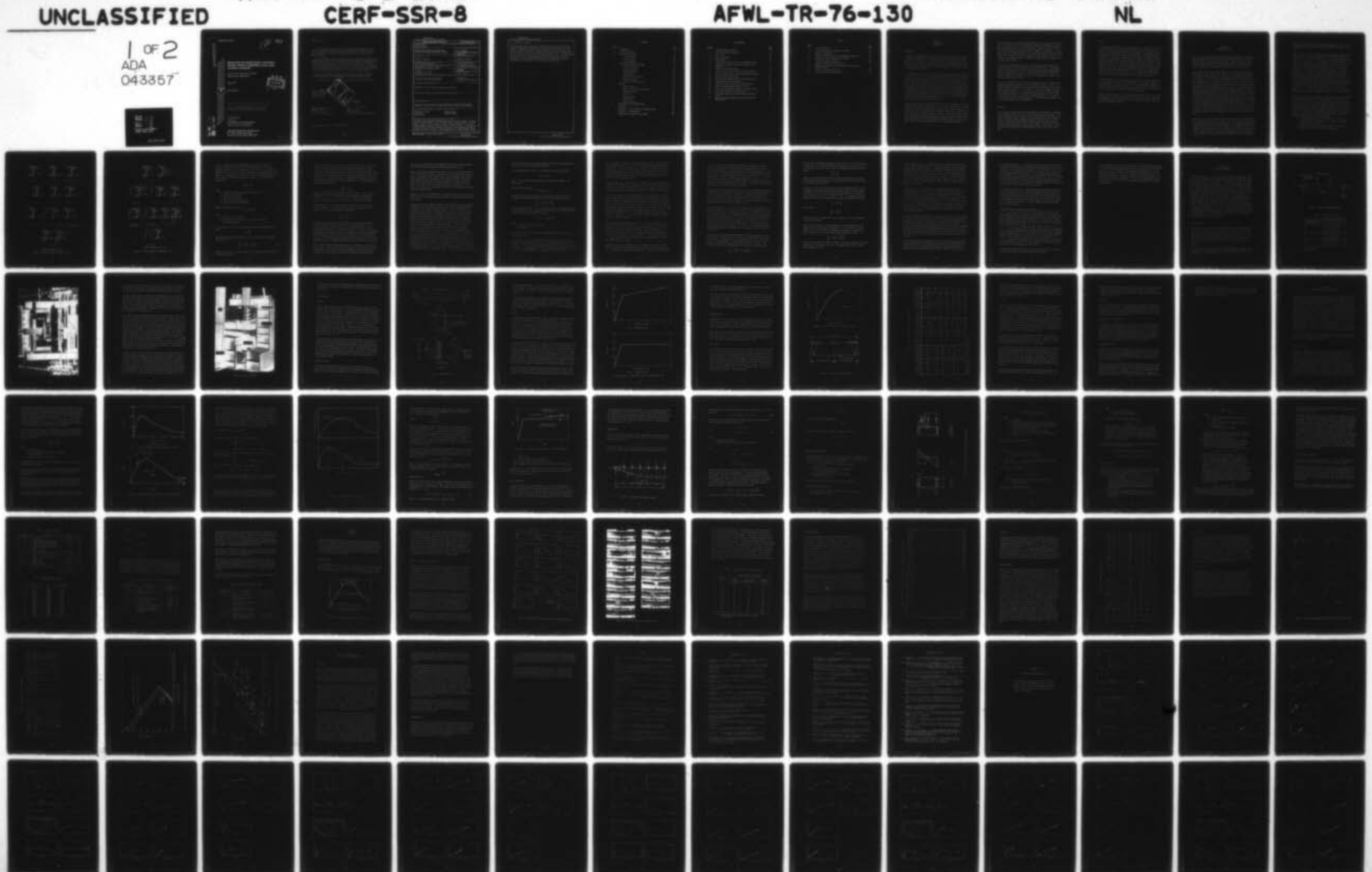

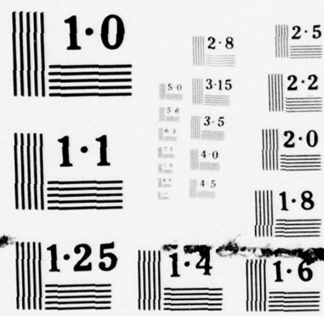
1·0
2·8
2·5
3·15
2·2
3·5
2·0
1·1
4·0
4·5
1·8
1·25
1·4
1·6

AFWL-TR-76-130

AFWL-TR-
76-130

BEHAVIOR OF REINFORCED CONCRETE BEAMS UNDER COMBINED AXIAL AND LATERAL LOADING

University of New Mexico/CERF
Albuquerque, NM 87131

May 1977

Final Report

Approved for public release; distribution unlimited.

This research was sponsored by the Defense Nuclear Agency under Subtask Y99AXSC157, Work Unit 04, "Strategic Structures Vulnerability Hardening."

Prepared for
Director
DEFENSE NUCLEAR AGENCY
Washington, DC 20305

AIR FORCE WEAPONS LABORATORY
Air Force Systems Command
Kirtland Air Force Base, NM 87117

AFWL-TR-76-130

This final report was prepared by the University of New Mexico, Eric H. Wang Civil Engineering Research Facility, under Contract F29601-76-C-0015, Job Order WDNS3423 with the Air Force Weapons Laboratory, Kirtland Air Force Base, New Mexico. Lt Rodney G. Galloway (DES) was the Laboratory Project Officer-in-Charge.

When US Government drawings, specifications, or other data are used for any purpose other than a definitely related Government procurement operation, the Government thereby incurs no responsibility nor any obligation whatsoever, and the fact that the Government may have formulated, furnished, or in any way supplied the said drawings, specifications, or other data is not to be regarded by implication or otherwise as in any manner licensing the holder or any other person or corporation or conveying any rights or permission to manufacture, use, or sell any patented invention that may in any way be related thereto.

This report has been reviewed by the Office of Information (OI) and is releasable to the National Technical Information Service (NTIS). At NTIS, it will be available to the general public, including foreign nations.

This technical report has been reviewed and is approved for publication.

Rodney G Galloway
RODNEY G. GALLOWAY
Lieutenant, USAF
Project Officer

FOR THE COMMANDER

James M Warren
JAMES M. WARREN
Lt Colonel, USAF
Chief, Survivability Branch

Frank J Leech
FRANK J. LEECH
Lt Colonel, USAF
Chief, Civil Engineering Research Div

DO NOT RETURN THIS COPY. RETAIN OR DESTROY.

UNCLASSIFIED

SECURITY CLASSIFICATION OF THIS PAGE (When Data Entered)

REPORT DOCUMENTATION PAGE		READ INSTRUCTIONS BEFORE COMPLETING FORM
1. REPORT NUMBER AFWL-TR-76-130	2. GOVT ACCESSION NO.	3. RECIPIENT'S CATALOG NUMBER
4. TITLE (and Subtitle) BEHAVIOR OF REINFORCED CONCRETE BEAMS UNDER COMBINED AXIAL AND LATERAL LOADING		5. TYPE OF REPORT & PERIOD COVERED Final Report
		6. PERFORMING ORG. REPORT NUMBER CERF-SSR-8
7. AUTHOR(s) Golden E. Lane, Jr.		8. CONTRACT OR GRANT NUMBER(s) F29601-76-C-0015
9. PERFORMING ORGANIZATION NAME AND ADDRESS University of New Mexico, Eric H. Wang Civil Engineering Research Facility, Albuquerque, New Mexico 87131		10. PROGRAM ELEMENT, PROJECT, TASK AREA & WORK UNIT NUMBERS 62704H/WDNS3423/Subtask No. Y99AXSC157/Work Unit 04
11. CONTROLLING OFFICE NAME AND ADDRESS Director, Defense Nuclear Agency, Washington, DC 20305		12. REPORT DATE May 1977
		13. NUMBER OF PAGES 148
14. MONITORING AGENCY NAME & ADDRESS(if different from Controlling Office) Air Force Weapons Laboratory (DES), Kirtland Air Force Base, NM 87117		15. SECURITY CLASS. (of this report) UNCLASSIFIED
		15a. DECLASSIFICATION/DOWNGRADING SCHEDULE

16. DISTRIBUTION STATEMENT (of this Report)

Approved for public release; distribution unlimited.

17. DISTRIBUTION STATEMENT (of the abstract entered in Block 20, if different from Report)

18. SUPPLEMENTARY NOTES

This research was sponsored by the Defense Nuslear Agency under Subtask Y99AXSC157, Work Unit 04, "Strategic Structures Vulnerability Hardening."

19. KEY WORDS (Continue on reverse side if necessary and identify by block number)

Reinforced Concrete
Axial Loads
Bending Loads
Concrete Beams
Combined Loading

20. ABSTRACT (Continue on reverse side if necessary and identify by block number)

Seventeen simply supported reinforced concrete beams were tested to collapse under combined flexural, axial, and shear forces. Each beam had a 12.5-foot span, a 9-by-15-inch cross section, and an effective depth of 12.5 inches. Reinforcement consisted of No. 2 stirrups, 6 inches on center. The beams were loaded laterally through a symmetrical two-point loading system and axially through the plastic centroid. Load was applied by a single hydraulic system designed to provide a constant ratio between axial and lateral loads for the over

DD FORM 1473, 1 JAN 73 — EDITION OF 1 NOV 65 IS OBSOLETE

UNCLASSIFIED

SECURITY CLASSIFICATION OF THIS PAGE (When Data Entered)

400 976

20. ABSTRACT (Continued)

duration of the tests. The two test parameters were axial-to-lateral-load ratio and shear-span-to-beam-depth ratio. Electrical measurements of beam behavior included steel strain on the longitudinal rebar, concrete strain, vertical deflections along the length of the beam, end rotations, and lateral and axial loads. In addition, a photoelastic coating sheet was bonded to one side of the beams and overlaid with a sheet of Polaroid film. The experimental results from the beam tests were compared with data calculated with an analytical behavioral model developed as part of this effort. The general beam behavior calculated from the analytical model agreed well with the measured results, especially in the region up to maximum load.

CONTENTS

ILLUSTRATIONS

TABLES

SECTION I
INTRODUCTION

BACKGROUND

Although a tremendous amount of research has been directed toward an understanding of the behavior of reinforced concrete structures, there are some areas in which knowledge is far from complete or is inadequate for some applications. For example, the behavior of a reinforced concrete beam loaded to collapse under the influence of combined flexural, shear, and axial loads is not completely understood.

Early endeavors in the analysis of reinforced concrete behavior were based on the theory of elasticity and the applicability of Hooke's Law. This approach allows elementary strength of materials procedures and an extension of elastic theory to be used for the analysis and design of reinforced concrete structures. Early investigators recognized that concrete is not an elastic material; however, the simplicity of the straight-line method was appealing from a computational viewpoint. As better understanding of the actual behavior of reinforced concrete structures developed, revisions and additions were made to accepted design procedures. This evolution has led to the widespread use of the ultimate strength design method or *strength method* used in the 1971 American Concrete Institute (ACI) Building Code.

During the past 25 years, extensive research has been conducted on individual aspects of reinforced concrete behavior (e.g., flexure, axial, shear, torsion, and bond). Also, many investigations concerning the interaction between various forces acting on reinforced concrete members (moment-shear, shear-torsion, and moment-axial) have been conducted. However, for a general loading condition, concrete member behavior depends on the interaction of all these behavioral aspects, and there exists no general theory or general behavioral model that accounts for the combined effects of all these behavioral aspects.

The state-of-the-art of reinforced concrete design is at a point where a great deal of confidence exists in the presently accepted strength design procedures when well-defined gravity loads are considered. However, there exist situations in which knowing just the strength of a member is not enough. To accurately predict the complete behavior of a multistory building to blast or earthquake loads or even the ultimate strength of a complex shell structure to static loads, the complete response of reinforced concrete members or elements to collapse must be known.

In recent years the complete behavior of reinforced concrete structures and structural systems has been investigated from two directions: scale models and full-sized prototype structures have been tested to provide experimental evidence of behavior, and analytical investigations have been conducted to establish methods for reasonable prediction of the response of complex structures to various types of loads.

During the past decade, there has been considerable success in analyzing the response of complex structures by the finite-element method, in which a continuum structure is modeled by an assemblage of discrete elements connected by selected points called *nodes*. The accuracy of the results depends on, among other things, the ability to accurately define the behavior of each element. If any analytical method is to predict the complete behavior or response of a complex structure, the complete behavior of reinforced concrete under a general loading condition must be understood.

OBJECTIVE

In an attempt to add to the basic understanding of the behavior of reinforced concrete members loaded to collapse, this investigation was undertaken. The specific objective of this research was to investigate the static behavior of reinforced concrete beams subjected to combined flexural, axial, and shear forces by developing a general model for beam behavior and comparing the results to those obtained from an experimental program. Of particular interest was member behavior during the large deflections which occur after maximum load.

SCOPE

The investigation included both an experimental and an analytical phase. The experimental phase of the investigation consisted of static testing, to collapse, 17 hinge-supported reinforced concrete beams. All beams had the same span length, cross-sectional geometry and properties, and nominal material properties. The beams were loaded laterally through a symmetrical two-point loading system and axially through the plastic centroid, as defined by the 1963 ACI Building Code. Load was applied through a single hydraulic system designed to provide a constant ratio between axial and lateral loads for the duration of the test. The two test parameters were axial-to-lateral-load ratio and shear-span-to-beam-depth ratio. Three shear-span-to-beam-depth ratios (3, 4, and 5) were considered. For each shear-span-to-beam-depth ratio, three axial-to-lateral-load ratios (3, 2, and 0) were used.

The experimental results provided data to describe the strength characteristics of the beams, including crack development, failure modes, strength interrelationships, and hinge performance. Also load-deformation behavior, including load-deflection characteristics, yield and collapse deflections, and load-strain behavior at various sections was determined.

In the analytical phase, a reinforced concrete behavioral model, which included beam response beyond the maximum load-carrying capacity, was formulated. The adequacy of the model was determined by comparing the model predictions with the experimental test data.

SECTION II
HISTORICAL REVIEW

Most of the uncertainties in predicting the flexural behavior of reinforced concrete members in the range of their maximum capacity result from the inelastic nature of the two materials involved. Accurate prediction of the flexural response depends on the ability to mathematically describe the inelastic characteristics of both the reinforcing steel and the concrete.

The reinforcing steel most commonly used has a distinct yield point and a flat plastic region; therefore, its behavior can be adequately expressed by a trapezoidal stress-strain curve. The stress-strain relationship for concrete, however, is more difficult to determine and also more difficult to express mathematically. Discussions of the stress-strain relationship of concrete and the stress distribution in the compression zone of flexural members have appeared in the literature since the late 1800s. Early design procedures for reinforced concrete were based on agreement between calculated and experimentally determined capacities (the same method the presently accepted ultimate strength design method is based on). Therefore, studies of stress distribution in the compression zone of reinforced concrete members have paralleled the development of ultimate strength design theories. Investigation of inelastic concrete stress distribution has been approached from two directions. One approach has been to determine the concrete stress distribution by analysis of the observed behavior and the ultimate strength from tests of reinforced concrete beams and columns; the other has been to determine the stress distribution by direct measurement of strain on plain concrete specimens.

One of the first rational methods for designing reinforced concrete members was reported by Koenen (ref. 1) in 1886. It concerned the analysis of simple reinforced concrete slabs subjected to bending. He assumed that there was a straight-line distribution of concrete stress in the compression zone, the neutral axis was at middepth of the section, and the concrete carried no tension. Koenen's work was followed by the development of many more flexural analysis theories on reinforced concrete. Hognestad (ref. 2) presented the

highlights of several of these theories published prior to 1951. Figure 1 presents the basic assumptions used in the theories discussed in this section.

Among the early theories published on flexure (following Koenen's) were other straight-line methods by Neumann (ref. 3) in 1890, Coignet and Tedesco (ref. 4) in 1894, Johnson (ref. 5) in 1895, and Ostenfeld (ref. 6) in 1902. (See figure 1.) In the Neumann and Ostenfeld Methods, the concrete was permitted to carry some tension. The Coignet/Tedesco theory was the first to include the modular ratio, n. Also about the same time, v. Thullie (ref. 7) in 1897 and Ritter (ref. 8) in 1899 published the first theories on the ultimate strength of reinforced concrete which considered the inelastic or nonlinear stress-strain relationship for concrete in the compression block. Ritter was the first to introduce the parabolic stress distribution. However, most of the investigators of this period agreed that the Coignet/Tedesco straight-line method was accurate enough for design purposes and its simplicity was appealing from a computational viewpoint. Hence, their theory became the *standard* theory at the turn of the century and led to rapid developments in the use of reinforced concrete as a construction material.

After the turn of the century and the general acceptance of the straight-line method of design, only a few investigators continued to research ultimate strength and inelastic stress distribution. Assumptions that were generally common to all of the proposed new theories included the validity of Bernoulli's hypothesis regarding strain proportional to the distance from the neutral axis, no bond slip between the concrete and reinforcing steel, and the concrete carried no tension. The reinforcing steel was assumed to have a trapezoidal stress-strain relationship. Normally, two modes of failure were considered:

(1) Tension Failure--after the reinforcing steel yields, the concrete crushes in compression as a result of the upward movement of the neutral axis.

(2) Compression Failure--the concrete crushes in compression prior to yielding of the tensile reinforcement.

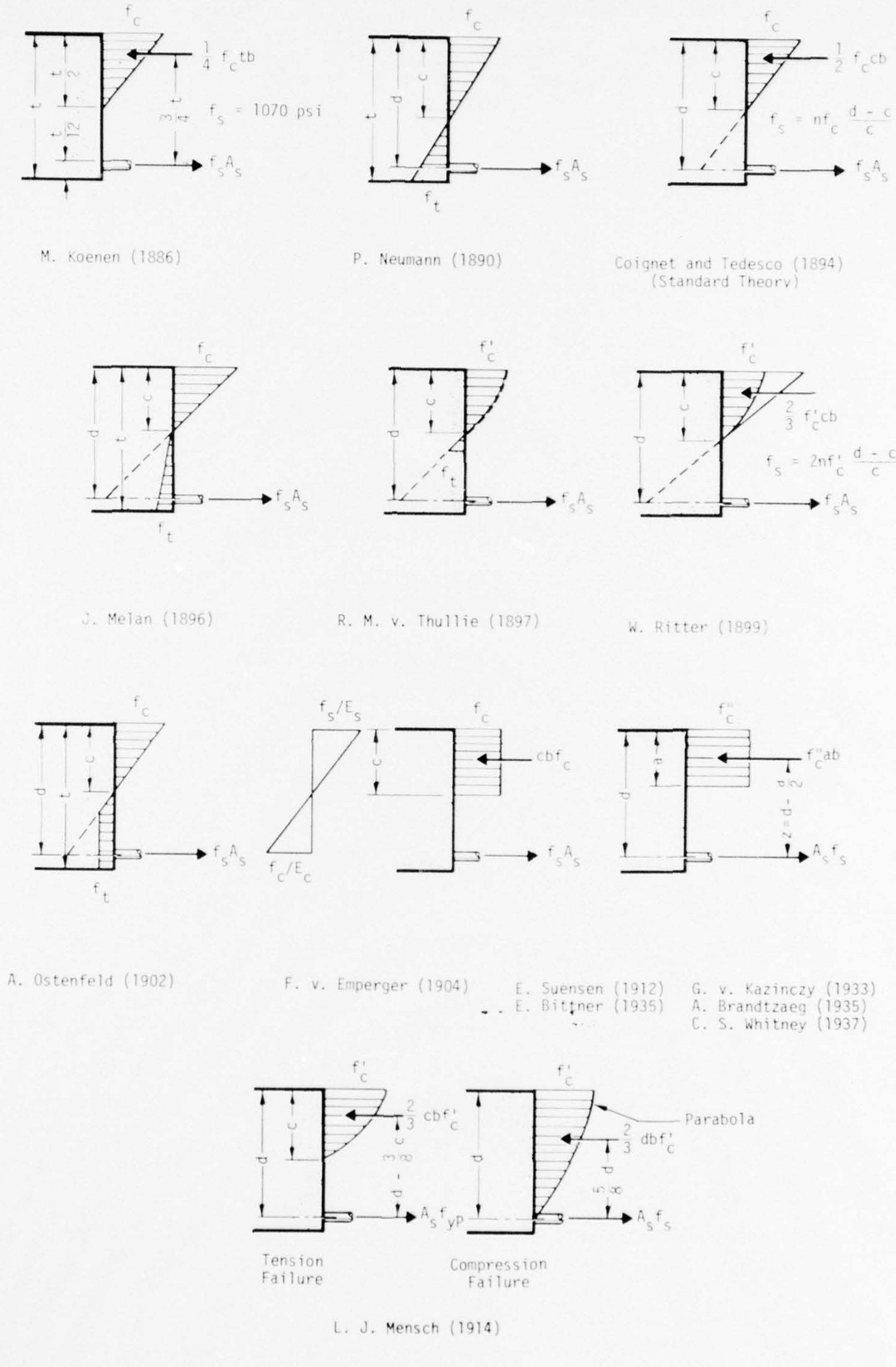

[after Hognestad (ref. 2)]

Figure 1. Flexural Analysis Theories (1 of 2)

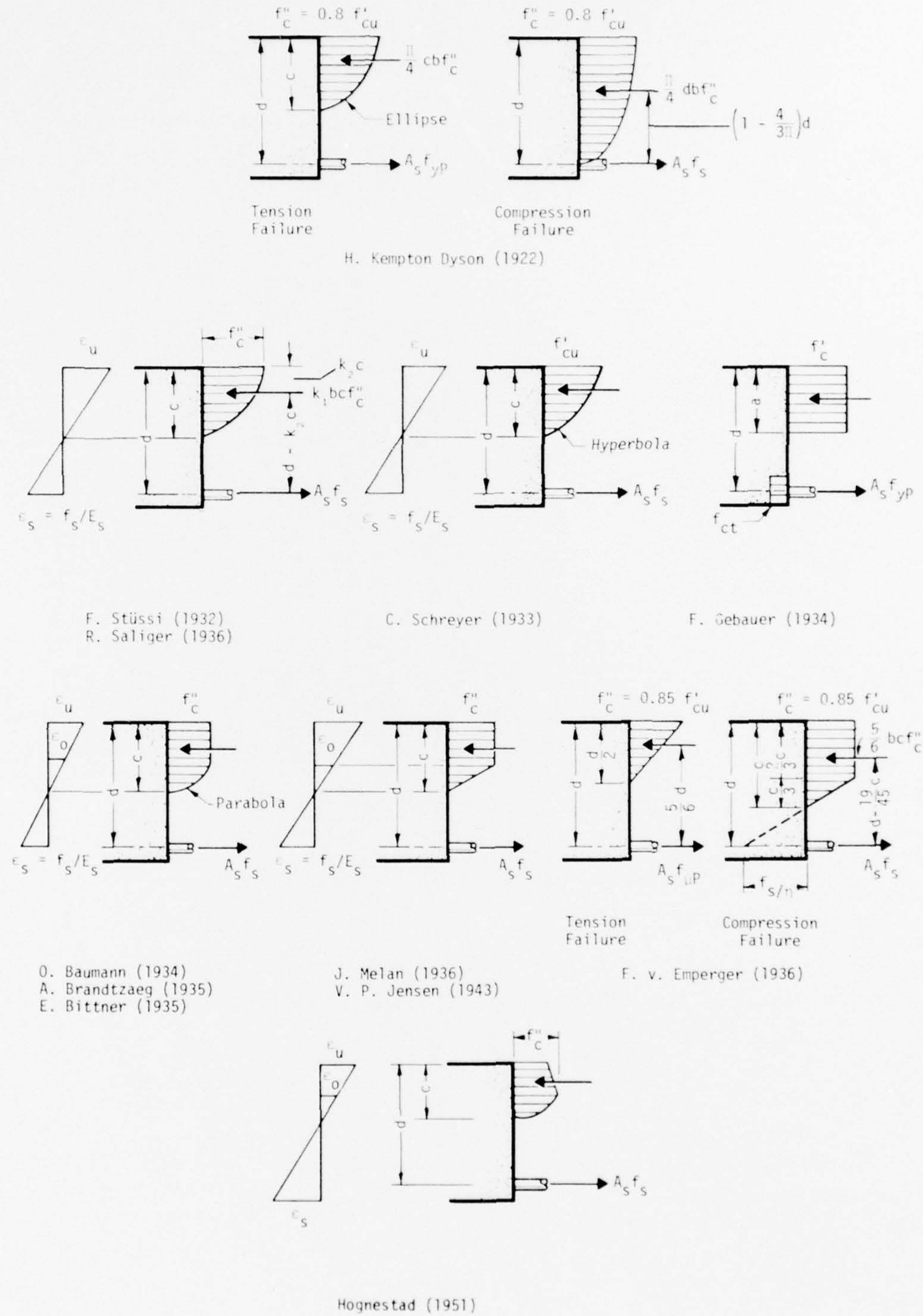

[after Hognestad (ref. 2)]

Figure 1. Flexural Analysis Theories (2 of 2)

The few investigators that continued with the research on ultimate strength included Talbot (refs. 9 and 10), Emperger (ref. 11), Suenson (ref. 12), Mensch (ref. 13), Kempton Dyson (ref. 14), and Lyse, Slater, and Zipprodt (refs. 15 and 16). Emperger and Suenson's proposed theories were based on a rectangular stress-block (fig. 1) but considered tension failures only. Hence, no compatibility equation was needed. Force equilibrium required that

$$f''_c ab = A_s f_s \tag{1}$$

where

f''_c = flexural strength of concrete in compression
a = depth of stress-block
b = width of cross section
A_s = area of tensile reinforcement
f_s = stress in tensile reinforcement

Moment equilibrium implied that

$$M = A_s f_s\left(d - \frac{a}{2}\right) \tag{2}$$

where

M = moment capacity of section
d = distance from compressive face of section to centroid of reinforcing steel

By combining eqs. (1) and (2) and substituting the reinforcement ratio, p, where

$$p = \frac{A_s}{bd}$$

the moment capacity can be expressed in the form that became well known in later years; i.e.,

$$\frac{M}{bd^2} = pf_s\left(1 - \frac{1}{2}\, p\, \frac{f_s}{f''_c}\right) \tag{3}$$

Suenson let f''_c equal f'_{cu} (cube strength) and f_s equal the yield strength of the reinforcing steel.

Mensch's proposed theory (ref. 13) in 1914 was based on Ritter's parabolic stress distribution and included both tension and compression failures. Compression reinforcement could also be included in the design method. No assumption was made regarding ultimate strain in the concrete nor was compatibility used. For tension failures, the computations were very similar to Suenson's; for compression failures, he assumed that the neutral axis was located at the centroid of the tension reinforcement. This resulted in the following moment capacity:

$$\frac{M}{bd^2} = \frac{1}{2.4} f'_c$$

where f'_c is the compressive strength of a test cylinder or prism. Mensch considered this limiting condition too extreme, however, and suggested for *balanced reinforcement* a factor of 1/2.6. Mensch also pointed out that the standard theory did not agree with test results at high loads.

Kempton Dyson (ref. 14) in 1922 proposed a theory based on an elliptical stress distribution. His results were not significantly different from Mensch's. For compression failures he found that

$$\frac{M}{bd^2} = \frac{1}{2.21} f''_c$$

During the first two decades of this century, the standard theory became so widely used that its approximate nature was often forgotten. The allowable concrete compressive stress, f_c, was normally taken as $0.325f'_c$, where f'_c was the strength of a 6-by-12-in cylinder. From this it was normally concluded that the safety factor against compression failure was about three. During this period, however, Slater and Zipprodt (ref. 15) and Slater and Lyse (ref. 16) pointed out that the actual safety factor was much larger than the ratio f'_c/f_c; this reemphasized the actual inelastic behavior of concrete.

Prior to 1920, bending stresses were ignored in the design of reinforced concrete columns. It was assumed that these stresses were provided for in the safety factor. These stresses were not considered mainly because suitable structural analysis methods for continuous structures were not available.

This lack was eliminated by the development of the Slope Deflection Method (ref. 17) and later by the Moment Distribution Method (ref. 18).

Another significant development took place in the early 1920s when McMillan (ref. 19) published a study on column test data that showed that, because of creep, reinforced concrete columns under a load may develop steel stresses much higher than those predicted by the straight-line method. McMillan's study led to an extensive ACI column investigation in the 1930s by Lyse, Slater, and Richart, which was reported by Richart and Brown (ref. 20). Their work resulted in the development of equations for the ultimate strength of axially loaded columns.

Another milestone in the advancement of reinforced concrete occurred in 1931; Emperger (ref. 21) published a critical study of the modular ratio and allowable stresses.

Prompted in the United States by the ACI column investigation and in Europe by Emperger's paper, a renewed interest in the ultimate strength behavior of reinforced concrete began in the early 1930s. In 1932, Stüssi (ref. 22) published a paper in which he discussed the ultimate strength of beams with tension reinforcement only. Considered in his study were compression and tension failures and the effect of strain hardening in the reinforcement. Brittle failures (failures due to rupture of the tension steel immediately after the formation of tension cracks in the concrete) were also discussed in terms of small percentages of reinforcing steel; Stüssi's method of analysis of the ultimate moment capacity was very general and several theories developed later were actually refinements and improvements on his work. Stüssi's theory was based on an arbitrary form of the compression stress-block but characterized by the stress-block constants k_1 and k_2, the compressive strength in flexure, f''_c, and an ultimate strain, ε_u (fig. 1). The constants k_1 and k_2 relate to the magnitude and location of the internal compressive force in the concrete. The compressive force is therefore $k_1bcf''_c$. He assumed f''_c was equal to f'_c. Stüssi determined his stress-block constants from concentric compression tests on prisms. He determined $k_1 = 0.70$ to 0.77. $k_2 = 0.39$ to 0.41, and $\varepsilon_u = 0.0020$ to 0.0025. These parameters were smaller

than those reported by later investigators because he did not recognize that larger strains could be developed in bending.

From the assumptions in figure 1, equilibrium of forces requires that

$$A_s f_s = k_1 bcf'_c$$

where c is the distance from the compressive face of the member to the neutral axis.

Moment equilibrium yields

$$M = k_1 bcf'_c(d - k_2 c)$$

For tension failures with f_s equal to f_y (the yield strength of the reinforcement), the ultimate moment capacity of a section was expressed as

$$\frac{M}{bd^2} = pf_y\left(1 - \frac{k^2}{k_1} p \frac{f_y}{f'_c}\right)$$

Stüssi suggested that $k_2/k_1 = 0.55$ was accurate enough for practical purposes. For compression failures, using the straight-line strain distribution, he developed the following compatibility equation:

$$f_s = E_s \varepsilon_s = E_s \varepsilon_u \left(\frac{d - c}{c}\right)$$

where

E_s = modulus of elasticity of steel

ε_s = steel strain

One of Stüssi's conclusions was that the safety factor with the standard theory was 2.3 to 4.1.

Schreyer (ref. 23) in 1933 reported on a Stüssi-type theory for which he established the stress-strain relationship for concrete in compression from cube tests. The stress-strain curve was hyperbolically shaped with $\varepsilon_u = 0.0063$. His value for ε_u was independent of concrete strength and his resulting expressions for moment capacity were, algebraically, quite involved.

The ultimate moment capacity of rectangular beams failing in tension was discussed by Kazinczy (ref. 24) in 1933. His theory was based on a rectangular stress-block. It was assumed that $f_s = f_y$ and $f''_c = f'_c$; therefore, the resulting expression of eq. (3) was used for the moment capacity of the beams. A major portion of Kazinczy's work consisted of the analysis of test results of two-span continuous beams--one of the first papers dealing with a plastic theory for reinforced concrete beams.

In 1934, Gebauer (ref. 25) reported on a theory for rectangular beams failing in tension. His theory was also based on a rectangular stress-block; however, he included some tensile strength of the concrete. Gebauer assumed that the tension was the result of shrinkage of the concrete around the reinforcement.

Also in 1934, Baumann (ref. 26) reported on a study of the buckling of reinforced concrete columns subjected to concentric or eccentric loads. In his study a relationship between moment and rotation for reinforced concrete members was required. Baumann found that a parabola satisfactorily approximated the stress-strain curve for concrete. However, he discovered through tests of eccentrically loaded prisms that the ultimate strain in flexure, ε_u, was larger than the corresponding strain at the maximum concrete stress, ε_o, for a concentric compression test. For a concrete strength of 3500 psi, he determined $\varepsilon_o = 0.0018$ and $\varepsilon_u = 0.0025$ to 0.0033. Baumann, therefore, used the stress-block shown in figure 1.

Bittner published two papers (refs. 27 and 28) in 1935 and 1936 on the inelastic behavior of reinforced concrete. For tension failures he assumed a rectangular stress-block and thus the moment capacity given by eq. (3) resulted. For compression failures he used a Stüssi-type analysis with a stress-block similar to Baumann's. However, Bittner used a constant value of $\varepsilon_o = 0.0015$, regardless of concrete strength. For his analysis he used $\varepsilon_u = 0.003$, 0.005, and 0.007 but did not make a recommendation as to which value should be used in design.

Between 1935 and 1937, Brandtzaeg (refs. 29 through 32) reported on studies that represented the first complete analysis of the ultimate strength capacity of rectangular, reinforced concrete sections. These studies included the

effect of compression reinforcement and bending in combination with axial load. For tension failures Brandtzaeg used a rectangular stress-block; for compression failures, he used a stress-block similar to Baumann's. However, it was improved by the development of a relationship between the ultimate strain, ε_u, and the compressive strength of the concrete. Also, f''_c was assumed equal to $0.85f'_c$. Brandtzaeg also introduced a *plasticity ratio* ($\eta = \varepsilon_u/\varepsilon_o$) into his expressions for ultimate moment. He verified his theory by comparing the results to the results from tests of 20 beams, 13 eccentrically loaded columns, and several auxiliary specimens.

Emperger, who in 1931 had written the paper critical of the modular ratio and the allowable stress approach to the design of reinforced concrete members (ref. 21), published a report (ref. 33) in 1936 based on his review of 5 years of discussion on ultimate strength design and concluded that satisfactory results for the ultimate strength of reinforced concrete beams could be obtained with the assumptions shown in figure 1.

In 1936, Saliger (ref. 34) presented a thorough study of rectangular beams in which he considered tension, compression, brittle, and balanced modes of failure. (Balanced failure is simultaneous crushing of the concrete and yielding of the tensile reinforcement.) Saliger used the same basic approach as Stüssi (ref. 22), but he assumed that $k_2 = 1/2k_1$; this is equivalent to replacing the curved stress-block with a rectangular one. He also assumed $f''_c = f'_c$; this results in eq. (3) becoming the expression for the ultimate moment capacity of a beam failing in tension. The value of k_1 was then determined by observing the position of the neutral axis at failure; he found values from 0.90 to 0.94.

Whitney, one of the better-known researchers in reinforced concrete in the United States, published papers on his ultimate strength theories from 1937 to 1948 (refs. 35 through 38). A rectangular stress-block was used in the analysis of tension failures with the assumption that $f''_c = 0.85f'_c$. The following expression was then developed for the ultimate moment capacity:

$$\frac{M}{bd^2} = pf_y\left(1 - \frac{1}{2}\, p\, \frac{f_y}{0.85f'_c}\right)$$

Whitney made no assumptions regarding ultimate strains, strain distribution, or bond slip. For compression failures he assumed from test results a limiting value of a/d = 0.537. This led to the following expression for ultimate moment:

$$\frac{M}{bd^2} = \frac{1}{3}f'_c$$

Whitney also developed expressions for the ultimate strength of rectangular and round sections subjected to axial load and bending moment and failing in either tension or compression.

In 1941, Cox (ref. 39) reported on tests of 110 rectangular beams. Using a rectangular stress-block, he developed expressions for tension and compression failures with and without compression reinforcement. He assumed f''_c = f'_c; this results in eq. (3) for tension failures. For compression failures, a value for the critical reinforcement, p_{cr}, was experimentally developed.

$$p_{cr} = 0.47 \frac{f'_c}{f_y}$$

This results in

$$\frac{M}{bd^2} = \frac{1}{2.76} f'_c$$

The 1/2.76 factor is between the 1/2.6 that Mensch (ref. 13) used and the 1/3 that Whitney found.

Jensen (refs. 40 and 41) in 1943 published a very complete report on rectangular beams with tension reinforcement only. His analysis was of the Stüssi type, but he considered a trapezoidal stress-block. He developed the following equation for the ultimate moment capacity of a beam:

$$\frac{M}{bd^2} = pf_s\left(1 - \frac{1}{N}\frac{pf_s}{f'_c}\right)$$

where N was a function of concrete strength. For tension failures, N = 2 was assumed; this is the same as eq. (3). For compression failures, a compatibility equation was used.

In 1951, Hognestad (ref. 2) published results of an extensive investigation of the ultimate strength behavior of reinforced concrete members subjected to combined bending and axial loads. He tested 120 specimens, which included both square tied and cylindrical spiral columns. In the investigation he developed an inelastic flexure theory of the Stüssi type. Hognestad used the concrete stress-strain relationship shown in figure 1. He also compared his results to the theories of Whitney and Jensen. Hognestad's paper included a compilation of previous theories and his theory seemed to include the best features of all of them.

In the early 1950s, a consolidation of information concerning ultimate strength design was initiated. Existing theories were extended to include combined bending and axial load as well as prestressed concrete members. Ultimate strength design methods were also introduced into the building codes of several countries. In October 1955 an ASCE-ACI Joint Committee on *Ultimate Strength Design* published its final report (ref. 42), which culminated more than 10 years of committee work. This report led to changes in the ACI Building Code, 318-56 (ref. 43), and thus permitted, for the first time in the United States, the use of ultimate strength design methods for reinforced concrete flexural members.

After the publication of the ASCE-ACI Joint Committee report and the inclusion of ultimate strength provisions in the 1956 ACI Building Code, Hognestad (ref. 44) published the results of a review of current literature regarding the inelastic stress distribution in flexure of reinforced concrete members. These results were compared with the recommendations of the Joint ASCE-ACI Committee, and from the comparison it was concluded that the committee's design coefficients were well substantiated by test results and that a simplified rectangular stress distribution gave satisfactory accuracy for common, practical design cases.

In 1961, Mattock, Kriz, and Hognestad (ref. 45) presented the development of an ultimate strength design theory based on an equivalent rectangular stress distribution in the concrete compression zone. The proposed theory was in general accord with the appendix to the 1956 ACI Building Code, but it had a

much broader application. The method was applied to a wide variety of reinforced concrete beams and columns under various combinations of axial load and flexure. These results were compared to results of experimental investigations and the agreement was excellent. Since a wide range of variables was considered in this investigation, it was concluded that the theory predicted ultimate strength with sufficient accuracy for all types of structural sections encountered in structural design, including odd-shaped sections. This work was the basis for the ultimate strength provisions for flexure and axial load in the 1963 ACI Building Code (ref. 46).

With the general acceptance of ultimate strength methods for the design of reinforced concrete structures and the acceptance of inelastic behavior of reinforced concrete, increased interest and attention were directed toward limit design of reinforced concrete structures. Even at the present time, in standard design procedures, an inelastic stress distribution is considered in designing cross sections to resist moments and loads determined from an elastic analysis.

In November 1964, an International Symposium on *Flexural Mechanics of Reinforced Concrete* (ref. 47) was held to present recent work directed specifically toward the goal of a more basic understanding of the flexural behavior of reinforced concrete and the elimination of the basic contradiction in design philosophy, e.g., ultimate strength design from an elastic analysis. Most of the papers presented were concerned with some aspect of limit design (e.g., Mattock's paper (ref. 48), *Rotational Capacity of Hinging Regions in Reinforced Concrete Beams*, and Roy and Sozen's paper (ref. 49), *Ductility of Concrete*.) Most of the papers were concerned with the behavior of reinforced concrete beams and slabs in the plastic region up to maximum load. However, Barnard presented one of the first reports (ref. 50) on beam behavior beyond maximum load to collapse. Based on the concept of concrete as a *strain-softening* material, Barnard showed that a beam could continue to rotate when the bending moment was falling off, but it would not collapse unless an energy balance in the beam ceased to be satisfied.

A comprehensive annotated bibliography (ref. 51) which covers limit design investigations between 1917 and 1968 was prepared by Cohn.

The most recent investigation into the behavior of reinforced concrete beams in the range beyond maximum moment capacity was reported by Iqbal and Hatcher (ref. 52) in 1975. The behavior of reinforced concrete beams in the post-crushing range (where moment is decreasing while deformations continue to increase) was studied. A theoretical model of the failure mechanism in the post-crushing region was presented. The results were compared with the experimental results of tests on six beams without compression or transverse reinforcement.

SECTION III
EXPERIMENTAL PROGRAM

The experimental phase of this investigation consisted of statically testing to collapse 17 rectangular, reinforced concrete beams. The duration of the beam tests varied from 2 to 12 minutes. All beams had the same span length, cross section, and hinged end supports. The two test parameters considered were the axial-to-lateral-load ratio and the shear-span-to-beam-depth ratio. For a two-point symmetrical lateral load, the shear span is the distance from the support to the load point. Figure 2 shows the general loading scheme for the beams. The axial-to-lateral-load ratio, P/F, remained constant for the duration of each test. The shear-span parameter is expressed as the a_s/d ratio; a_s is the shear span and d is the distance from the compression face of the concrete to the centroid of the tensile reinforcement (effective depth). The parameters considered in this investigation were a_s/d ratios of 5, 4, and 3 and P/F ratios of 3, 2, and 0. Each beam test was identified by a three-number designation (e.g., 5-3-1). The first number refers to the nominal a_s/d ratio, the second refers to the nominal P/F ratio, and the third to the beam number of that particular configuration. Table 1 presents the test designations for each configuration.

TEST APPARATUS

The loading device used in this investigation was a test frame used by Crist (ref. 53) in a reinforced concrete deep beam study; but it was modified to accommodate the axial load application. Figure 3 shows the modified test frame which consisted of an upper portion that provided reaction for the lateral load and a lower portion that provided the axial load and support system. The two portions were tied together by five vertical structural T-sections.

Lateral load was applied by a 100,000-lb-capacity hydraulic ram with a 13-in stroke. Axial load was applied by two 200,000-lb-capacity double acting rams with 26-in strokes mounted in a horizontal position. A single hydraulic

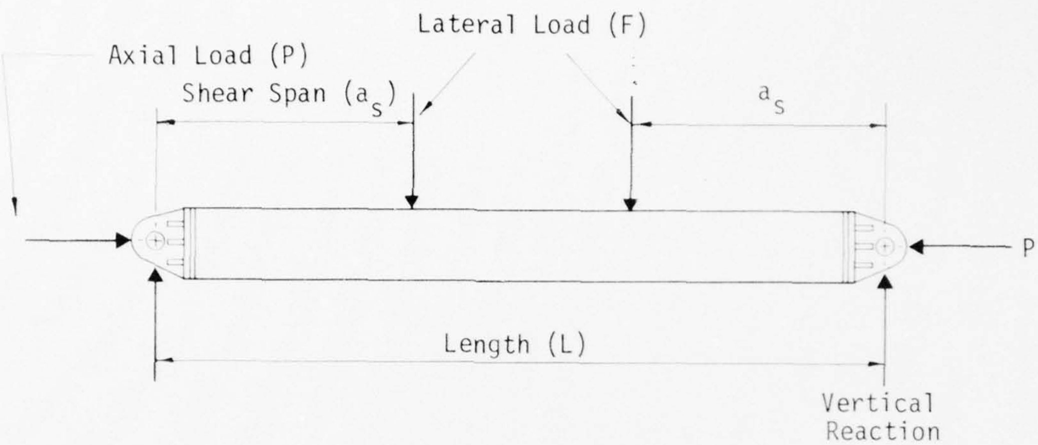

Figure 2. General Loading Configuration

Table 1. Test Designations

Shear-Span-to-Beam-Depth Ratio	Axial-to-Lateral-Load Ratio		
	3	2	0
5	5-3-1* 5-3-2 5-3-3	5-2-1 5-2-2	5-0-1 5-0-2
4	4-3-1 4-3-2	4-2-1 4-2-2	4-0-1
3	3-3-1 3-3-2 3-3-3	3-2-1 3-2-2	3-0-1

*Not reported.

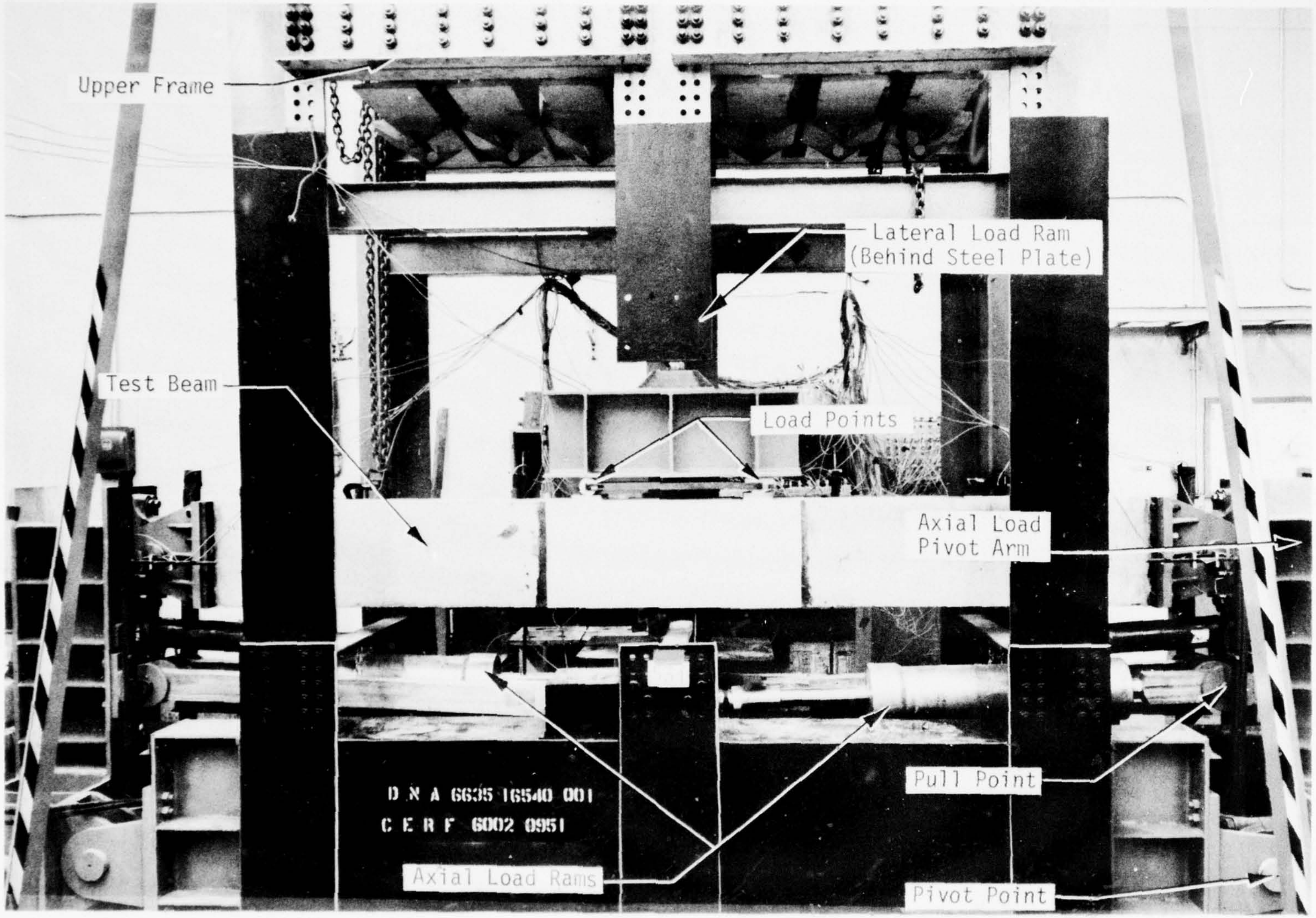

Figure 3. Test Frame

system was used to activate the rams to insure a constant P/F ratio throughout each test. The hydraulic system had a capacity of 9,500 psi and could be operated from a portable remote control with an adjustable load rate.

The total lateral load was divided into a two-point load by a steel distribution beam which imparted force to the beams through 2-1/2-in-diameter rollers and 4-by-9-by-3/4-in steel bearing plates. One end of the distribution beam was free to translate and rotate while the other end was only free to rotate. The bearing plates were seated to the beams with a thin layer of high-strength gypsum compound. The length of the shear span was established by the position of the lateral loads.

Axial load was applied to the beams by using the two horizontal rams in tension; this resulted in compression on the beam because of the pivoting of the vertical reaction arms (fig. 4). The ratio of axial to lateral load was defined by the pull-point position of the rams on the reaction arms. To adjust the axial-to-lateral-load ratio, the connection point of the tension rams to the pivot arm was changed. For zero axial load, the horizontal rams were mechanically and hydraulically disconnected from the system. The hinged condition at the ends of the beams was insured by transmitting the axial load through self-aligning, roller-bearing pillow blocks and 4-in-diameter steel shafts. The axial force was applied through the *plastic centroid* of the beam cross section. The plastic centroid of a section, as defined by the 1963 ACI Building Code (ref. 46), is the centroid of resistance to load computed under the assumption that the concrete is uniformly stressed to f''_c and the reinforcing steel is uniformly stressed to f_y.

To insure that the forces measured in the horizontal rams during the tests could be accurately converted to axial forces in the test beams, a series of calibration tests was conducted prior to actual beam testing. The calibration tests consisted of loading a dummy beam axially while measuring both the forces in the hydraulic rams with force links and the axial load in the beam with a load cell. Under the assumption that all joints in the mechanical linkage between the horizontal rams and the dummy beam were frictionless, the calculated axial load in the beam was compared to the load indicated by the load cell. The agreement between calculated and measured forces in the

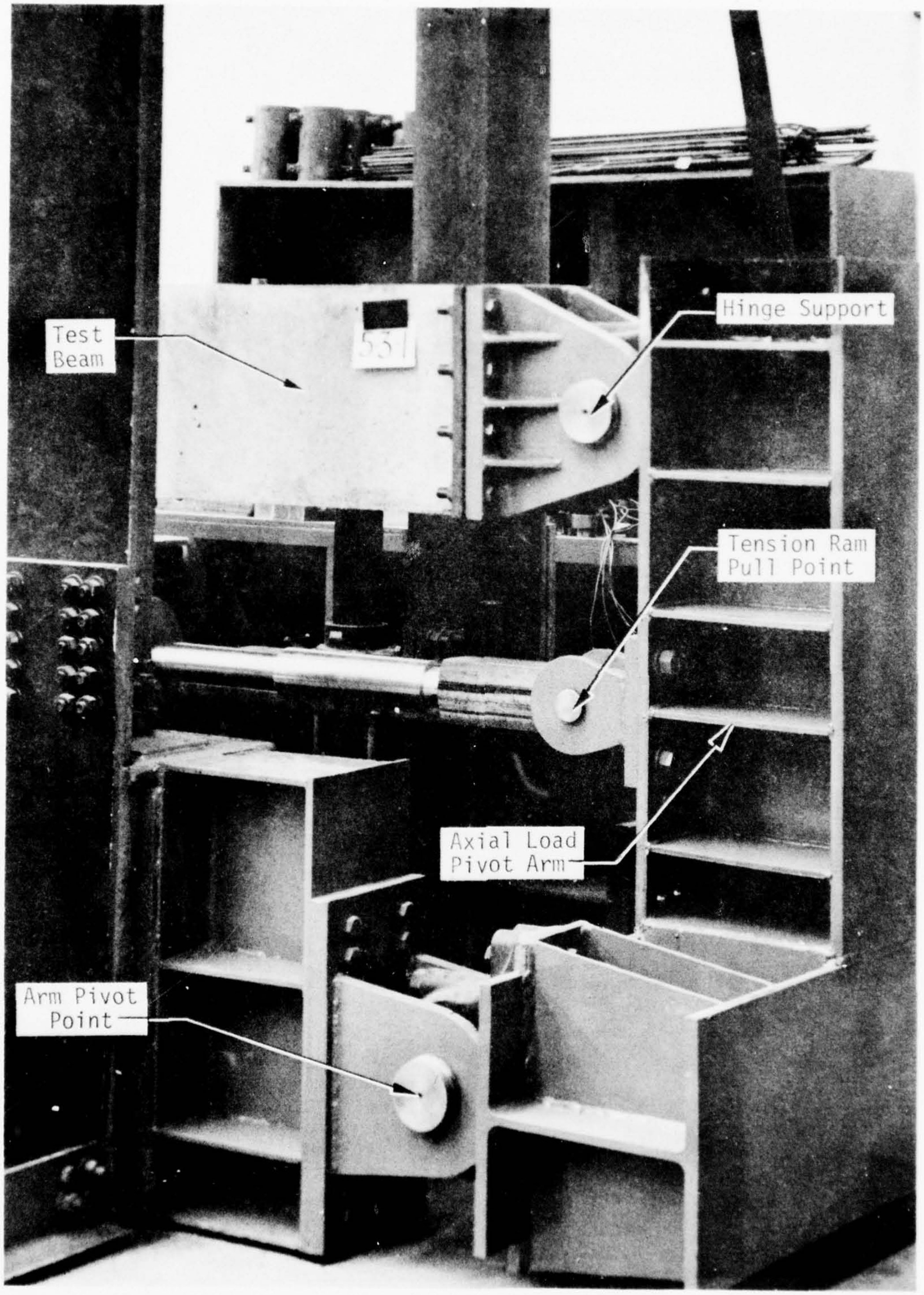

Figure 4. Axial Load System

dummy beam was within 10 percent; however, the corrections derived from the calibration tests were used to determine axial loads in the beams during the actual tests.

BEAM SPECIMENS

Geometry

The beam span was 12 ft, 6-1/4 in measured from center to center of the pivotal shafts at the beam ends. This length included the steel end reaction devices shown in figures 4 and 5. Cross-sectional properties and geometry were the same for all specimens. The beams were 15 in in overall depth and 9 in wide with a depth from the compressive face of the concrete to the centroid of the tensile steel of 12-1/2 in. Tensile reinforcement consisted of three No. 6 (3/4-in-diameter) bars. Although it was intended that the specimens be essentially singly reinforced, two No. 2 (1/4-in-diameter) bars were placed in the top of the beams. These were included to assist in beam fabrication and to facilitate making strain measurements in the compression zone of the beams. No. 2 stirrups were placed at 6-in intervals along the length of the beams (fig. 5).

To facilitate axial load application, the concrete portion of the beams was terminated at end bearing plates to which the end reaction devices were bolted. The longitudinal reinforcement was welded to the end bearing plates to assure adequate anchorage for the bars and to assure development of the full flexural and shear capacities of the beams. Additional reinforcement was also welded to the end plates to provide a mechanism for shear transfer between the concrete and the end supports. Figure 5 shows the details of the end bearing plates.

Reinforcing Steel

The principal longitudinal reinforcing, which consisted of three No. 6 bars, had a yield strength of 62,000 psi and conformed to ASTM Specification A615-60. All the steel was produced from the same heat to insure consistency

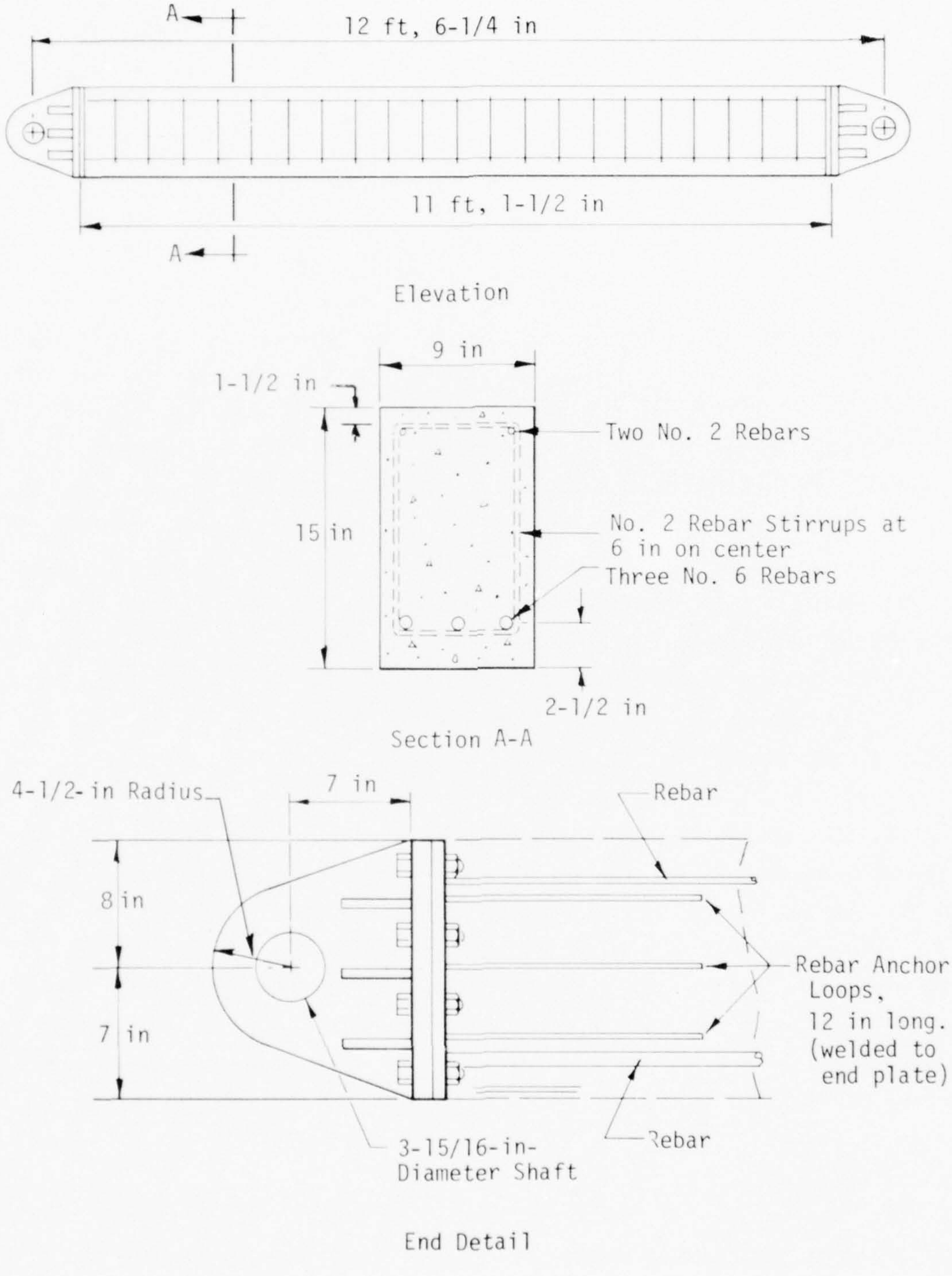

Figure 5. Beam Geometry

among the beam specimens. Tensile tests were performed on samples from several lengths of the rebar to insure control and to determine the mechanical properties of the steel. A typical stress-strain curve is shown in figure 6a.

The stirrups and compression reinforcement were intermediate-grade steel conforming to ASTM Specification A15 with a yield strength of 52,000 psi. Although not covered by Specification A305, beams with the No. 2 bars had deformations similar to those with the No. 6 bars. A typical stress-strain curve is shown in figure 6b.

Concrete

The concrete used in the beams had a nominal compressive strength of 5,000 psi and was produced with Type III Portland cement and a maximum-size aggregate of 3/8 in. The coarse aggregate was mostly well-rounded natural material of uniform gradation (100 percent by weight passing the 3/8-in sieve with less than 12 percent by weight passing the No. 4 sieve) with less than 10 percent by weight crushed material. The fine aggregate was a washed material conforming to ASTM Specification C-33 for concrete fine aggregate and had less than 2 percent by weight passing the No. 200 sieve. The fineness modulus of the sand varied from 2.6 to 3.1.

The concrete was mixed at the Eric H. Wang Civil Engineering Research Facility (CERF) in a 16-ft^3 nontilting, rotating drum, electric-powered concrete mixer. Three to six control cylinders for each beam were cast in 6-in-diameter, 12-in-high, waxed cardboard molds. The beams were cast in their normal position in steel forms. Each beam and its control cylinders were cast from a single batch of concrete. The beam concrete was compacted with a 1-in-diameter, 12-in-long, electric vibrator probe which operated at about 10,000 rpm. The control cylinders were compacted by vertical vibration at a frequency of 10 Hz for about 1-1/2 minutes on a vibrating table designed and fabricated at CERF.

The beams and control cylinders were cured under polyethylene plastic sheets for at least 48 hours before the forms were removed and the cylinder molds stripped. The beams and cylinders were then left to cure together under the

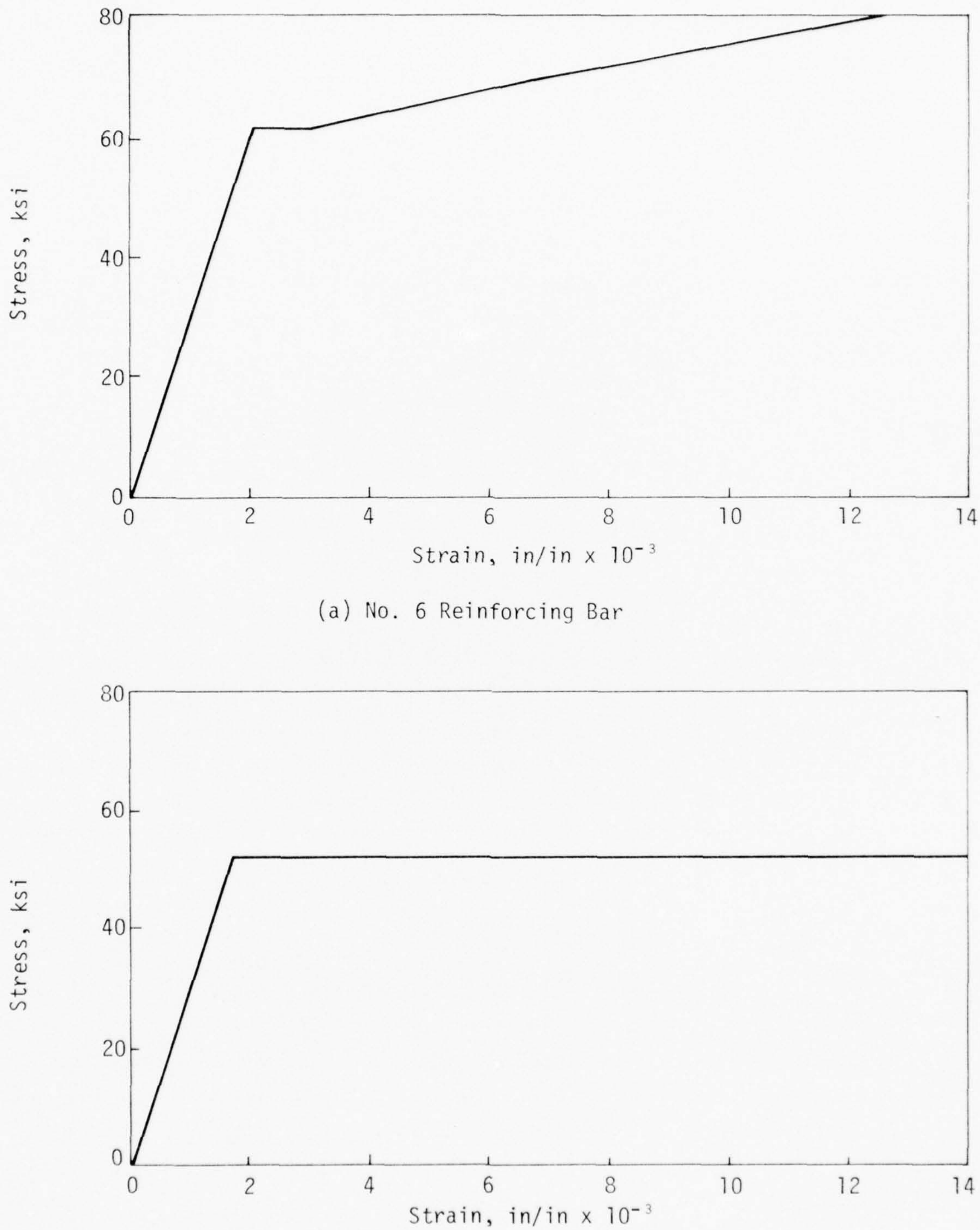

(a) No. 6 Reinforcing Bar

(b) No. 2 Reinforcing Bar

Figure 6. Typical Stress-Strain Curves for Reinforcing Steel

polyethylene sheets until about 2 weeks prior to the beam test, at which time curing continued at ambient conditions.

The control cylinders were tested to failure the day of the beam test. Tensile splitting tests and stress-strain curves were made for a limited number of the control cylinders. Figure 7 shows a typical stress-strain curve for the concrete. The portion of the curve beyond maximum stress could not be measured because of the characteristics of the testing machine used. Table 2 presents the concrete strengths for the various beams.

INSTRUMENTATION

Instrumentation for all beams, with a few exceptions, was similar. Measurements were made at nodal locations that corresponded to nodes used in the behavioral model development. Figure 8 shows the location of the reference nodes. Measurement locations were symmetrical about the beam centerline.

Measurements made included vertical deflections along the beam, vertical and horizontal deflections at the support shafts, relative horizontal displacements along the beam, steel and concrete strain at various locations, rotations at the beam ends, and lateral and horizontal loads.

Displacement

Vertical deflection measurements were made at seven locations along the beam (1, 2, 4, and 6 in figure 8). At the beam centerline, station 6, the measurement was made from the ground to the bottom surface of the beam. At the other six locations, the measurements were made from the ground to aluminum brackets bonded to the beam side at middepth. Support movement during the tests was monitored by vertical and horizontal displacement measurements on both sides of the support shafts at each end of the beams. Linear potentiometers with gage lengths from 1 to 6 in, depending on the location of the measurement, were used for these measurements.

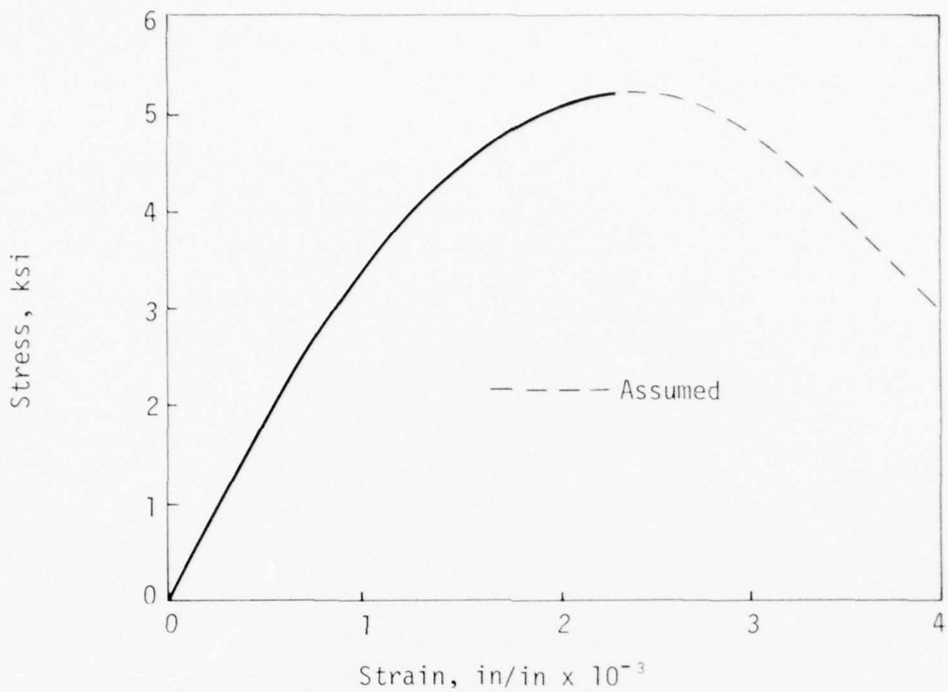

Figure 7. Typical Stress-Strain Curve for Concrete

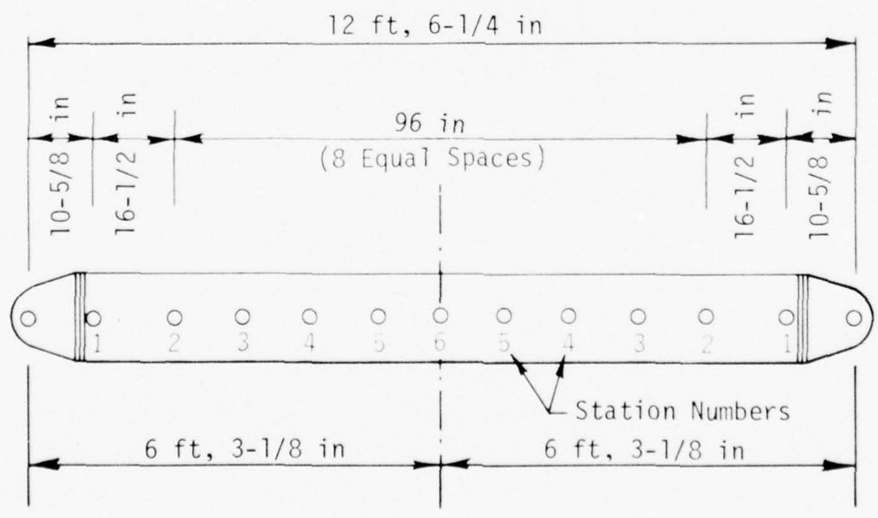

Figure 8. Location of Reference Nodes

Table 2. Test-Day Compressive Strength of Concrete

Beam Designation	Cylinder Strength, psi	Average Strength, psi
5-0-1	5023 4952 5067	5014 (58)*
5-0-2	5058 5129 4934 4828 4952	4980 (117)
5-2-1	4298 4333 4377	4336 (40)
5-2-2	5200 4032 4864 4633 5075 4103	4651 (492)
5-3-2	4837 4767 4690 4533 4899 4793	4753 (129)

Beam Designation	Cylinder Strength, psi	Average Strength, psi
5-3-3	5571 5500 5571 5606 5667	5583 (61)
4-0-1	5359 5164 5369 5309 5238	5288 (87)
4-2-1	5199 5288 5129	5205 (80)
4-2-2	4969 5093 5129 5129 4740 4881	4990 (158)
4-3-1	5164 5270 5182	5205 (57)

Beam Designation	Cylinder Strength, psi	Average Strength, psi
4-3-2	5270 5500 5500	5423 (133)
3-0-1	5129 5146 5199 5093	5142 (44)
3-2-1	4810 4633 4934	4792 (151)
3-2-2	4952 4399 4793	4881 (81)
3-3-1	5217 5252 5288	5252 (36)
3-3-2	4916 5022 5146	5028 (115)
3-3-3	4244 4492 4297	4344 (131)

*Standard deviations are shown in parenthesis.

Horizontal displacement measurements were also made at six locations along the beams. These measurements were made as relative displacements between stations 1 and 2, 2 and 4, and 4 and 6. The measurements were made with direct current differential transformer (DCDT) displacement transducers with full-scale ranges of $\pm$ 0.05 in.

Strain

Steel strain in the longitudinal tensile reinforcement was measured at stations 2 through 6. The measurements were made on the middle reinforcing bar. Strain measurements on the two compression steel bars were also taken at stations 2 through 6, except under the load points, in which case no measurement was made. At station 6 (the beam centerline) a strain gage was mounted on each bar. At the remaining stations, the measurements were taken on alternate sides of the beams. Strain measurements were also taken in the first two stirrups outside the load points in all but the first four beams tested, in which the gages were inadvertantly left out. Measurements of the steel strain were made with 350-ohm, epoxy-backed, foil strain gages which had a 1/2-in gage length and a gage factor of 2.125.

The steel strain gages were mounted with epoxy cement on a widened and smoothed portion of a longitudinal rib of the bars. Lead wires were then attached and the gage was waterproofed with a plastic sealant. The lead wires exited the beams through holes in the side forms.

All concrete strain measurements were made on the beam surface. Three concrete strain measurements were taken at the beam centerline--one at the middle of the top surface, one 1 in from the top on the side of the beam, and one 2-1/2 in from the top on the side. In addition, in the 5-series (i.e., $a_s/d = 5$), the two side measurements were also made at station 4; in the 4-series, the two side measurements were also made at stations 5 and 3; and in the 3-series the side measurements were also made at stations 5 and 2.

Concrete strain measurements were made with 300-ohm, paper-backed, wire strain gages which had a 1-in gage length and a gage factor of 2.05. The

surface on which a strain gage was to be mounted was first ground or sanded to remove foreign material and to smooth the surface. The surface was cleaned, filled with epoxy, and sanded smooth. Epoxy was then used to bond the gage to the surface.

Rotation

Rotation measurements were made at both ends of the beams with gages specially fabricated at CERF. The rotation gages consisted of a pendulum suspended from the paddle portion of a DX type velocity gage. The rotation of the pendulum relative to the gage body was measured by the variable inductance transducer of the velocity gage.

Data Acquisition and Reduction

The electrical instrumentation measurements were continuously recorded on 1-in magnetic tape. Recording was accomplished at a tape speed of 30 in/sec; thus, each test could have a maximum recording time of 15 minutes. However, to reduce the computer time associated with the digitizing of the analog tapes, it was intended that each test be less than 7-1/2 minutes. Analog data tapes were digitized and data reduction and presentation were performed at the Kirtland Air Force Base computing facilities.

Photoelastic Coating

In addition to the electrical measurements, photoelastic coating was used on the sides of the beams to determine the complete concrete strain distribution in compression in the constant moment region. Since only the compression strain pattern was of interest, the coating was applied to the top half of the beams only.

The strain pattern was observed by taping a Polaroid sheet over the coating and then photographing the resulting fringe patterns that occurred during loading of the specimens. Slow-speed (six frames per second), color motion pictures were taken of the coated area during the tests. Theoretically, based on the characteristics and thickness of the coating, the number and

order of the fringes can be related to the strain in the coating. To relate the strain pattern to a load condition, a digital voltmeter, which displayed the output from the lateral load force link, was located on the test frame and photographed with the strain patterns.

SECTION IV
DEVELOPMENT OF ANALYTICAL MODEL

A behavioral model for static response prediction of hinge-ended reinforced concrete beams under combined axial and lateral loads was formulated. The beam response was analyzed by dividing the beam along its length into a number of segments connected at points called *nodes* and assuming the curvature varied linearly between these nodes. The lateral loads were applied as point loads at the nodes and the axial loads were applied longitudinally at the end nodes (hinge points). Only beams of symmetrical geometry and loads about the centerline were considered. A constant axial-to-lateral-load ratio was maintained throughout the calculated beam response. A maximum concrete strain was not specified in the model; consequently, the collapse point was not determined. However, the response was described beyond any significant load-carrying capacity. A CDC 6600 digital computer was used to solve for the beam behavior (i.e., deflections, concrete and rebar strains, and curvatures at the node points as a function of applied loading) from the developed model.

Results of the behavioral model calculation, plotted with the experimental results, are presented in appendix A. Appendix B presents the computer program used for the analytical calculations.

MATERIAL BEHAVIOR

The behavioral model used predicted the response well beyond the maximum resistance of the beam. It was necessary, therefore, that the concrete stress-strain relationship used in this model development represent the complete stress-strain behavior and not just that to maximum stress. When a standard universal testing machine is used to test concrete cylinders, the specimens normally crush when the maximum stress is reached. This behavior leads to difficulties in obtaining data on the stress-strain relationship of concrete beyond the point of maximum stress. Barnard (ref. 50) and other researchers cited by Barnard have tested concrete cylinders using specially constructed very stiff constant-strain-rate testing machines. These machines

permitted concrete specimens to be tested to very large compressive strains, well beyond those occurring at maximum stress. Figure 9 shows the complete stress-strain curve for concrete obtained with the special testing machines. Based on the descending portion of the curve where stress decreases with increasing strain, Barnard describes concrete as a *strain-softening* material (unlike mild steel which is a *strain-hardening* material). This strain-softening characteristic of concrete has a significant effect on the behavior of the beam after maximum resistance has been attained.

Figure 10 shows the concrete stress-strain curve used for this model formulation. This curve was assumed to represent the complete stress-strain behavior of the concrete in the beam. The initial portion of the curve is defined by the parabola

$$f_c = f''_c\left[\frac{2\varepsilon}{\varepsilon_o} - \left(\frac{\varepsilon}{\varepsilon_o}\right)^2\right]$$

where

f_c = concrete stress

f''_c = flexural strength of concrete in compression

ε = concrete strain

ε_o = strain at maximum concrete stress

This parabolic form was first used by Hognestad (ref. 2) and subsequently by many other investigators.

The second portion of the curve is a descending straight line connecting the top of the parabola at a strain of ε_o and a horizontal line at a stress of $0.2f''_c$.

The third portion of the stress-strain curve, a horizontal line, suggests that concrete can sustain a stress of $0.2f''_c$ to infinity. This approach has been used previously by Barnard (ref. 54), Yamashiro and Siess (ref. 55), and Kent and Park (ref. 56).

The maximum moment capacity of a beam with no axial load, singly reinforced with steel having a bilinear stress-strain relationship, and the concrete

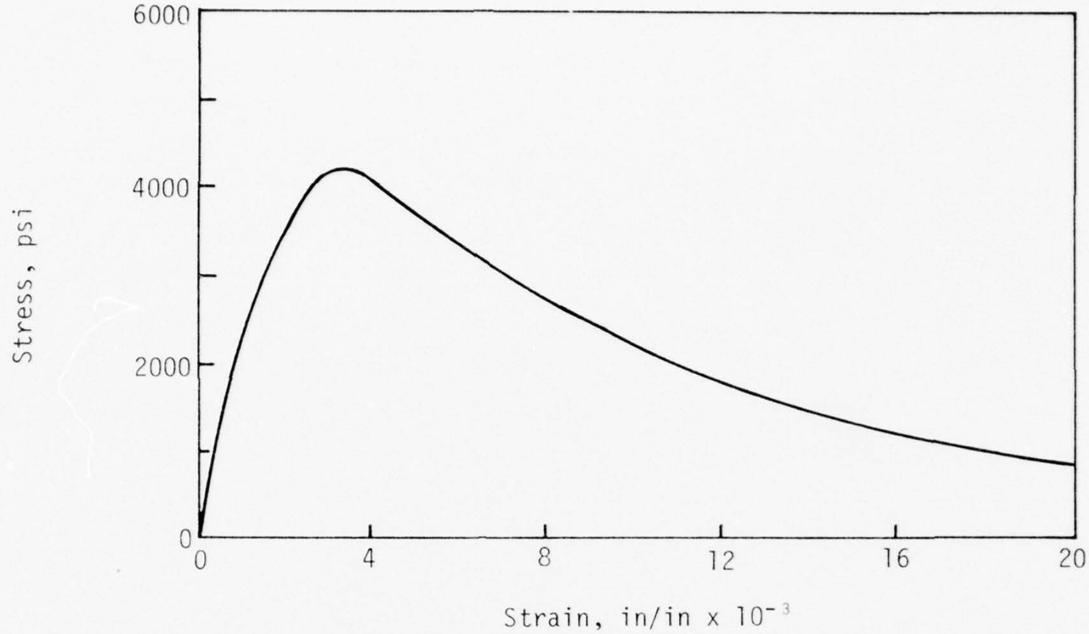

[after Barnard (ref. 50)]

Figure 9. Typical Complete Stress-Strain Curve for Concrete

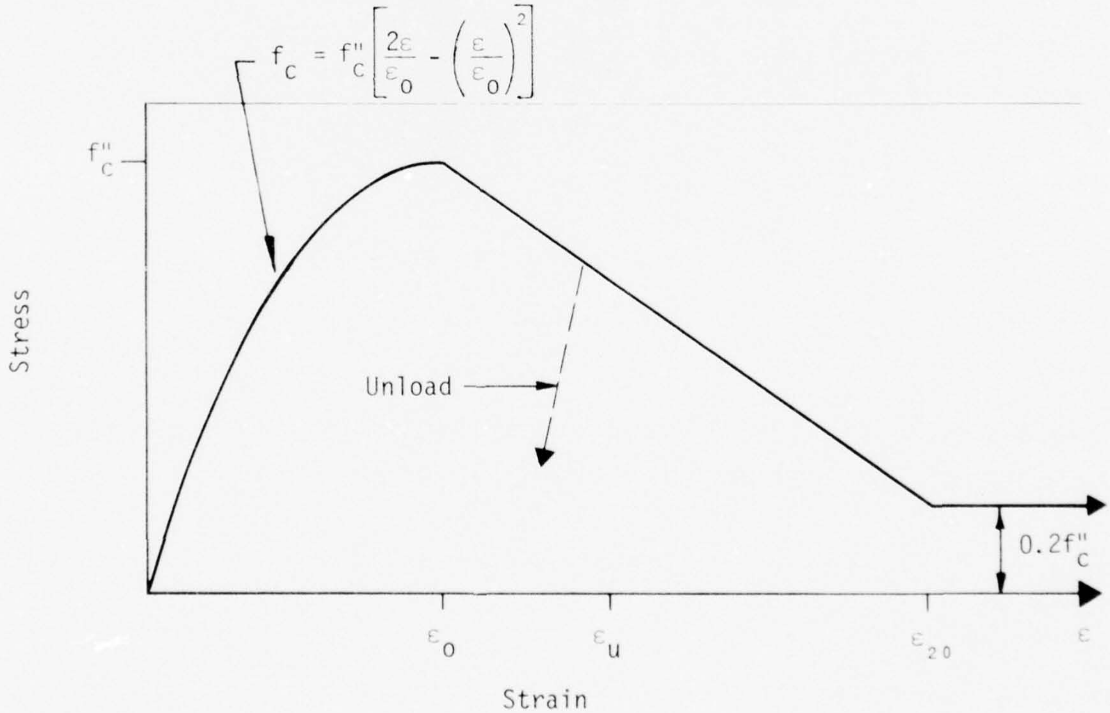

Figure 10. Concrete Stress-Strain Curve Used in Analytical Model

stress-strain characteristics shown in figure 10 occurs at a strain between ε_0 and ε_{20} (the strain at which the concrete stress becomes 20 percent of f''_c). The exact value of the strain corresponding to the maximum moment capacity depends on the slope of the descending straight line and occurs at the strain where the ratio of the area under the stress-strain curve to the area of the rectangle $f''_c\varepsilon$, designated k_1, becomes a maximum. The strain at which k_1 becomes maximum is designated as ε_u. Figure 11 further illustrates the relationship between the concrete stress-strain curve and k_1.

With reference to figure 11 and for

$$\varepsilon_0 \leq \varepsilon \leq \varepsilon_{20}$$

the area, A, under the concrete stress-strain curve is

$$A = f''_c\left[\frac{2}{3}\varepsilon_0 + (\varepsilon - \varepsilon_0) - \frac{1}{2}m(\varepsilon - \varepsilon_0)^2\right]$$

$$= f''_c\left[\varepsilon - \frac{1}{2}m\varepsilon^2 + m\varepsilon\varepsilon_0 - \left(\frac{1}{2}m\varepsilon_0^2 + \frac{1}{3}\varepsilon_0\right)\right]$$

The ratio of the area under the concrete stress-strain curve to the area of the rectangle $f''_c\varepsilon$ is k_1.

$$k_1 = \frac{A}{f''_c\varepsilon} = 1 - \frac{1}{2}m\varepsilon + m\varepsilon_0 - \frac{1}{\varepsilon}\left(\frac{1}{2}m\varepsilon_0^2 + \frac{1}{3}\varepsilon_0\right)$$

The strain at which k_1 is maximum can be determined from

$$\frac{dk_1}{d\varepsilon} = -\frac{1}{2}m + \frac{1}{\varepsilon^2}\left(\frac{1}{2}m\varepsilon_0^2 + \frac{1}{3}\varepsilon_0\right) = 0$$

By designating ε_u the strain corresponding to maximum k_1, the slope of the descending portion of the curve required to make k_1 maximum at ε_u is

$$m = \frac{2}{3} \cdot \frac{\varepsilon_0}{\varepsilon_u^2 - \varepsilon_0^2}$$

Why the maximum moment capacity of an under-reinforced concrete flexural member (tension failure) occurs at maximum k_1 can be explained by considering the internal forces in the beam. After the tension reinforcement yields

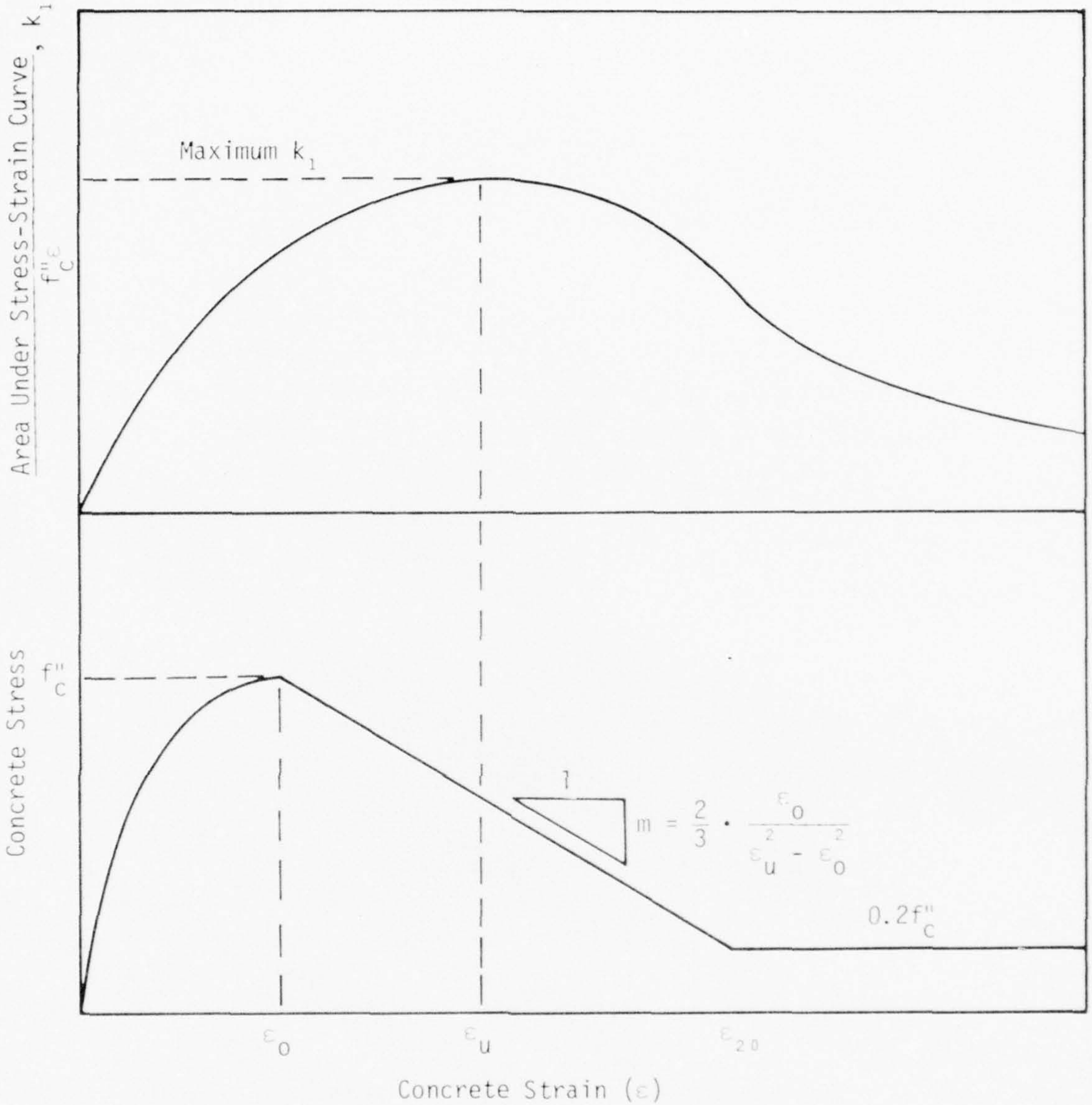

Figure 11. Concrete Stress-Strain and k_1

and the curvature is increasing, the tension force, T_s, remains constant. Force equilibrium requires that the compression force in the concrete, C_c, be equal to the tension force, or

$$C_c = T_s$$

However,

$$C_c = k_1 f''_c \, bc$$

where b is the beam width and c is the distance from the compression face of the beam to the neutral axis. Therefore, with increasing curvature prior to a concrete strain of ε_u, k_1 increases; this requires a decrease in c. As the neutral axis moves upward, the internal moment arm between C_c and T_s also increases and this results in an increasing moment. Beyond an extreme fiber strain of ε_u and as the curvature increases, k_1 decreases. Consequently, c must increase; this results in a decreasing internal moment arm and decreasing moment.

The tensile strength of the concrete was not ignored. Concrete cracking was specified by a limiting concrete tensile strain, ε_{cr}. The modulus of elasticity of concrete in tension was assumed as suggested in the ACI Building Code (ref. 46); i.e.,

$$E_{conc} = 33\omega^{1.5} \sqrt{f'_c} \quad \text{in psi}$$

where ω is the unit weight of concrete (145 lb/ft^3). Unloading of the concrete was assumed to occur at a slope parallel to the initial slope of the compression portion of the curve.

$$E_{unload} = \frac{2f'_c}{\varepsilon_o}$$

REINFORCING STEEL

Figure 12 illustrates the stress-strain relationship assumed for the tension reinforcing steel. The curve is bilinear and includes a second-degree curve representation of strain hardening. The equation of the curve beyond strain hardening for $\varepsilon \geq \varepsilon_{sh}$ is

$$f_s = f_y + A_{sh} (\varepsilon - \varepsilon_{sh}) - B_{sh}(\varepsilon - \varepsilon_{sh})^2 \qquad (4)$$

where f_s is the steel stress and f_y is the yield stress.

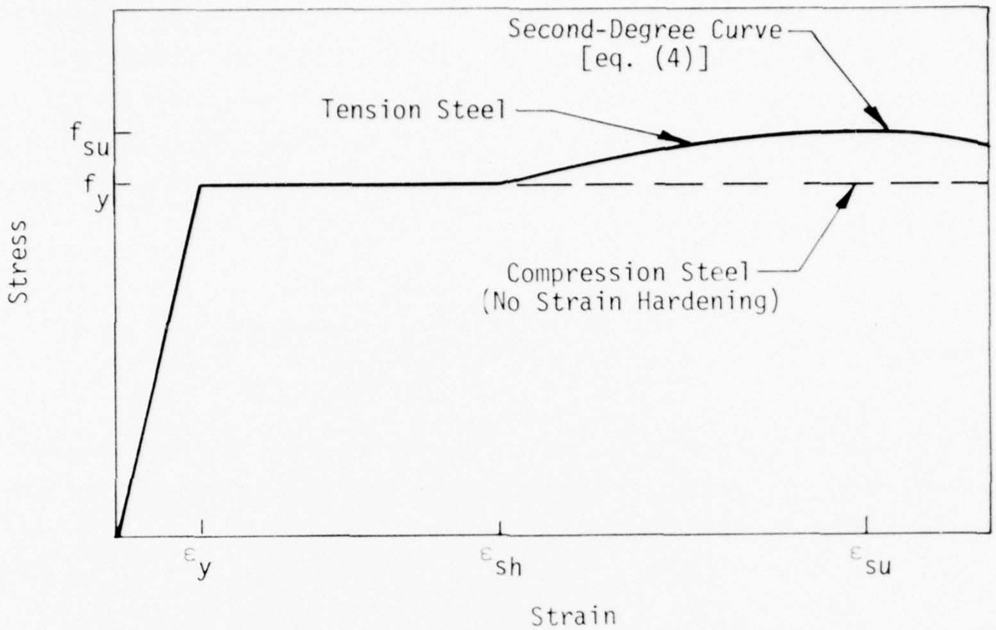

Figure 12. Typical Stress-Strain Curve for Reinforcing Steel

ε = steel strain

ε_{sh} = strain at start of strain hardening

A_{sh} = initial slope of strain hardening curve

B_{sh} = constant determined to match actual steel stress-strain behavior

In compression, the reinforcement was assumed to behave as in tension except with no strain hardening. Unloading of the steel was assumed to occur at the initial slope of the curve, E_s.

MODEL FORMULATION

A common method for solving the response of a statically loaded beam is to increment the applied load and calculate the resulting strains, stresses, rotations, and deflections. This method, however, presents numerical instability problems when the material involved has a strain-softening characteristic and the response is calculated into the decreasing-load region. Consequently,

the method used to calculate the responses in this investigation consisted of incrementing the strain at the top of the beam at the centerline and then computing the associated loads, rotations, deflections, and the strains and resulting stresses at the centerline and at the remaining node points. The solution was repeated until the strain at the top of the beam reached some large value (e.g., 0.05).

BEAM BEHAVIOR

Figure 13 illustrates the model used for the overall response calculations. The axial load, P, and the total lateral load, F, on half the beam are related by the factor K; i.e.,

$$K = P/F$$

For no axial load (i.e., K = 0), a very small K was used in the calculations (e.g., 0.005) because subsequent calculations involved division by K.

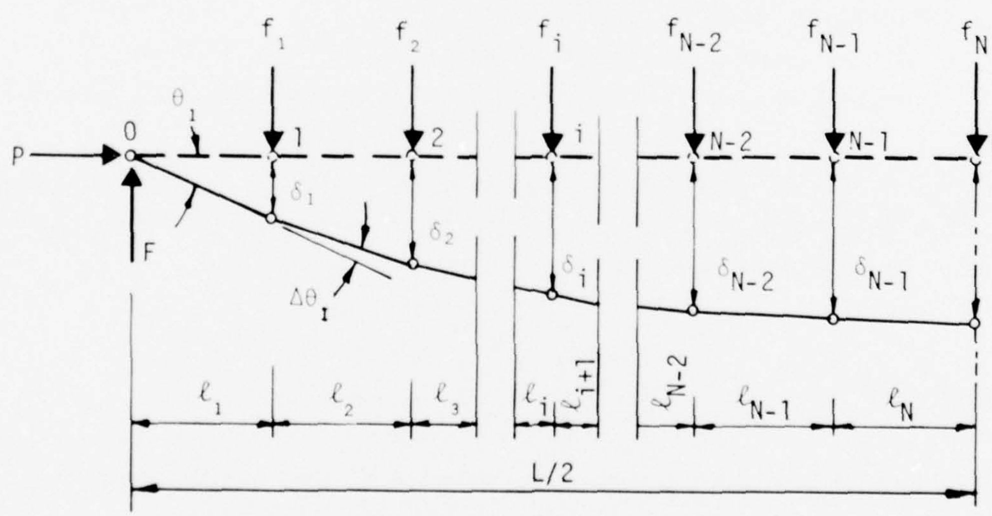

Figure 13. Beam Model for Overall Response

Distribution of the lateral load was specified by the factors A_i, i = 1, N, such that

$$f_i = A_i F = A_i P/K, \; 0 \leq A_i \leq 1.0 \tag{5}$$

The shear force in any segment and the bending moment at any node were expressed in terms of the axial load, P, by

$$v_i = V_i P, \; i=1, N$$

and

$$m_i = M_i P, \; i=1, N \tag{6}$$

where

v_i = shear force in segment i

m_i = bending moment at node i due to lateral load only

and

$$V_1 = 1.0/K$$

$$V_i = V_{i-1} - A_{i-1}/K, \; i=2, N$$

$$M_0 = 0.0$$

$$M_i = M_{i-1} + V_i \ell_i, \; i=1, N$$

Node deflections and rotations can be calculated if curvatures, ϕ_i, are known at each node and the distribution of the curvature between nodes is assumed to be linear. The curvatures, ϕ_i, were determined from force equilibrium at the nodes. It was also assumed, then, for the calculation of the deflections, that the beam rotations were concentrated at the nodes and segments between the nodes remained straight. The angle change or change in rotation at a node i was computed as follows:

$$\Delta\theta_i = \left[\left(2\phi_i + \phi_{i-1}\right)\ell_i + \left(2\phi_i + \phi_{i+1}\right)\ell_{i+1}\right]/6$$

The slope of the segment at the hinged end was computed as follows:

$$\theta_1 = \sum_{i=1}^{N} \Delta\theta_i$$

The slope, then, of any segment was

$$\theta_i = \theta_1 - \sum_{j=1}^{i-1} \Delta\theta_j$$

The beam deflection at any node was computed as follows:

$$\delta_i = \delta_{i-1} + \theta_i \ell_i$$

with

$$\delta_0 = 0$$

BEAM SECTION EQUILIBRIUM

Figure 14 illustrates the stresses and associated forces acting on a beam section resulting from a known strain distribution. The assumptions associated with section equilibrium are as follows:

(1) Strain is proportional to the distance from the neutral axis.

(2) Concrete and steel stress-strain relationships are as described previously.

(3) Shear behavior does not affect the flexural behavior of the beams.

The force resultants shown in figure 14 are discussed below.

<u>Compressive Concrete Force (C_c)</u>

C_c was determined by integrating the concrete stress-strain curve presented in figure 10.

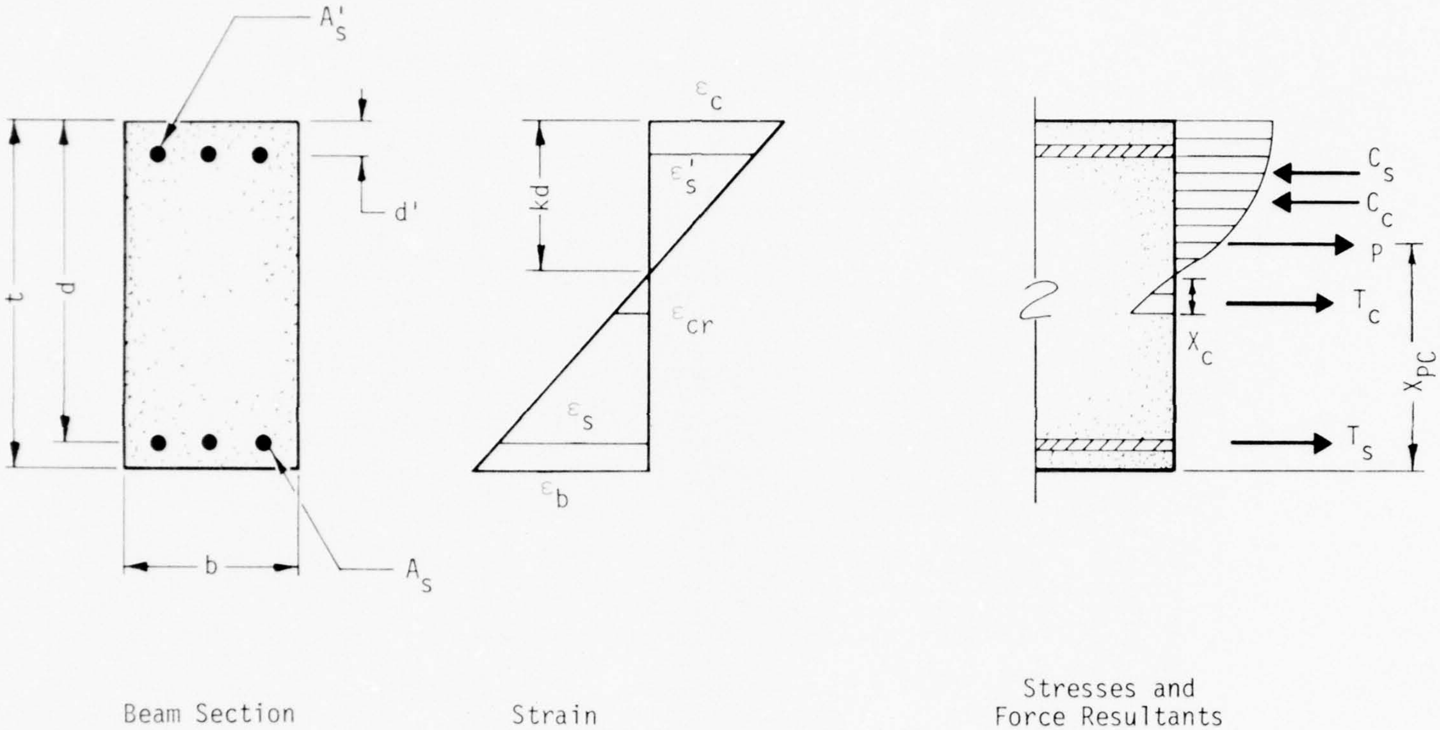

Figure 14. Stresses, Strains, and Forces on Beam Section

$$C_c = bkdk_3 \int_0^{\varepsilon_c} f_c d\varepsilon = bkdk_1 k_3 f'_c$$

where

b = beam width

kd = distance from compressive face of beam to neutral axis

k_3 = factor relating flexural strength of concrete in beam to concrete cylinder strength

ε = strain in concrete at extreme fiber of beam

k_1 = concrete stress-strain curve shape factor previously discussed

Force in Compression Reinforcement (C_s)

$$C_s = A'_s f'_s$$

where

A'_s = area of compression reinforcement

f'_s = stress in compression reinforcement

However, when $\varepsilon'_s \geq \varepsilon_u$, the compression reinforcement is assumed to buckle and no longer carry load.

Tensile Force in Concrete (T_c)

$$T_c = \frac{1}{2} E_{conc} \varepsilon_{cr} bX_c$$

where

X_c = depth of tension stress block (determined from strain distribution)

Tensile Force in Main Reinforcement (T_s)

$$T_s = A_s f_s$$

where

A_s = area of reinforcing steel

f_s = stress in reinforcing steel

Horizontal force equilibrium requires that

$$P = C_c + C_s - T_c - T_s$$

The axial force, P, acts through the *plastic centroid* of the beam section which is located a distance X_{PC} from the bottom of the beam. The plastic centroid of a section is the centroid of resistance to load computed under the assumption that the concrete is uniformly stressed to $k_3 f'_c$ and the reinforcing steel is uniformly stressed to f_y.

Moment equilibrium about the plastic centroid, X_{PC}, yields an expression for the moment resistance of the beam.

$$M_R = C_c(\text{moment arm abt PC}) + C_s(\text{moment arm abt PC})$$

$$+ T_c(\text{moment arm abt PC}) + T_s(\text{moment arm abt PC}) \qquad (7)$$

RESPONSE SOLUTION

The concrete strain at the top of the centerline section was incremented and the associated forces and displacements were calculated. The following steps were employed in determining the response:

(1) A set of displacements (δ_i, i=0, N) was assumed at the start of each response cycle. For the first cycle, the deflections were assumed to be zero (δ_i=0, i=0, N) and subsequently the final deflections calculated from the previous cycle were used as the assumed deflections for the next cycle.

(2) With ε_{cN}($\varepsilon_{cN} = \varepsilon_c$ at node N) and the load ratio (K = P/F) known, the strain at the bottom of the section was incremented until

$$M_{RN} = m_N + P\delta_N$$

where

M_{RN} = moment resistance of the section at node N [eq. (7)]

m_N = moment at node N due to applied lateral loads [eq. (6)]

δ_N = assumed deflection at node N

At this time in the solution, an axial load, P, and the corresponding moments at each node were known as well as the curvature at the centerline, ϕ_N.

(3) With the axial load and moments known at the remaining nodes, the concrete strain and the strain at the bottom of the beam at each remaining node were incremented until the resisting and applied forces were equal; i.e.,

$$M_{Ri} = m_i + P\delta_i \qquad i=1,\ N-1$$

This established a set of curvatures (ϕ_i, i=1, N-1).

(4) With the new set of curvatures known, a revised set of nodal deflections was calculated. The new deflection at the centerline was compared to the previously assumed deflection. If the agreement was within a specified tolerance, the cycle was ended and a new cycle was started with the next increment of ε_c at node N. If the centerline deflections did not agree with the specified tolerance, the old deflections were replaced with the new and the cycle was repeated with the same ε_c at node N. The tolerance used in comparing new and previous deflections was a relative error of 0.01, or

$$\left|\delta_{new} - \delta_{old}\right| / \delta_{new} \leq 0.01$$

There was no failure (collapse) criterion associated with the model; therefore, the response was calculated to some large ε_c (e.g., 0.05). The terminal value of ε_c was selected large enough to obtain the response well

beyond the maximum beam resistance and far enough to establish significant behavioral characteristics.

Beyond the maximum moment resistance of a beam, the curvature at the node of maximum moment (the centerline node) continues to increase with decreasing moment. However, at the remaining nodes the curvature and associated strains decrease with decreasing moment. As the beam is forced through further deflection, the curvature at the center becomes more concentrated as the remaining portions of the beam unload and decrease in curvature. To adequately model the unloading of portions of the beam, the maximum strains encountered at each node were stored for comparison with subsequent strains. Also, based on observed behavior beyond maximum moment, the portion of beam undergoing the extremely large curvature has a finite length that must be accounted for in the deflection calculations. Therefore, at the center node, whenever the strain at the compression face was greater than ε_u, deflections were calculated based on an assumed width of maximum curvature of d (the beam depth).

ANALYTICAL MODEL PARAMETERS

The geometric parameters used were the same as those for the experimental beam specimens described in section 3 and are summarized in table 3.

Table 4 presents the compressive concrete strength, f'_c, and the load ratio, $K = P/F$, used in the calculations. The concrete strengths presented are the average of several (3 to 6) compression tests performed the day of the beam tests on 6-by-12-in cylinders cast with the beams. The load ratios were determined from lateral and horizontal force measurements made during the beam tests.

The load factors, A_i, that relate the individual concentrated nodal forces to the total lateral load on half of the beam (eq. 5) were as follows:

Table 3. Geometric Parameters

Parameter	Description	Value
b	Beam Width	9.0 in
d	Depth of Tension Reinforcement from Compressive Face of Beam	12.5 in
d'	Depth of Compressive Reinforcement from Compressive Face of Beam	1.5 in
t	Total Beam Depth	15.0 in
A_s	Area of Tensile Reinforcement	1.32 in^2
A_s'	Area of Compressive Reinforcement	0.10 in^2
L	Beam Length	150.25 in
N	Number of Nodes	6
ℓ_i	Length of i^{th} Beam Segment	ℓ_1 = 10.625 in ℓ_2 = 16.5 in $\ell_{3,4,5,6}$ = 12.0 in

Table 4. Average Concrete Compressive Strength and Load Ratio

Beam Designation	f_c', psi	Load Ratio (K = P/F)
5-0-1	5014	0.005
5-0-2	4980	0.005
5-2-1	4336	1.91
5-2-2	4651	1.88
5-3-2	4753	3.10
5-3-3	5583	3.21
4-0-1	5288	0.005
4-2-1	5205	1.97
4-2-2	4990	1.88
4-3-1	5205	3.18
4-3-2	5423	3.15
3-0-1	5142	0.005
3-2-1	4792	1.85
3-2-2	4881	1.87
3-3-1	5252	3.03
3-3-2	5028	3.08
3-3-3	4344	3.11

Series 5

$$A_{1,2,3,4,6} = 0$$
$$A_5 = 1.0$$

Series 4

$$A_{1,2,3,5,6} = 0$$
$$A_4 = 1.0$$

Series 3

$$A_{1,2,4,5,6} = 0$$
$$A_3 = 1.0$$

Table 5 presents the parameters associated with the concrete model. The modulus of elasticity, used only when the tensile strength of the concrete was considered, was the value suggested in the ACI Building Code. The unload modulus was arbitrarily selected as the initial tangent to the parabolic portion of the stress-strain curve. The strain at maximum stress, ε_0, was selected as an average from the cylinder tests on the beam concrete.

Table 5. Parameters Associated With Concrete Model

Parameter	Description	Value
E_c	Modulus of Elasticity	$57{,}400\sqrt{f'_c}$ psi
E_{unload}	Modulus of Elasticity for Unloading Concrete	$\frac{2f'_c}{\varepsilon_o}$
ε_o	Strain at Maximum Stress	0.0022
ε_u	Strain at Maximum k_1	0.0035
ε_{cr}	Strain at Concrete Cracking	0.0001
k_3	Ratio of Flexure Strength of Concrete to Cylinder Strength	1.00

The few tensile splitting tests conducted on the concrete indicated an approximate tensile strength of 400 psi. This value with a modulus of 4×10^6 psi leads to the value of the cracking strain, ε_{cr}, that was used in the calculations. The value of ε_u used was selected based on some observed behavior and also on a value that seemed to yield better comparisons in some areas between calculated and experimental beam response.

The tensile reinforcement was assumed to be elastic-plastic and to include strain hardening. The strain hardening portion of the steel behavior was described by a second-degree curve [eq. (4)].

The compression reinforcement was also assumed to be elastic-plastic, but not to include strain hardening. Also, the compression reinforcement was assumed to have no strength beyond a strain of ε_u. Table 6 presents the reinforcing steel parameters that were determined from tensile tests on the rebar.

The calculations of the beam behavior were made to a maximum compressive strain at the top of the beam of 0.05 in/in.

Table 6. Reinforcing Steel Parameters

Parameter	Description	Value
E_s	Modulus of Elasticity	30×10^6 psi
f_y	Yield Stress for Tensile Reinforcement	62.0 ksi
f'_y	Yield Stress for Compressive Reinforcement	52.0 ksi
ε_{sh}	Strain at Onset of Strain Hardening (Tensile reinforcement only)	0.003
A_{sh} B_{sh}	Parameters Used to Describe Strain-Hardening Portion of Tensile Reinforcement	2.2×10^6 psi 29.6×10^6 psi

SECTION V
RESULTS

Results from both the experimental investigation and the behavioral model analysis are presented. Analytical data were obtained for the node points at which experimental measurements were made. When possible, both results are presented together so that comparisons may be made and the results discussed. Appendix A presents all the measured experimental and the calculated analytical data for each beam.

GENERAL BEHAVIOR

The general response of the beams can be illustrated by their load-centerline deflection curves. Figure 15 presents an idealized response curve. The behavior of the beams was generally stiff for the initial 10 percent of the

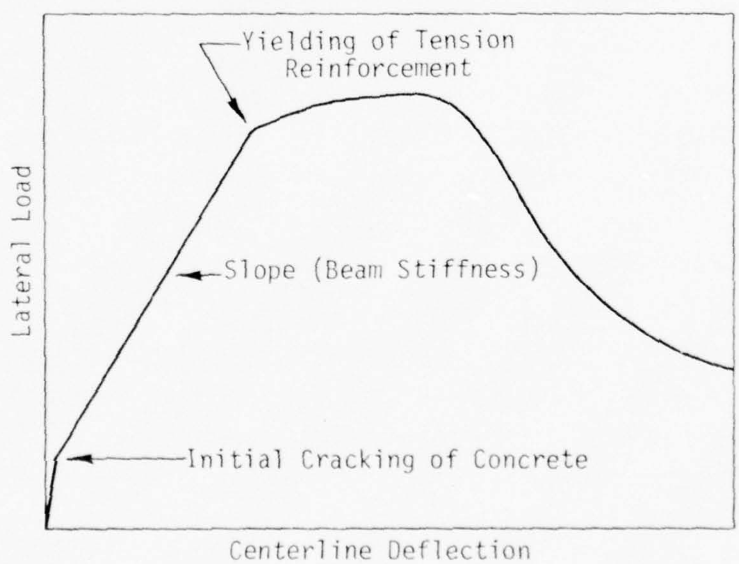

Figure 15. Typical Load-Centerline Deflection Curve

loading, followed by a fairly linear portion of reduced stiffness. Upon yielding of the tensile reinforcement the curve flattened considerably until the maximum load was achieved. The behavior beyond yield was a function of the magnitude of the axial load. When the axial load was zero, or very small, the flattened portion of the curve was relatively long. With high axial load the flattened portion was either short or nonexistent. Upon reaching maximum load, with no axial load, the load decreased at a gradual rate with increasing deflection. With high axial load, the load dropped rapidly upon reaching the maximum load. Figure 16 presents the load-centerline deflection curves for the 17 beams tested.

MODE OF FAILURE AND CRACK PATTERN

The mode of failure of the beams was flexural tension; i.e., the tension reinforcement began yielding before the concrete crushed. The beams collapsed when the concrete at the top of the beams was crushed. Based on the ultimate shear strength of the beams predicted by the ACI Building Code, the beams with short shear spans could have failed in shear. However, the small percentage of shear reinforcement was very effective in preventing shear failure. In the analytical calculations, shear behavior was not considered; therefore, only flexural failures were predicted. Also, prediction of crack spacing and width was beyond the scope of the analytical effort; consequently, only observed crack behavior is reported.

Because the experimental test measurements were continuously recorded on magnetic tape, the duration of each test could be no longer than 15 minutes (maximum time on one roll of tape when recording at 30 in/sec). However, to conserve magnetic tape and to reduce data-reduction costs, the test times were held to 2 to 12 minutes. These relatively short test times precluded the marking of cracks at specific load increments, which is commonly done in static tests of reinforced concrete components.

Following each test, the cracks were marked and the beams were photographed. Figure 17 presents the final crack patterns. Visible crack formation was documented by slow-speed motion pictures taken to record the fringe patterns

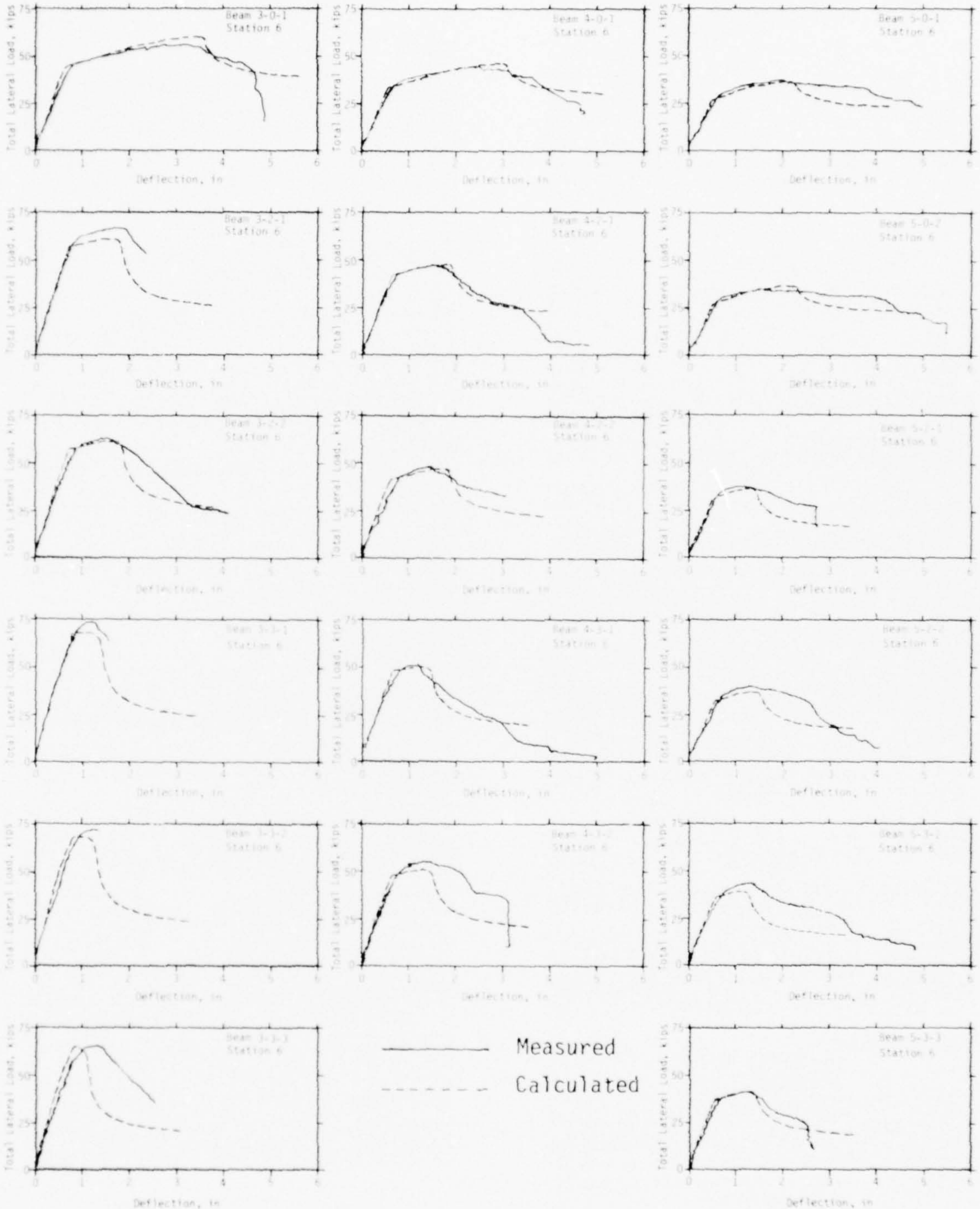

Figure 16. Load-Centerline Deflection Curves for Beams Tested

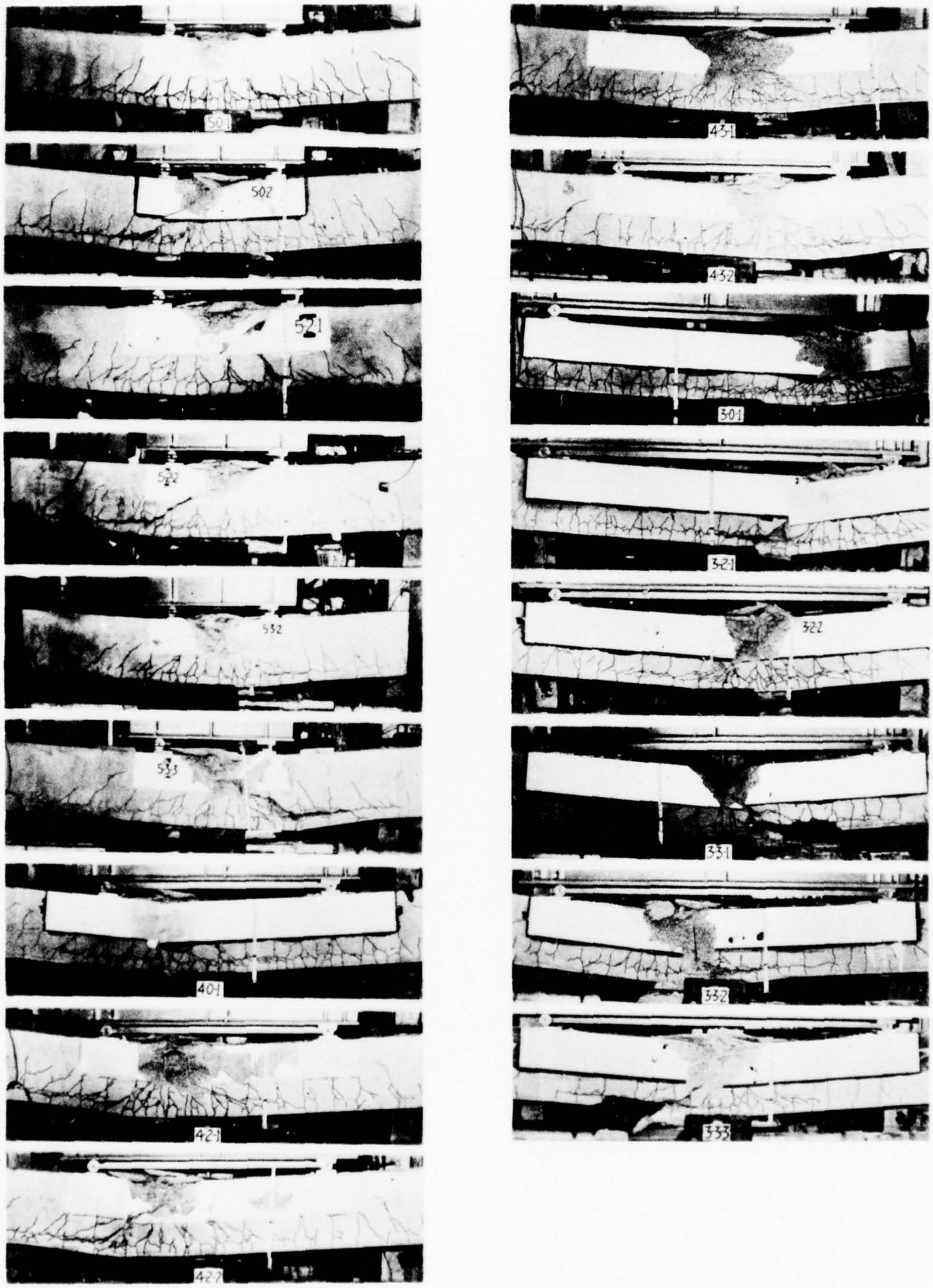

Figure 17. Final Crack Patterns for Beams Tested

from the photoelastic coating. The motion pictures indicated that cracking first occurred in the middle of the constant-moment region of the beams and then spread toward the supports. The initial cracks generally formed at the stirrups. At advanced stages of loading, additional cracks formed between the initial cracks. Near the maximum load capacity of the beams, horizontal cracks formed at the level of the tensile reinforcing steel; this indicated bond failure. In general, the beams with high axial load were cracked less than those with no axial load. It can also be seen from figure 17 that inclined diagonal tension cracks extended from the tensile reinforcement level to the vicinity of the load points. Table 7 presents the percentages of maximum load at which first visible cracking, first diagonal cracking, and concrete spalling occurred (based on the slow-speed motion pictures).

Table 7. Concrete Cracking and Spalling Data

Beam Designation	Load, Percentage of Maximum		
	First Flexural Cracking	First Visible Diagonal Cracking	Concrete Spalling
5-0-1	14	39	95
5-2-2	12	34	100
5-3-3	23	38	100
4-0-1	12	32	92
4-2-2	16	64	100
4-3-1	25	74	100
3-0-1	15	52	100
3-2-1	13	59	100
3-3-2	22	81	100

Note: These values were taken from motion pictures of the tests.

FLEXURAL BEHAVIOR

The agreement between calculated and measured behavior prior to cracking of the concrete was good. The agreement from cracking to maximum load resistance of the beams is summarized in table 8. Comparisons are made for yield and maximum loads and for deflections at yield and maximum loads. Load agreement was good. Comparisons ranged from -3 to 9 percent for yield load and from -7 to 9 percent for maximum loads, with an average in both cases of 3 percent. The deflection agreement was not as good as the load agreement (generally the case in reinforced concrete investigations). All measured yield deflections were higher than those calculated; this indicated that the beams were not as stiff as predicted. Yield deflection ratios varied from 10 to 36 percent, with an average of 24 percent. Deflection agreement at maximum load was much more erratic than the yield deflection agreement; even though the average was -2 percent, the ratios ranged from -21 to 44 percent.

Deflections at collapse or the actual collapse load could not be compared since the theoretical calculations did not include a criterion for this phenomenon. The calculations were arbitrarily continued to a compression strain at the top of the beam of 0.05 in/in. The actual collapse behavior of a beam is related to the stiffness of the testing apparatus and the energy released into the crushing portion of the beam. Therefore, collapse behavior in this experimental configuration would not be applicable to prototype behavior under real loads.

A comparison of the tensile steel strain data for the various beams (appendix A) shows that the agreement between calculated and measured strain became worse with distance from the load point. This indicates that bond failure or slip between the end of the beam and the load point is at least partially the reason why the actual deflections prior to yield were greater than the calculated deflections.

Table 8. Summary of Calculated and Measured Load and Centerline Deflection Data

Beam Designation	f'_c, psi	Load Ratio (K = P/F)	Calculated				Measured				Comparison - Measured/Calculated			
			Yield Load, kips	Maximum Load, kips	Yield Deflection, in	Deflection at Maximum Load, in	Yield Load, kips	Maximum Load, kips	Yield Deflection, in	Deflection at Maximum Load, in	Yield Load	Maximum Load	Yield Deflection	Deflection at Maximum Load
5-0-1	5014	0	27.5	36.5	0.52	2.22	28.8	38.0	0.65	2.00	1.05	1.04	1.25	0.90
5-0-2	4980	0	27.5	36.8	0.52	2.22	29.4	34.8	0.62	1.75	1.07	0.95	1.19	0.79
5-2-1	4336	1.91	32.5	35.8	0.60	1.40	33.0	37.2	0.70	1.20	1.04	1.04	1.17	0.86
5-2-2	4651	1.88	32.5	36.5	0.55	1.50	34.5	39.2	0.75	1.40	1.06	1.07	1.36	0.93
5-3-2	4753	3.10	35.8	38.3	0.60	1.20	38.8	43.4	0.75	1.35	1.08	1.13	1.25	1.13
5-3-3	5583	3.21	36.8	40.8	0.55	1.30	37.3	41.4	0.65	1.30	1.01	1.01	1.18	1.00
4-0-1	5288	0	33.8	46.0	0.58	3.02	35.0	44.1	0.70	2.50	1.04	0.96	1.21	0.83
4-2-1	5205	1.97	42.3	47.5	0.62	1.80	42.5	46.7	0.80	1.60	1.00	0.98	1.29	0.89
4-2-2	4990	1.88	41.5	46.3	0.64	1.80	42.8	47.6	0.87	1.50	1.03	1.03	1.36	0.83
4-3-1	5205	3.18	48.0	50.0	0.68	1.30	47.5	51.3	0.75	1.20	0.99	1.03	1.10	0.92
4-3-2	5423	3.15	48.0	50.5	0.65	1.40	47.5	55.2	0.78	1.50	0.99	1.09	1.20	1.07
3-0-1	5142	0	43.0	60.0	0.61	3.55	45.0	56.0	0.80	3.30	1.05	0.93	1.31	0.93
3-2-1	4792	1.85	57.5	60.5	0.72	1.72	60.0	66.0	0.90	1.90	1.04	1.09	1.25	1.10
3-2-2	4831	1.87	57.5	61.3	0.72	1.80	57.5	62.5	0.90	1.60	1.00	1.02	1.25	0.89
3-3-1	5252	3.03	67.5	68.0	0.78	1.25	72.0	74.0	1.00	1.20	1.07	1.09	1.28	0.96
3-3-2	5028	3.08	67.5	67.8	0.80	1.10	67.5	72.0	0.90	1.30	1.00	1.06	1.13	1.18
3-3-3	4344	3.11	65.0	65.0	0.82	0.90	63.0	65.2	1.00	1.30	0.97	1.00	1.22	1.44
									Average		1.03	1.03	1.24	0.98
									Standard Deviation		0.033	0.055	0.072	0.163

DUCTILITY

A common way to express the ductility of reinforced concrete beams is to compare deflection of the beam at first yielding of the tensile steel, Δ_{yield}, to the deflection at maximum load, Δ_{ML}. Table 9 presents both calculated and measured ductility ratios ($\mu = \Delta_{ML}/\Delta_{yield}$) and measured collapse ductility ratios ($\mu' = \Delta_{collapse}/\Delta_{yield}$) where $\Delta_{collapse}$ is the deflection of the beam at collapse. The ductility ratios decreased as the axial load increased. This occurs because the higher axial stress in the compression zone of the beam causes failure of the concrete prior to a significant amount of tensile steel yielding and accompanying deflection.

HINGE FORMATION

Normally, hinge formation is associated with beam behavior after yielding of the tensile reinforcement and before crushing of the concrete. Beams subjected to a single concentrated load or fixed-end beams display very pronounced hinge formations at the concentrated load or at the fixed ends. In these cases the hinge is concentrated at the maximum moment point and is confined to a finite length of the beam because of the moment gradient. In this investigation, because of the two-point loading, which results in a constant-moment region, this type of hinging was not experienced, even though there was a small moment gradient in some of the beams because of the P-Δ effect. There was instead a general yielding of the tensile reinforcement along the constant-moment region. However, a secondary hinge formed in the constant-moment region. This hinge was formed when the concrete, at some point, became stressed beyond its maximum load-carrying capacity and entered the strain-softening region. At this point, the load-carrying capacity of the beam began to decrease. Thereafter, the strain at the secondary hinge point continued to increase, while the strain in the remainder of the beam decreased. The farther the beam deflected, the more concentrated the hinge became. Final collapse of the beams occurred when the secondary hinge region could accommodate no more rotation and almost completely disintegrated. Usually a diagonal crack formed across the hinge region simultaneously with the collapse of the beam.

Table 9. Summary of Beam Ductility Data

Beam Designation	Calculated			Measured				
	Yield Deflection, in	Deflection at Maximum Load, in	Ductility Ratio (μ)	Yield Deflection, in	Deflection at Maximum Load, in	Deflection at Collapse, in	Ductility Ratio (μ)	Collapse Ductility Ratio (μ')
5-0-1	0.52	2.22	4.27	0.65	2.00	5.00	3.08	7.69
5-0-2	0.52	2.22	4.27	0.62	1.75	5.50	2.82	8.87
5-2-1	0.60	1.40	2.33	0.70	1.20	2.75	1.71	3.93
5-2-2	0.55	1.50	2.73	0.75	1.40	4.00	1.87	5.33
5-3-2	0.60	1.20	2.00	0.75	1.35	5.00	1.80	6.67
5-3-3	0.55	1.30	2.36	0.65	1.30	2.50	2.00	3.85
4-0-1	0.58	3.02	5.21	0.70	2.50	4.80	3.57	6.86
4-2-1	0.62	1.80	2.90	0.80	1.60	4.00	2.00	5.00
4-2-2	0.64	1.80	2.81	0.87	1.50	3.00	1.72	3.45
4-3-1	0.68	1.30	1.91	0.75	1.20	4.00	1.60	5.33
4-3-2	0.65	1.40	2.15	0.78	1.50	3.20	1.92	4.10
3-0-1	0.61	3.55	5.82	0.80	3.30	4.80	4.13	6.00
3-2-1	0.72	1.72	2.39	0.90	1.90	2.40	2.11	2.66
3-2-2	0.72	1.80	2.50	0.90	1.60	4.00	1.78	4.44
3-3-1	0.78	1.25	1.60	1.00	1.20	1.50	1.20	1.50
3-3-2	0.80	1.10	1.38	0.90	1.30	1.30	1.44	1.44
3-3-3	0.82	0.90	1.10	1.00	1.30	2.40	1.30	2.40

INTERACTION

Interaction between axial load and bending moment was demonstrated by a comparison of beam behavior as the axial load was increased and also by an interaction diagram of axial load versus applied moment for both calculated and measured behavior. Figure 18 presents both measured and calculated centerline deflection versus total lateral load for each series of beam tests. The increase in maximum load and the decrease in ductility with increased axial load are evident. Also, the variation in behavior with a variation in concrete strength is demonstrated. Table 10 presents a summary of interaction data at maximum load for all beams. These data are plotted on the theoretical interaction diagram (fig. 19), which was derived with the analytical model developed in section 4.

ANALYTICAL MODEL

In evaluating the results of this investigation, some areas of possible error in the calculated beam behavior should be considered. The method used to calculate the beam behavior involved replacing a continuous structure with an assemblage of discrete elements connected at nodes. Thus, the resulting calculated beam response is an approximation of the actual behavior. The accuracy of this approximation depends on the element size and the mathematical representation of the material characteristics of the beam. Also, in calculating the nodal rotations and deflections, the distribution of curvature between nodes was assumed to be linear. Because of the nonlinear moment-curvature relationship, a higher-order assumption would result in less error.

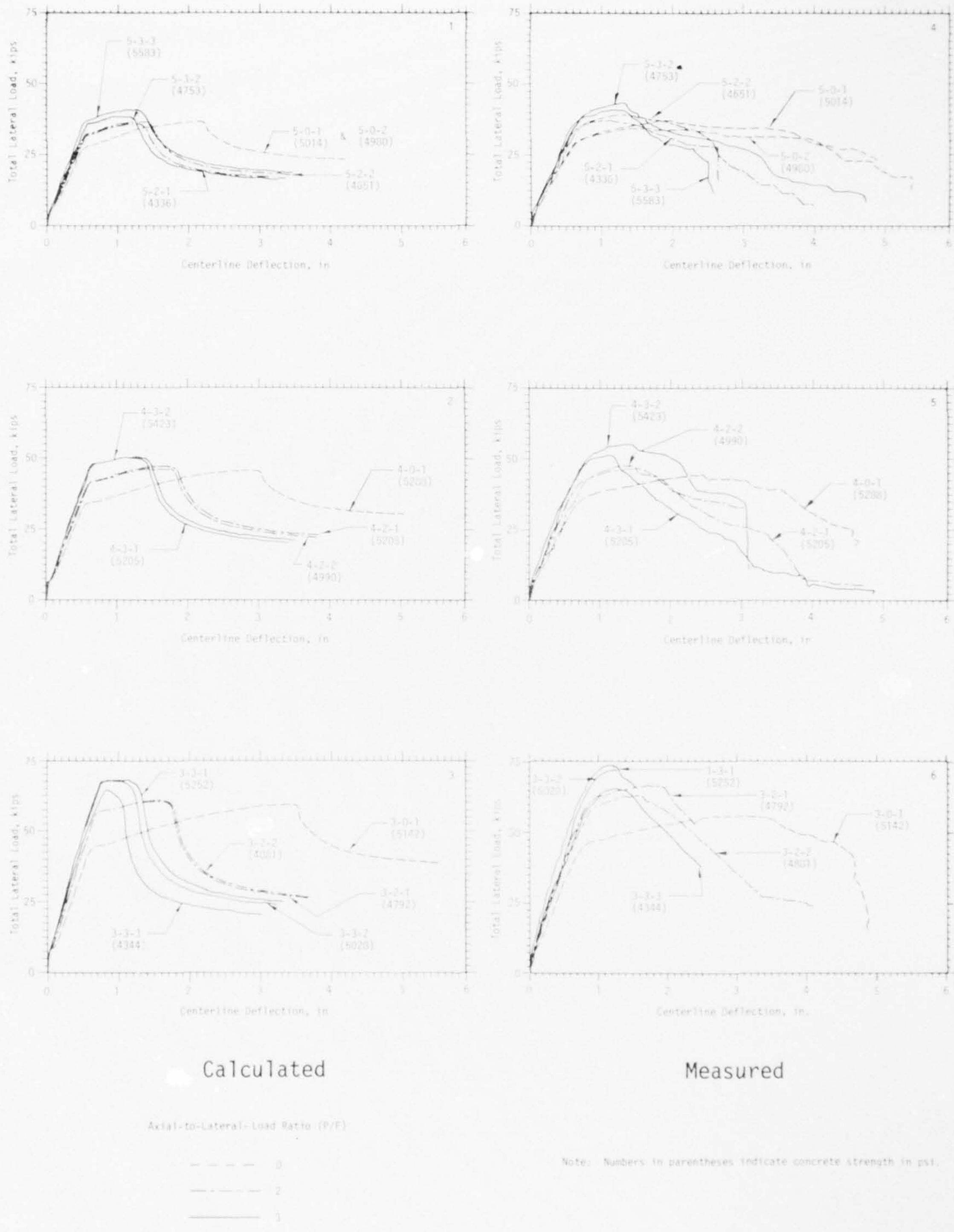

Figure 18. Calculated and Measured Load-Centerline Deflection Curves

Table 10. Interaction Data at Maximum Load

Beam Designation	f'_c, psi	Shear Span (a_s), in	Load Ratio ($K = P/F$)	Total Lateral Load (2F), kips	Centerline Deflection at Maximum Load (Δ), in	Axial Load ($P = K \cdot F$), kips	Lateral Load Moment ($M_1 = F \cdot a_s$), in-kips	P - Δ Moment ($M_2 = P \cdot \Delta$), in-kips	Total Moment ($M = M_1 + M_2$), in-kips
5-0-1	5014	63.125	0	38.0	2.00	0	1199.38	0	1199.38
5-0-2	4980	63.125	0	34.8	1.75	0	1098.38	0	1098.38
5-2-1	4336	63.125	1.91	37.2	1.20	35.60	1174.13	42.72	1216.85
5-2-2	4651	63.125	1.88	39.2	1.40	36.87	1237.25	51.62	1288.87
5-3-2	4753	63.125	3.10	43.4	1.35	67.37	1369.81	90.94	1460.75
5-3-3	5583	63.125	3.21	41.4	1.30	66.45	1306.69	86.39	1398.08
4-0-1	5288	51.125	0	44.1	2.50	0	1127.31	0	1127.31
4-2-1	5205	51.125	1.97	46.7	1.60	45.93	1193.77	73.49	1267.26
4-2-2	4990	51.125	1.88	47.6	1.50	44.70	1216.78	67.05	1283.83
4-3-1	5205	51.125	3.18	51.3	1.20	81.52	1311.36	97.82	1409.18
4-3-2	5423	51.125	3.15	55.2	1.50	87.02	1411.05	130.53	1541.58
3-0-1	5142	39.125	0	56.0	3.30	0	1095.50	0	1095.50
3-2-1	4792	39.125	1.85	66.0	1.90	61.15	1291.13	116.19	1407.32
3-2-2	4881	39.125	1.87	62.5	1.60	58.34	1222.66	93.34	1316.00
3-3-1	5252	39.125	3.03	74.0	1.20	111.93	1447.63	134.32	1581.95
3-3-2	5028	39.125	3.08	72.0	1.30	110.88	1408.50	144.14	1552.64
3-3-3	4344	39.125	3.11	65.2	1.30	101.42	1275.48	131.85	1407.33

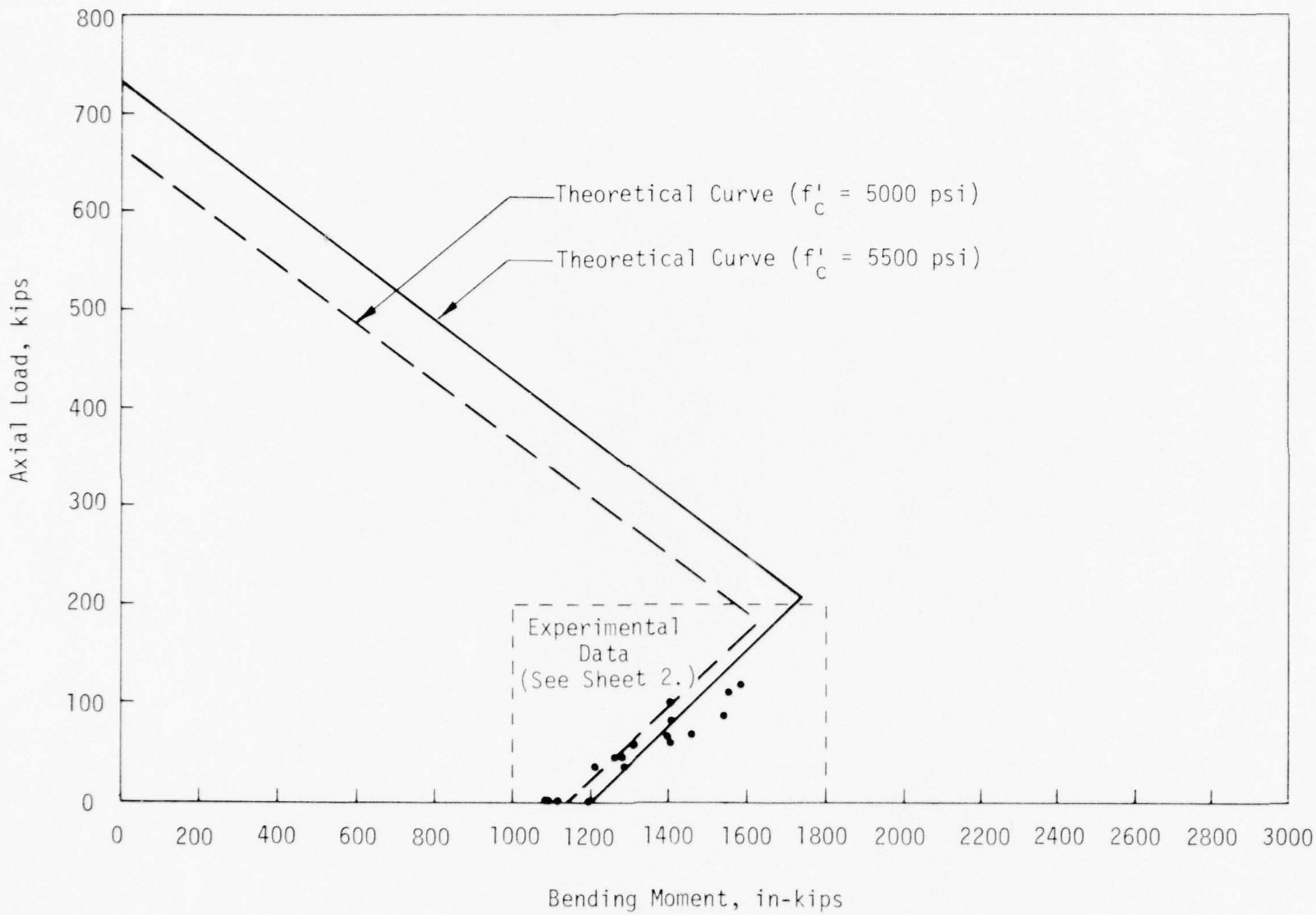

Figure 19. Axial Load-Bending Moment Interaction Diagram for Maximum Load (1 of 2)

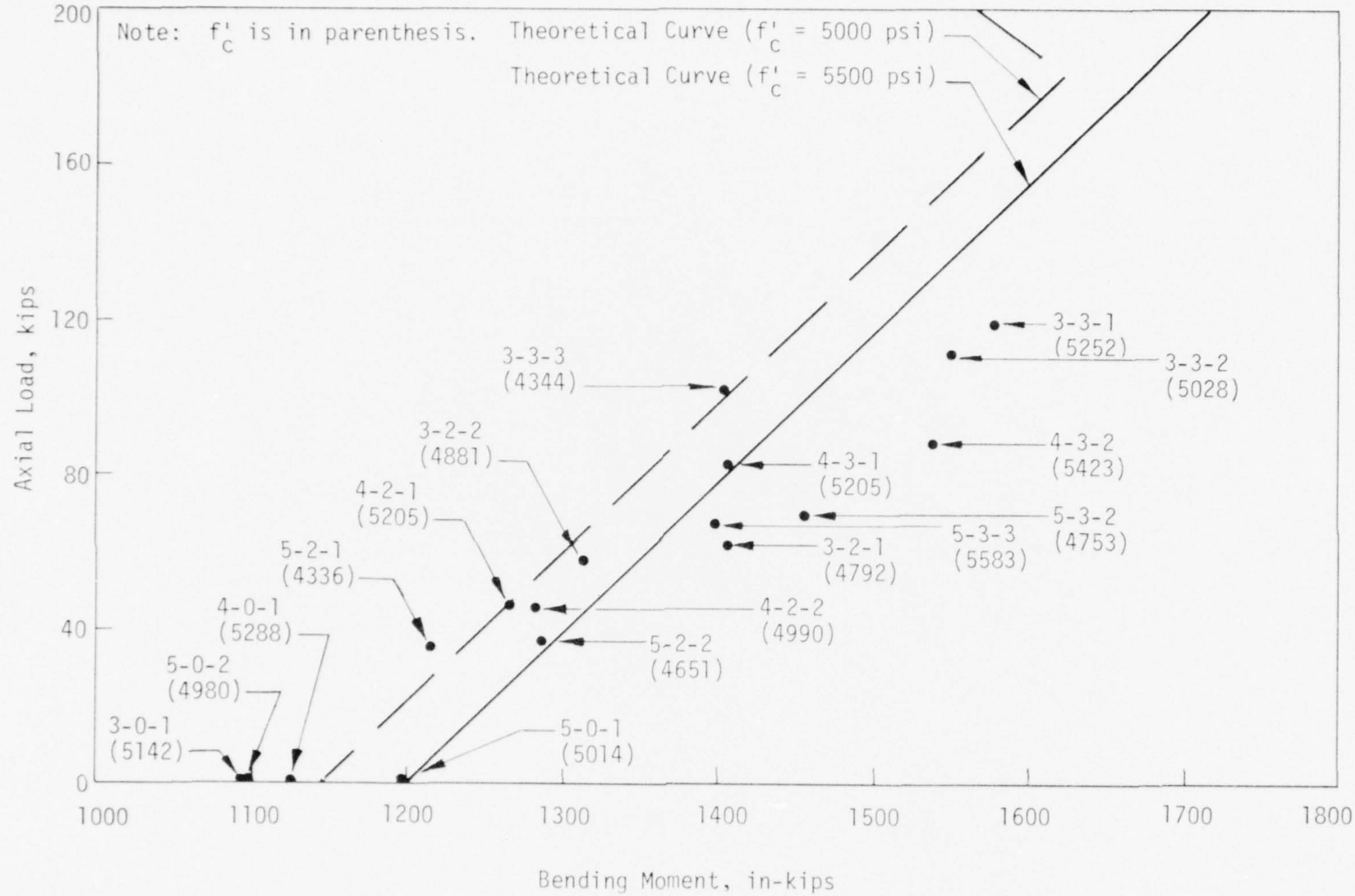

Figure 19. Axial Load-Bending Moment Interaction Diagram for Maximum Load (2 of 2)

SECTION VI
CONCLUSIONS AND RECOMMENDATIONS

CONCLUSIONS

One of the main objectives of this investigation was to study the static behavior of reinforced concrete beams under combined flexural, axial, and shear effects. However, none of the beams failed in shear and, therefore, no real data on shear interaction or transition of failure modes under the combined effects were obtained. The investigation did provide good information on ductility and behavior of beams in the large deflection region.

In general, the procedures and methods employed in this investigation for beam specimen fabrication, testing, and experimental data acquisition were carefully controlled in order to produce the best results possible. Each size of reinforcement was controled by using bars from the same heat. The concrete, however, varied in compressive strength between -13 and 12 percent from the nominal 5000 psi. Although load application techniques and control were kept as constant as possible for all tests, the total time of each test varied from 2 to 12 minutes (2 minutes is not short enough to cause dynamic effects and 12 minutes is not long enough to involve creep). But, a more constant test time would have been more desirable.

Most of the instrumentation and the data-acquisition techniques used produced satisfactory results. There were some exceptions, however. The data from the strain gages mounted on stirrups that were expected to be in the region of diagonal tension shear cracks were very erratic and of very little value in determining beam response. Another measurement that provided very little insight into beam behavior was the horizontal measurement made between stations. The most notable data-acquisition method that did not provide satisfactory results was the photoelastic coating. This coating was applied to obtain data on hinge formation in the constant-moment region of the beams. However, the nonhomogeneity of the concrete caused irregular and erratic fringe patterns and, consequently, no useful data were obtained. Also, near maximum load, the concrete began to spall,

causing the coating to debond. The one positive aspect of using the photoelastic material was the slow-speed motion pictures that provided good visual documentation of the sequence of events in the response of the beams.

The general beam behavior calculated from the analytical model agreed well with the measured results, especially in the region up to maximum load. The measured beam stiffness (the slope of the load-deflection curve between first concrete cracking and yielding of the tensile reinforcement) was always less than that predicted; this seemed to be the result of bond slip or failure between the rebar and the concrete. (This was not considered in the analytical model.) The yield and maximum loads predicted by the model were within 9 percent of the test results. Deflection calculations were not as good as load calculations. Calculated yield deflections were all lower (10 to 36 percent) than those predicted. Comparison of calculated and measured deflections at maximum load showed very erratic differences. The ratio of measured to calculated deflections ranged from -21 to 44 percent.

The analytical model did not calculate the collapse point of the beams; it calculated the behavior to an arbitrary compression strain (0.05 in/in) at the top of the beam. Therefore, no comparison could be made of collapse behavior; however, beyond maximum load, the general behavior predicted by the model was good.

RECOMMENDATIONS

Since the objective of this investigation was to study beam behavior to beam collapse under combined flexural, axial, and shear forces and since the mode of failure for all test beams was flexural tension, it is recommended that another group of beams without stirrups be tested under the same general loading conditions. This would provide information on the transition from a flexural tension mode of failure to a shear mode.

It is further recommended that another group of beams be tested with axial-to-lateral-load ratios high enough to provide data above the balance point on the axial load-bending moment interaction diagram. This group should include beams with and without stirrups in order to provide shear-interaction data.

Further work with the behavioral model is suggested. There are three obvious areas not considered in the present model: (1) bond behavior between the reinforcing steel and the concrete, (2) calculations of beam shear strength, and (3) calculation of the point of collapse of the beam.

REFERENCES

1. Koenen, M., "Für die Berechnung der Stärke der Monierschen Zementplatten," *Zentralblatt der Bauverwaltung*, Vol. 6, No. 47, November 1886, p. 462.

2. Hognestad, E., *A Study of Combined Bending and Axial Load in Reinforced Concrete Members*, University of Illinois Engineering Experiment Station, Bulletin No. 399, November 1951, 128 pp.

3. Neumann, P., "Ueber die Berechnung der Monier-Constructionen," *Wochenschrift des Oesterr. Ing. und Arch. Vereines*, Vol. 15, No. 22, May 1890, pp. 209-212.

4. Coignet, E., and Tedesco, N. de, "Du calcu des ouvrages en ciment avec ossature métallique," *Mémoires de la société des ingénieurs civils de France*, 1894 I, pp. 282-363.

5. Johnson, J. B., "Strength of Concrete and Steel in Combination," *Engineering News and American Railway Journal*, Vol. 33, No. 1, January 1895, pp. 10-11.

6. Ostenfeld, A., "Einige Folgerungen aus den Sanders'schen Belastungsversuchen," *Beton und Eisen*, Vol. 1, No. 5, October 1902, pp. 19-22.

7. Thullie, R. M. v., "Ueber die Berechnung der Monierplatten," *Zeitschrift des Oesterr. Ing. und Arch. Vereins*, Vol. 49, No. 13, March 1897, pp. 193-197.

8. Ritter, W., "Die Bauweise Hennebique," *Schweizerische Bauzeitung*, Vol. 33, Nos. 5, 6, and 7, February 1899, pp. 41-43, 49-52, 59-61.

9. Talbot, A. N., *Tests of Reinforced Concrete Beams*, University of Illinois Engineering Experiment Station Bulletin No. 1, September 1904, 64 pp.

10. Talbot, A. N., *Tests of Reinforced Concrete Beams Series of 1905*, University of Illinois Engineering Experiment Station Bulletin No. 4, April 1906, 84 pp.

11. Emperger, F. v., *Handbuch für Eisenbetonbau, Vol. I: Entwicklungsgeschichte und Theorie des Eisenbetons*, Wilhelm Ernst und Sohn, Berlin, 1908.

12. Suenson, E., "Jaernprocentens Indflydelse paa Jaernbetonpladers Baereevne," *Ingenøiren*, Copenhagen, Vol. 21, No. 72, September 1921, p. 568.

13. Mensch, L. J., "New-Old Theory of Reinforced Concrete Beams in Bending," *ACI Journal*, Vol. 2, No. 7, December 1914, pp. 28-41.

14. Kempton Dyson, H., "What is the use of the Modular Ratio?" *Concrete and Constructional Engineering*, Vol. 17, Nos. 5, 6, and 7, London, May-July 1922, pp. 330-336, 408-415, 486-491.

15. Slater, W. A., and Zipprodt, R. R., "Compressive Strength of Concrete in Flexure," *Proceedings ACI*, Vol. 16, 1920, pp. 120-151.

16. Slater, W. A., and Lyse, I., "Compressive Strength in Flexure as Determined from Tests of Reinforced Beams," *Proceedings ACI*, Vol. 26, 1930, pp. 831-874.

17. Maney, G.A., *Studies in Engineering No. 1*, University of Minnesota Press, 1915.

18. Cross, Hardy, "Analysis of Continuous Frames by Distributing Fixed-End Moments," *Trans. Am. Soc. Civil Engineers*, 96, 1932, pp. 1-10.

19. McMillan, F. R., "A Study of Column Test Data," *Proceedings ACI*, Vol. 17, 1921, pp. 150-171.

20. Richart, F. E., and Brown, R. L., *An Investigation of Reinforced Concrete Columns*, University of Illinois Engineering Station Bulletin No. 267, June 1934, 91 pp.

21. Emperger, F. v., "Der Beiwert n = 15 und die zulässigen Biegungs-Spannungen," *Beton und Eisen*, Vol. 30, No. 19, October 1931, pp. 340-346.

22. Stüssi, F., "Ueber die Sicherheit des einfach bewehrten Eisenbeton-Rechteckbalkens," *Publications, International Association for Bridge and Structural Engineering*, Vol. 1, Zürich, April 1932, pp. 487-495.

23. Schreyer, C., "Elastizität und Festigkeit des Betons auf Grund von Würfelversuchen und relativen Spannungen," *Beton und Eisen*, Vol. 32, Nos. 3 and 4, February 1933, pp. 42-49, 60.

24. Kazinczy, C. v., "Die Plastizität des Eisenbetons," *Beton und Eisen*, Vol. 32, No. 5, March 1933, pp. 74-80.

25. Gebauer, F., "Berechnung der Eisenbetonbalken unter Berücksichtigung der Schwindspannungen der Eisen," *Beton und Eisen*, Vol. 33, No. 9, May 1934, pp. 137-143.

26. Baumann, O., "Die Knickung der Eisenbeton-Säulen," *Eidg. Material-Prüfungsanstalt an der E. T. H. in Zürich, Bericht*, No. 89, December 1934, 56 pp.

27. Bittner, E., "Zur Klärung der n-Frage bei Eisenbetonbalken," *Beton und Eisen*, Vol. 34, No. 14, July 1935, pp. 226-228.

28. Bittner, E., "Die Berechnung der Eisenbetonbalken nach Zustand III," *Beton und Eisen*, Vol. 35, No. 9, May 1936, pp. 143-146.

29. Brandtzaeg, A., "Der Bruchspannungszustand und der Sicherheitsgrad von rechteckigen Eisenbetonquerschnitten unter Biegung oder aussermittigem Druck," *Norges Tekniske Høiskole, Avhandlinger til 25-arsjubileet*, 1935, pp. 667-764.

REFERENCES (Cont'd)

30. Brandtzaeg, A., "Die Bruchspannungen und die zulässigen Randspannungen in rechteckigen Eisenbetonbalken," *Beton und Eisen*, Vol. 35, No. 13, July 1936, pp. 219-222.

31. Brandtzaeg, A., "Zulässige Betondruckspannungen in rechteckigen Eisenbetonquerschnitten bei aussermittigem Druck," Final Report, Second Congress, *International Association for Bridge and Structural Engineering*, Berlin-Munich, October 1936, pp. 121-135.

32. Brandtzaeg, A., "Forelesninger i jernbetong ved Norges tekniske høiskole," *Tapirs forlag*, Trondheim, Norway, 1937.

33. Emperger, F. v., "Der Beiwert n," *Beton und Eisen*, Vol. 35, No. 19, October 1936, pp. 324-332.

34. Saliger, R., "Bruchzustand und Sicherheit im Eisenbetonbalken," *Beton und Eisen*, Vol. 35, Nos. 19 and 20, October 1936, pp. 317-320 and 339-346.

35. Whitney, C. S., "Design of Reinforced Concrete Members Under Flexure and Combined Flexure and Direct Compression," *ACI Journal*, Vol. 33, March-April 1937, pp. 483-498.

36. Whitney, C. S., "Eccentrically Loaded Reinforced Concrete Columns," *Concrete and Constructional Engineering*, Vol. 33, No. 11, November 1938, pp. 549-561.

37. Whitney, C. S., "Plastic Theory in Reinforced Concrete Design," *Proceedings ASCE*, December 1940; *Transactions ASCE*, Vol. 107, 1942, pp. 251-326.

38. Whitney, C. S., "Application of Plastic Theory to the Design of Modern Reinforced Concrete Structures," *Journal of the Boston Society of Civil Engineers*, Vol. 35, No. 1, January 1948, pp. 30-53.

39. Cox, K. C., "Tests of Reinforced Concrete Beams with Recommendations for Attaining Balanced Design," *ACI Journal*, September 1941; *Proceedings*, Vol. 38, pp. 65-80.

40. Jensen, V. P., "The Plasticity Ratio of Concrete and its Effect on the Ultimate Strength of Beams," *ACI Journal*, June 1943; *Proceedings*, Vol. 39, pp. 565-582.

41. Jensen, V. P., *Ultimate Strength of Reinforced Concrete Beams as Related to the Plasticity Ratio of Concrete*, University of Illinois Engineering Experiment Station Bulletin No. 345, June 1943, 60 pp.

42. "Report of ASCE-ACI Joint Committee on Ultimate Strength Design," *Proceedings ASCE*, Vol. 81, Paper No. 809, October 1955, 68 pp.

43. "Building Code Requirements for Reinforced Concrete (ACI 318-56)," *ACI Journal*, May 1956, *Proceedings*, Vol. 52, pp. 913-986.

44. Hognestad, E., "Confirmation of Inelastic Stress Distribution in Concrete," *Proceedings ASCE*, Vol. 83, Paper No. 1189, March 1957, 17 pp.

45. Mattock, A. H., Kriz, L. B., and Hognestad, E., "Rectangular Concrete Stress Distribution in Ultimate Strength Design," *ACI Journal, Proceedings*, Vol. 57, No. 8, February 1961, pp. 875-928. Also *Development Department Bulletin D-49*, Portland Cement Association, Skoke, Illinois.

46. *Building Code Requirements for Reinforced Concrete, ACI (318-63)*, American Concrete Institute, Detroit, Michigan, 1963.

47. "Flexural Mechanics of Reinforced Concrete," *Proceedings of the International Symposium*, November 10-12, 1964, Miami, Florida, 1965.

48. Mattock, A. H., "Rotational Capacity of Hinging Regions in Reinforced Concrete Beams," *Proceedings, International Symposium on Flexural Mechanics of Reinforced Concrete*, Miami, Florida, November 1964, ACI Special Publication SP-12, pp. 143-182.

49. Roy, H. E. H., and Sozen, M. A., "Ductility of Concrete," *Proceedings, International Symposium on the Flexural Mechanics of Reinforced Concrete*, Miami, Florida, November 1964, ACI Special Publication SP-12, pp. 213-236.

50. Barnard, P. R., "The Collapse of Reinforced Concrete Beams," *Proceedings, International Symposium on Flexural Mechanics of Reinforced Concrete*, Miami, Florida, November 1964, ACI Special Publication SP-12, pp. 501-520.

51. Cohn, M. Z., "Limit Design for Reinforced Concrete Structures: An Annotated Bibliography," ACI Bibliography No. 8, American Concrete Institute, Detroit, Michigan, 1968.

52. Iqbal, M., and Hatcher, D., "Post-Crushing Behavior of Unbound Concrete Beams," *Journal of the Structural Division, ASCE*, Vol. 101, No. ST. 11, November 1975, pp. 2303-2316.

53. Crist, R. A., *Shear Behavior of Deep Reinforced Concrete Beams, Vol. II: Static Tests*, AFWL-TR-67-61, Kirtland Air Force Base, New Mexico October 1967.

54. Barnard, P. R., "Researches into the Complete Stress-Strain Curve for Concrete," *Magazine of Concrete Research*, Vol. 16, No. 49, December 1964, pp. 203-210.

55. Yamashiro, R., and Siess, C. P., "Moment-Rotation Characteristics of Reinforced Concrete Members Subjected to Bending, Shear and Axial Load," Civil Engineering Studies, *Structural Research Series No. 260*, University of Illinois, December 1962.

56. Kent, Dudley Charles, and Park, Robert, "Flexural Members with Confined Concrete," *Journal of the Structural Division, ASCE*, Vol. 97, No. ST7, Proc. Paper 8243, July 1971, pp. 1969-1990.

APPENDIX A

CALCULATED AND EXPERIMENTAL DATA

This appendix presents both experimental and analytical results of the behavior of the 17 beams tested. Where possible, the corresponding analytical and experimental data are presented on one graph for comparison.

Beam 5-0-1

f'_c 5014 psi

K = P/F 0

Test Date 4/26/73

Test Duration 12 min

Legend:

——— Experimental Results

– – – – Analytical Results

▼ Gage Failure

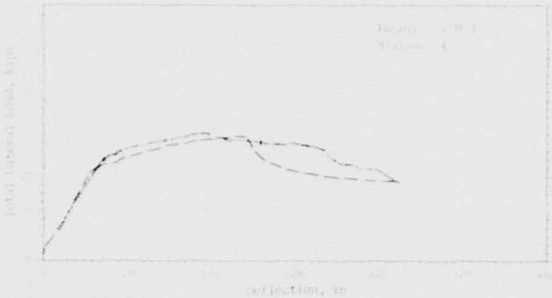

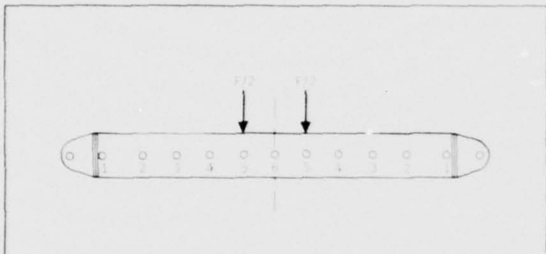

Loading Configuration and Station Location

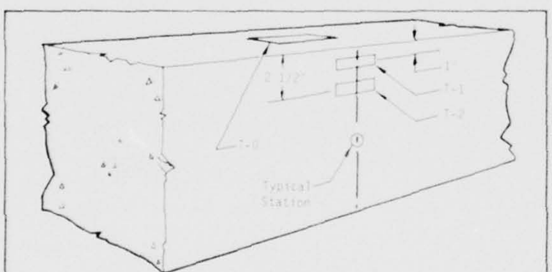

Concrete Strain Measurement Location

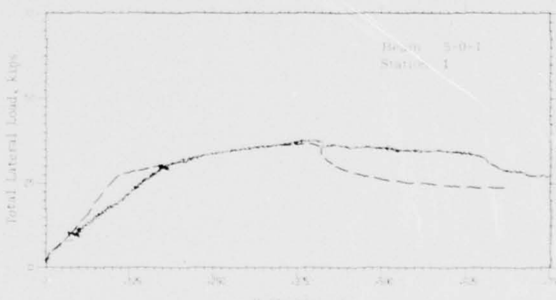

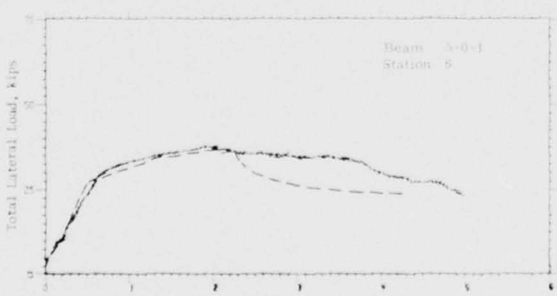

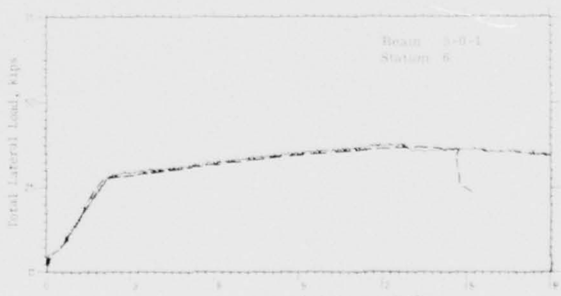

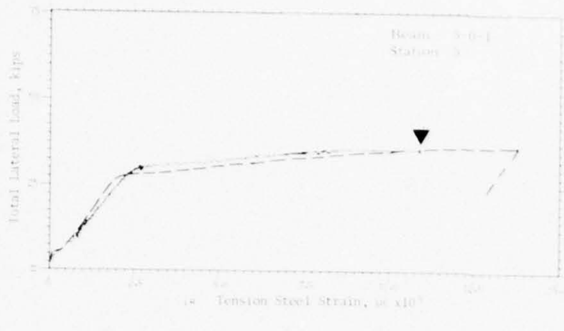
Beam 3-0-1
Station 5
Total Lateral Load, kips
Tension Steel Strain, με x10

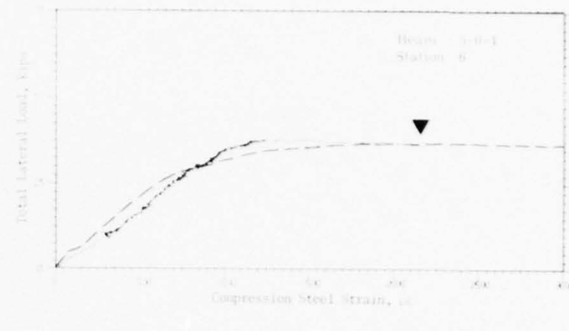
Beam 3-0-1
Station 6
Total Lateral Load, kips
Compression Steel Strain, με

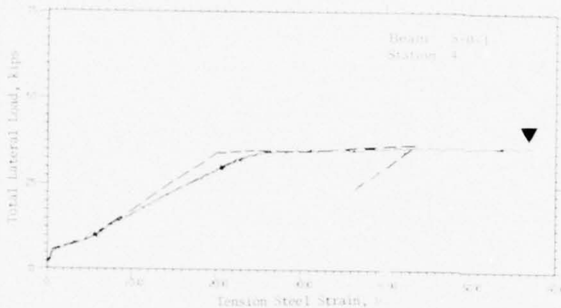
Beam 3-0-1
Station 4
Total Lateral Load, kips
Tension Steel Strain,

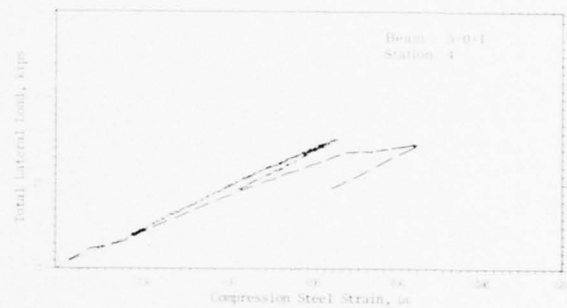
Beam 3-0-1
Station 4
Total Lateral Load, kips
Compression Steel Strain, με

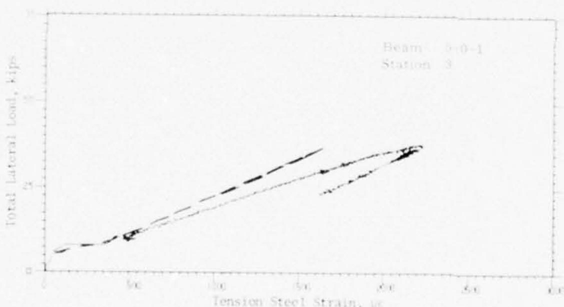
Beam 3-0-1
Station 3
Total Lateral Load, kips
Tension Steel Strain, με

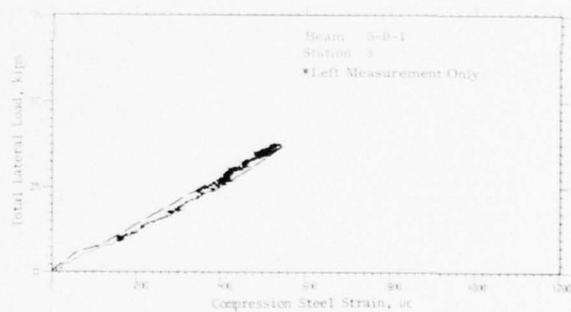
Beam 3-0-1
Station 3
*Left Measurement Only
Total Lateral Load, kips
Compression Steel Strain, με

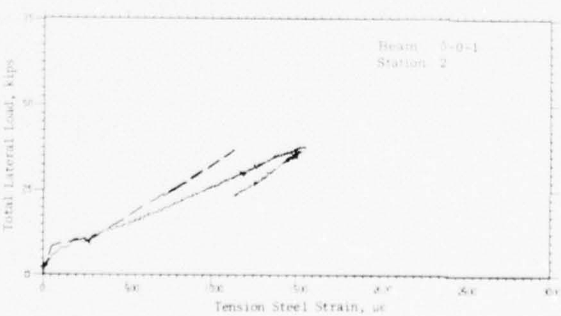
Beam 3-0-1
Station 2
Total Lateral Load, kips
Tension Steel Strain, με

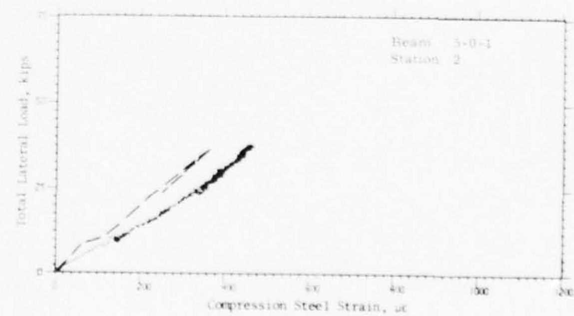
Beam 3-0-1
Station 2
Total Lateral Load, kips
Compression Steel Strain, με

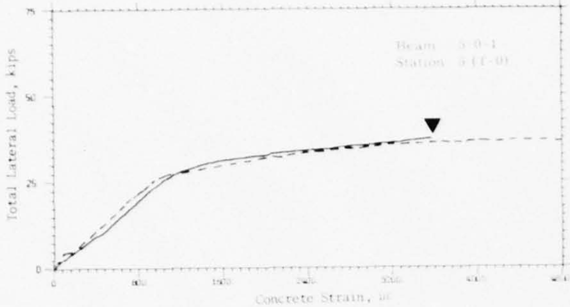
Beam 5-0-1
Total Lateral Load, kips
Concrete Strain, με

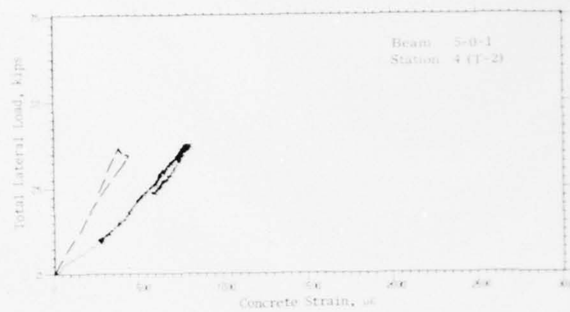
Beam 5-0-1
Station 4 (T-2)
Total Lateral Load, kips
Concrete Strain, με

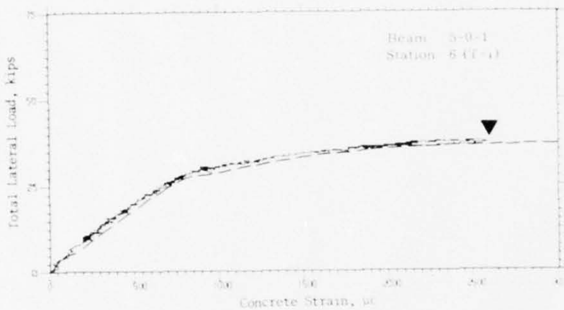
Beam 5-0-1
Total Lateral Load, kips
Concrete Strain, με

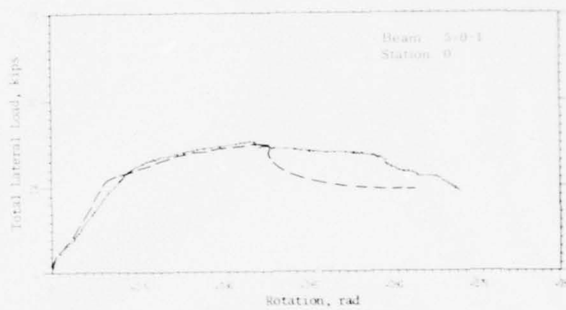
Beam 5-0-1
Station 0
Total Lateral Load, kips
Rotation, rad

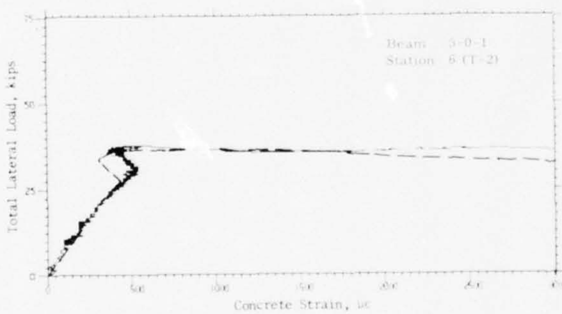
Beam 5-0-1
Station 6 (T-2)
Total Lateral Load, kips
Concrete Strain, με

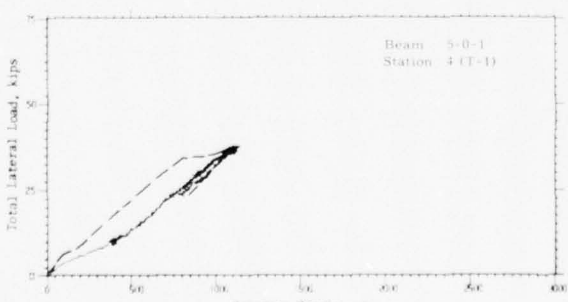
Beam 5-0-1
Station 4 (T-1)
Total Lateral Load, kips
Concrete Strain, με

Beam	5-0-2
f'_c	4980 psi
K = P/F	0
Test Date	6/7/73
Test Duration	2 min

Legend:

- ———— Experimental Results
- — — — — Analytical Results
- ▼ Gage Failure

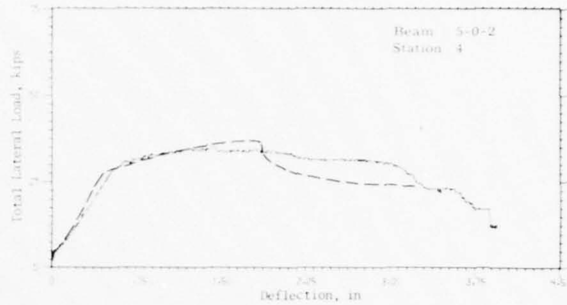

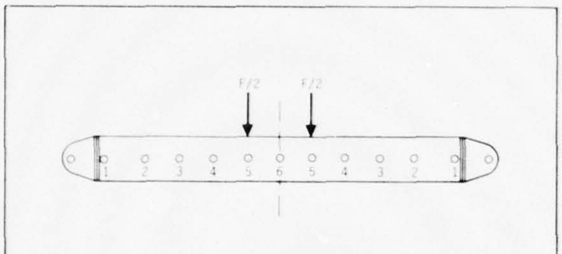

Loading Configuration and Station Location

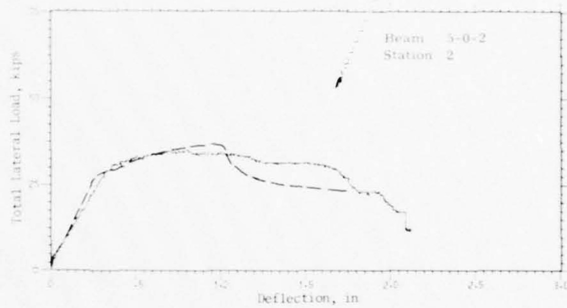

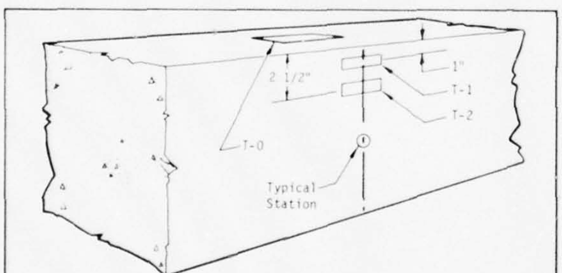

Concrete Strain Measurement Location

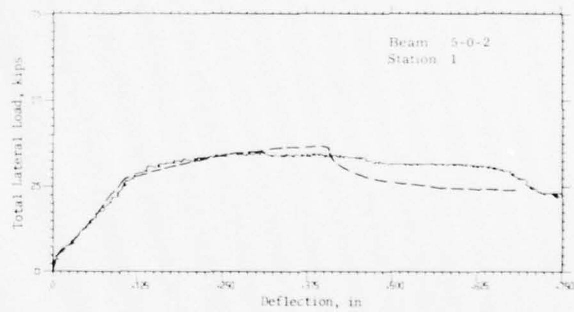

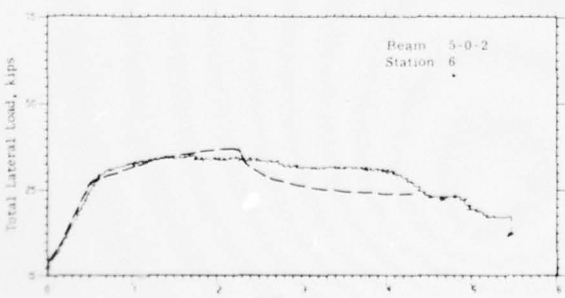

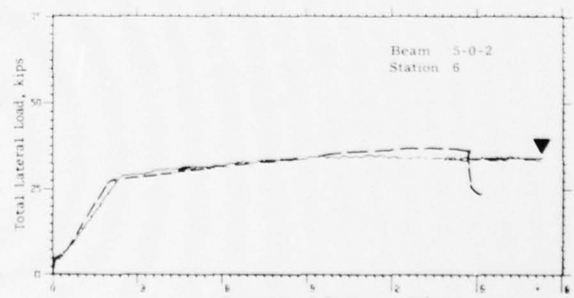

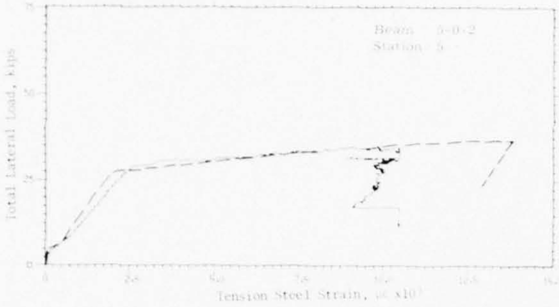
Beam 5-0-2
Station 5
Total Lateral Load, kips
Tension Steel Strain, με x10³

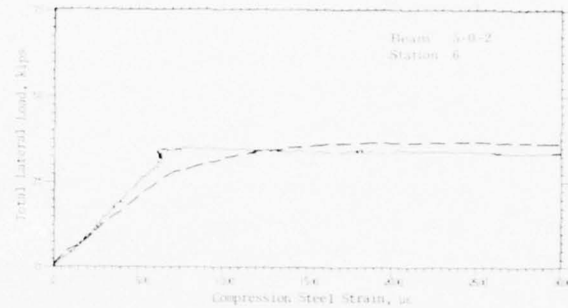
Beam 5-0-2
Station 6
Total Lateral Load, kips
Compression Steel Strain, με

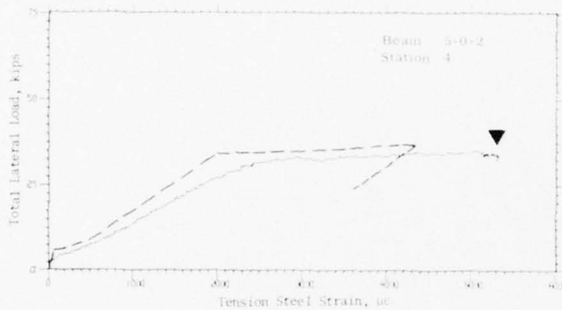
Beam 5-0-2
Station 4
Total Lateral Load, kips
Tension Steel Strain, με

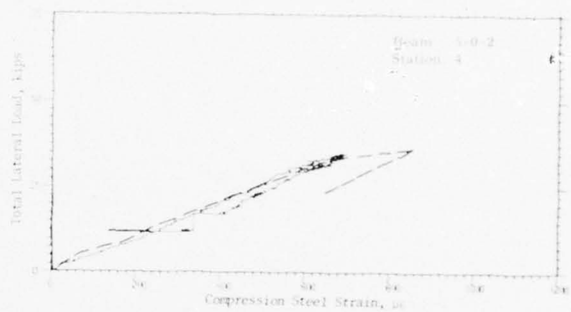
Beam 5-0-2
Station 4
Total Lateral Load, kips
Compression Steel Strain, με

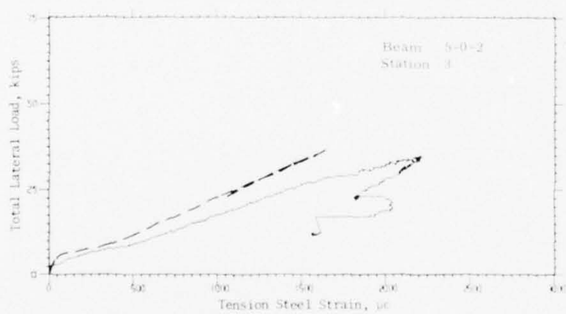
Beam 5-0-2
Station 3
Total Lateral Load, kips
Tension Steel Strain, με

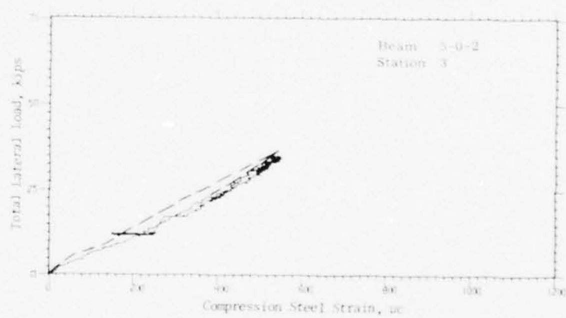
Beam 5-0-2
Station 3
Total Lateral Load, kips
Compression Steel Strain, με

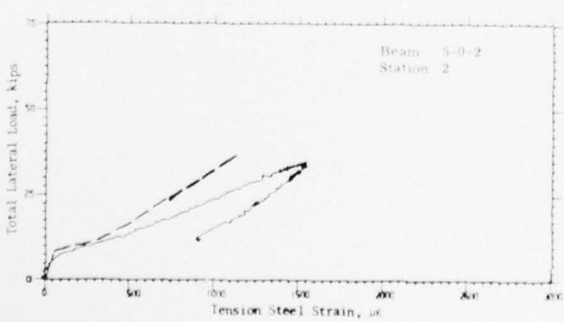
Beam 5-0-2
Station 2
Total Lateral Load, kips
Tension Steel Strain, με

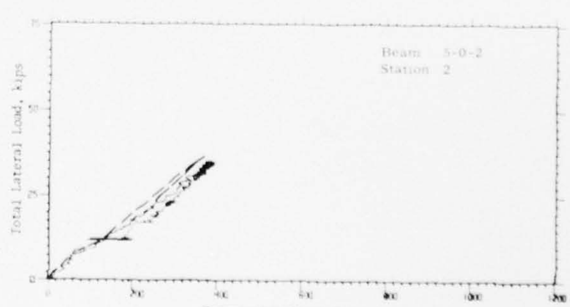
Beam 5-0-2
Station 2
Total Lateral Load, kips
Compression Steel Strain, με

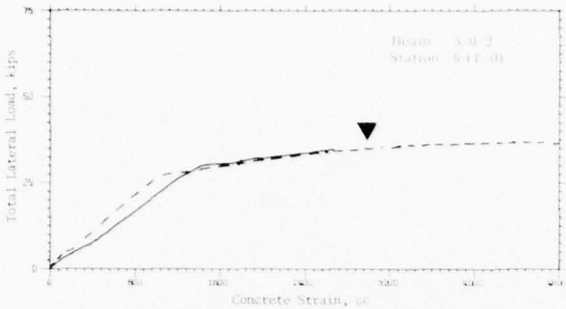

Beam 5-0-2
Station 6 (T-0)
Total Lateral Load, kips
Concrete Strain, με

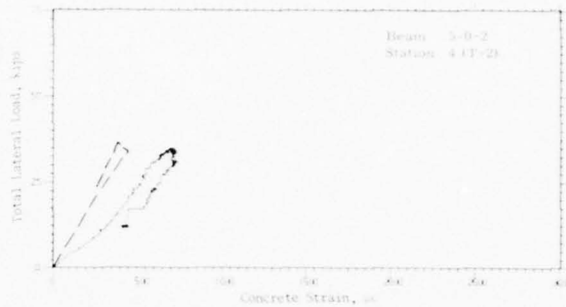

Beam 5-0-2
Station 4 (T-2)
Total Lateral Load, kips
Concrete Strain, με

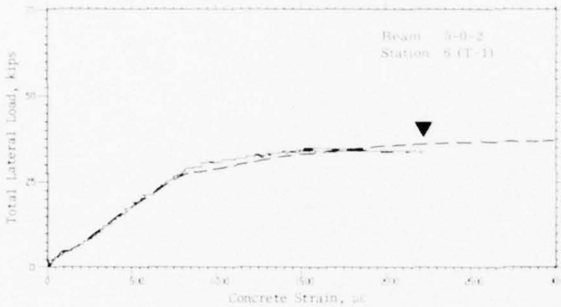

Beam 5-0-2
Station 6 (T-1)
Total Lateral Load, kips
Concrete Strain, με

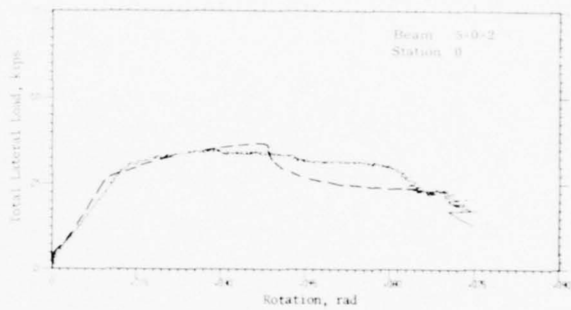

Beam 5-0-2
Station 0
Total Lateral Load, kips
Rotation, rad

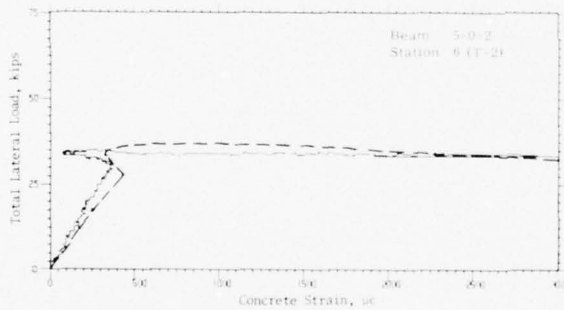

Beam 5-0-2
Station 6 (T-2)
Total Lateral Load, kips
Concrete Strain, με

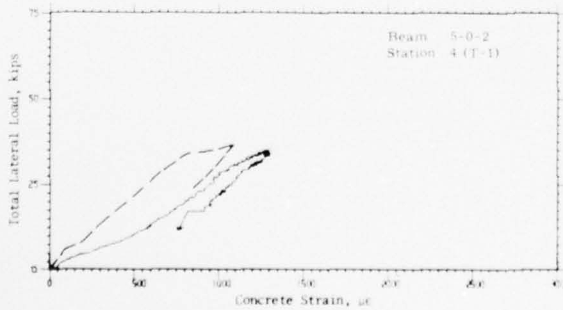

Beam 5-0-2
Station 4 (T-1)
Total Lateral Load, kips
Concrete Strain, με

Beam	5-2-1
f'_c	4336 psi
K = P/F	1.91
Test Date	4/19/73
Test Duration	9 min

Legend:

——————— Experimental Results

— — — — — Analytical Results

▼ Gage Failure

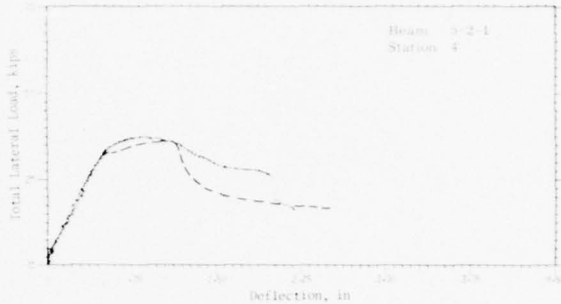

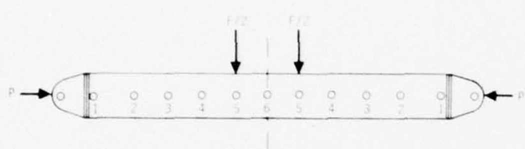

Loading Configuration
and Station Location

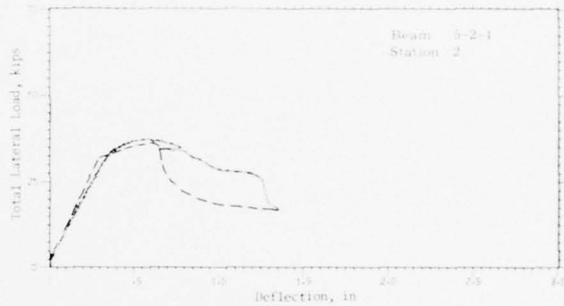

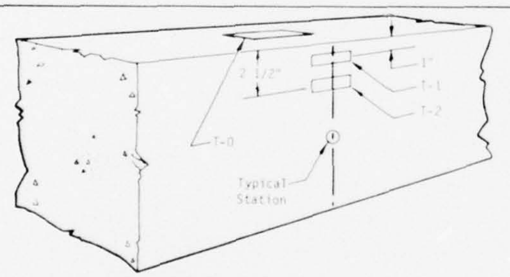

Concrete Strain Measurement Location

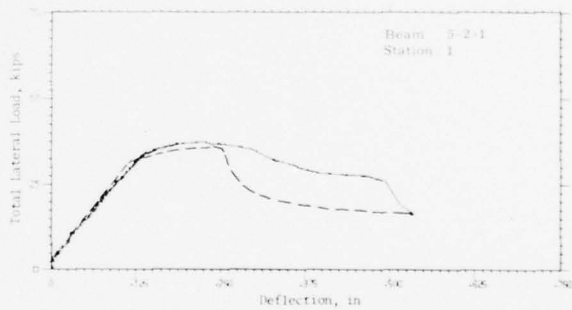

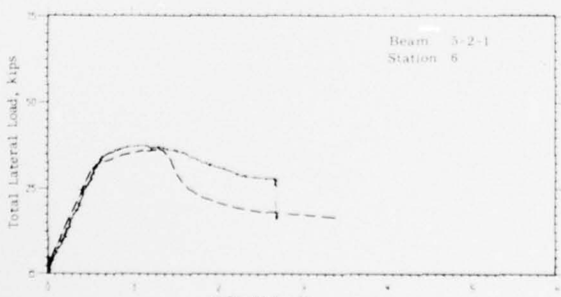

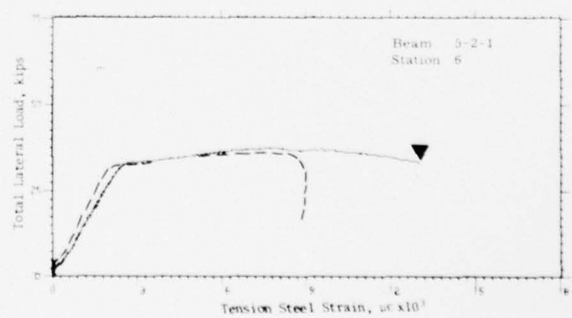

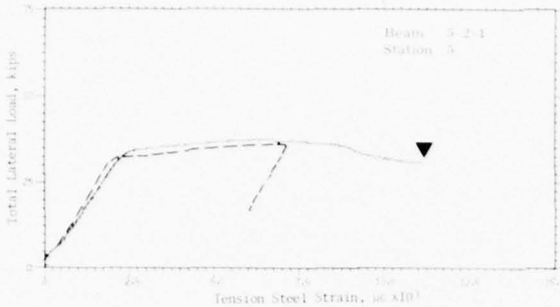
Beam 5-2-1
Station 5
Total Lateral Load, kips
Tension Steel Strain, με x10³

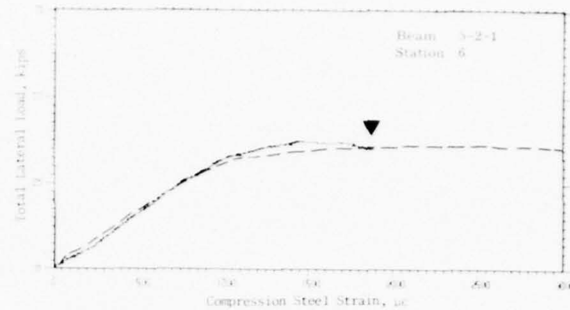
Beam 5-2-1
Station 6
Total Lateral Load, kips
Compression Steel Strain, με

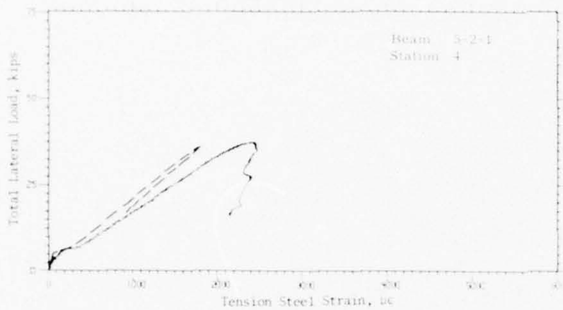
Beam 5-2-1
Station 4
Total Lateral Load, kips
Tension Steel Strain, με

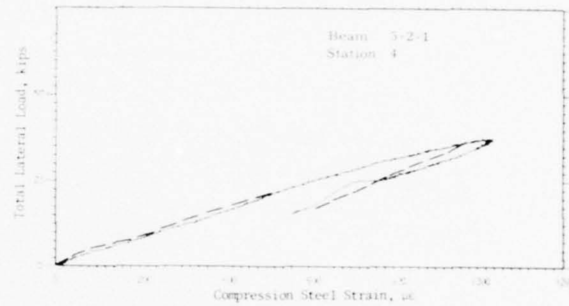
Beam 5-2-1
Station 4
Total Lateral Load, kips
Compression Steel Strain, με

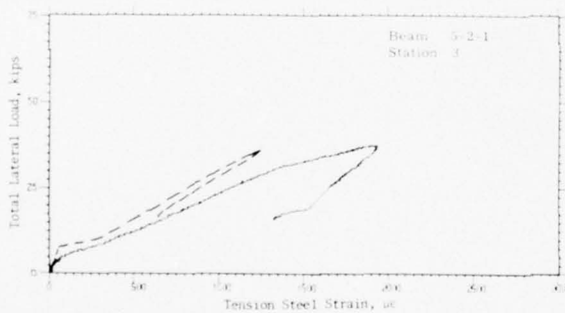
Beam 5-2-1
Station 3
Total Lateral Load, kips
Tension Steel Strain, με

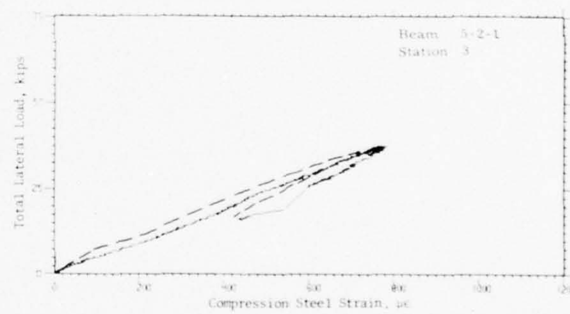
Beam 5-2-1
Station 3
Total Lateral Load, kips
Compression Steel Strain, με

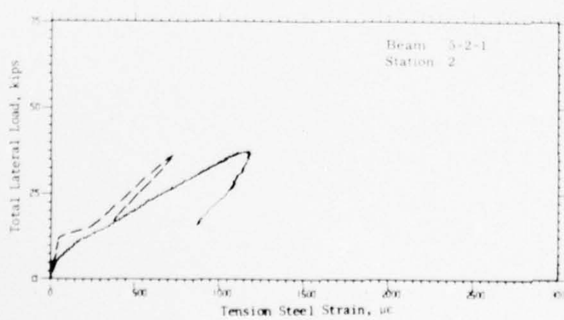
Beam 5-2-1
Station 2
Total Lateral Load, kips
Tension Steel Strain, με

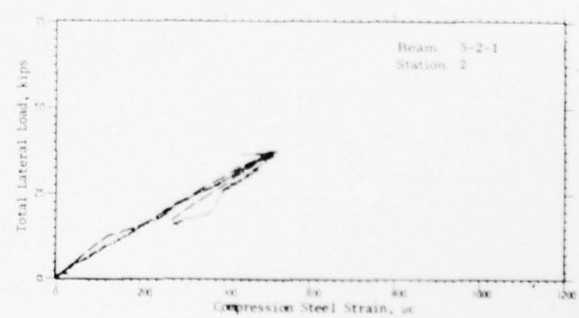
Beam 5-2-1
Station 2
Total Lateral Load, kips
Compression Steel Strain, με

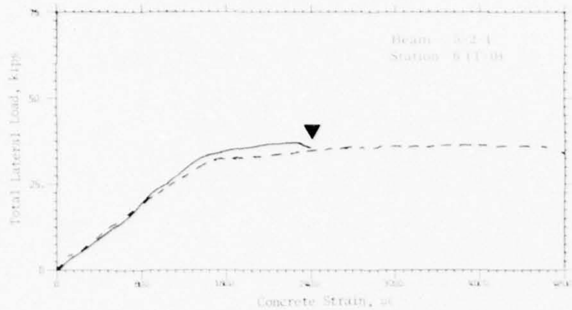
Beam 5-2-1
Station 6 (T-0)
Total Lateral Load, kips
Concrete Strain, με

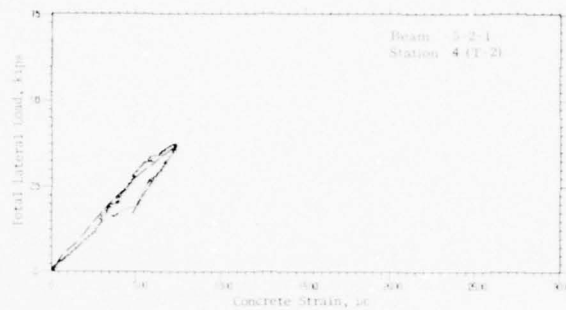
Beam 5-2-1
Station 4 (T-2)
Total Lateral Load, kips
Concrete Strain, με

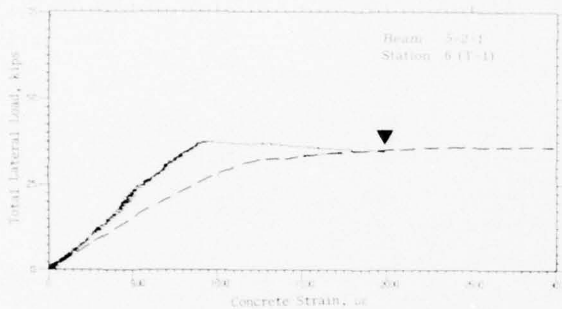
Beam 5-2-1
Station 6 (T-1)
Total Lateral Load, kips
Concrete Strain, με

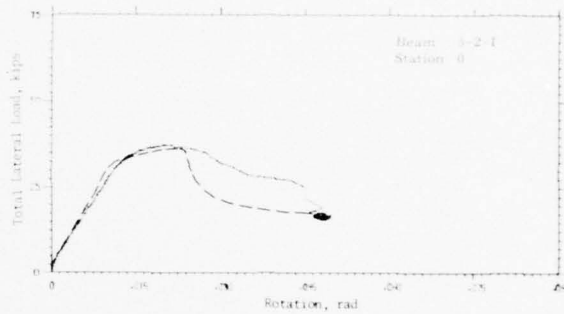
Beam 5-2-1
Station 0
Total Lateral Load, kips
Rotation, rad

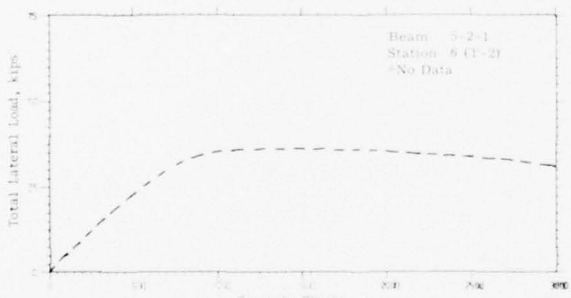
Beam 5-2-1
Station 6 (T-2)
*No Data
Total Lateral Load, kips
Concrete Strain, με

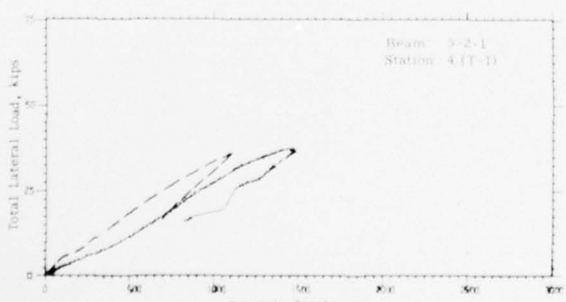
Beam 5-2-1
Station 4 (T-1)
Total Lateral Load, kips
Concrete Strain, με

Beam	5-2-2
f'_c	4651 psi
K = P/F	1.88
Test Date	5/16/73
Test Duration	4.5 min

Legend:

————	Experimental Results
– – – – –	Analytical Results
▼	Gage Failure

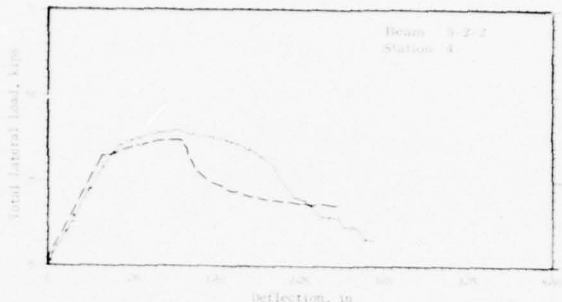

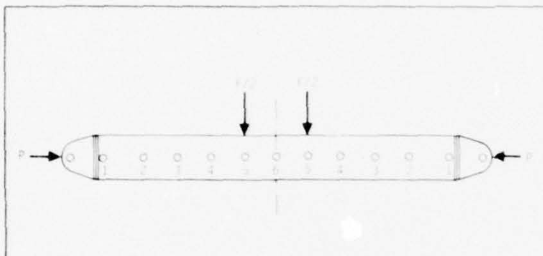

Loading Configuration
and Station Location

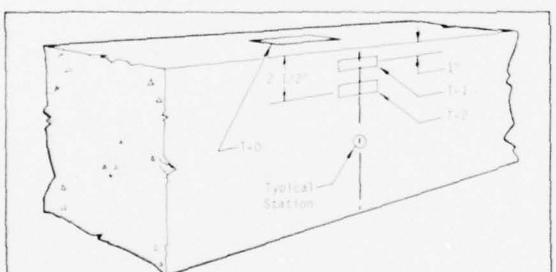

Concrete Strain Measurement Location

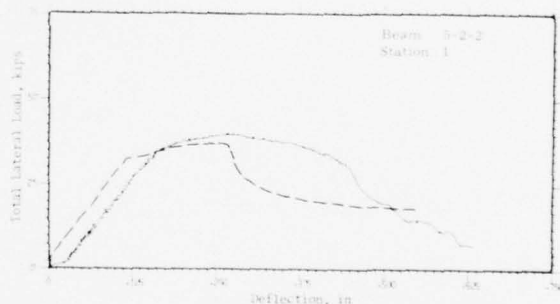

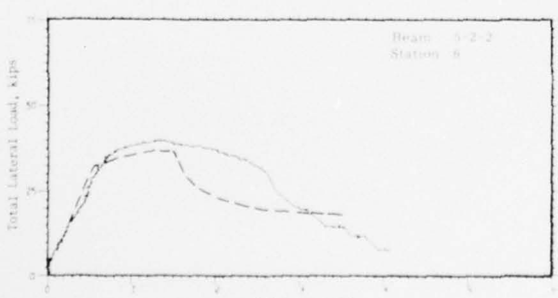

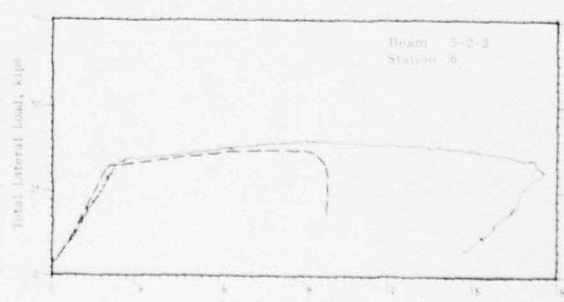

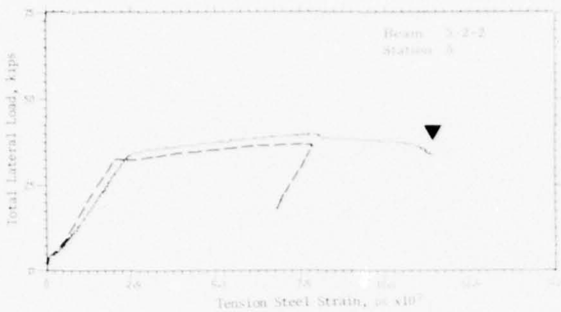
Beam 5-2-2
Station 5
Total Lateral Load, kips
Tension Steel Strain, με x10³

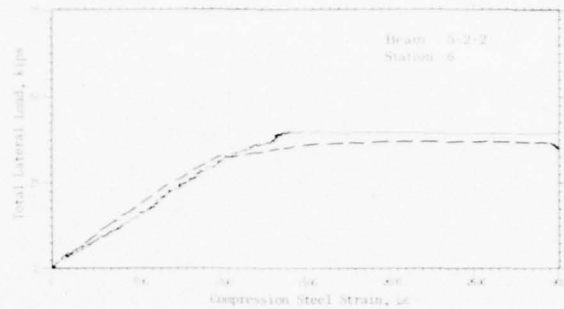
Beam 5-2-2
Station 6
Total Lateral Load, kips
Compression Steel Strain, με

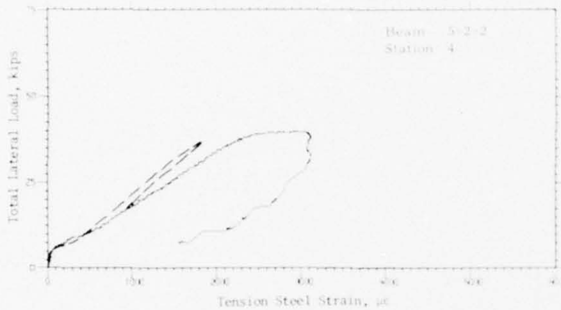
Beam 5-2-2
Station 4
Total Lateral Load, kips
Tension Steel Strain, με

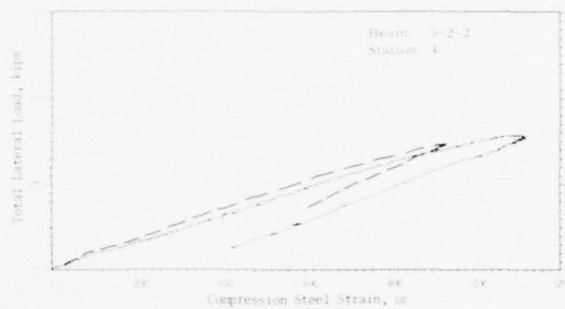
Beam 5-2-2
Station 4
Total Lateral Load, kips
Compression Steel Strain, με

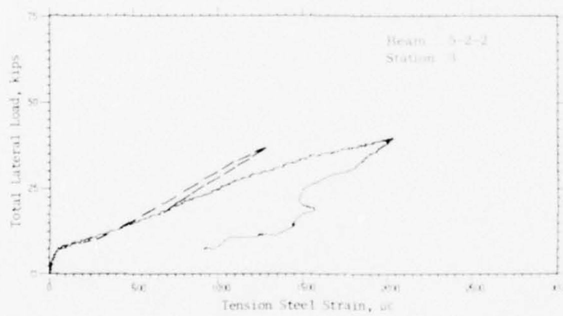
Beam 5-2-2
Station 3
Total Lateral Load, kips
Tension Steel Strain, με

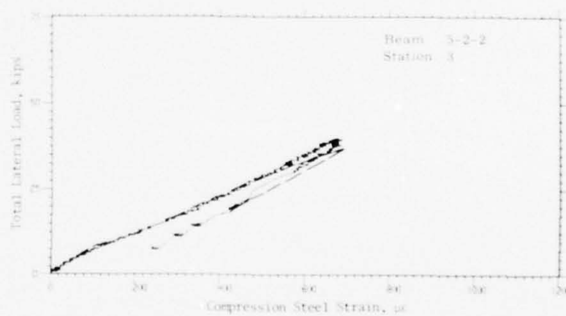
Beam 5-2-2
Station 3
Total Lateral Load, kips
Compression Steel Strain, με

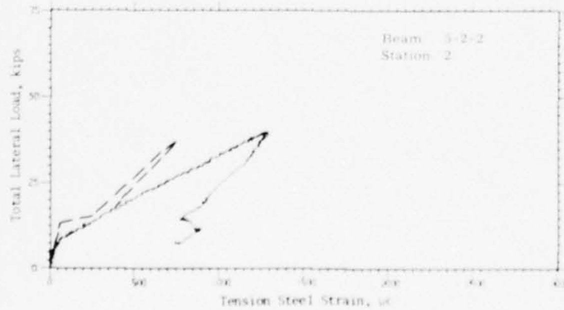
Beam 5-2-2
Station 2
Total Lateral Load, kips
Tension Steel Strain, με

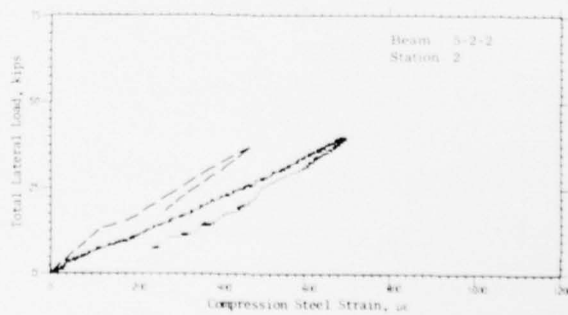
Beam 5-2-2
Station 2
Total Lateral Load, kips
Compression Steel Strain, με

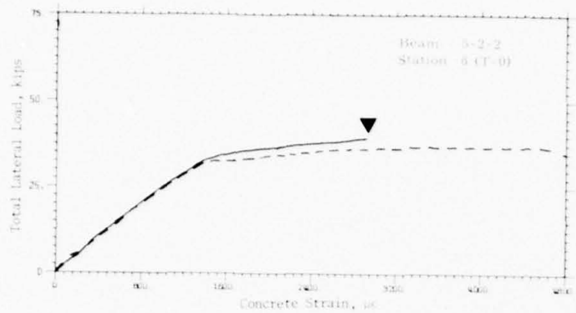
Beam 5-2-2
Station 6 (T-0)
Total Lateral Load, kips
Concrete Strain, με

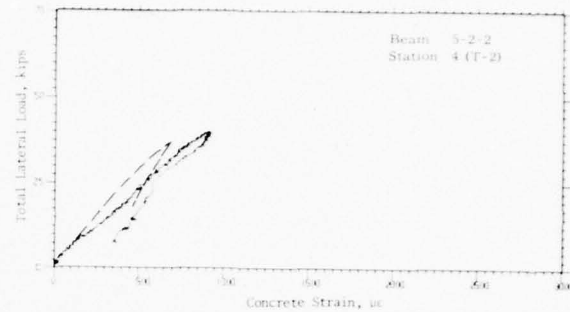
Beam 5-2-2
Station 4 (T-2)
Total Lateral Load, kips
Concrete Strain, με

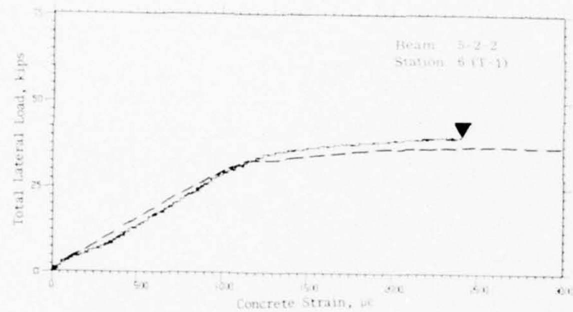
Beam 5-2-2
Station 6 (T-1)
Total Lateral Load, kips
Concrete Strain, με

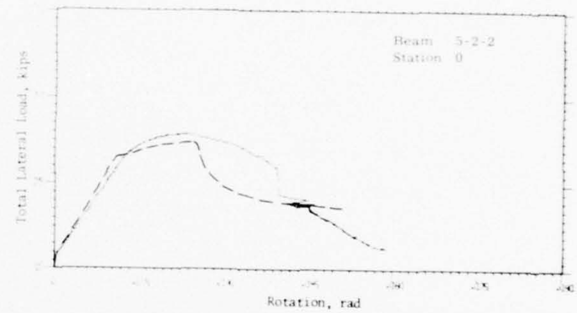
Beam 5-2-2
Station 0
Total Lateral Load, kips
Rotation, rad

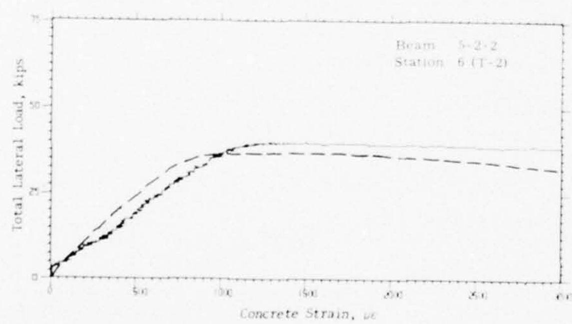
Beam 5-2-2
Station 6 (T-2)
Total Lateral Load, kips
Concrete Strain, με

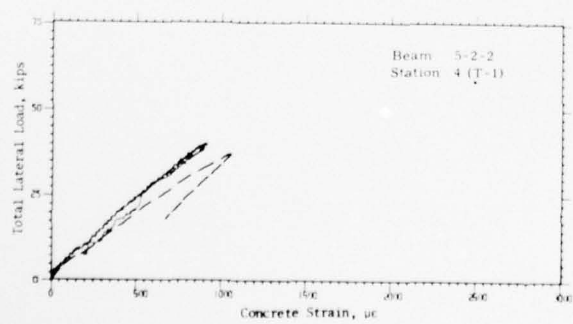
Beam 5-2-2
Station 4 (T-1)
Total Lateral Load, kips
Concrete Strain, με

Beam	5-3-2
f'_c	4753 psi
K = P/F	3.10
Test Date	5/25/73
Test Duration	10 min

Legend:

———	Experimental Results
— — —	Analytical Results
▼	Gage Failure

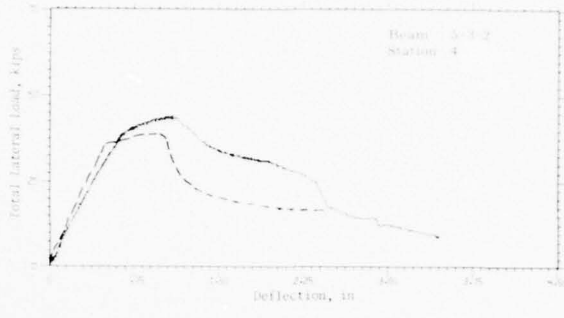

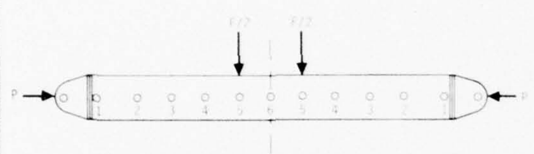

Loading Configuration and Station Location

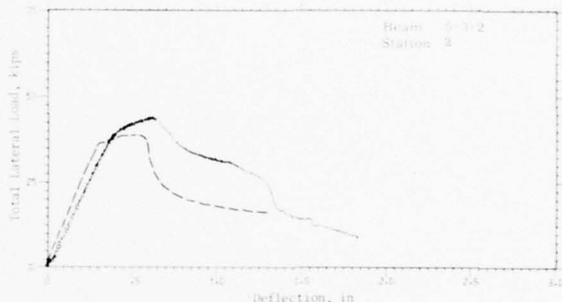

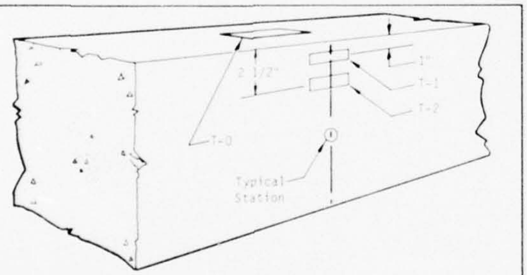

Concrete Strain Measurement Location

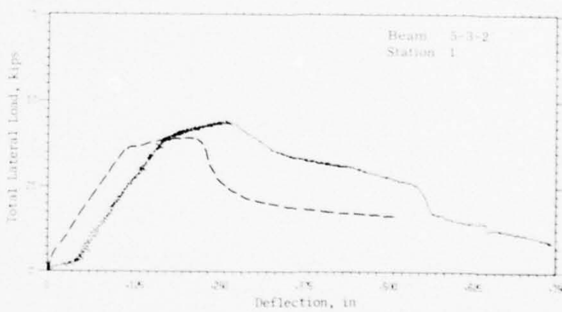

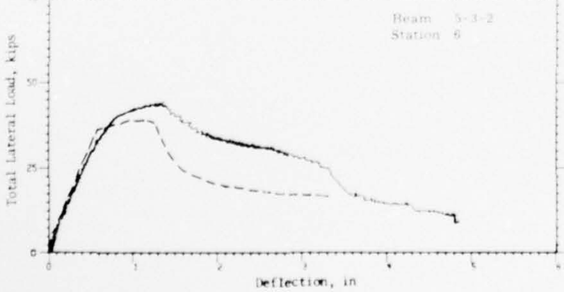

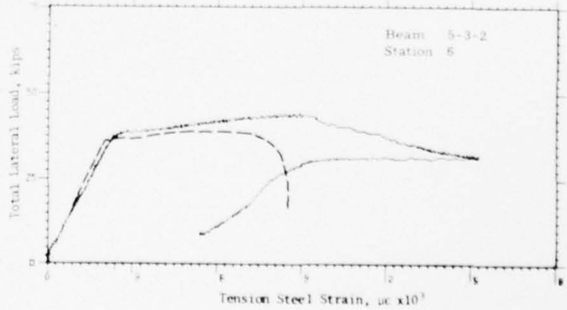

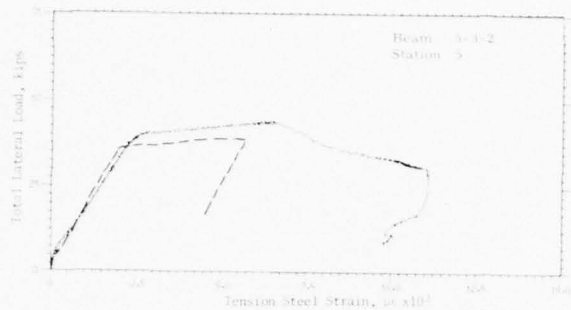
Beam 5-3-2
Station 5
Total Lateral Load, kips
Tension Steel Strain, με x10³

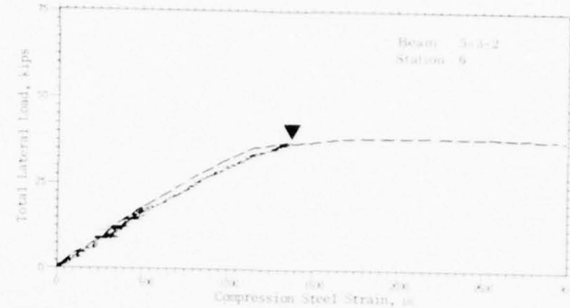
Beam 5-3-2
Station 6
Total Lateral Load, kips
Compression Steel Strain, με

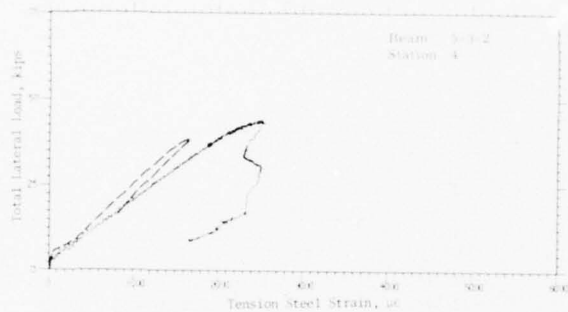
Beam 5-3-2
Station 4
Total Lateral Load, kips
Tension Steel Strain, με

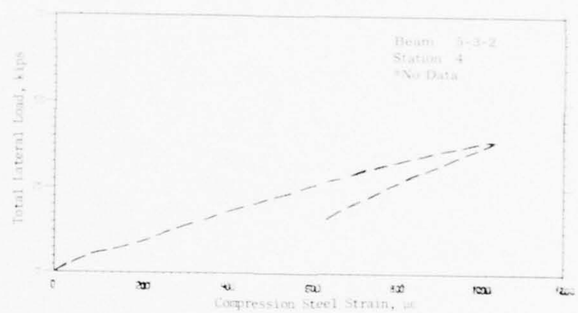
Beam 5-3-2
Station 4
*No Data
Total Lateral Load, kips
Compression Steel Strain, με

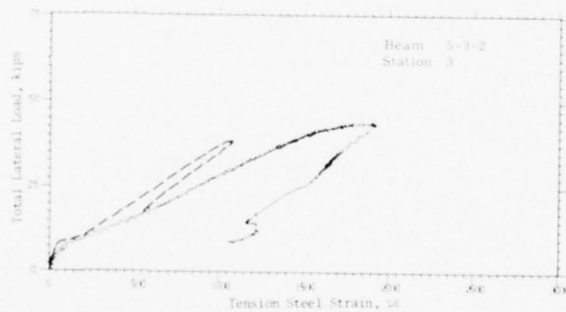
Beam 5-3-2
Station 3
Total Lateral Load, kips
Tension Steel Strain, με

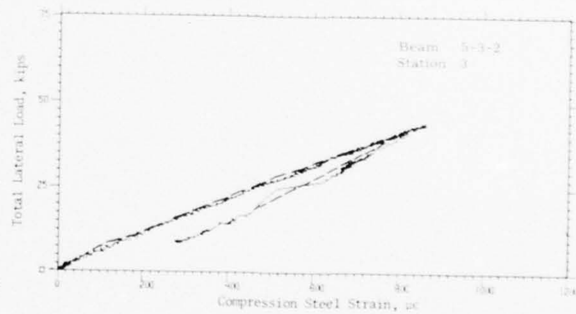
Beam 5-3-2
Station 3
Total Lateral Load, kips
Compression Steel Strain, με

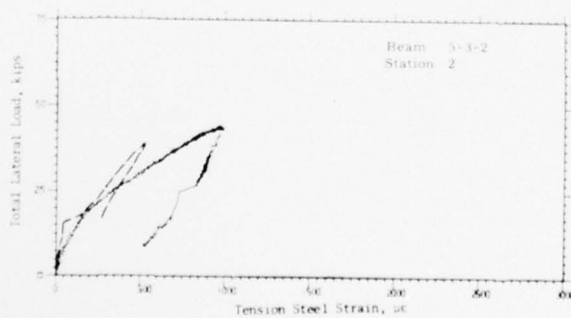
Beam 5-3-2
Station 2
Total Lateral Load, kips
Tension Steel Strain, με

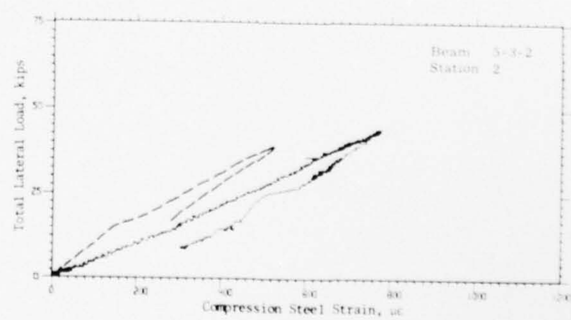
Beam 5-3-2
Station 2
Total Lateral Load, kips
Compression Steel Strain, με

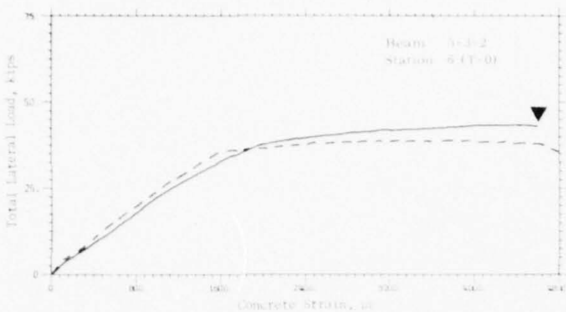
Beam 5-3-2
Station 6 (T-0)
Total Lateral Load, kips
Concrete Strain, με

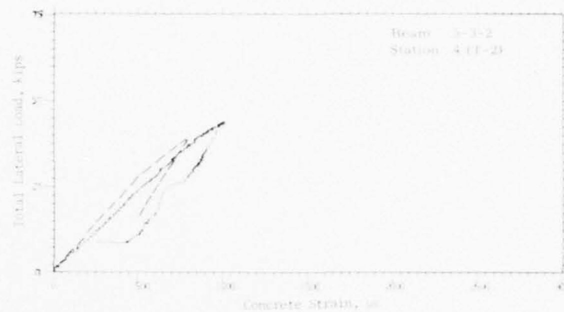
Beam 5-3-2
Station 4 (T-2)
Total Lateral Load, kips
Concrete Strain, με

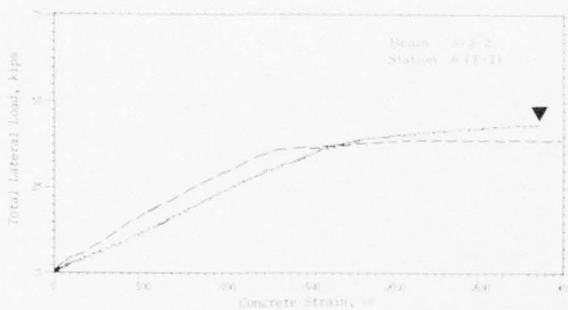
Beam 5-3-2
Station 6 (T-1)
Total Lateral Load, kips
Concrete Strain, με

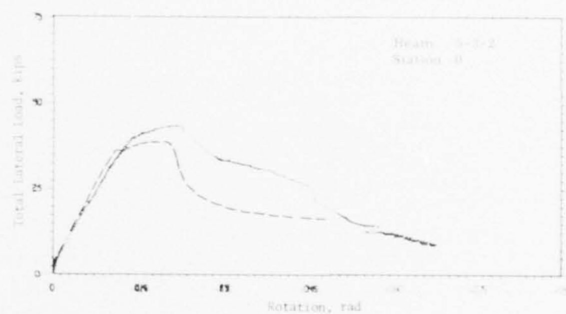
Beam 5-3-2
Station 0
Total Lateral Load, kips
Rotation, rad

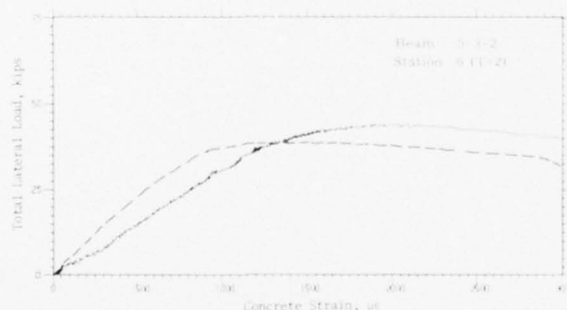
Beam 5-3-2
Station 6 (T-2)
Total Lateral Load, kips
Concrete Strain, με

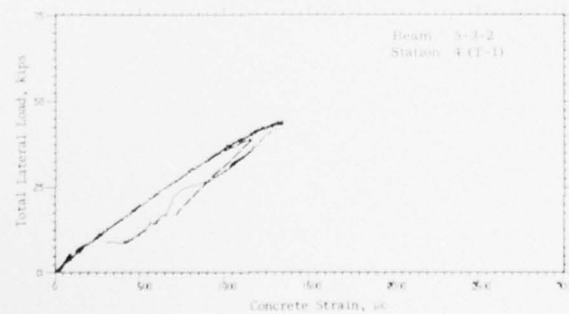
Beam 5-3-2
Station 4 (T-1)
Total Lateral Load, kips
Concrete Strain, με

Beam	5-3-3
f'_c	5583 psi
K = P/F	3.21
Test Date	6/1/73
Test Duration	7 min

Legend:

———	Experimental Results
– – – –	Analytical Results
▼	Gage Failure

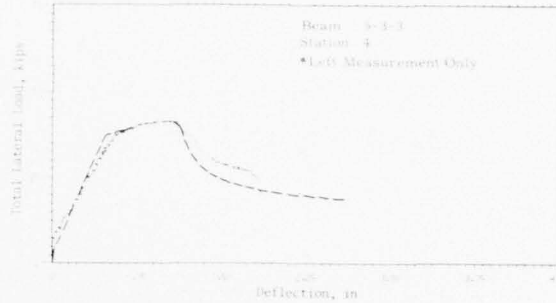

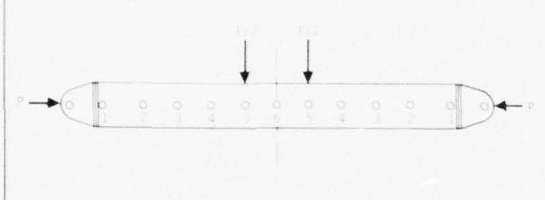

Loading Configuration
and Station Location

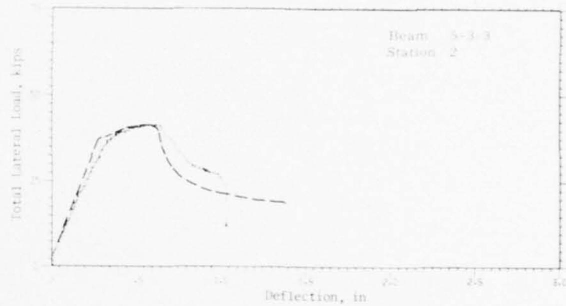

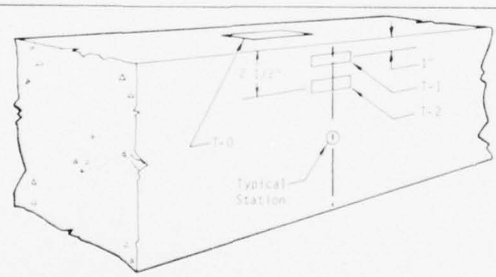

Concrete Strain Measurement Location

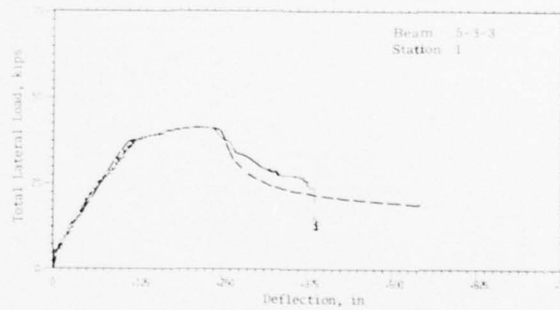

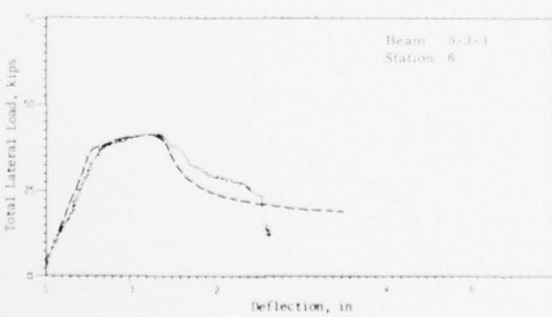

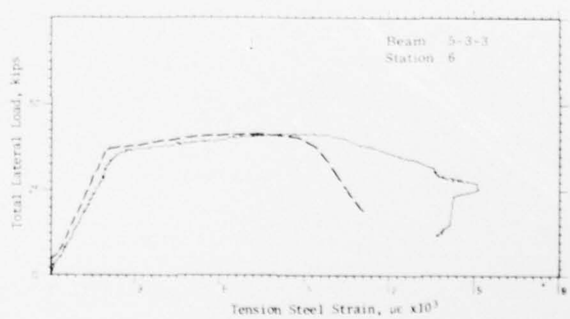

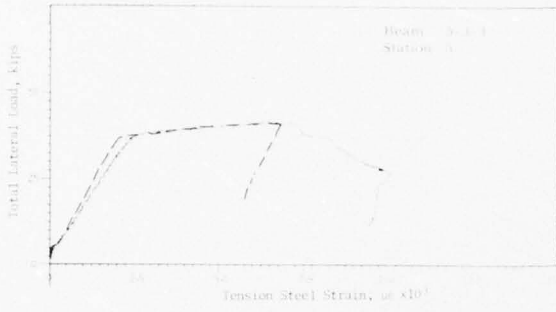
Beam
Total Lateral Load, kips
Tension Steel Strain, $\mu\epsilon \times 10^3$

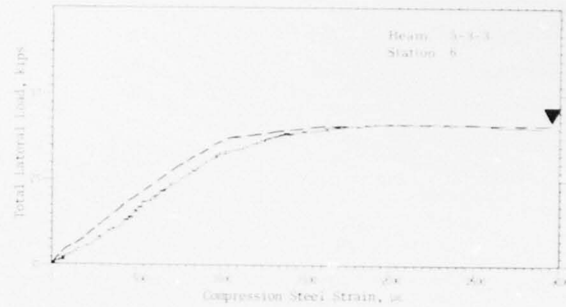
Beam 5-3-3
Station 6
Total Lateral Load, kips
Compression Steel Strain, $\mu\epsilon$

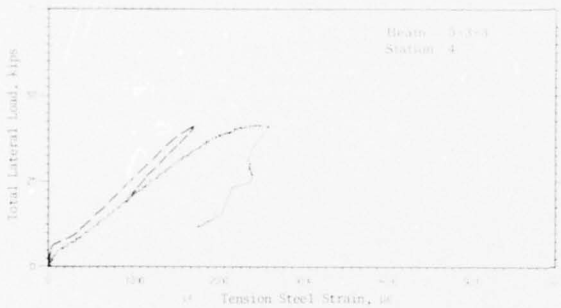
Beam 5-3-3
Station 4
Total Lateral Load, kips
Tension Steel Strain, $\mu\epsilon$

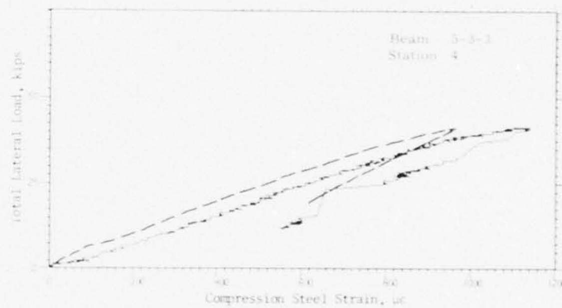
Beam 5-3-3
Station 4
Total Lateral Load, kips
Compression Steel Strain, $\mu\epsilon$

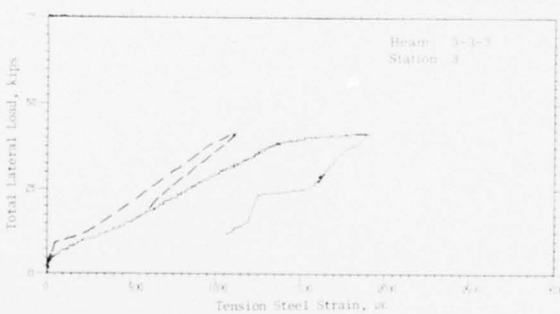
Beam
Station 3
Total Lateral Load, kips
Tension Steel Strain, $\mu\epsilon$

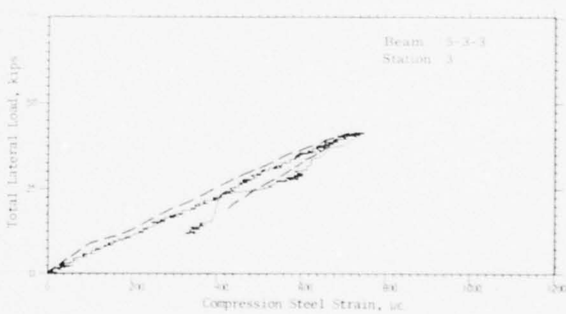
Beam 5-3-3
Station 3
Total Lateral Load, kips
Compression Steel Strain, $\mu\epsilon$

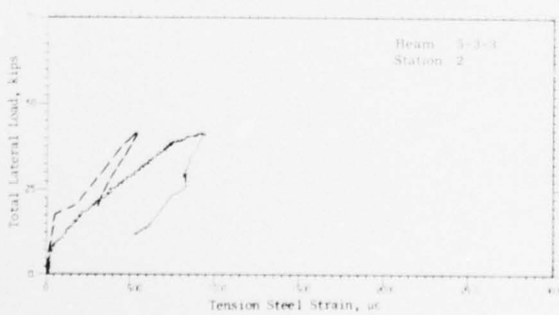
Beam 5-3-3
Station 2
Total Lateral Load, kips
Tension Steel Strain, $\mu\epsilon$

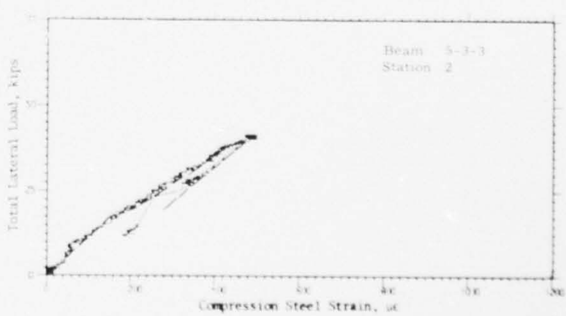
Beam 5-3-3
Station 2
Total Lateral Load, kips
Compression Steel Strain, $\mu\epsilon$

AD-A043 357 NEW MEXICO UNIV ALBUQUERQUE ERIC H WANG CIVIL ENGINE--ETC F/G 11/2
BEHAVIOR OF REINFORCED CONCRETE BEAMS UNDER COMBINED AXIAL AND --ETC(U)
MAY 77 G E LANE F29601-76-C-0015

UNCLASSIFIED CERF-SSR-8 AFWL-TR-76-130 NL

2 OF 2
ADA
043357

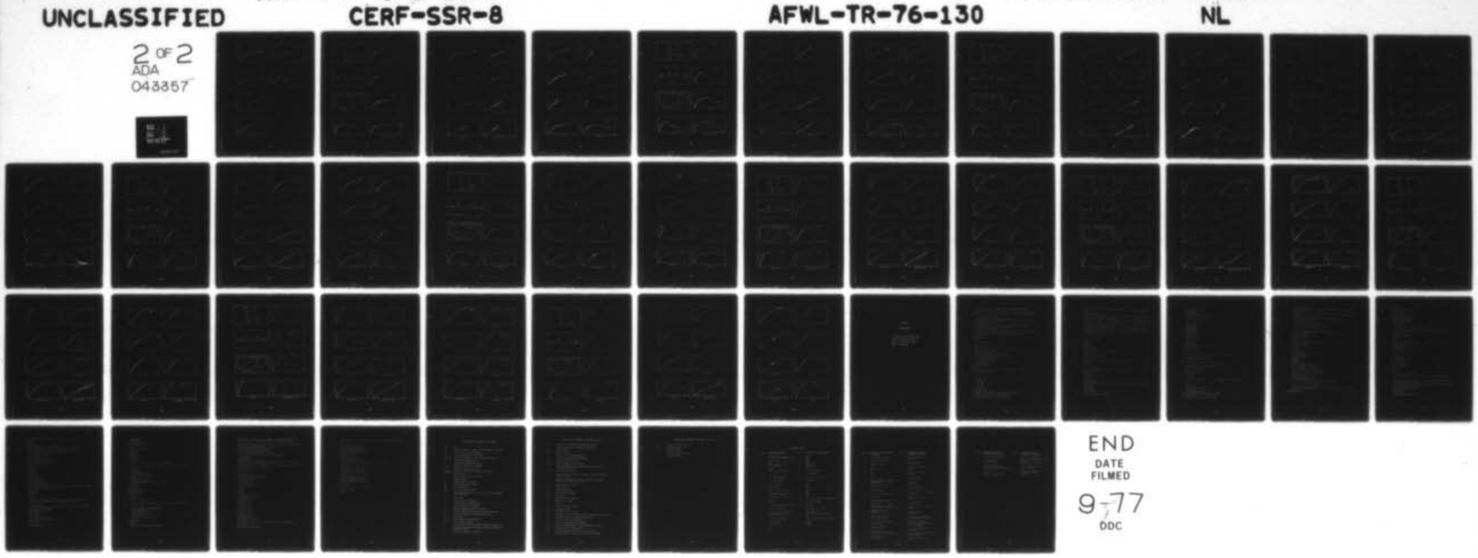

END
DATE
FILMED
9-77
DDC

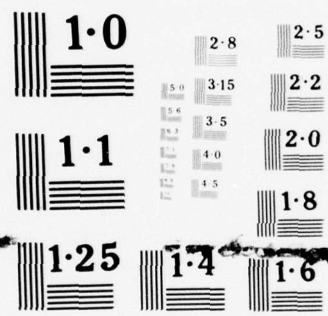

NATIONAL BUREAU OF STANDARDS
MICROCOPY RESOLUTION TEST CHART

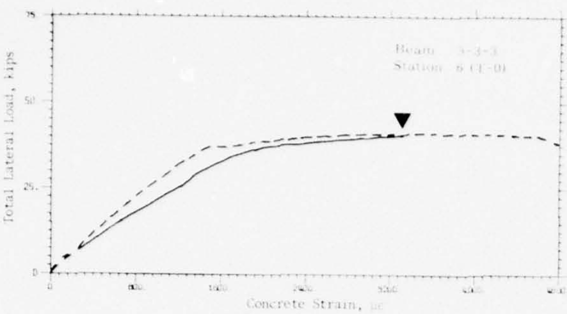
Beam 5-3-3
Station 6 (T-0)
Total Lateral Load, kips
Concrete Strain, με

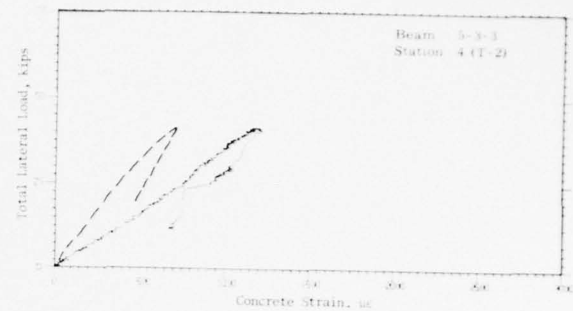
Beam 5-3-3
Station 4 (T-2)
Total Lateral Load, kips
Concrete Strain, με

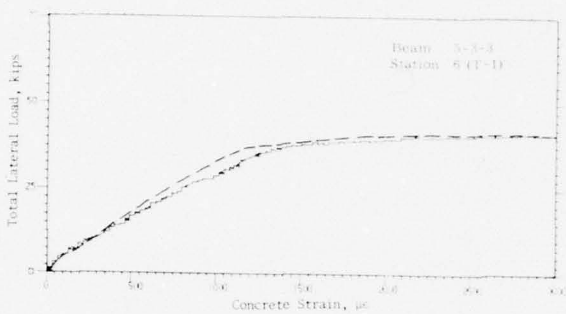
Beam 5-3-3
Station 6 (T-1)
Total Lateral Load, kips
Concrete Strain, με

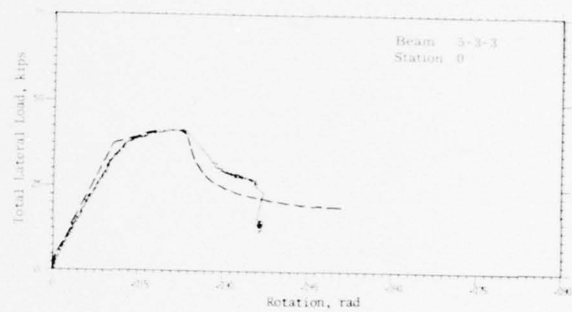
Beam 5-3-3
Station 0
Total Lateral Load, kips
Rotation, rad

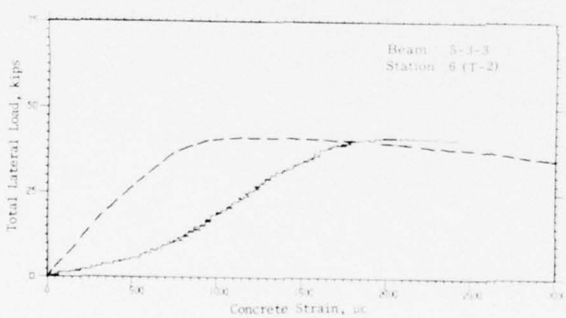
Beam 5-3-3
Station 6 (T-2)
Total Lateral Load, kips
Concrete Strain, με

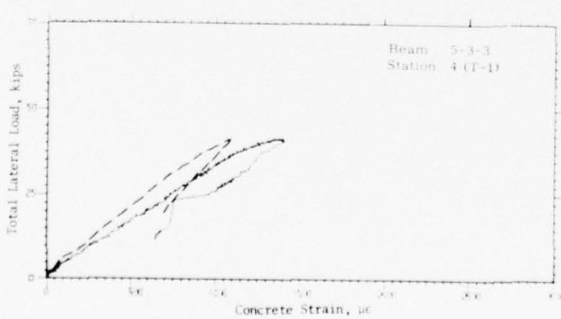
Beam 5-3-3
Station 4 (T-1)
Total Lateral Load, kips
Concrete Strain, με

Beam	4-0-1
f'_c	5288 psi
K = P/F	0
Test Date	7/11/73
Test Duration	7 min

Legend:

——— Experimental Results

— — — Analytical Results

▼ Gage Failure

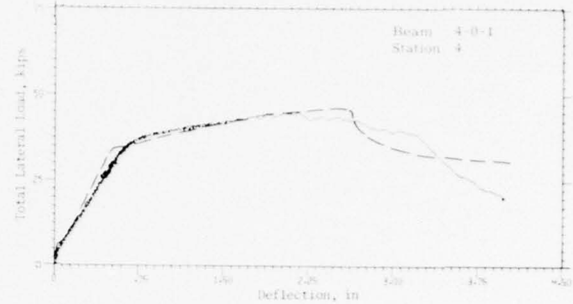

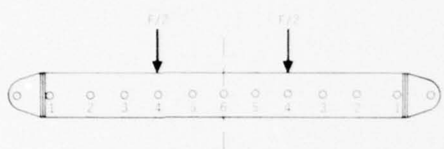

Loading Configuration
and Station Location

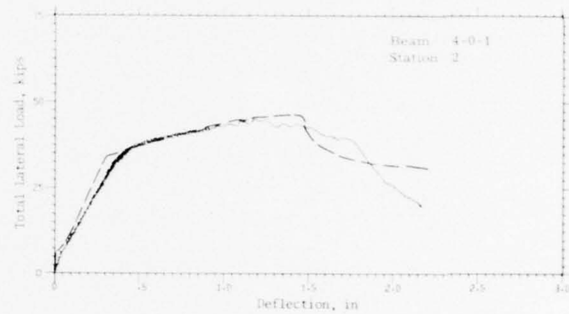

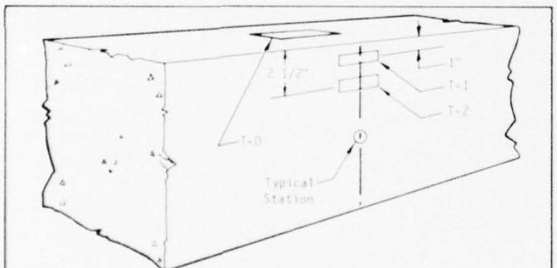

Concrete Strain Measurement Location

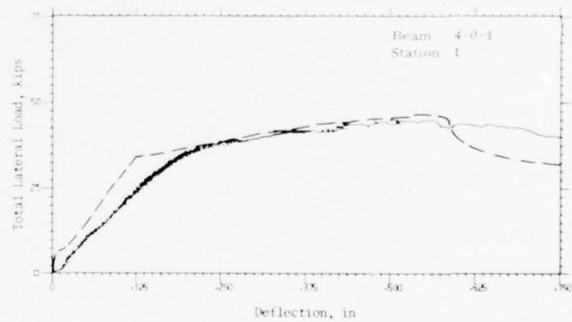

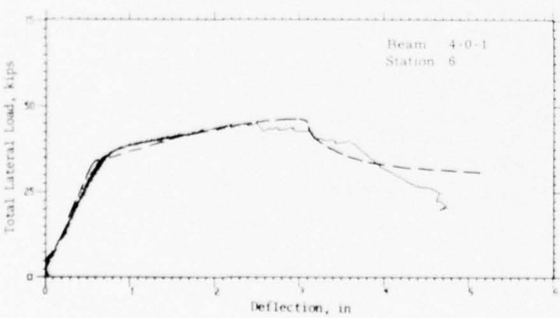

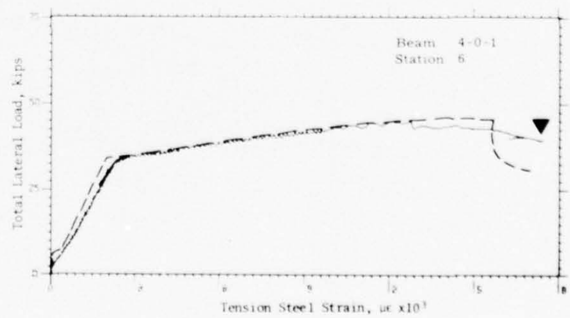

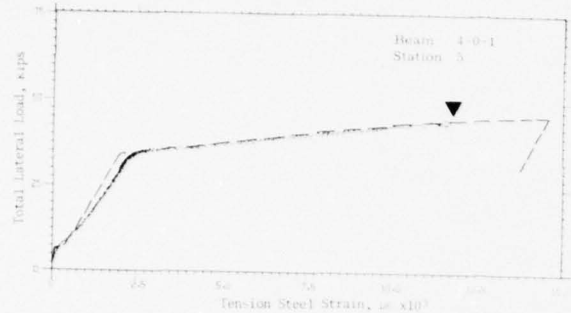
Beam 4-0-1
Station 5
Total Lateral Load, kips
Tension Steel Strain, με x10³

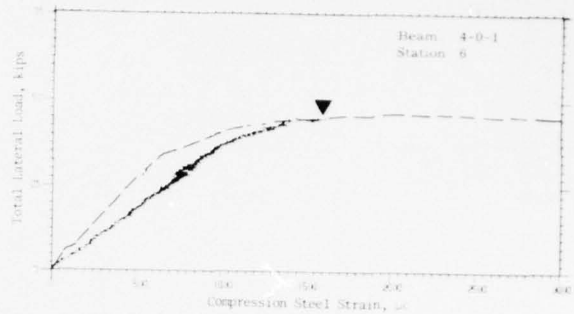
Beam 4-0-1
Station 6
Total Lateral Load, kips
Compression Steel Strain, με

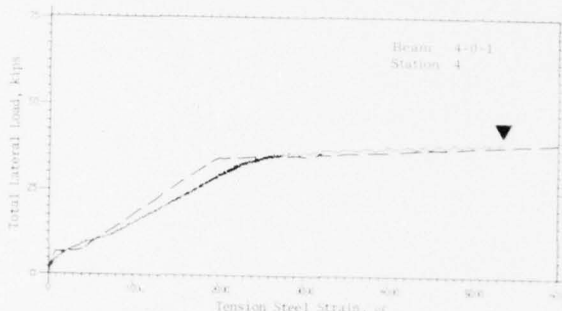
Beam 4-0-1
Station 4
Total Lateral Load, kips
Tension Steel Strain, με

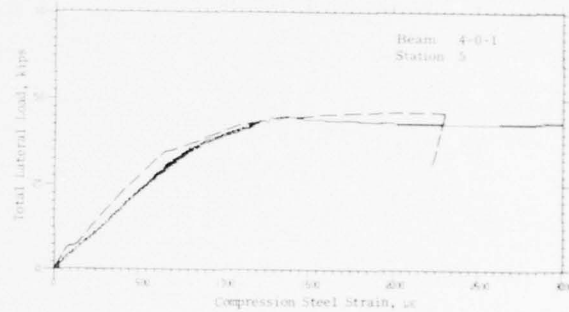
Beam 4-0-1
Station 5
Total Lateral Load, kips
Compression Steel Strain, με

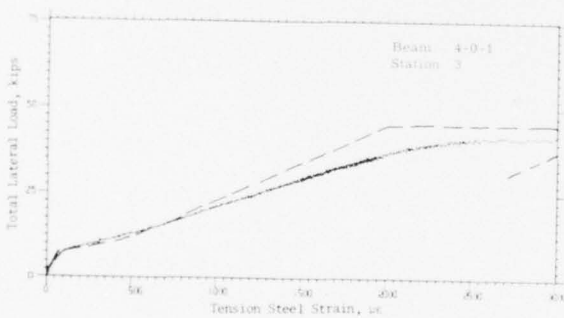
Beam 4-0-1
Station 3
Total Lateral Load, kips
Tension Steel Strain, με

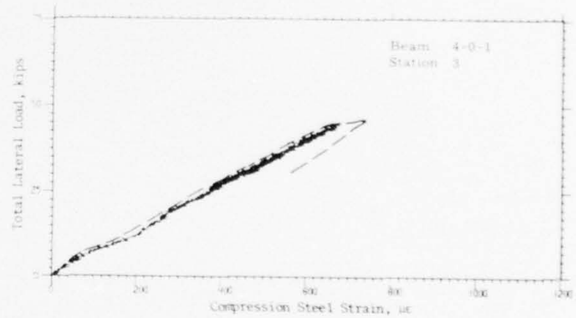
Beam 4-0-1
Station 3
Total Lateral Load, kips
Compression Steel Strain, με

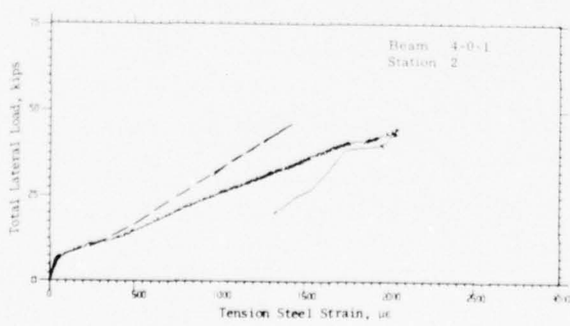
Beam 4-0-1
Station 2
Total Lateral Load, kips
Tension Steel Strain, με

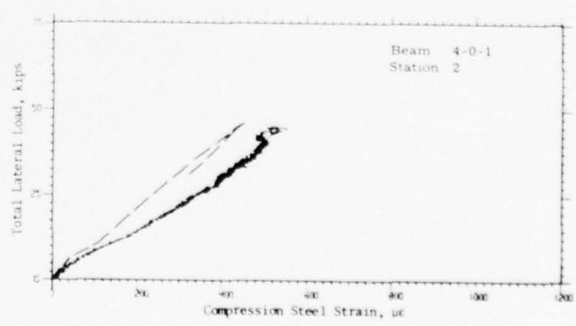
Beam 4-0-1
Station 2
Total Lateral Load, kips
Compression Steel Strain, με

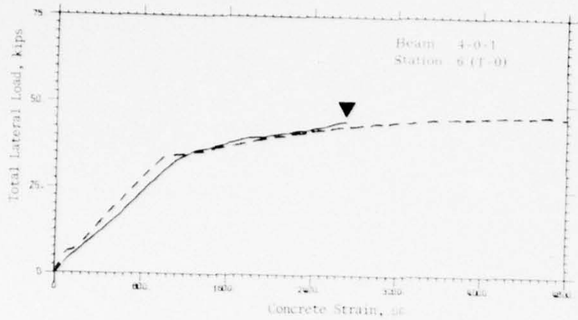
Beam 4-0-1
Station 6 (T-0)
Total Lateral Load, kips
Concrete Strain, με

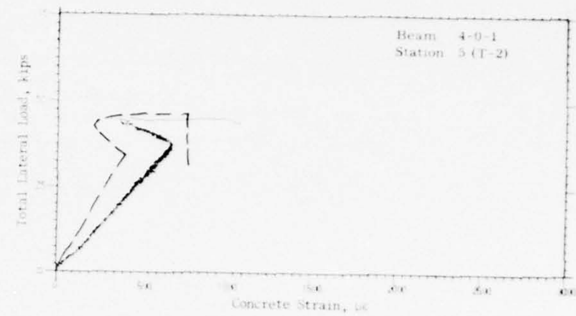
Beam 4-0-1
Station 5 (T-2)
Total Lateral Load, kips
Concrete Strain, με

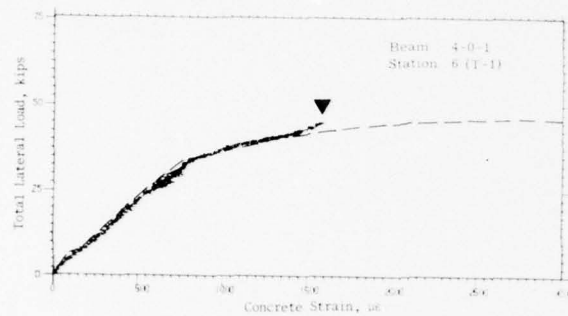
Beam 4-0-1
Station 6 (T-1)
Total Lateral Load, kips
Concrete Strain, με

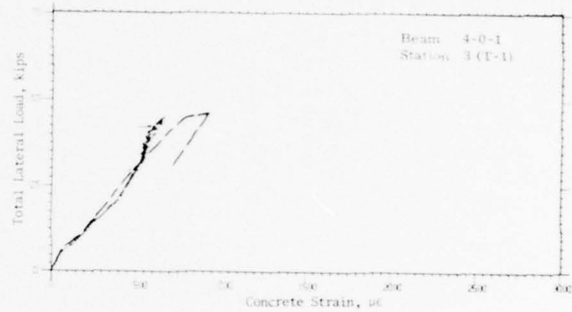
Beam 4-0-1
Station 3 (T-1)
Total Lateral Load, kips
Concrete Strain, με

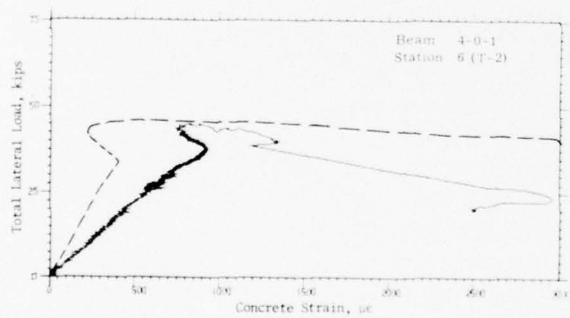
Beam 4-0-1
Station 6 (T-2)
Total Lateral Load, kips
Concrete Strain, με

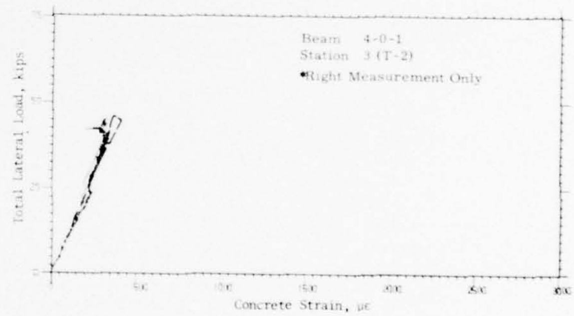
Beam 4-0-1
Station 3 (T-2)
*Right Measurement Only
Total Lateral Load, kips
Concrete Strain, με

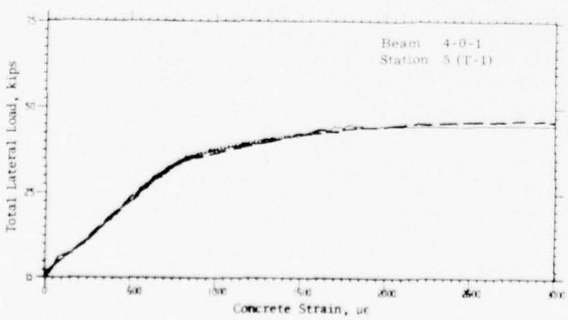
Beam 4-0-1
Station 5 (T-1)
Total Lateral Load, kips
Concrete Strain, με

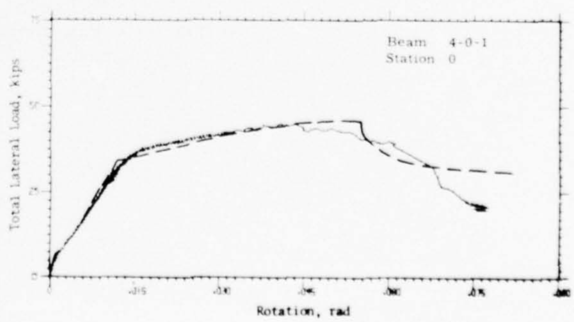
Beam 4-0-1
Station 0
Total Lateral Load, kips
Rotation, rad

Beam	4-2-1
f'_c	5205 psi
K = P/F	1.97
Test Date	6/29/73
Test Duration	8.9 min

Legend:

———	Experimental Results
— — —	Analytical Results
▼	Gage Failure

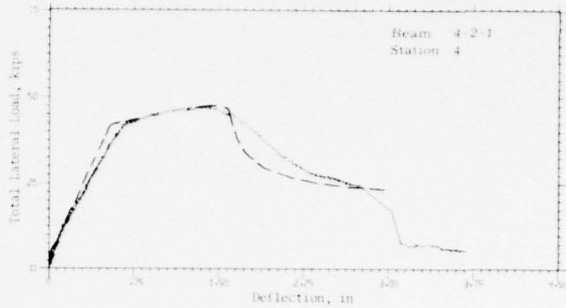

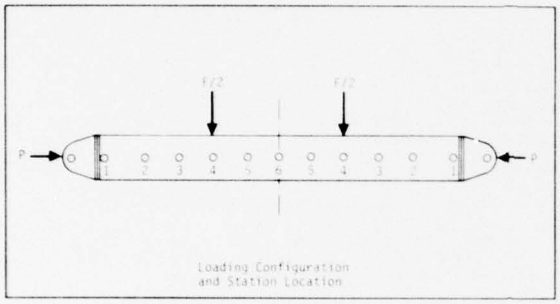

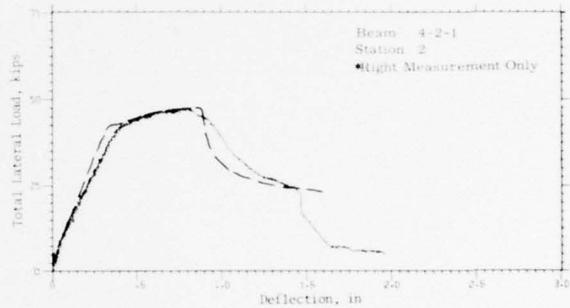

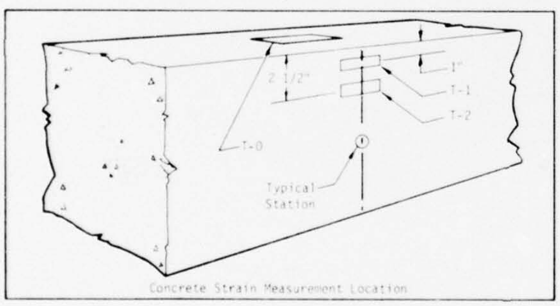

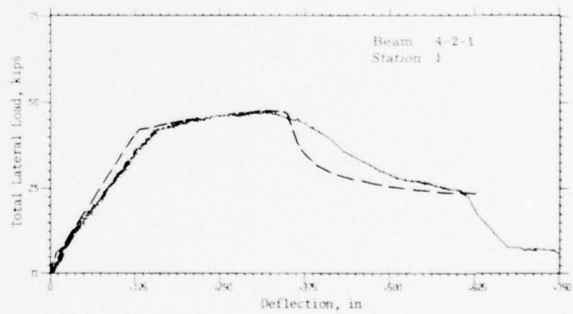

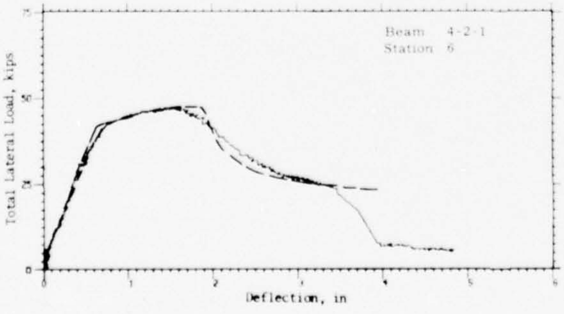

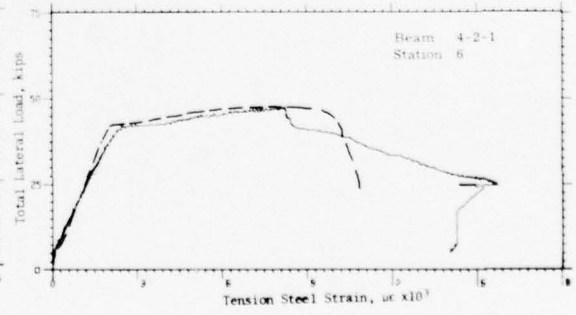

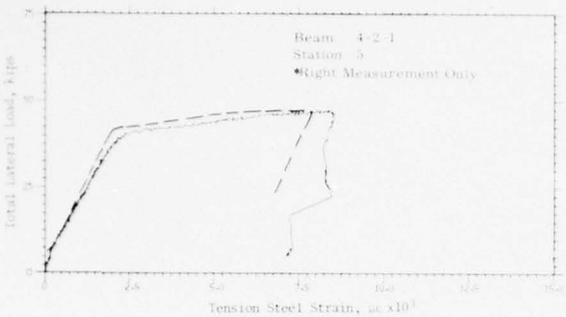
Beam 4-2-1
Station 5
*Right Measurement Only
Total Lateral Load, kips
Tension Steel Strain, με x10³

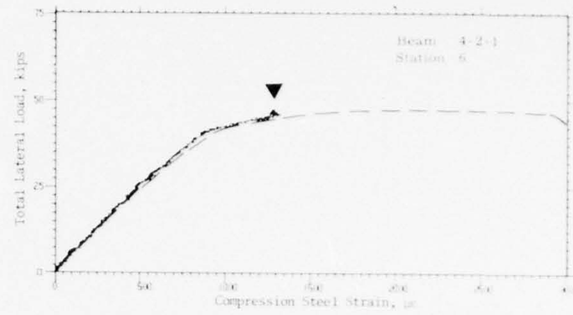
Beam 4-2-1
Station 6
Total Lateral Load, kips
Compression Steel Strain, με

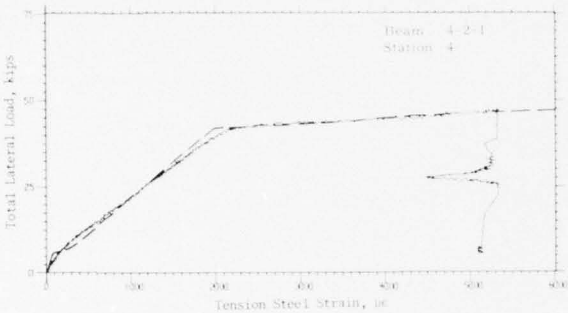
Beam 4-2-1
Station 4
Total Lateral Load, kips
Tension Steel Strain, με

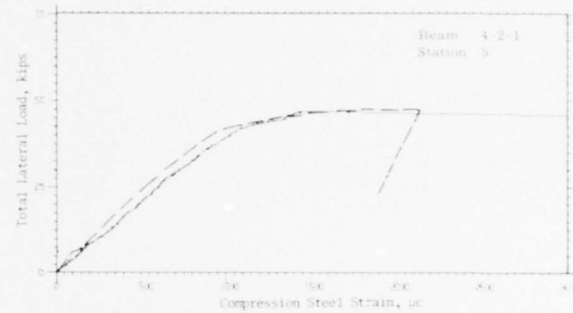
Beam 4-2-1
Station 5
Total Lateral Load, kips
Compression Steel Strain, με

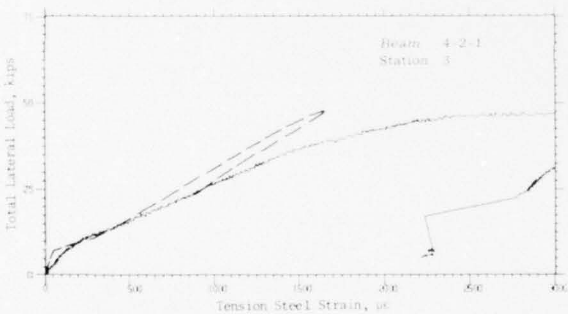
Beam 4-2-1
Station 3
Total Lateral Load, kips
Tension Steel Strain, με

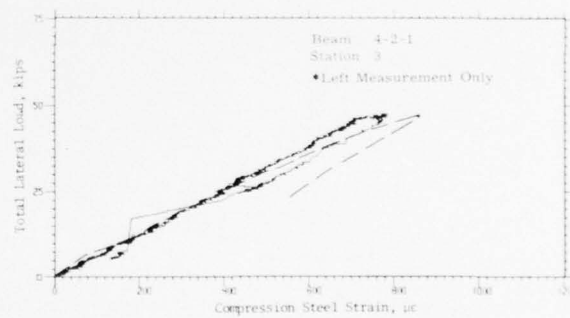
Beam 4-2-1
Station 3
*Left Measurement Only
Total Lateral Load, kips
Compression Steel Strain, με

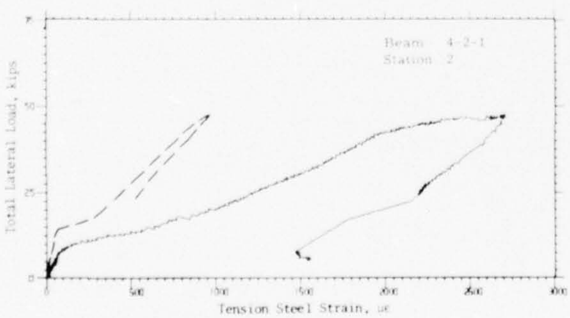
Beam 4-2-1
Station 2
Total Lateral Load, kips
Tension Steel Strain, με

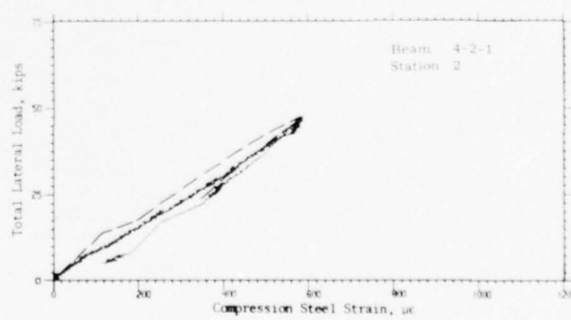
Beam 4-2-1
Station 2
Total Lateral Load, kips
Compression Steel Strain, με

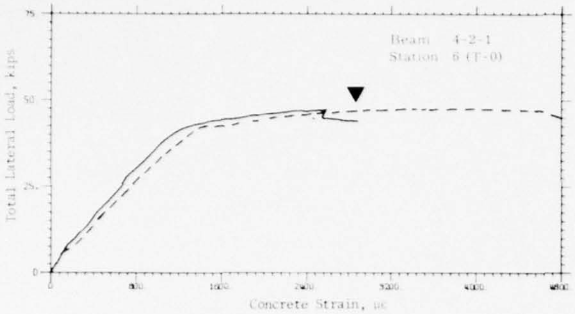
Beam 4-2-1
Station 6 (T-0)
Total Lateral Load, kips
Concrete Strain, με

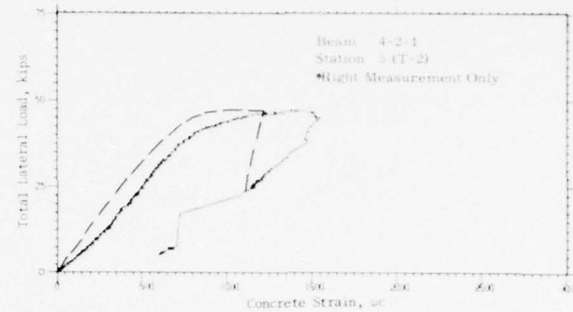
Beam 4-2-1
Station 5 (T-2)
*Right Measurement Only
Total Lateral Load, kips
Concrete Strain, με

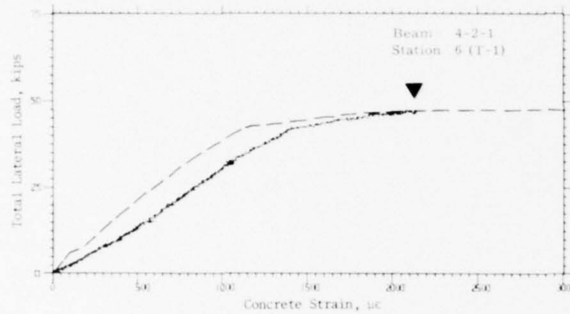
Beam 4-2-1
Station 6 (T-1)
Total Lateral Load, kips
Concrete Strain, με

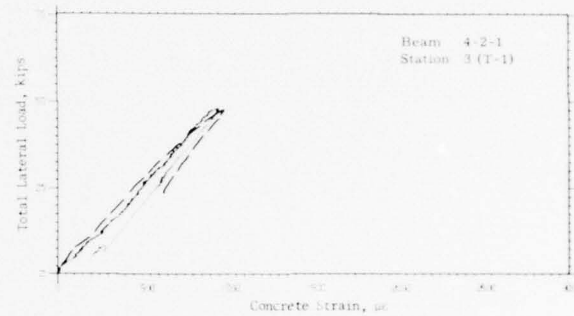
Beam 4-2-1
Station 3 (T-1)
Total Lateral Load, kips
Concrete Strain, με

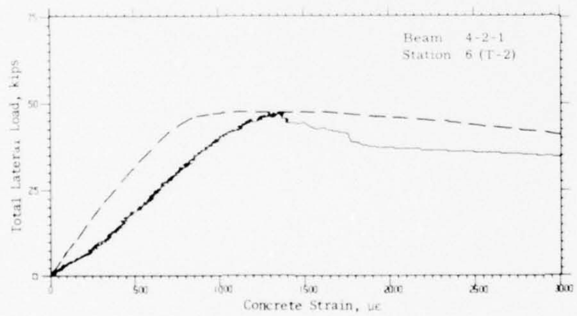
Beam 4-2-1
Station 6 (T-2)
Total Lateral Load, kips
Concrete Strain, με

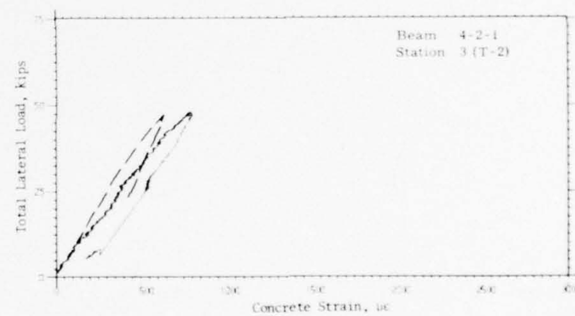
Beam 4-2-1
Station 3 (T-2)
Total Lateral Load, kips
Concrete Strain, με

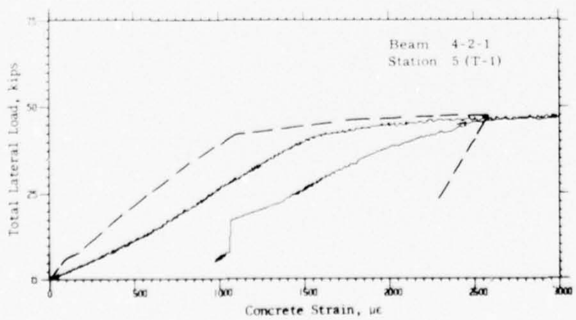
Beam 4-2-1
Station 5 (T-1)
Total Lateral Load, kips
Concrete Strain, με

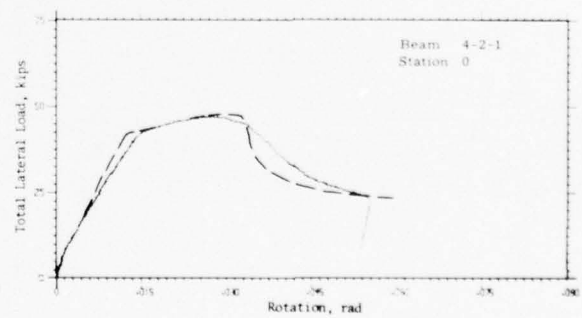
Beam 4-2-1
Station 0
Total Lateral Load, kips
Rotation, rad

Beam	4-2-2
f'_c	4990 psi
K = P/F	1.88
Test Date	7/5/73
Test Duration	6.8 min

Legend:

———————	Experimental Results
— — —	Analytical Results
▼	Gage Failure

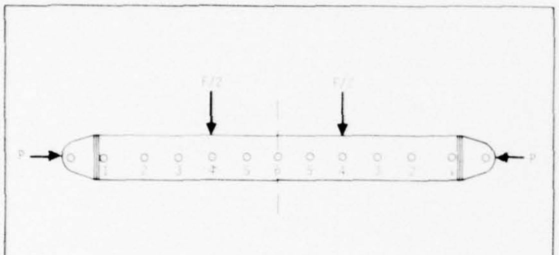

Loading Configuration and Station Location

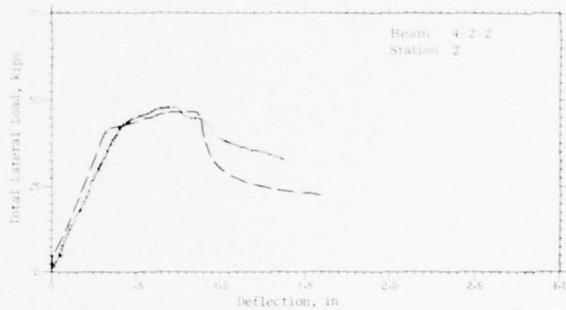

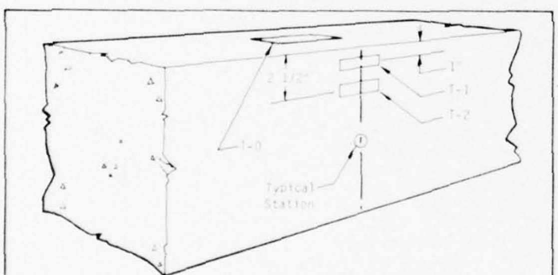

Concrete Strain Measurement Location

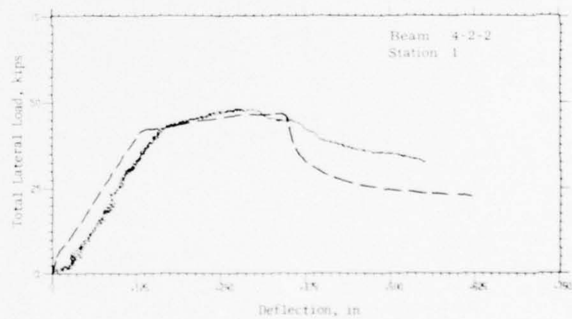

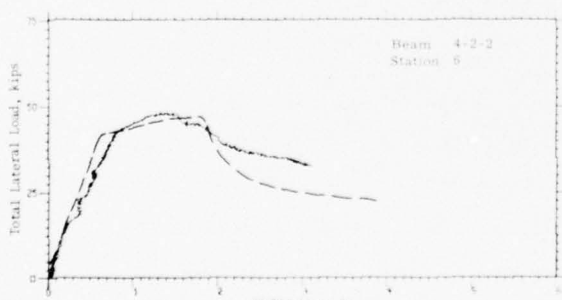

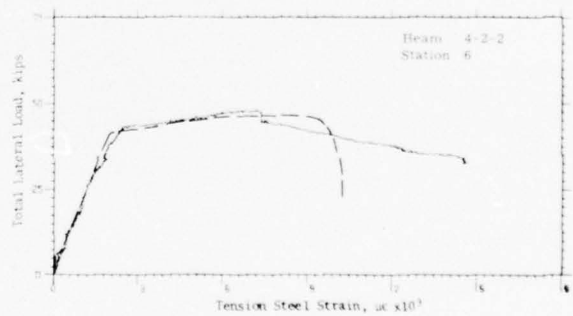

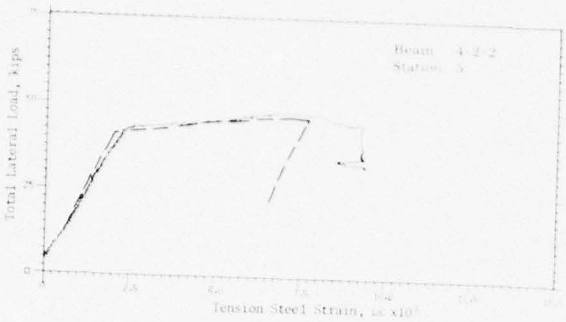
Beam 4-2-2
Station 5
Total Lateral Load, kips
Tension Steel Strain, με x10

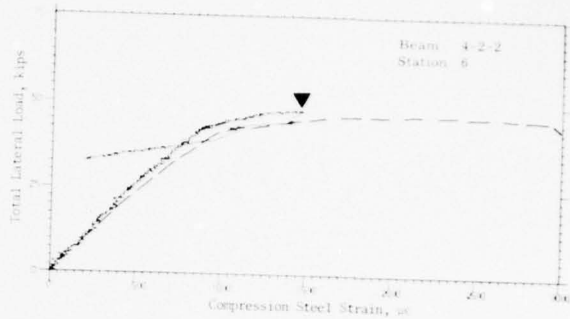
Beam 4-2-2
Station 6
Total Lateral Load, kips
Compression Steel Strain, με

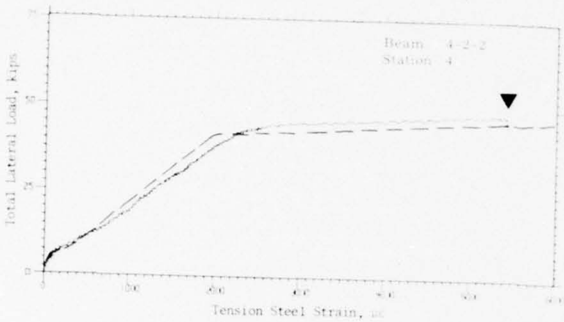
Beam 4-2-2
Station 4
Total Lateral Load, kips
Tension Steel Strain, με

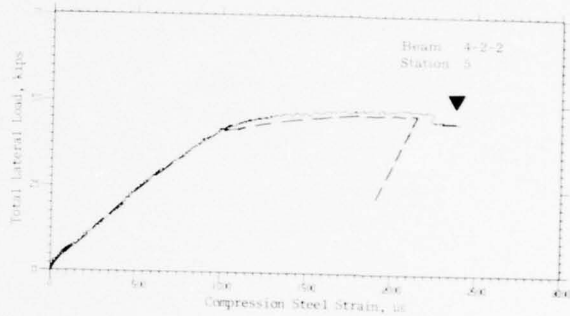
Beam 4-2-2
Station 5
Total Lateral Load, kips
Compression Steel Strain, με

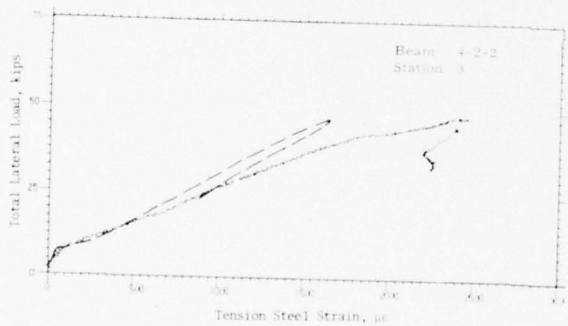
Beam 4-2-2
Station 3
Total Lateral Load, kips
Tension Steel Strain, με

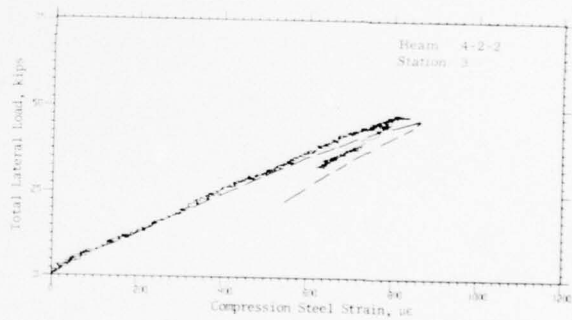
Beam 4-2-2
Station 3
Total Lateral Load, kips
Compression Steel Strain, με

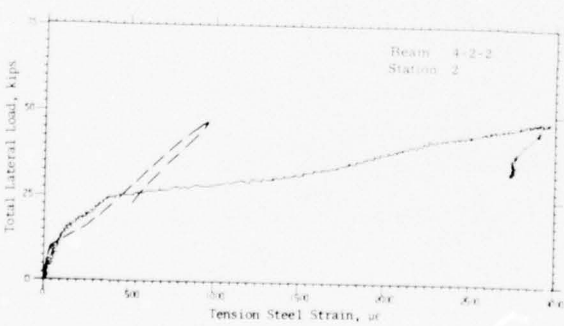
Beam 4-2-2
Station 2
Total Lateral Load, kips
Tension Steel Strain, με

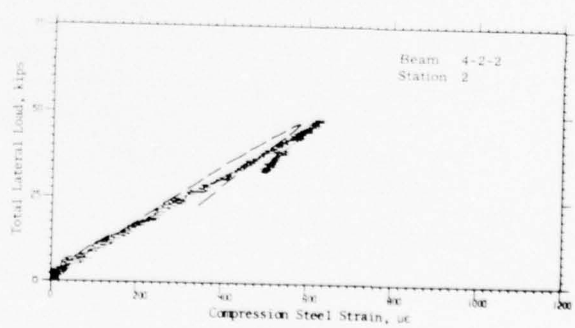
Beam 4-2-2
Station 2
Total Lateral Load, kips
Compression Steel Strain, με

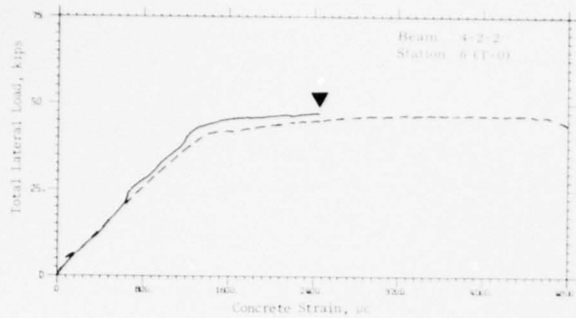
Beam 4-2-2
Station 6 (T-0)
Total Lateral Load, kips
Concrete Strain, με

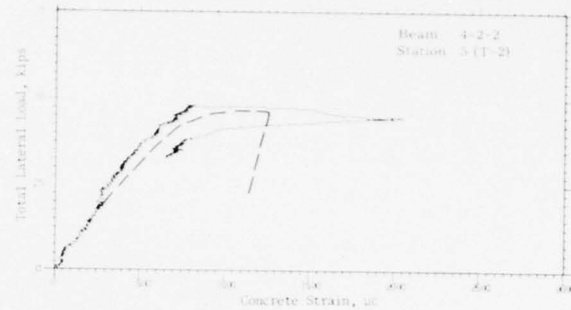
Beam 4-2-2
Station 5 (T-2)
Total Lateral Load, kips
Concrete Strain, με

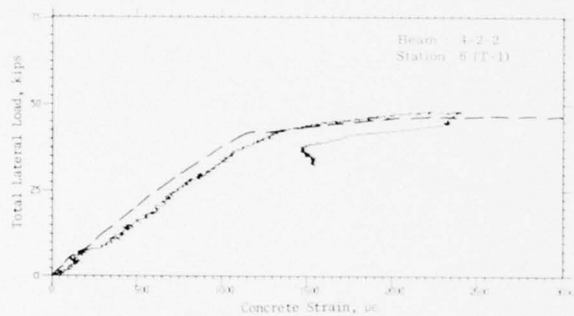
Beam 4-2-2
Station 6 (T-1)
Total Lateral Load, kips
Concrete Strain, με

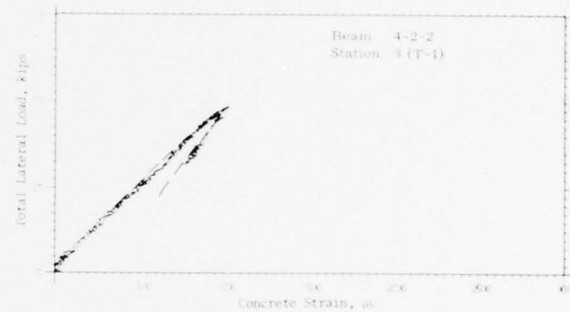
Beam 4-2-2
Station 3 (T-1)
Total Lateral Load, kips
Concrete Strain, με

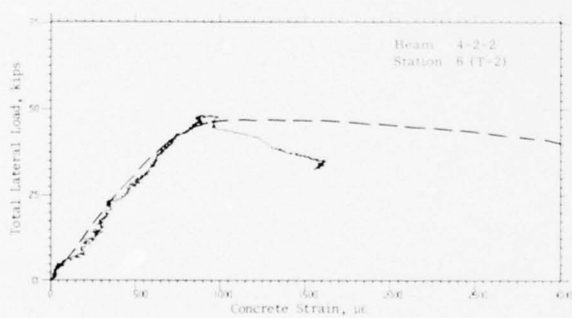
Beam 4-2-2
Station 6 (T-2)
Total Lateral Load, kips
Concrete Strain, με

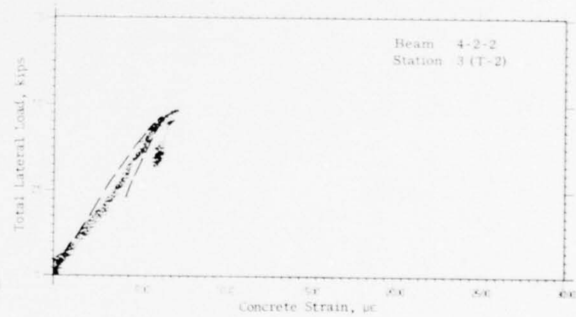
Beam 4-2-2
Station 3 (T-2)
Total Lateral Load, kips
Concrete Strain, με

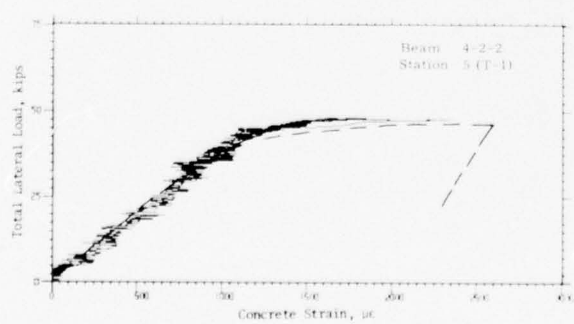
Beam 4-2-2
Station 5 (T-1)
Total Lateral Load, kips
Concrete Strain, με

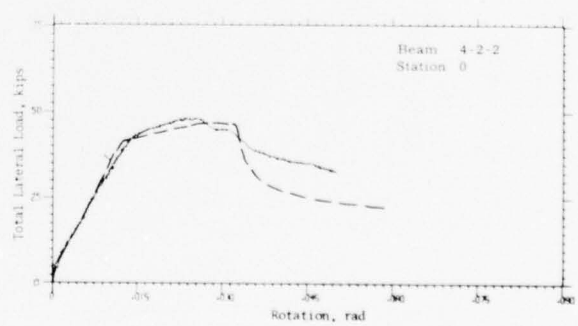
Beam 4-2-2
Station 0
Total Lateral Load, kips
Rotation, rad

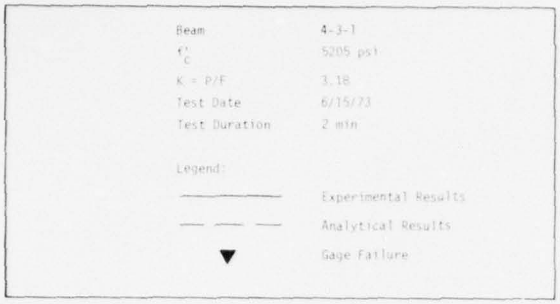
Beam 4-3-1
5205 psi
K = P/F 3.18
Test Date 6/15/73
Test Duration 2 min
Legend:
Experimental Results
Analytical Results
Gage Failure

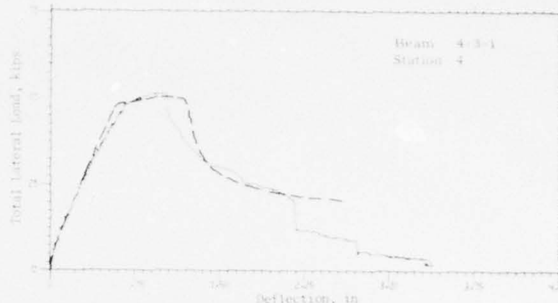
Beam 4-3-1
Station 4
Total Lateral Load, kips
Deflection, in

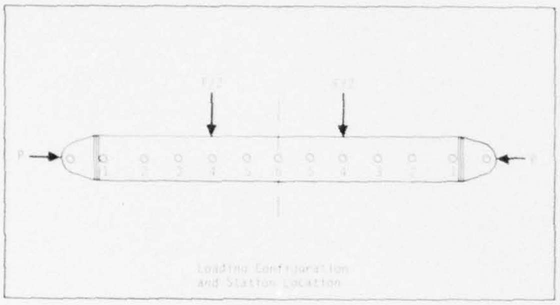
Loading Configuration
and Station Location

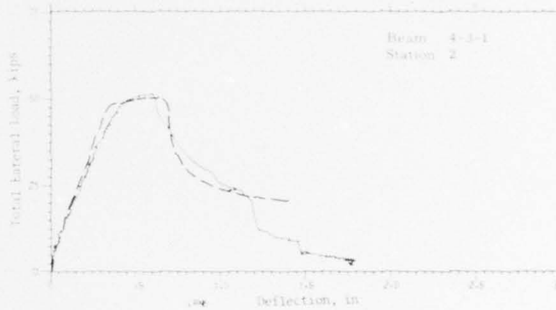
Beam 4-3-1
Station 2
Total Lateral Load, kips
Deflection, in

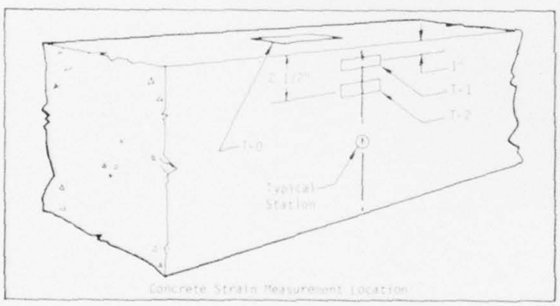
T-1
T-2
Typical
Station
Concrete Strain Measurement Location

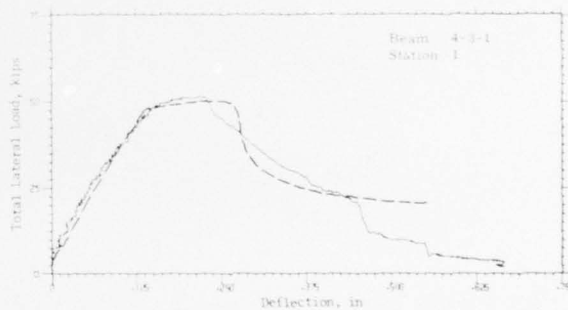
Beam 4-3-1
Station 1
Total Lateral Load, kips
Deflection, in

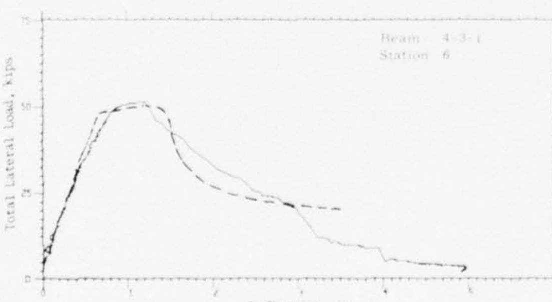
Beam 4-3-1
Station 6
Total Lateral Load, kips
Deflection, in

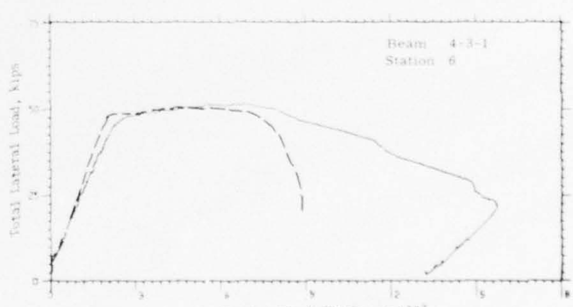
Beam 4-3-1
Station 6
Total Lateral Load, kips
Tension Steel Strain, με x10³

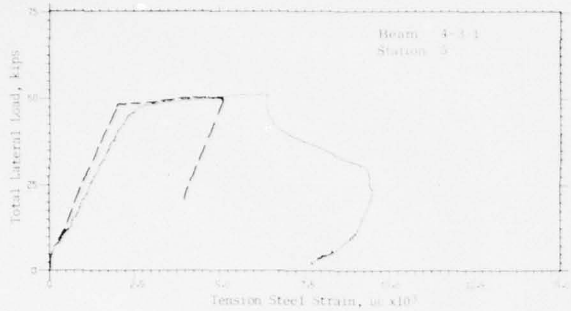
Beam 4-3-1
Station 5
Total Lateral Load, kips
Tension Steel Strain, $\mu\epsilon \times 10^3$

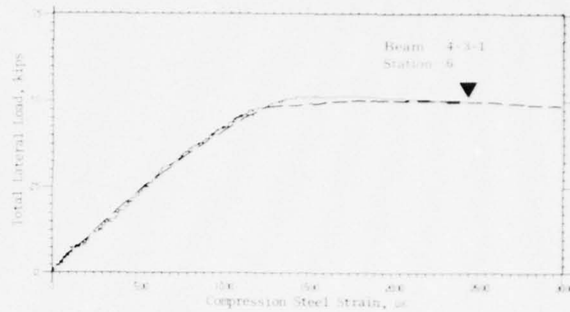
Beam 4-3-1
Station 6
Total Lateral Load, kips
Compression Steel Strain, $\mu\epsilon$

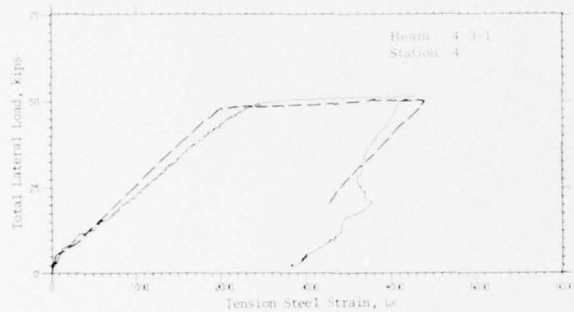
Beam 4-3-1
Station 4
Total Lateral Load, kips
Tension Steel Strain, $\mu\epsilon$

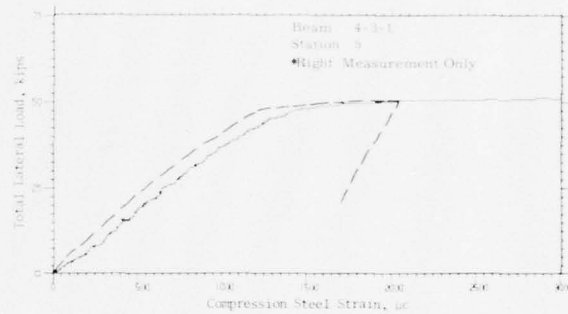
Beam 4-3-1
Station 5
*Right Measurement Only
Total Lateral Load, kips
Compression Steel Strain, $\mu\epsilon$

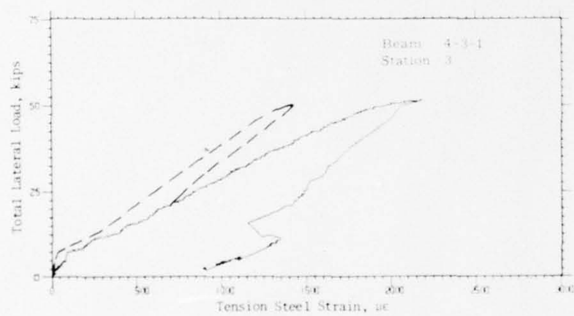
Beam 4-3-1
Station 3
Total Lateral Load, kips
Tension Steel Strain, $\mu\epsilon$

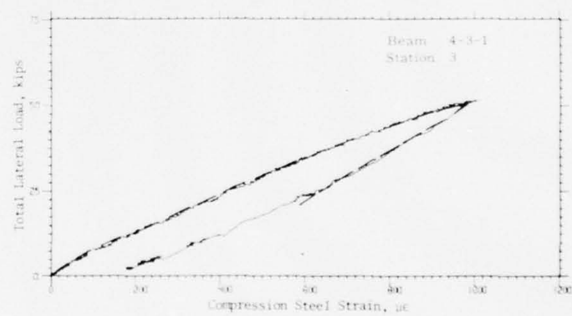
Beam 4-3-1
Station 3
Total Lateral Load, kips
Compression Steel Strain, $\mu\epsilon$

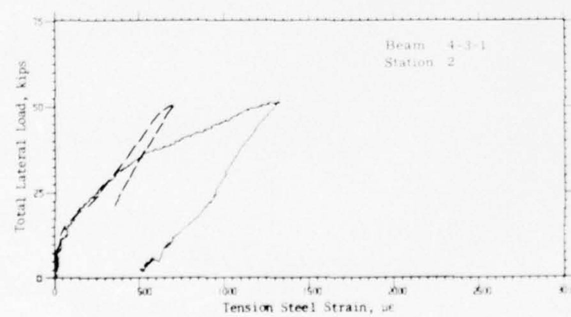
Beam 4-3-1
Station 2
Total Lateral Load, kips
Tension Steel Strain, $\mu\epsilon$

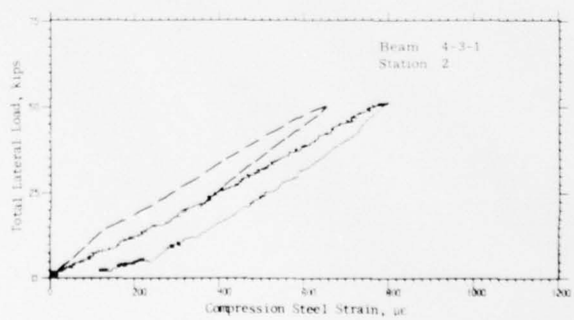
Beam 4-3-1
Station 2
Total Lateral Load, kips
Compression Steel Strain, $\mu\epsilon$

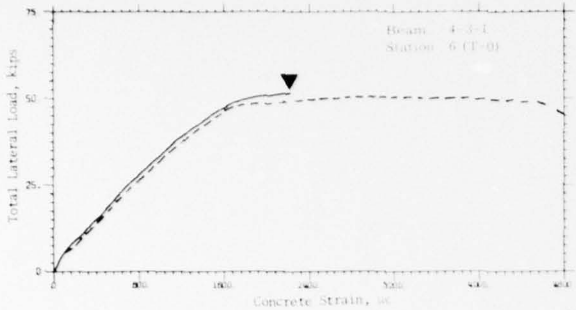
Beam 4-3-1
Station 6 (T-0)
Total Lateral Load, kips
Concrete Strain, με

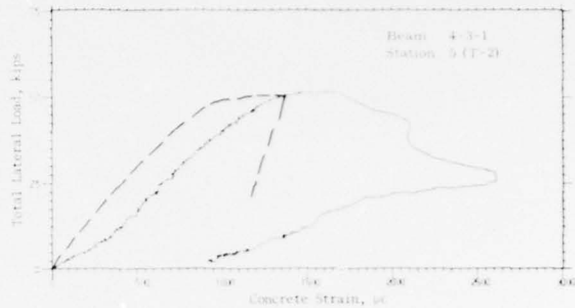
Beam 4-3-1
Station 5 (T-2)
Total Lateral Load, kips
Concrete Strain, με

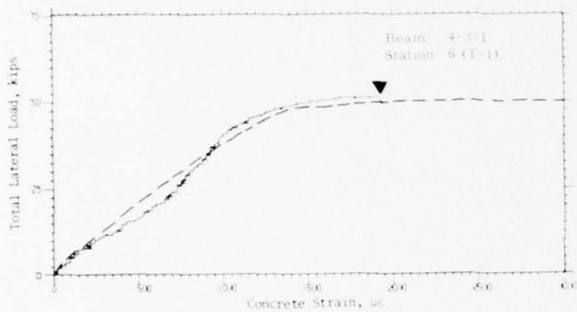
Beam 4-3-1
Station 6 (T-1)
Total Lateral Load, kips
Concrete Strain, με

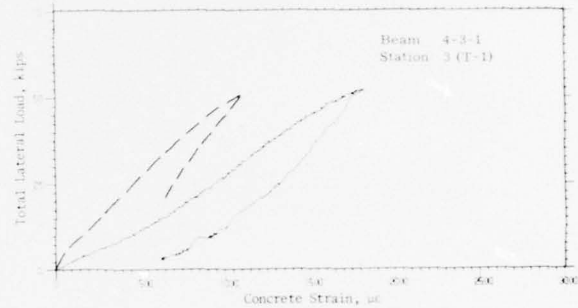
Beam 4-3-1
Station 3 (T-1)
Total Lateral Load, kips
Concrete Strain, με

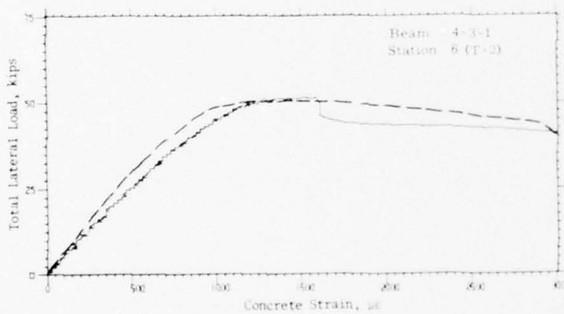
Beam 4-3-1
Total Lateral Load, kips
Concrete Strain, με

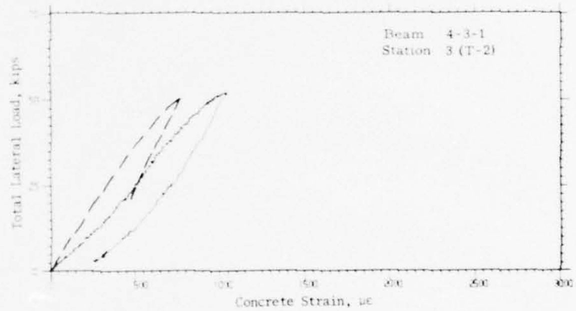
Beam 4-3-1
Station 3 (T-2)
Total Lateral Load, kips
Concrete Strain, με

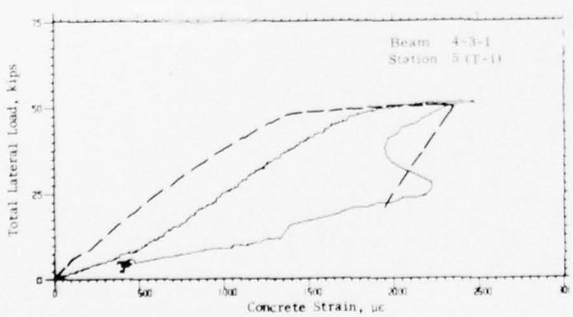
Beam 4-3-1
Station 5 (T-1)
Total Lateral Load, kips
Concrete Strain, με

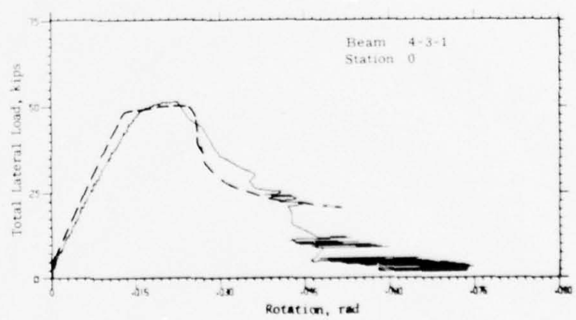
Beam 4-3-1
Station 0
Total Lateral Load, kips
Rotation, rad

Beam	4-3-2
f'_c	5423 psi
K = P/F	3.15
Test Date	6/26/73
Test Duration	9.9 min

Legend:

———————	Experimental Results
— — — —	Analytical Results
▼	Gage Failure

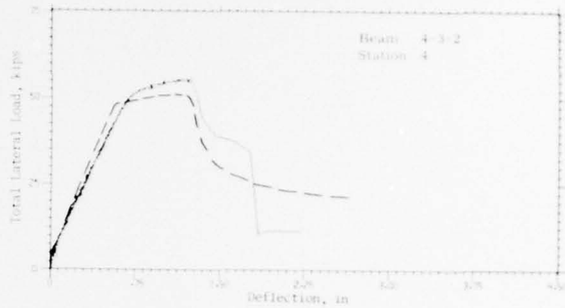

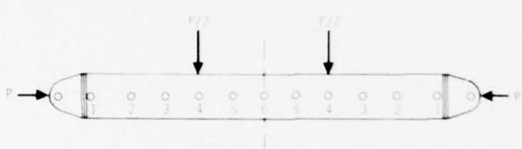

Loading Configuration and Station Location

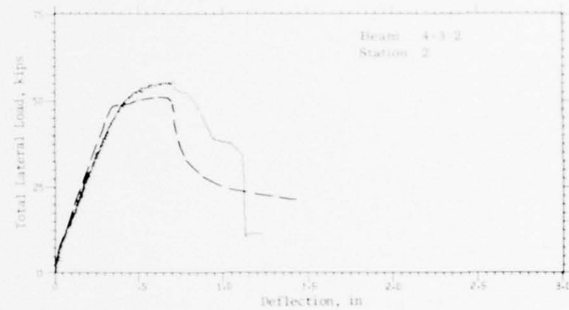

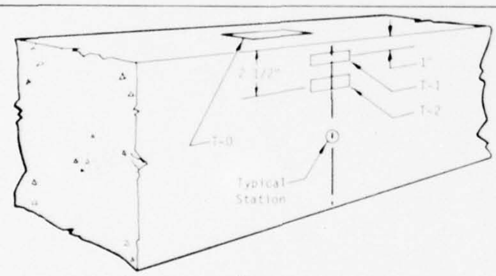

Concrete Strain Measurement Location

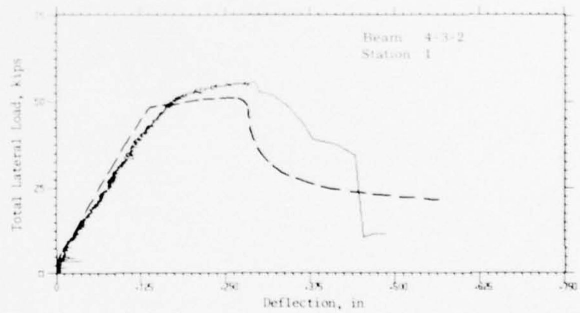

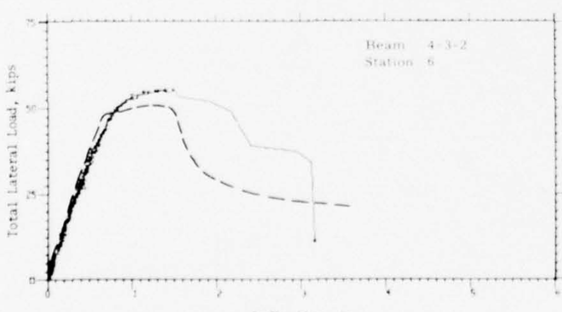

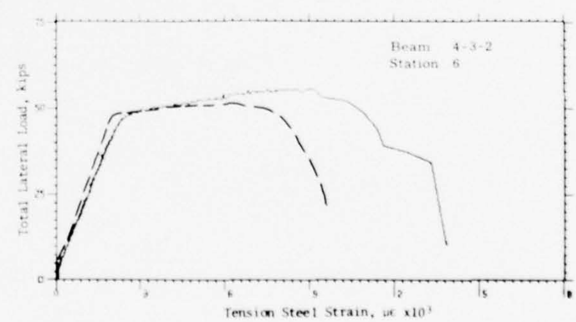

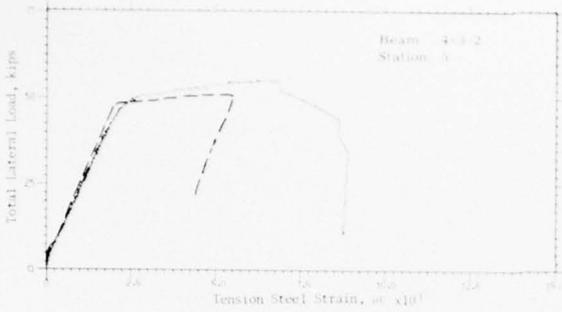
Beam 4-3-2
Station 5
Total Lateral Load, kips
Tension Steel Strain, με x10¹

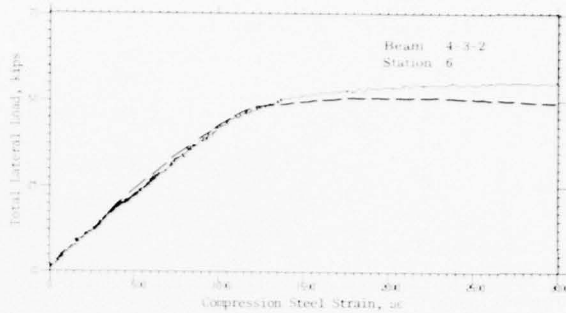
Beam 4-3-2
Station 6
Total Lateral Load, kips
Compression Steel Strain, με

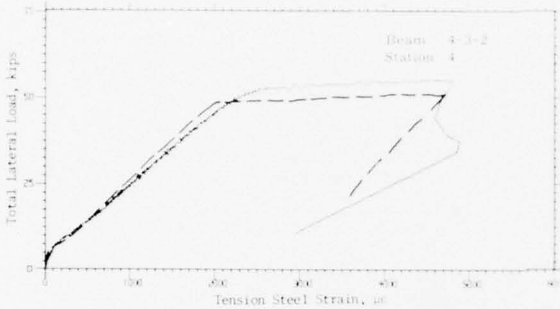
Beam 4-3-2
Station 4
Total Lateral Load, kips
Tension Steel Strain, με

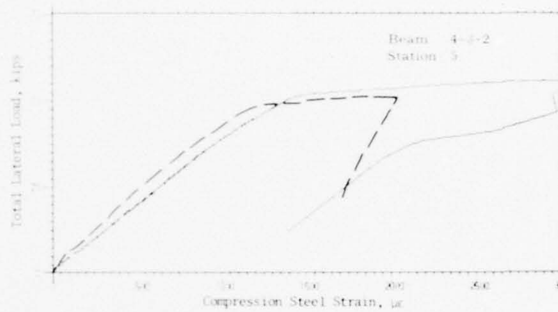
Beam 4-3-2
Station 5
Total Lateral Load, kips
Compression Steel Strain, με

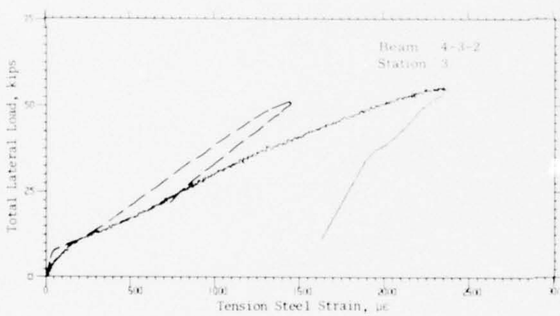
Beam 4-3-2
Station 3
Total Lateral Load, kips
Tension Steel Strain, με

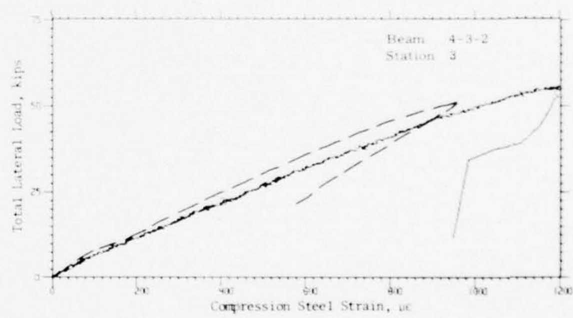
Beam 4-3-2
Station 3
Total Lateral Load, kips
Compression Steel Strain, με

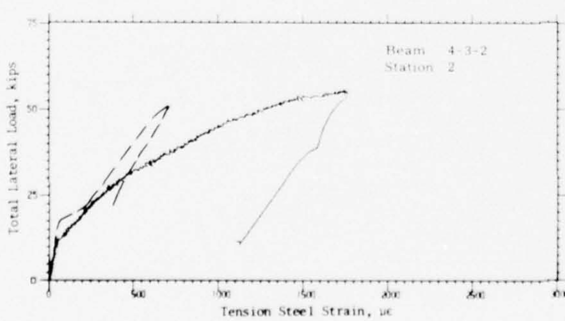
Beam 4-3-2
Station 2
Total Lateral Load, kips
Tension Steel Strain, με

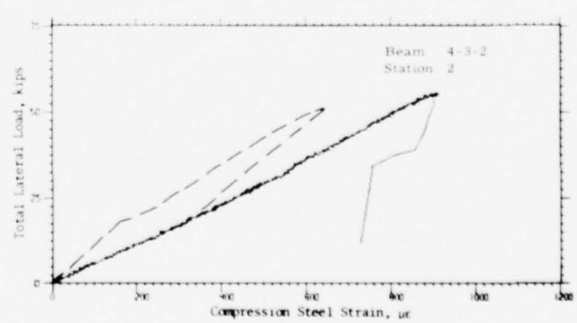
Beam 4-3-2
Station 2
Total Lateral Load, kips
Compression Steel Strain, με

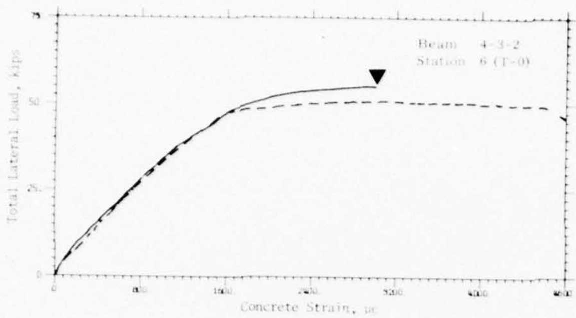
Beam 4-3-2
Station 6 (T-0)
Total Lateral Load, kips
Concrete Strain, με

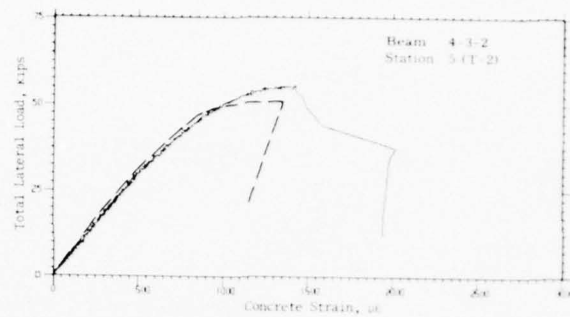
Beam 4-3-2
Station 5 (T-2)
Total Lateral Load, kips
Concrete Strain, με

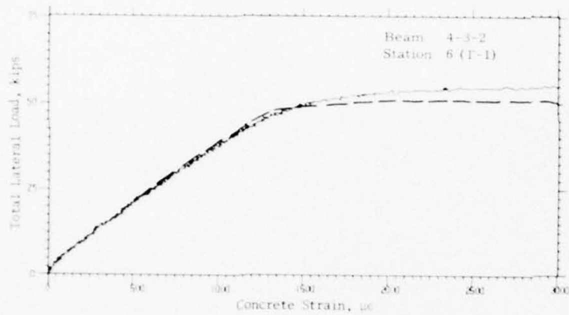
Beam 4-3-2
Station 6 (T-1)
Total Lateral Load, kips
Concrete Strain, με

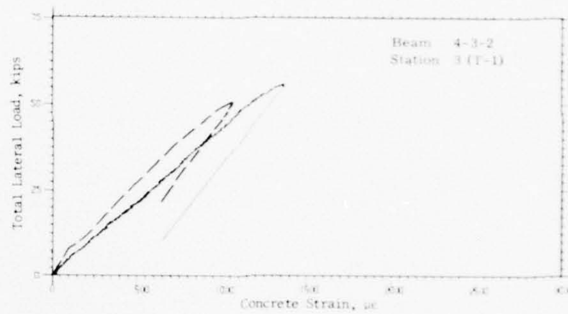
Beam 4-3-2
Station 3 (T-1)
Total Lateral Load, kips
Concrete Strain, με

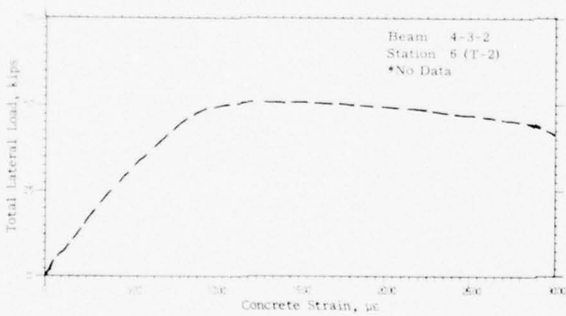
Beam 4-3-2
Station 6 (T-2)
*No Data
Total Lateral Load, kips
Concrete Strain, με

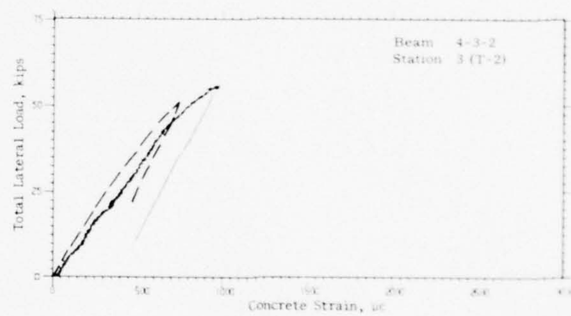
Beam 4-3-2
Station 3 (T-2)
Total Lateral Load, kips
Concrete Strain, με

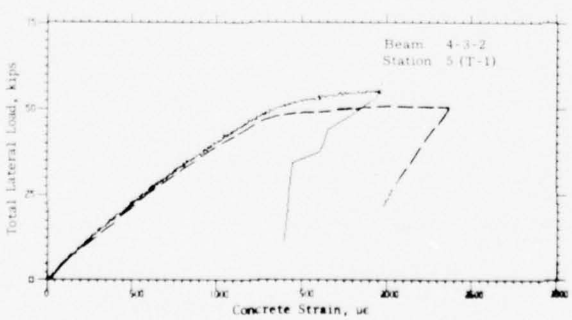
Beam 4-3-2
Station 5 (T-1)
Total Lateral Load, kips
Concrete Strain, με

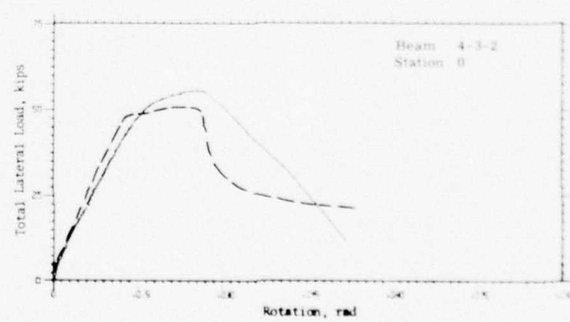
Beam 4-3-2
Station 0
Total Lateral Load, kips
Rotation, rad

Beam	3-0-1
f'_c	5142 psi
K = P/F	0
Test Date	7/17/73
Test Duration	6.3 min

Legend:

————	Experimental Results
– – – –	Analytical Results
▼	Gage Failure

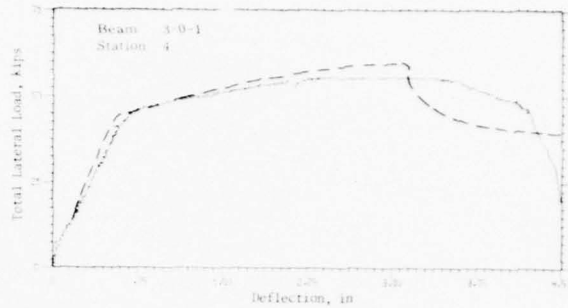

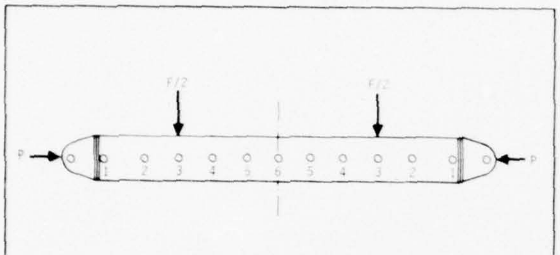

Loading Configuration and Station Location

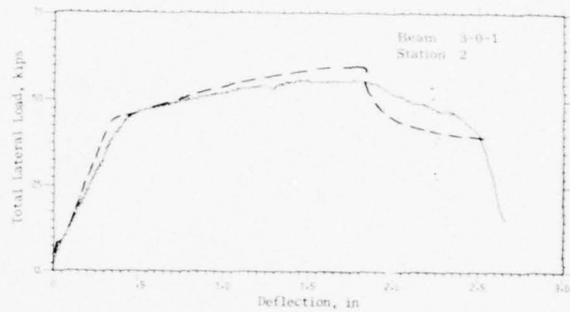

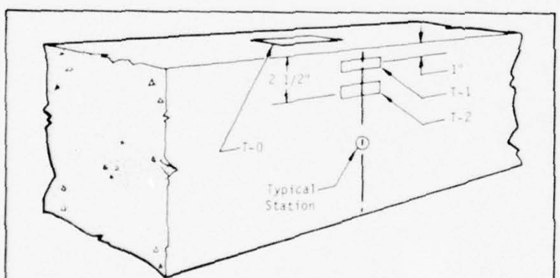

Concrete Strain Measurement Location

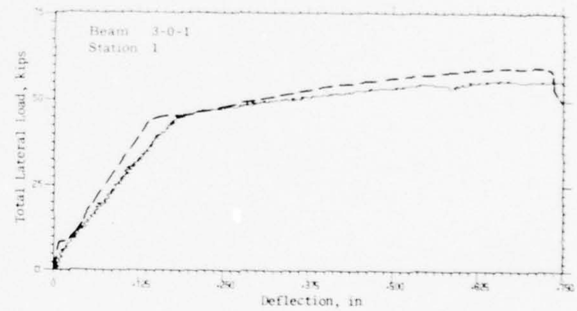

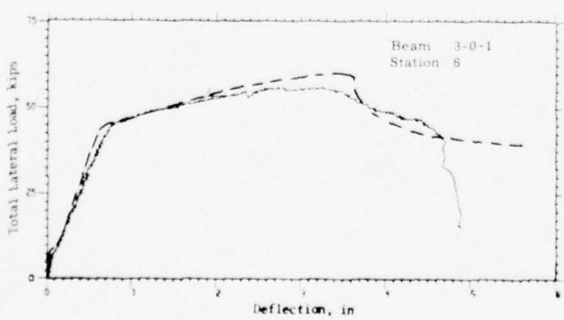

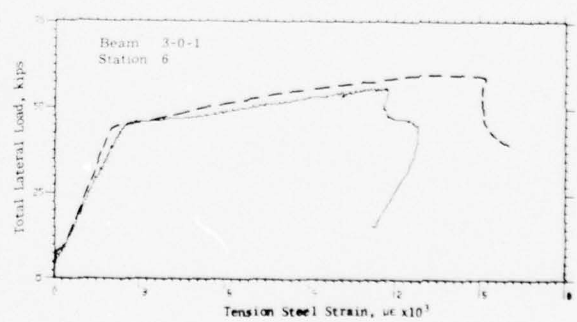

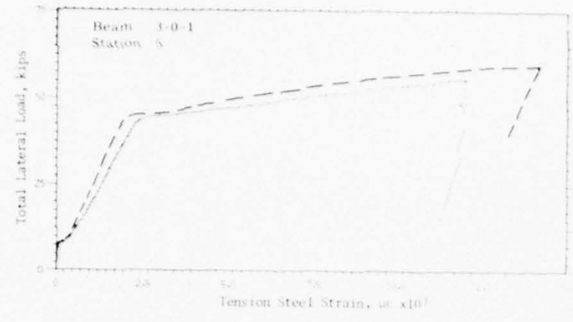
Beam 3-0-1
Station 5
Total Lateral Load, kips
Tension Steel Strain, με x10³

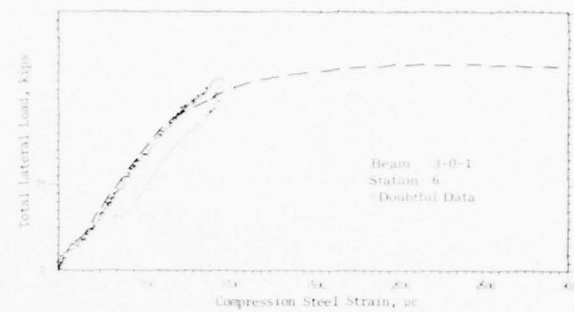
Beam 3-0-1
Station 6
Doubtful Data
Total Lateral Load, kips
Compression Steel Strain, με

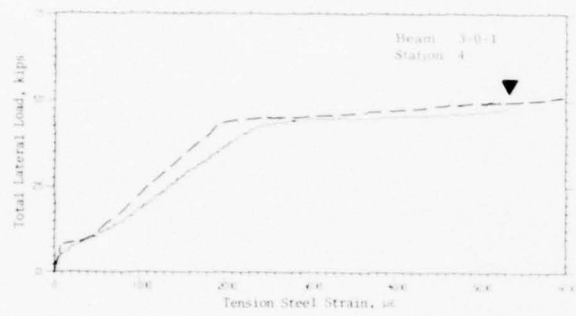
Beam 3-0-1
Station 4
Total Lateral Load, kips
Tension Steel Strain, με

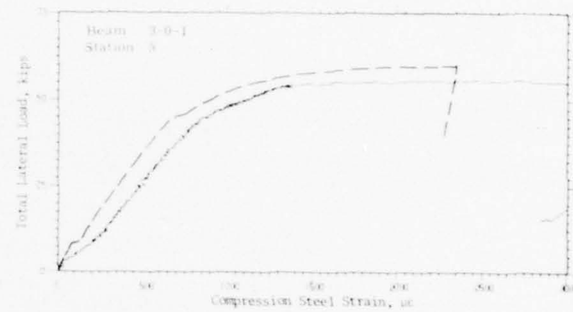
Beam 3-0-1
Station 3
Total Lateral Load, kips
Compression Steel Strain, με

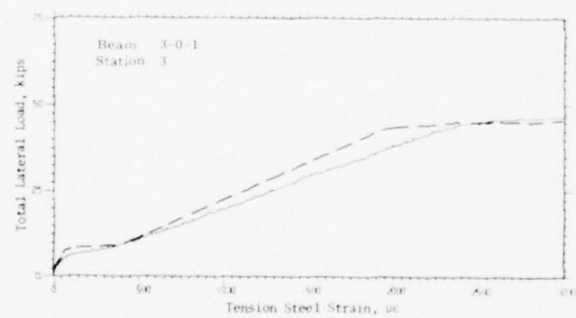
Beam 3-0-1
Station 3
Total Lateral Load, kips
Tension Steel Strain, με

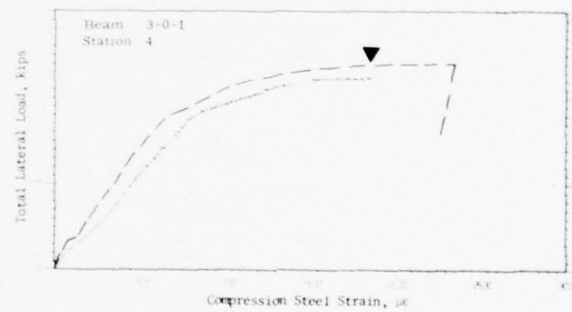
Beam 3-0-1
Station 4
Total Lateral Load, kips
Compression Steel Strain, με

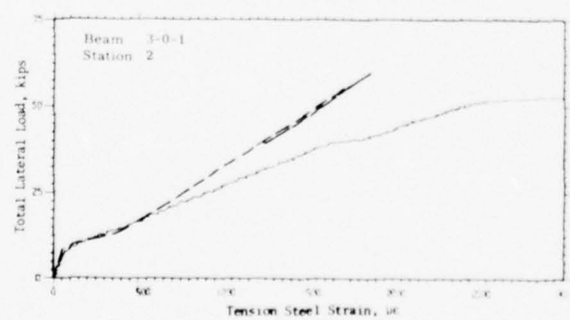
Beam 3-0-1
Station 2
Total Lateral Load, kips
Tension Steel Strain, με

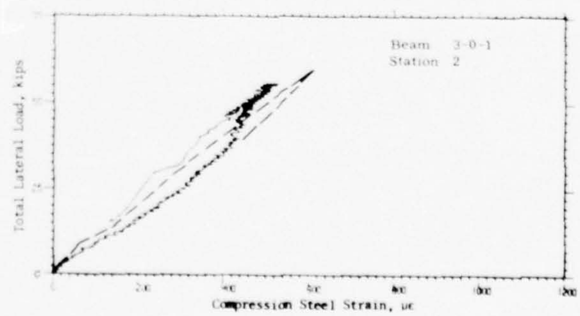
Beam 3-0-1
Station 2
Total Lateral Load, kips
Compression Steel Strain, με

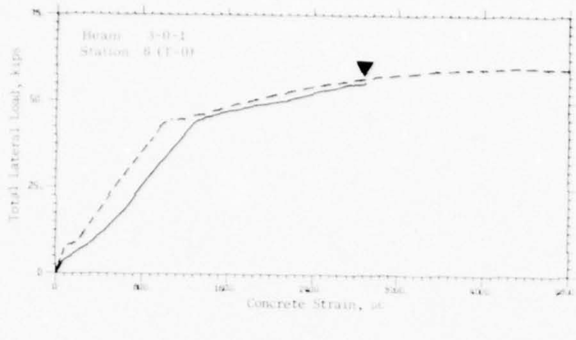
Beam 3-0-1
Station 6 (T-0)
Total Lateral Load, kips
Concrete Strain, με

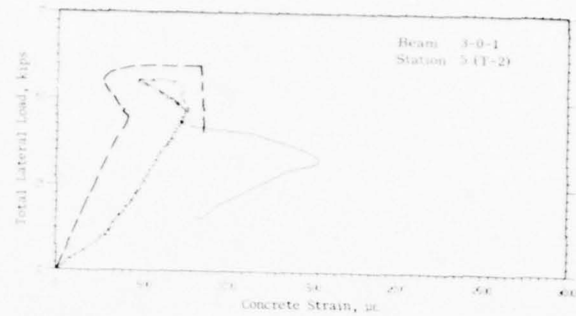
Beam 3-0-1
Station 5 (T-2)
Total Lateral Load, kips
Concrete Strain, με

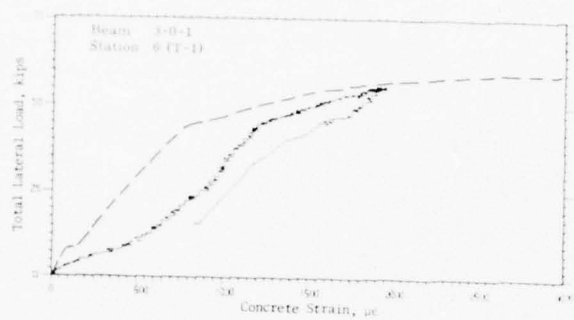
Beam 3-0-1
Station 6 (T-1)
Total Lateral Load, kips
Concrete Strain, με


Beam 3-0-1
Station 2 (T-1)
Total Lateral Load, kips
Concrete Strain, με

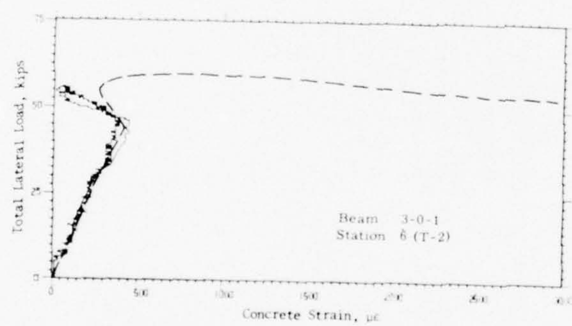
Beam 3-0-1
Station 6 (T-2)
Total Lateral Load, kips
Concrete Strain, με

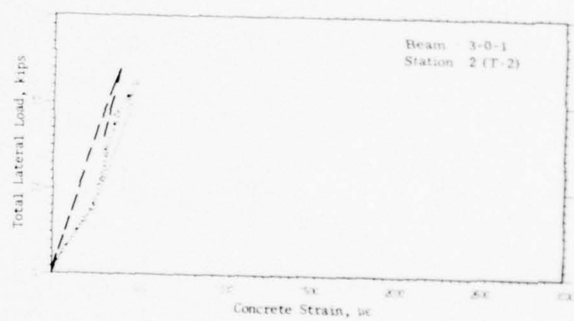
Beam 3-0-1
Station 2 (T-2)
Total Lateral Load, kips
Concrete Strain, με

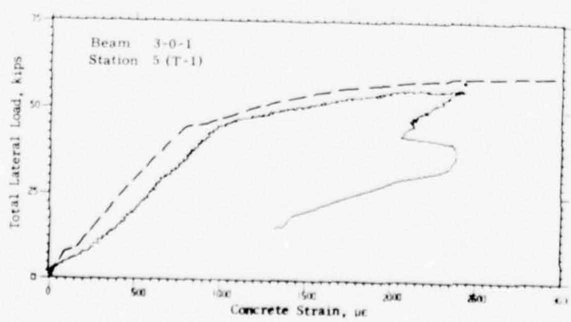
Beam 3-0-1
Station 5 (T-1)
Total Lateral Load, kips
Concrete Strain, με

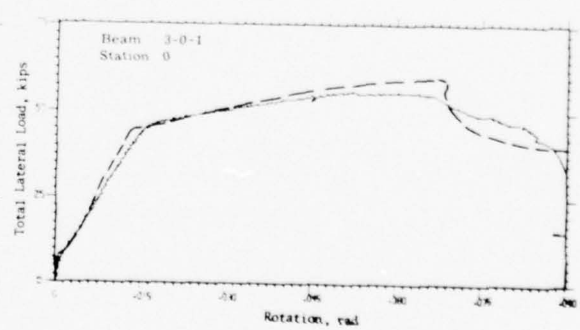
Beam 3-0-1
Station 0
Total Lateral Load, kips
Rotation, rad

Beam	3-2-1
f'_c	4792 psi
K = P/F	1.85
Test Date	7/20/73
Test Duration	6.3 min

Legend:

——————— Experimental Results

– – – – – – Analytical Results

▼ Gage Failure

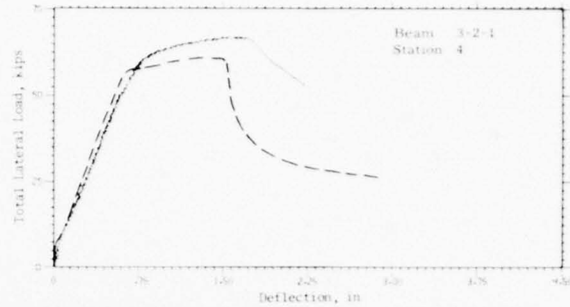

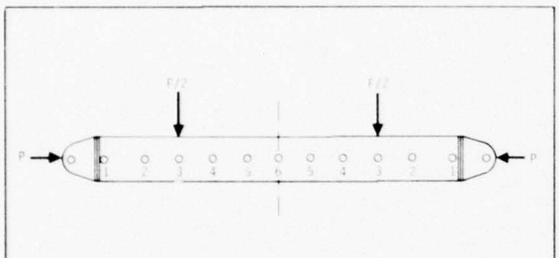

Loading Configuration
and Station Location

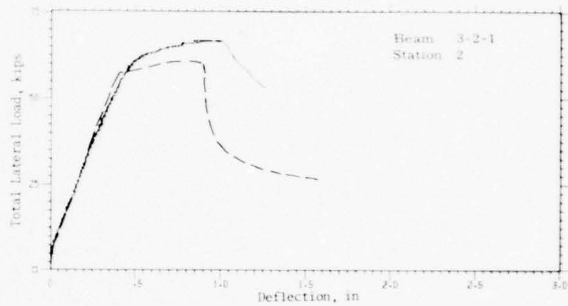

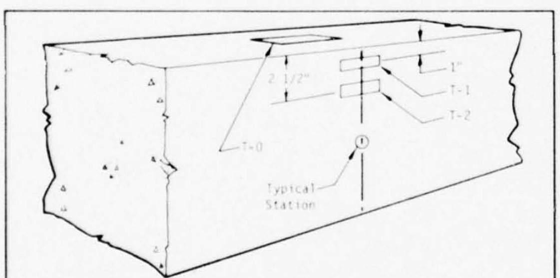

Concrete Strain Measurement Location

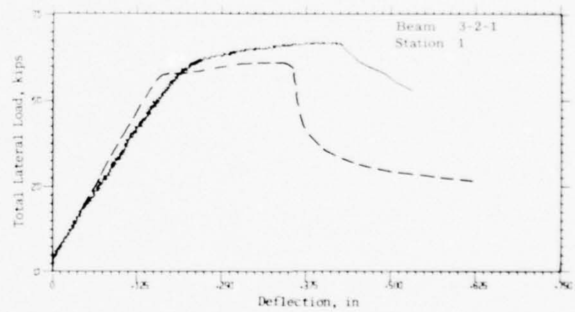

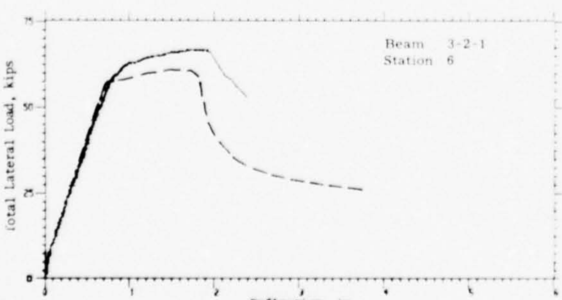

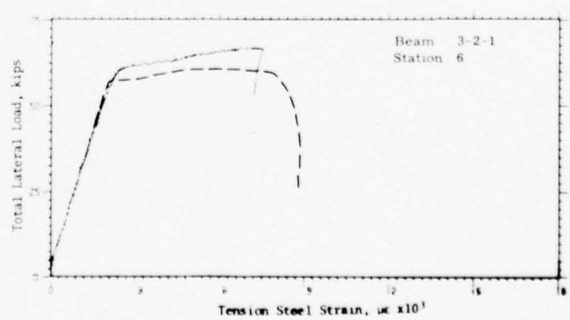

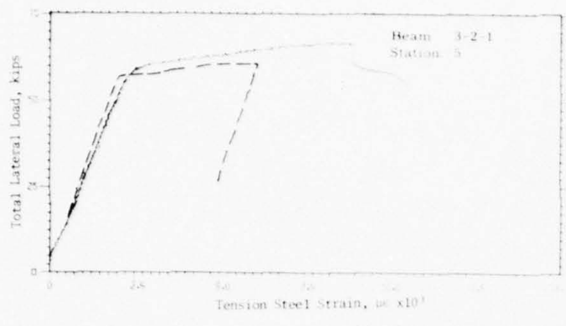
Beam 3-2-1
Station 5
Total Lateral Load, kips
Tension Steel Strain, με x10³

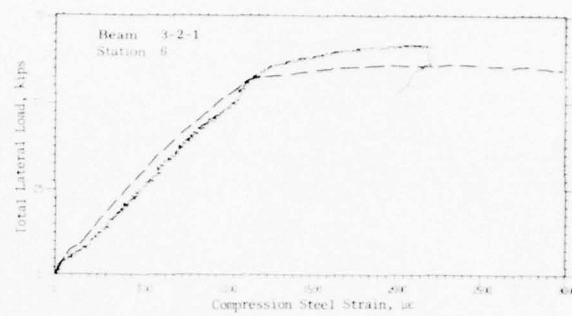
Beam 3-2-1
Station 6
Total Lateral Load, kips
Compression Steel Strain, με

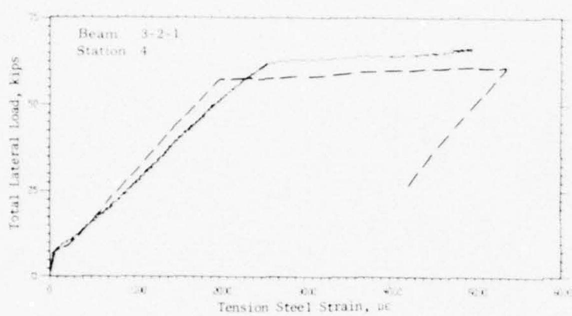
Beam 3-2-1
Station 4
Total Lateral Load, kips
Tension Steel Strain, με

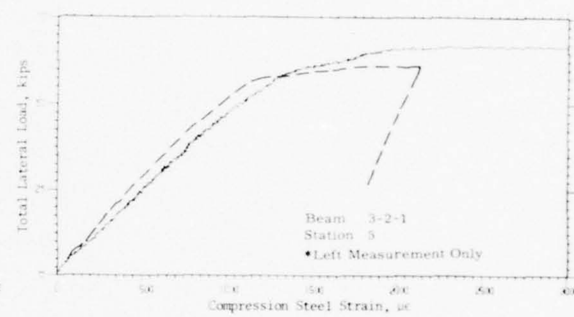
Beam 3-2-1
Station 5
*Left Measurement Only
Total Lateral Load, kips
Compression Steel Strain, με

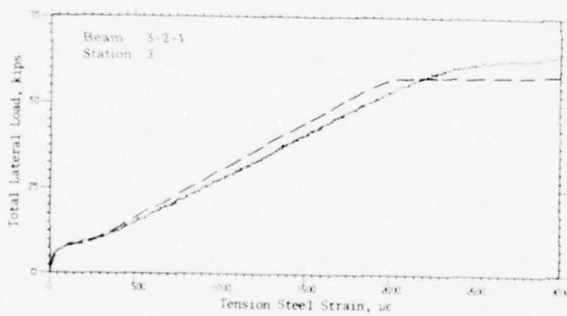
Beam 3-2-1
Station 3
Total Lateral Load, kips
Tension Steel Strain, με

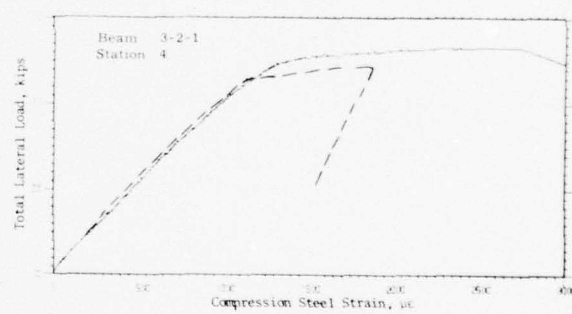
Beam 3-2-1
Station 4
Total Lateral Load, kips
Compression Steel Strain, με

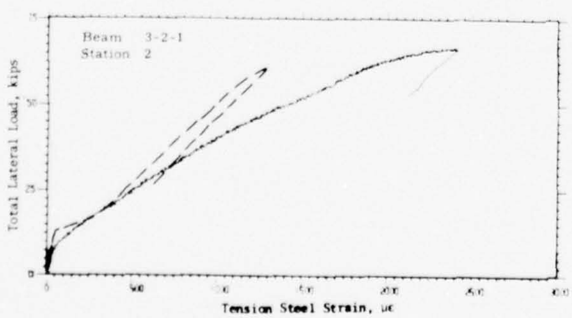
Beam 3-2-1
Station 2
Total Lateral Load, kips
Tension Steel Strain, με

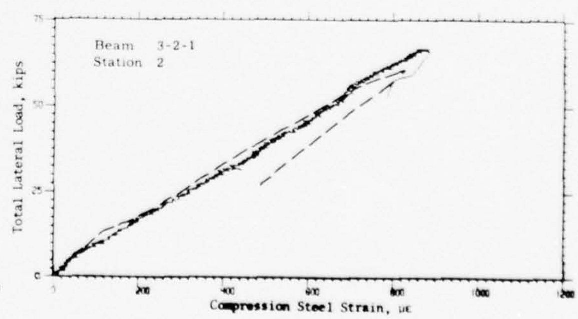
Beam 3-2-1
Station 2
Total Lateral Load, kips
Compression Steel Strain, με

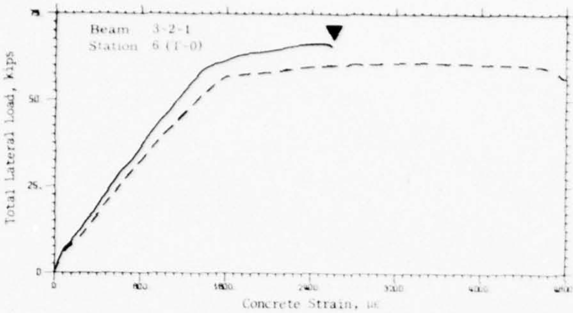
Beam 3-2-1
Station 6 (T-0)
Total Lateral Load, kips
Concrete Strain, με

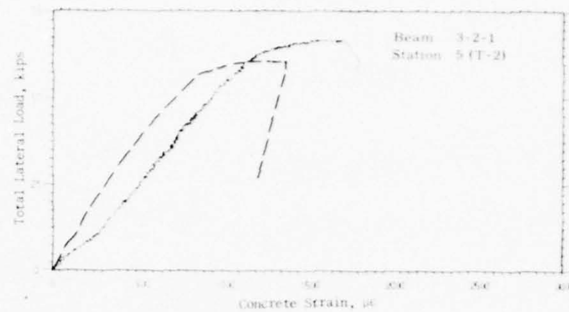
Beam 3-2-1
Station 5 (T-2)
Total Lateral Load, kips
Concrete Strain, με

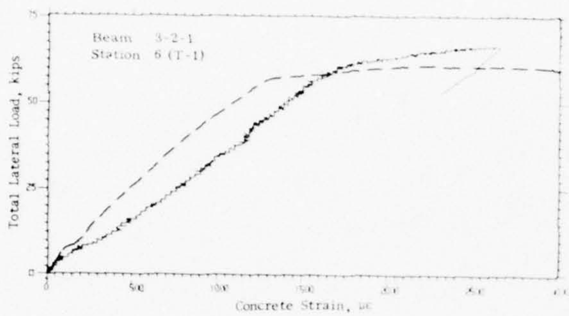
Beam 3-2-1
Station 6 (T-1)
Total Lateral Load, kips
Concrete Strain, με

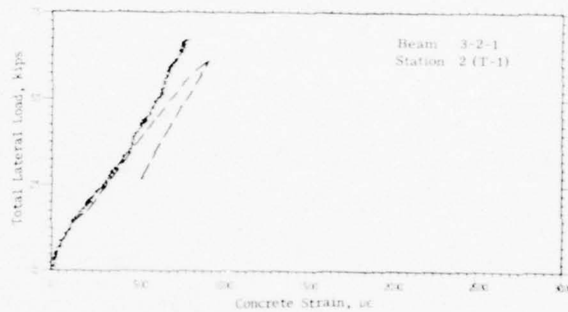
Beam 3-2-1
Station 2 (T-1)
Total Lateral Load, kips
Concrete Strain, με

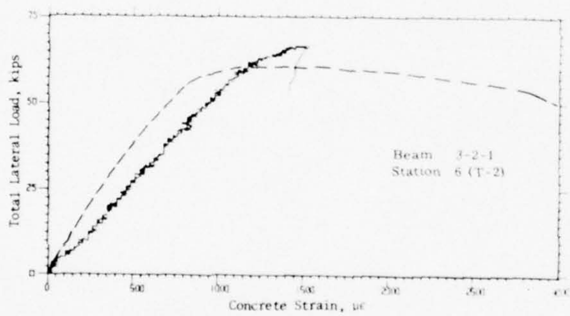
Beam 3-2-1
Station 6 (T-2)
Total Lateral Load, kips
Concrete Strain, με

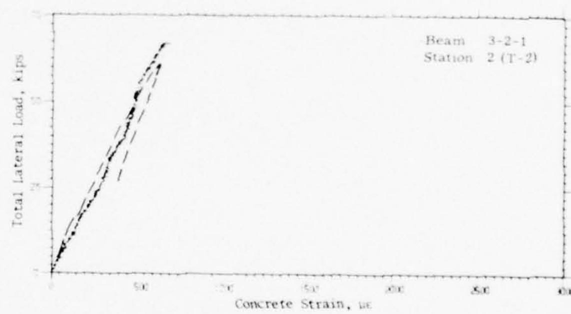
Beam 3-2-1
Station 2 (T-2)
Total Lateral Load, kips
Concrete Strain, με

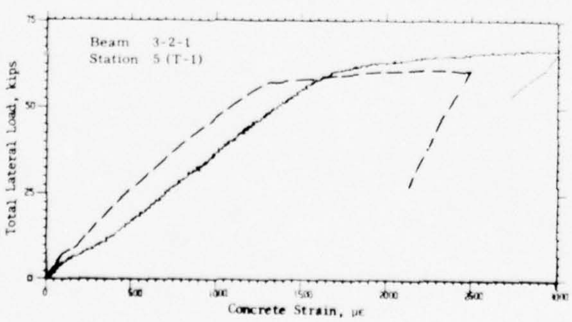
Beam 3-2-1
Station 5 (T-1)
Total Lateral Load, kips
Concrete Strain, με

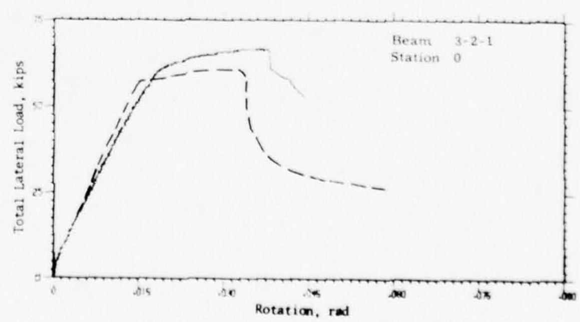
Beam 3-2-1
Station 0
Total Lateral Load, kips
Rotation, rad

Beam 3-2-2
f'_c 4881 psi
K = P/F 1.87
Test Date 7/24/73
Test Duration 4.3 min

Legend:
———— Experimental Results
– – – – Analytical Results
▼ Gage Failure

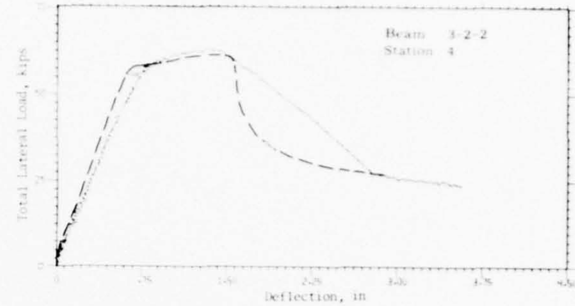

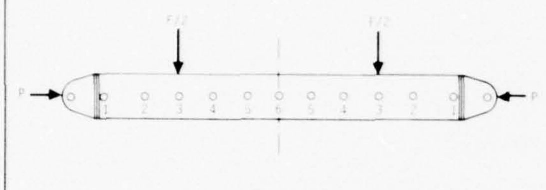

Loading Configuration
and Station Location

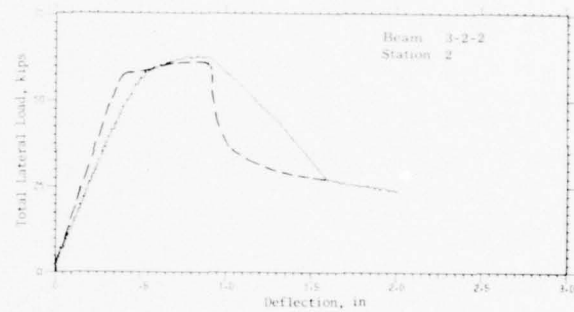

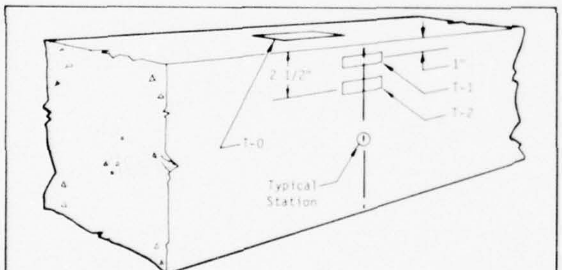

Concrete Strain Measurement Location

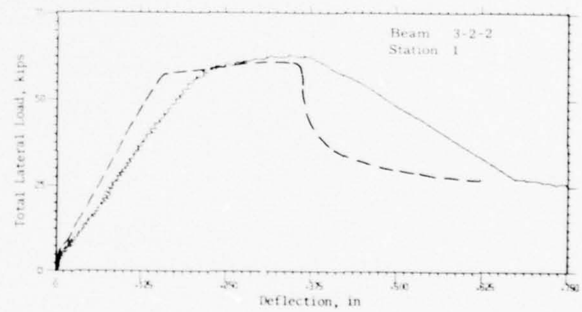

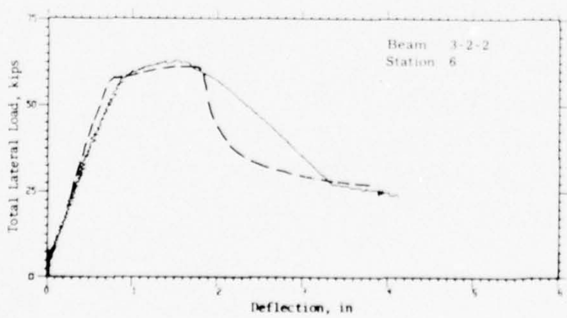

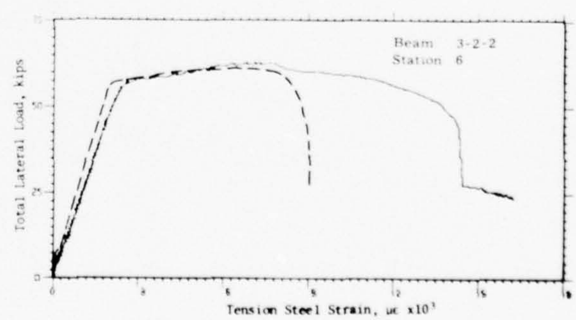

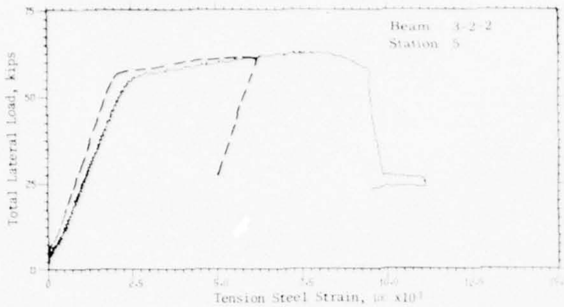
Beam 3-2-2
Station 5
Total Lateral Load, kips
Tension Steel Strain, με x10³

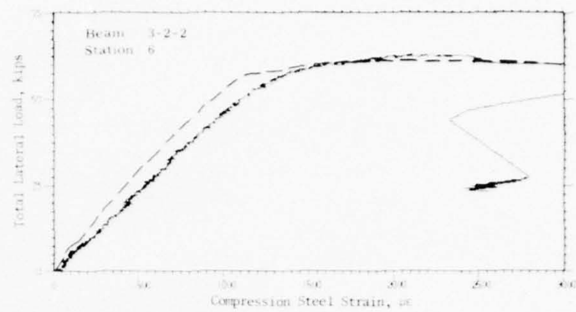
Beam 3-2-2
Station 6
Total Lateral Load, kips
Compression Steel Strain, με

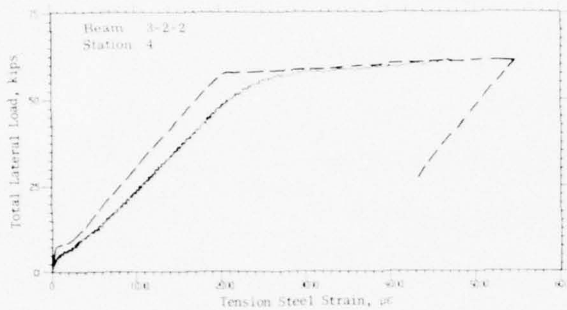
Beam 3-2-2
Station 4
Total Lateral Load, kips
Tension Steel Strain, με

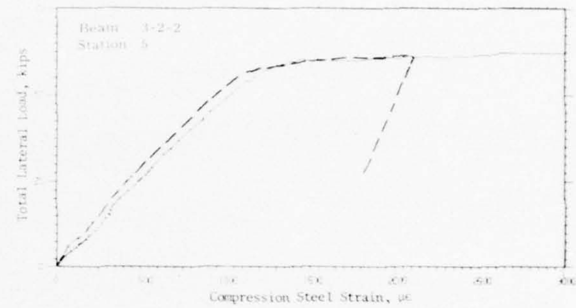
Beam 3-2-2
Station 5
Total Lateral Load, kips
Compression Steel Strain, με

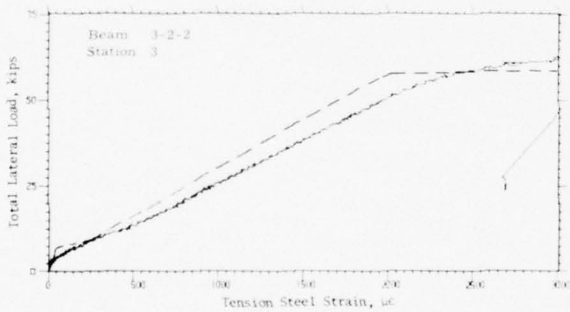
Beam 3-2-2
Station 3
Total Lateral Load, kips
Tension Steel Strain, με

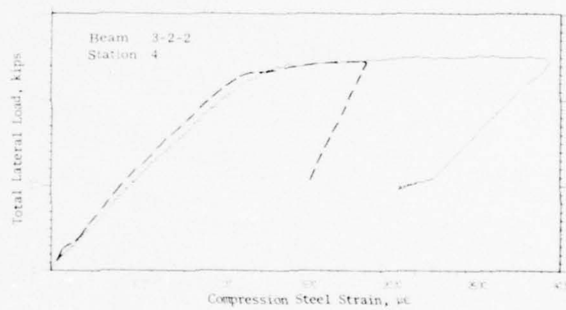
Beam 3-2-2
Station 4
Total Lateral Load, kips
Compression Steel Strain, με

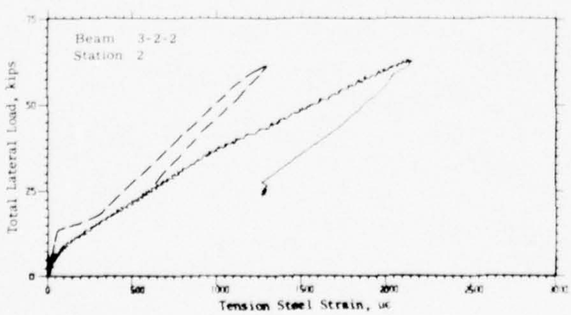
Beam 3-2-2
Station 2
Total Lateral Load, kips
Tension Steel Strain, με

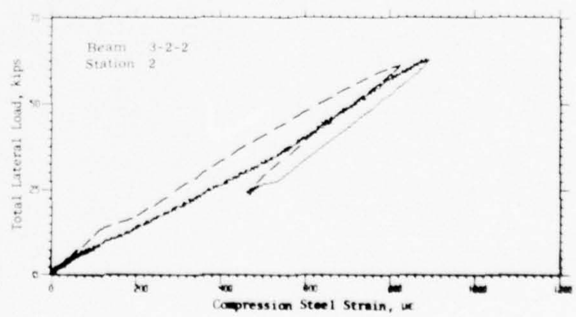
Beam 3-2-2
Station 2
Total Lateral Load, kips
Compression Steel Strain, με

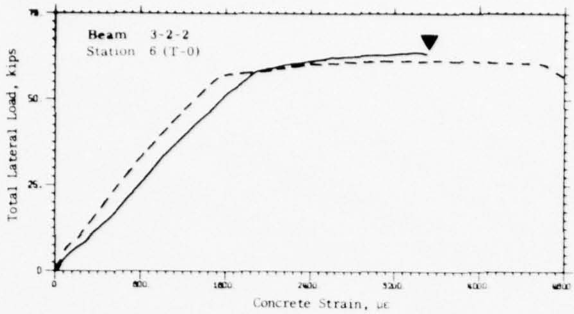
Beam 3-2-2
Station 6 (T-0)
Total Lateral Load, kips
Concrete Strain, με

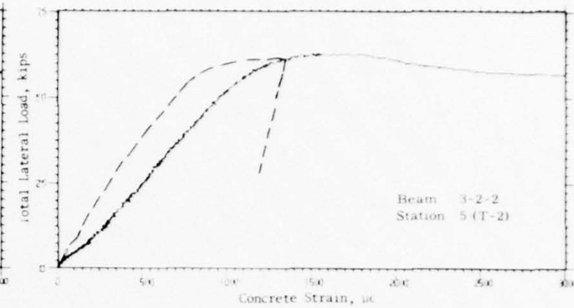
Beam 3-2-2
Station 5 (T-2)
Total Lateral Load, kips
Concrete Strain, με

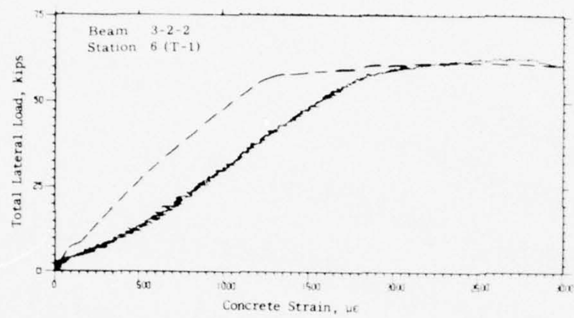
Beam 3-2-2
Station 6 (T-1)
Total Lateral Load, kips
Concrete Strain, με

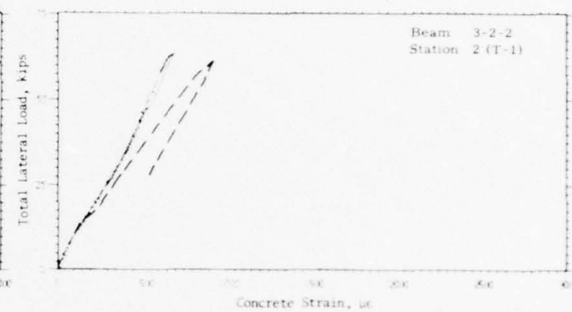
Beam 3-2-2
Station 2 (T-1)
Total Lateral Load, kips
Concrete Strain, με

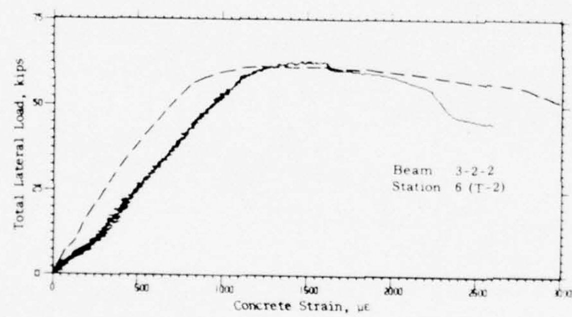
Beam 3-2-2
Station 6 (T-2)
Total Lateral Load, kips
Concrete Strain, με

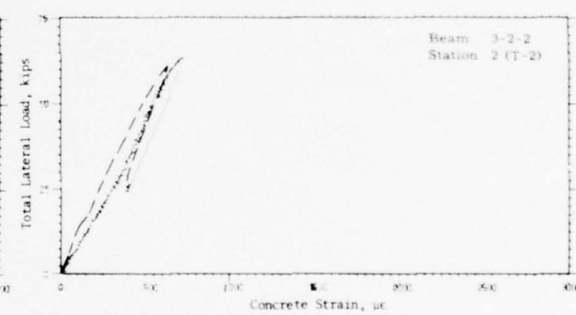
Beam 3-2-2
Station 2 (T-2)
Total Lateral Load, kips
Concrete Strain, με

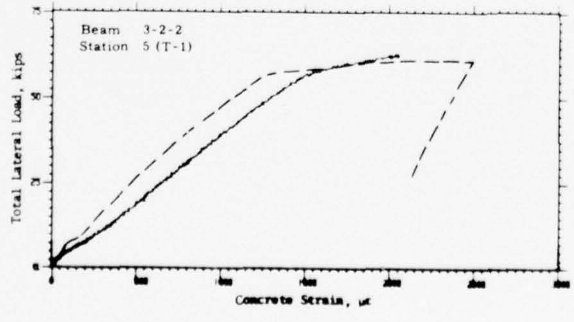
Beam 3-2-2
Station 5 (T-1)
Total Lateral Load, kips
Concrete Strain, με

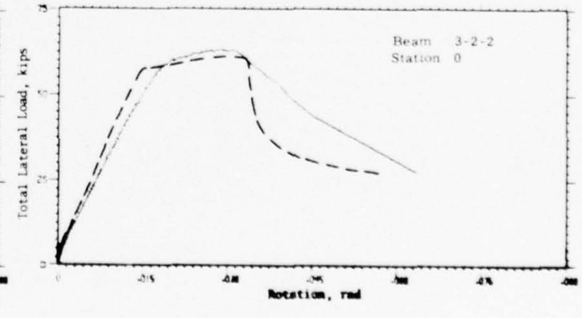
Beam 3-2-2
Station 0
Total Lateral Load, kips
Rotation, rad

Beam	3-3-1
f'_c	5252 psi
K = P/F	3.03
Test Date	7/26/73
Test Duration	7.5 min

Legend:

———————— Experimental Results

– – – – – – Analytical Results

▼ Gage Failure

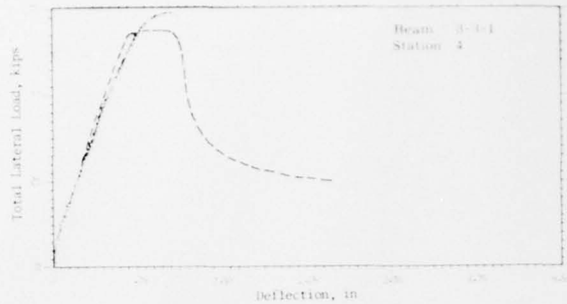

Loading Configuration and Station Location

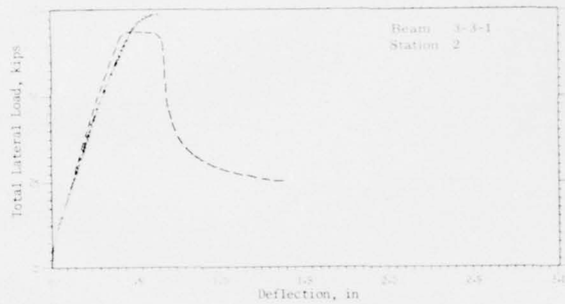

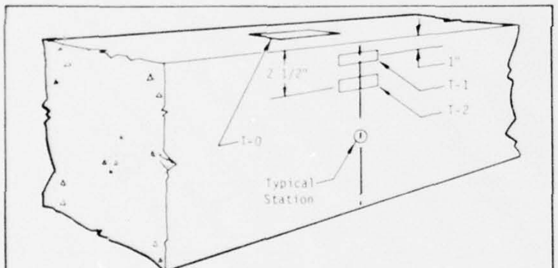

Concrete Strain Measurement Location

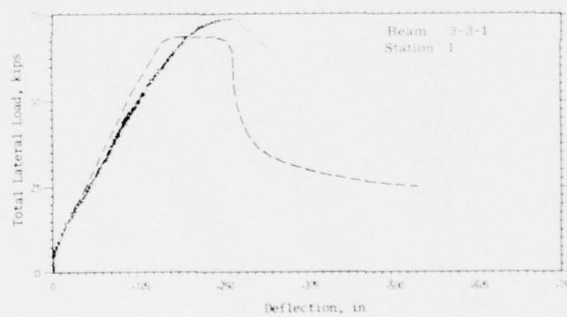

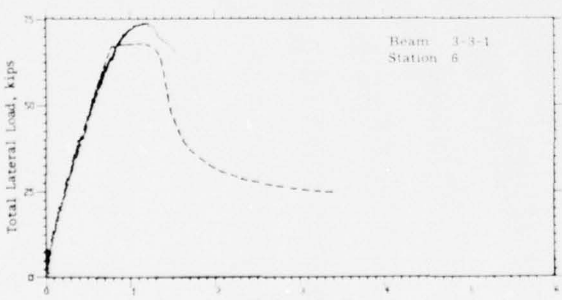

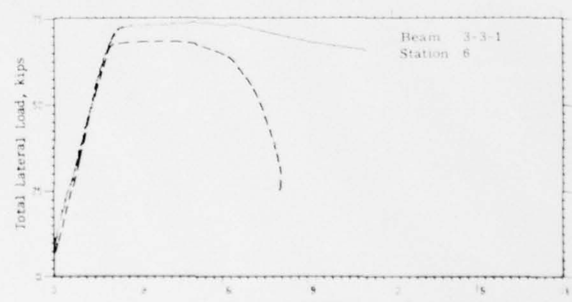

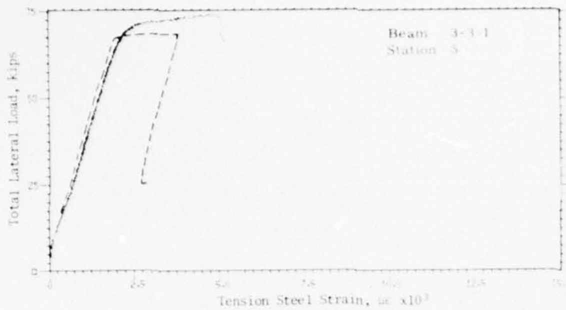
Beam 3-3-1
Station 3
Total Lateral Load, kips
Tension Steel Strain, με x10³

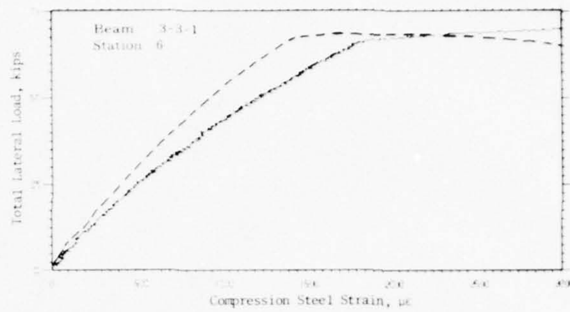
Beam 3-3-1
Station 6
Total Lateral Load, kips
Compression Steel Strain, με

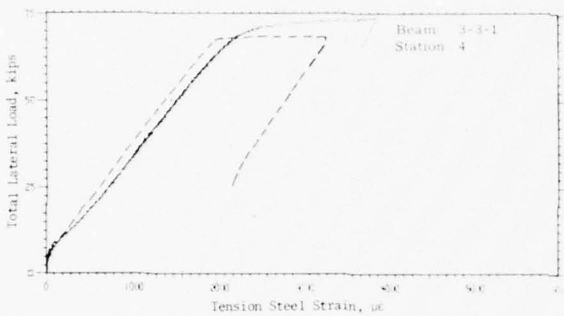
Beam 3-3-1
Station 4
Total Lateral Load, kips
Tension Steel Strain, με

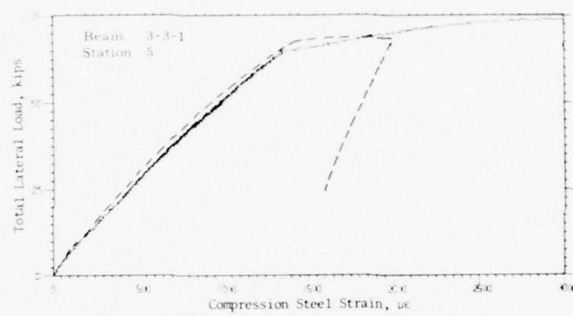
Beam 3-3-1
Station 5
Total Lateral Load, kips
Compression Steel Strain, με

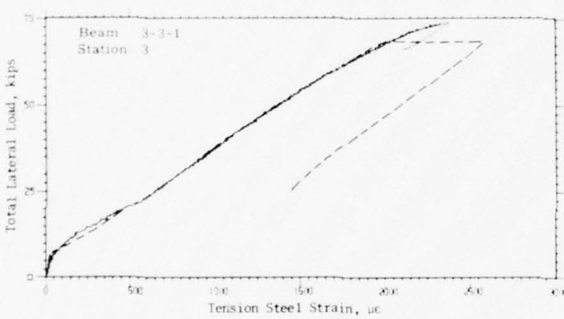
Beam 3-3-1
Station 3
Total Lateral Load, kips
Tension Steel Strain, με

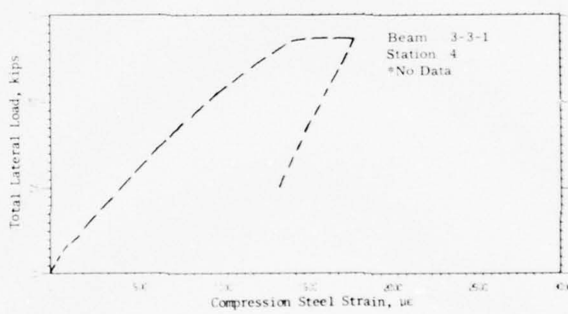
Beam 3-3-1
Station 4
*No Data
Total Lateral Load, kips
Compression Steel Strain, με

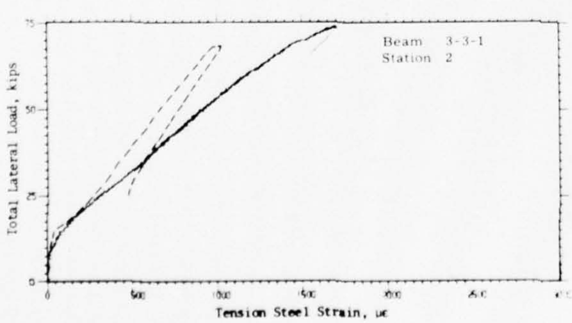
Beam 3-3-1
Station 2
Total Lateral Load, kips
Tension Steel Strain, με

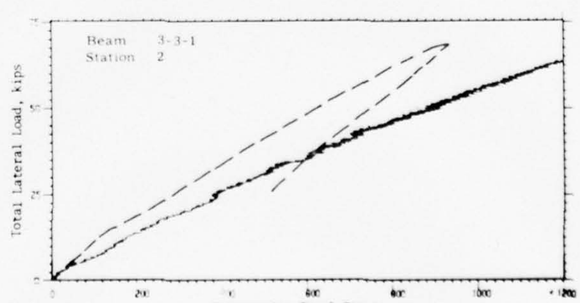
Beam 3-3-1
Station 2
Total Lateral Load, kips
Compression Steel Strain, με

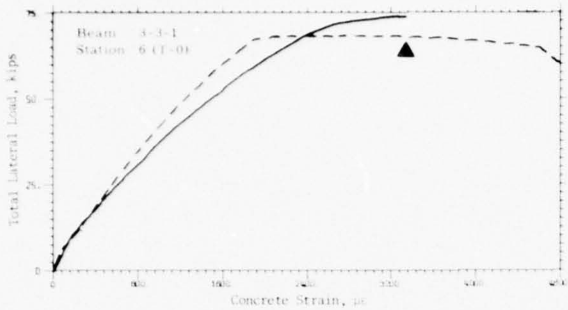
Beam 3-3-1
Station 6 (T-0)
Total Lateral Load, kips
Concrete Strain, µε

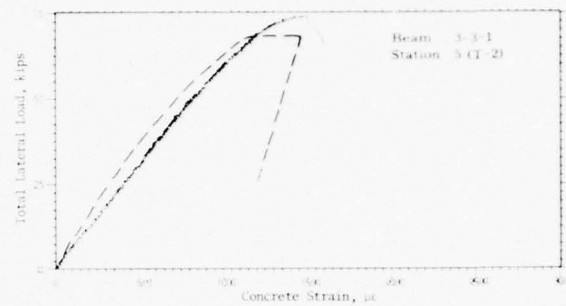
Beam 3-3-1
Station 5 (T-2)
Total Lateral Load, kips
Concrete Strain, µε

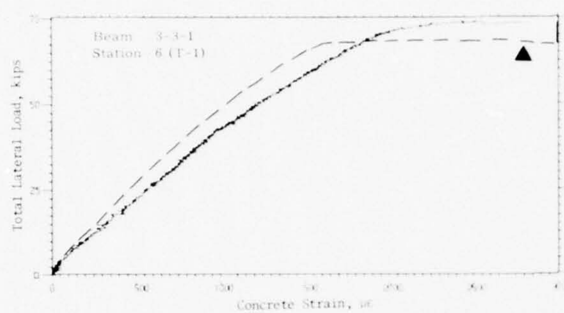
Beam 3-3-1
Station 6 (T-1)
Total Lateral Load, kips
Concrete Strain, µε

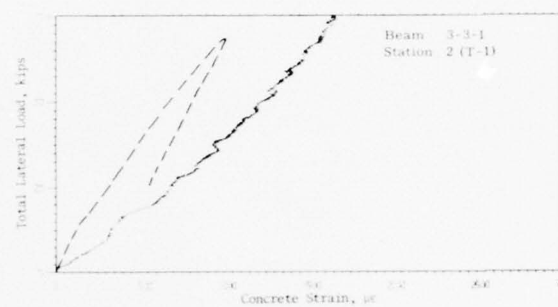
Beam 3-3-1
Station 2 (T-1)
Total Lateral Load, kips
Concrete Strain, µε

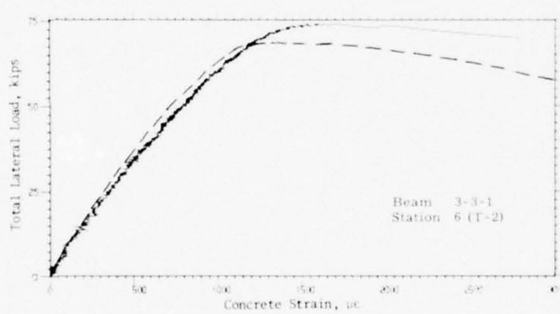
Beam 3-3-1
Station 6 (T-2)
Total Lateral Load, kips
Concrete Strain, µε

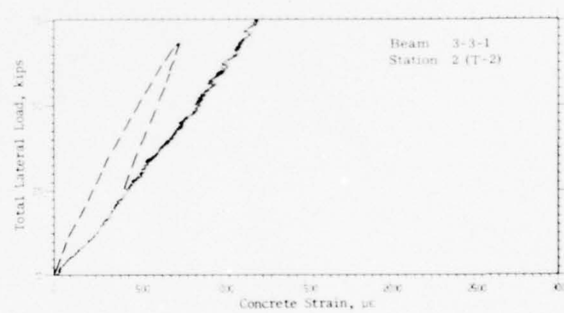
Beam 3-3-1
Station 2 (T-2)
Total Lateral Load, kips
Concrete Strain, µε

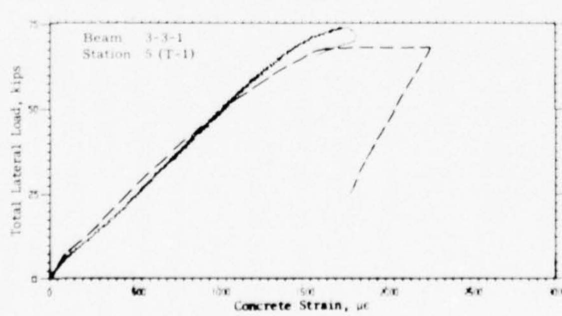
Beam 3-3-1
Station 5 (T-1)
Total Lateral Load, kips
Concrete Strain, µε

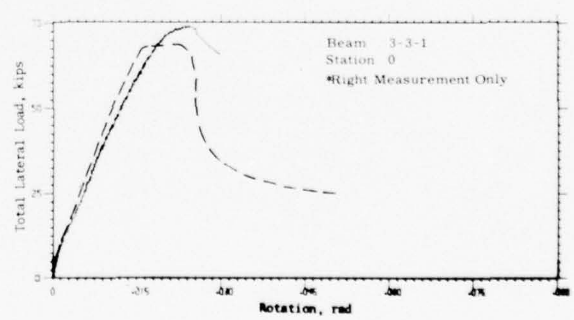
Beam 3-3-1
Station 0
*Right Measurement Only
Total Lateral Load, kips
Rotation, rad

Beam	3-3-2
f'_c	5028 psi
K = P/F	3.08
Test Date	7/30/73
Test Duration	1.7 min

Legend:

————	Experimental Results
– – – – –	Analytical Results
▼	Gage Failure

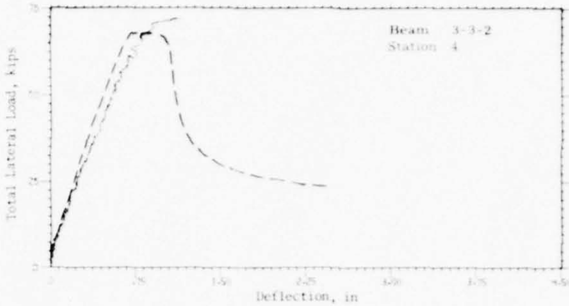

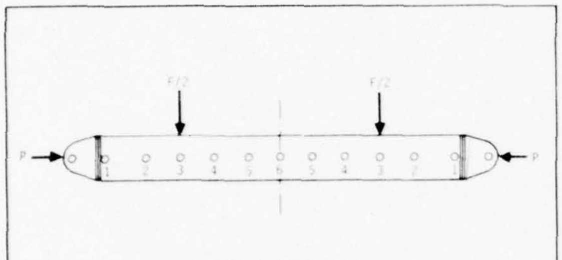

Loading Configuration
and Station Location

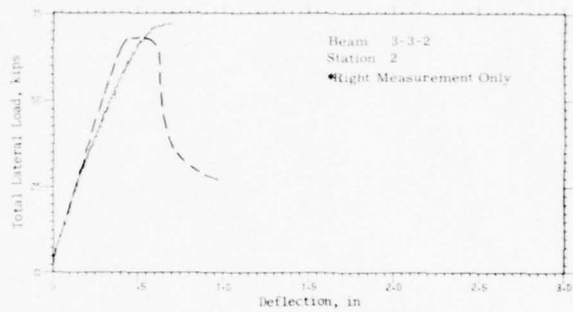

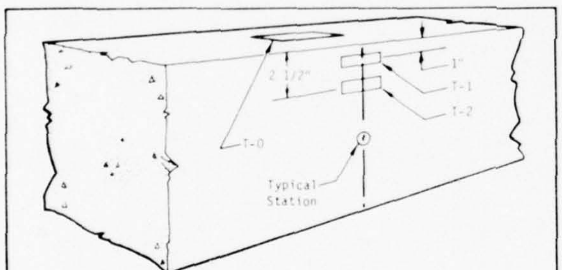

Concrete Strain Measurement Location

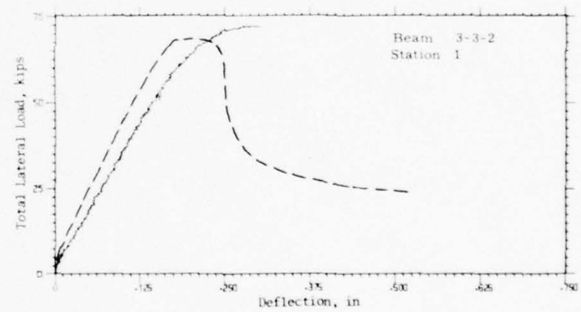

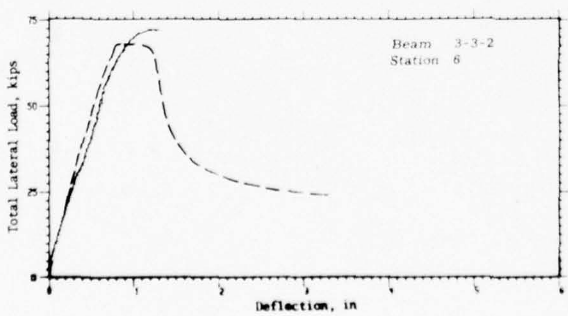

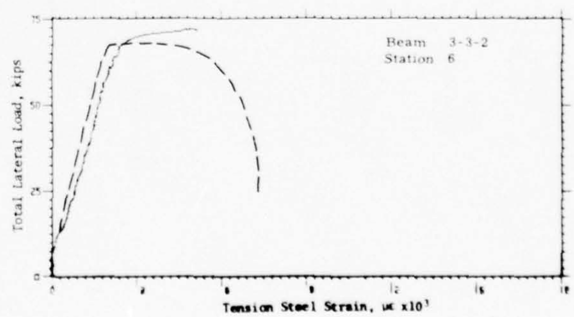

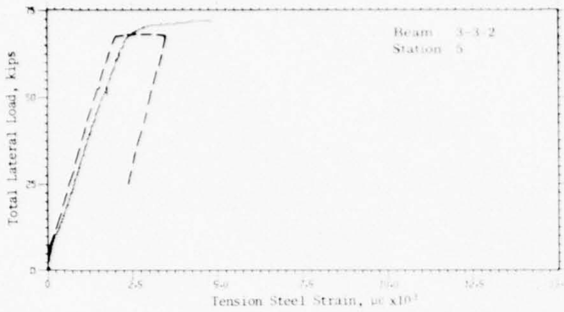
Beam 3-3-2
Station 5
Total Lateral Load, kips
Tension Steel Strain, με x10³

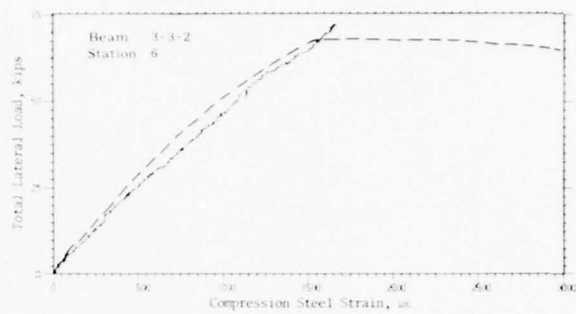
Beam 3-3-2
Station 6
Total Lateral Load, kips
Compression Steel Strain, με

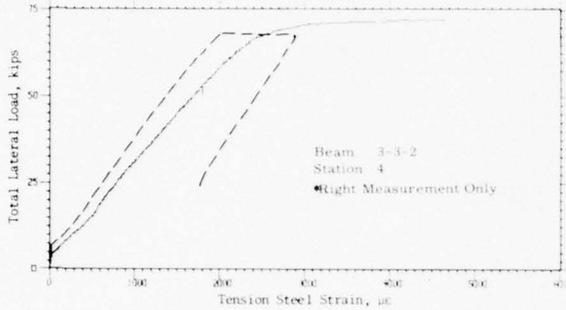
Beam 3-3-2
Station 4
*Right Measurement Only
Total Lateral Load, kips
Tension Steel Strain, με

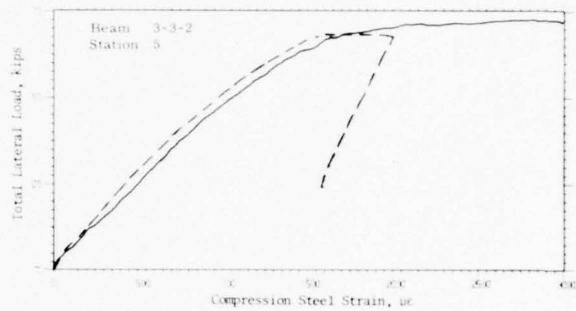
Beam 3-3-2
Station 5
Total Lateral Load, kips
Compression Steel Strain, με

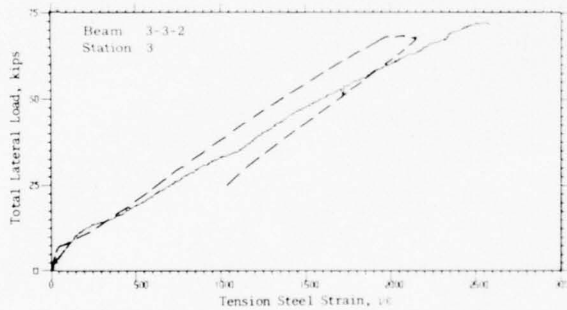
Beam 3-3-2
Station 3
Total Lateral Load, kips
Tension Steel Strain, με

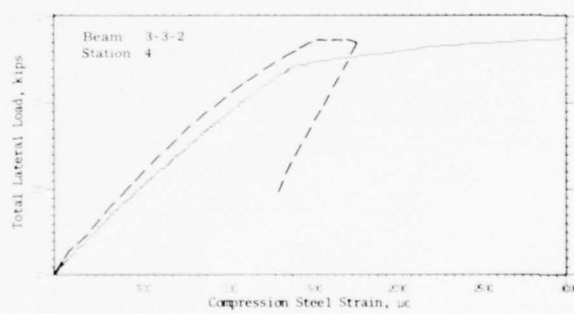
Beam 3-3-2
Station 4
Total Lateral Load, kips
Compression Steel Strain, με

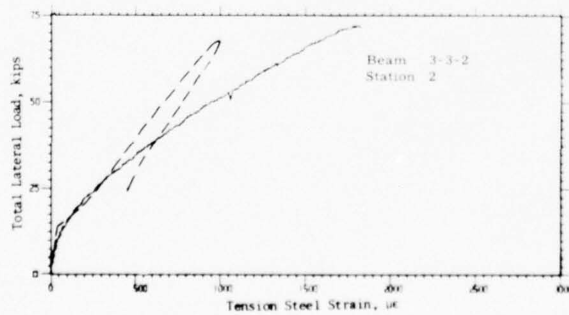
Beam 3-3-2
Station 2
Total Lateral Load, kips
Tension Steel Strain, με

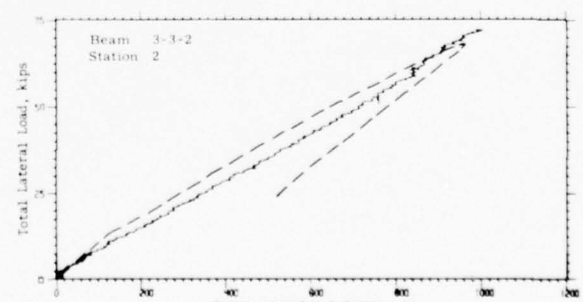
Beam 3-3-2
Station 2
Total Lateral Load, kips
Compression Steel Strain, με

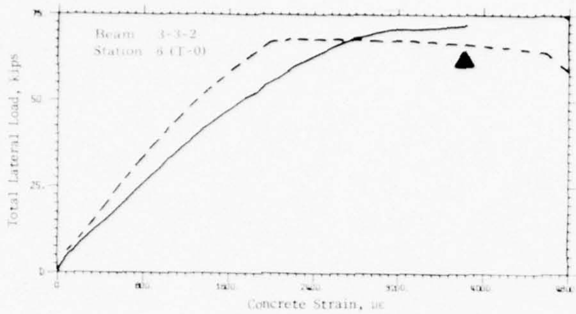
Beam 3-3-2
Station 6 (T-0)
Total Lateral Load, kips
Concrete Strain, με

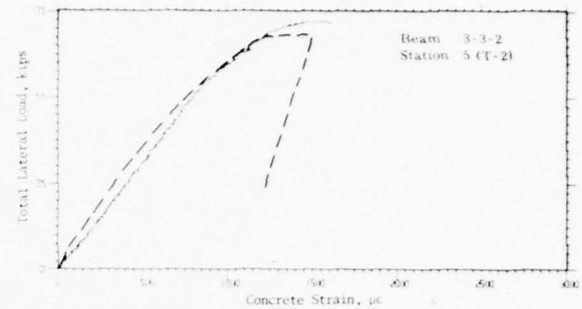
Beam 3-3-2
Station 5 (T-2)
Total Lateral Load, kips
Concrete Strain, με

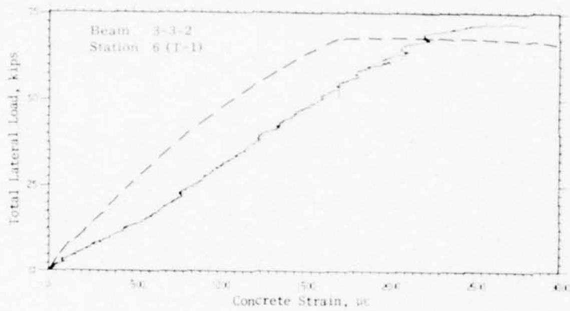
Beam 3-3-2
Station 6 (T-1)
Total Lateral Load, kips
Concrete Strain, με

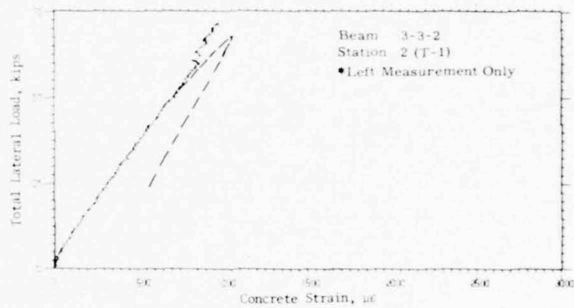
Beam 3-3-2
Station 2 (T-1)
*Left Measurement Only
Total Lateral Load, kips
Concrete Strain, με

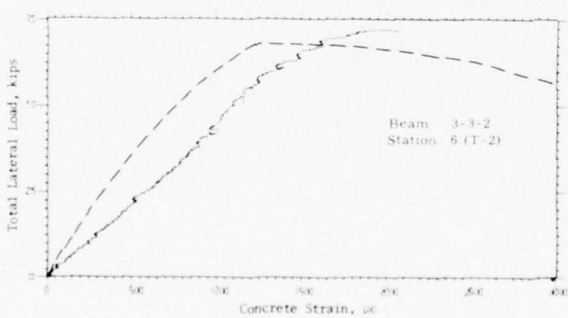
Beam 3-3-2
Station 6 (T-2)
Total Lateral Load, kips
Concrete Strain, με

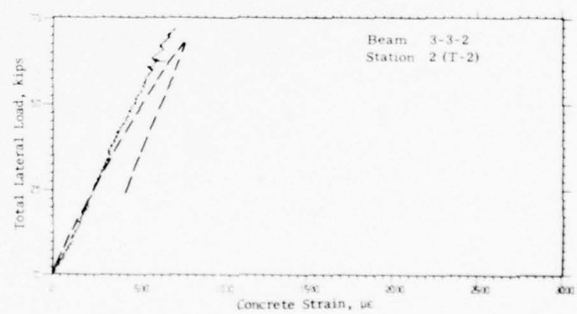
Beam 3-3-2
Station 2 (T-2)
Total Lateral Load, kips
Concrete Strain, με

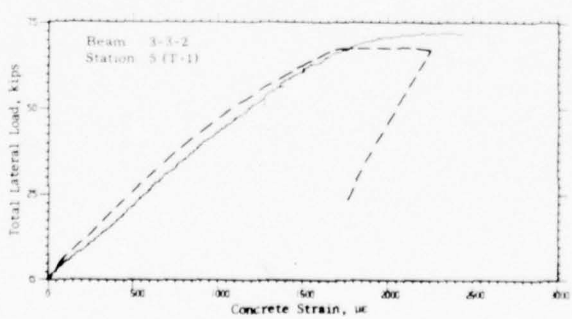
Beam 3-3-2
Station 5 (T-1)
Total Lateral Load, kips
Concrete Strain, με

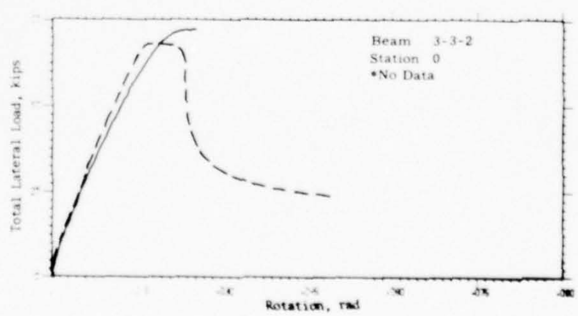
Beam 3-3-2
Station 0
*No Data
Total Lateral Load, kips
Rotation, rad

Beam	3-3-3
f'_c	4344
K = P/F	3.11
Test Date	8/2/73
Test Duration	2.5 min

Legend:

————	Experimental Results
– – – – –	Analytical Results
▼	Gage Failure

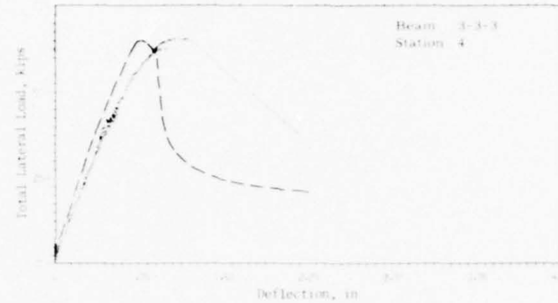

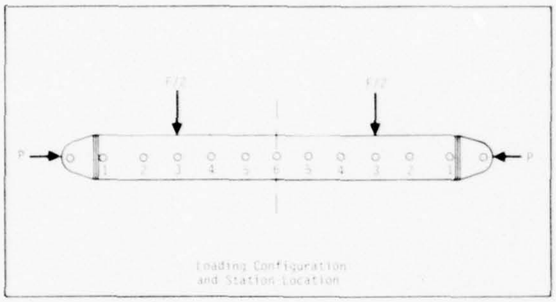

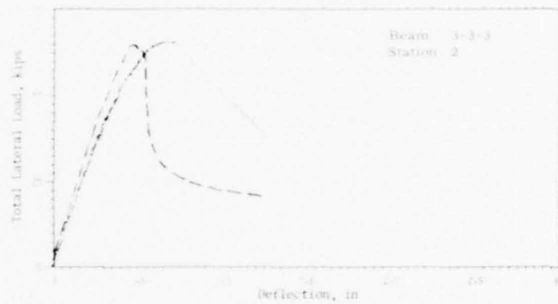

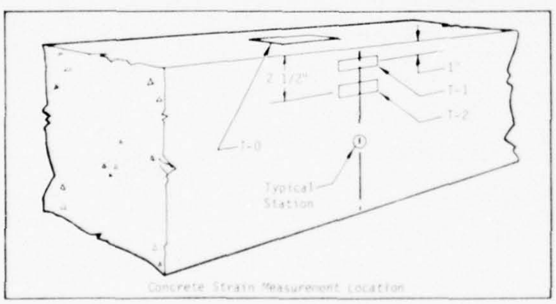

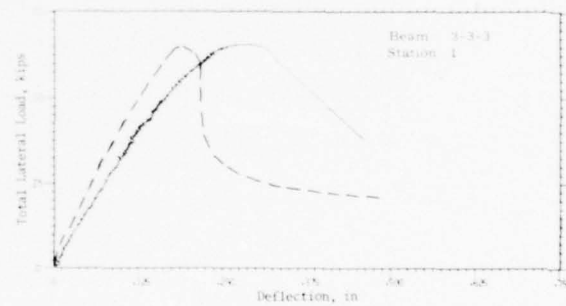

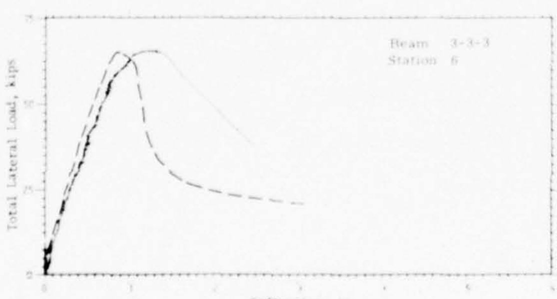

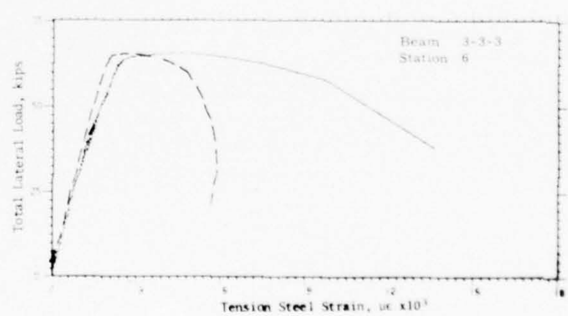

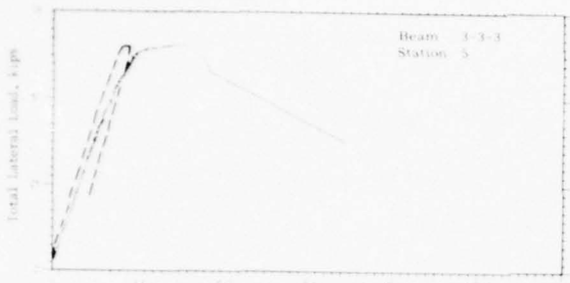
Beam 3-3-3
Station 5
Total Lateral Load, kips
Tension Steel Strain, με x10³

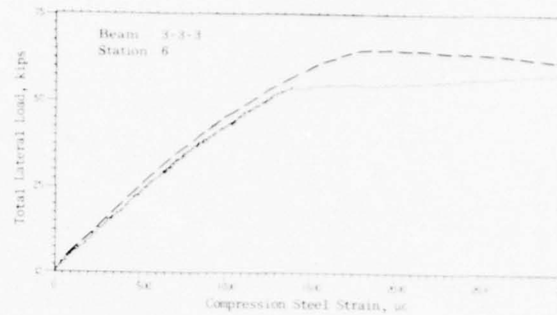
Beam 3-3-3
Station 6
Total Lateral Load, kips
Compression Steel Strain, με

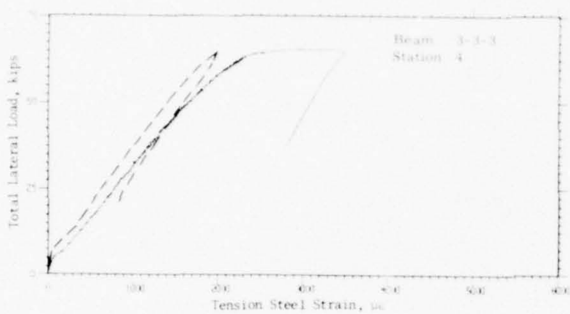
Beam 3-3-3
Station 4
Total Lateral Load, kips
Tension Steel Strain, με

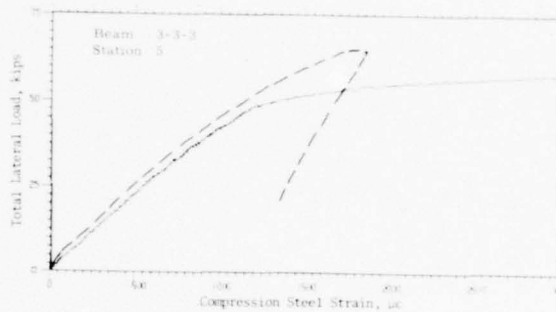
Beam 3-3-3
Station 5
Total Lateral Load, kips
Compression Steel Strain, με

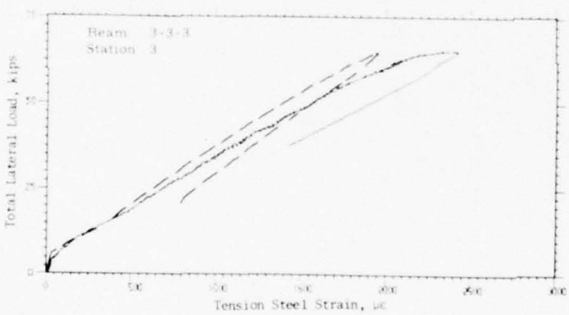
Beam 3-3-3
Station 3
Total Lateral Load, kips
Tension Steel Strain, με

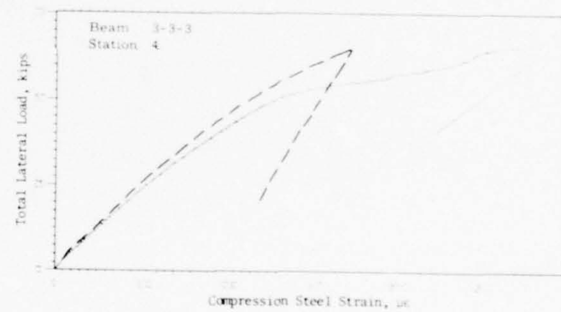
Beam 3-3-3
Station 4
Total Lateral Load, kips
Compression Steel Strain, με

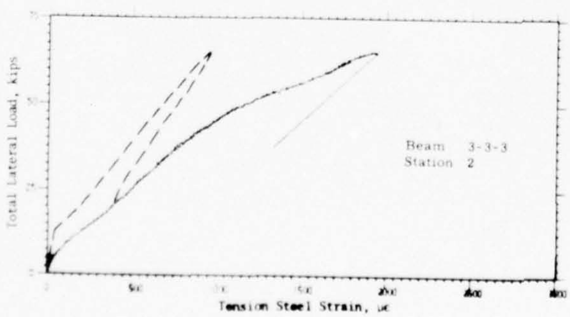
Beam 3-3-3
Station 2
Total Lateral Load, kips
Tension Steel Strain, με

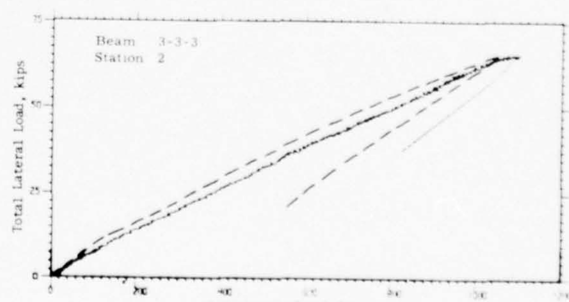
Beam 3-3-3
Station 2
Total Lateral Load, kips
Compression Steel Strain, με

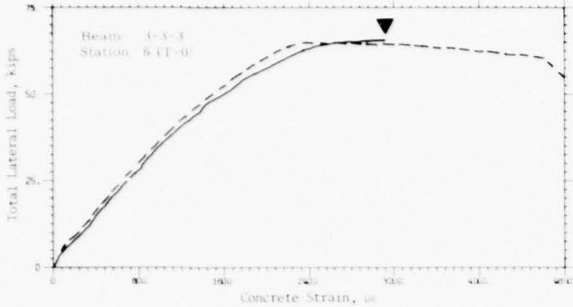
Beam 3-3-3
Station 6 (T-0)
Total Lateral Load, kips
Concrete Strain, με

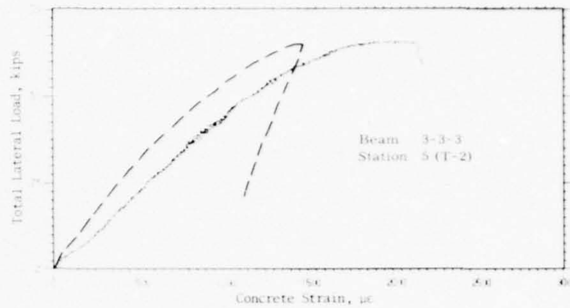
Beam 3-3-3
Station 5 (T-2)
Total Lateral Load, kips
Concrete Strain, με

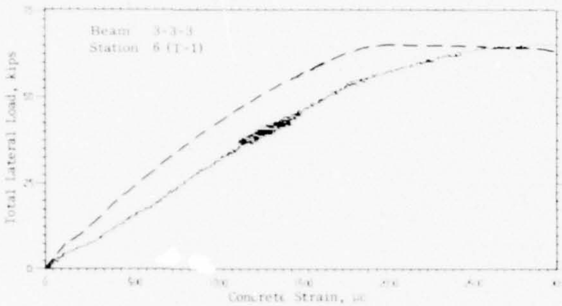
Beam 3-3-3
Station 6 (T-1)
Total Lateral Load, kips
Concrete Strain, με

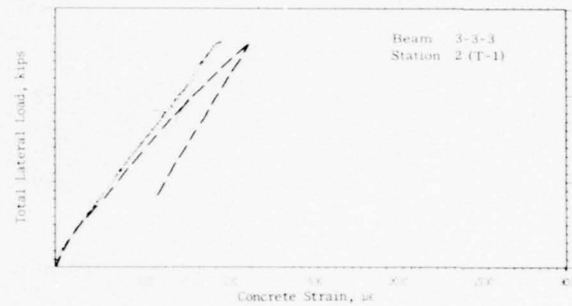
Beam 3-3-3
Station 2 (T-1)
Total Lateral Load, kips
Concrete Strain, με

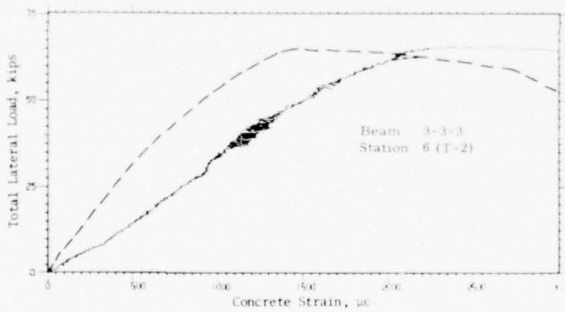
Beam 3-3-3
Station 6 (T-2)
Total Lateral Load, kips
Concrete Strain, με

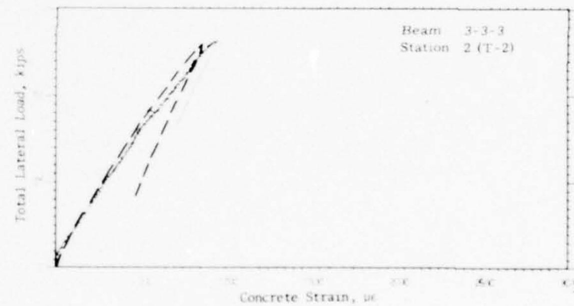
Beam 3-3-3
Station 2 (T-2)
Total Lateral Load, kips
Concrete Strain, με

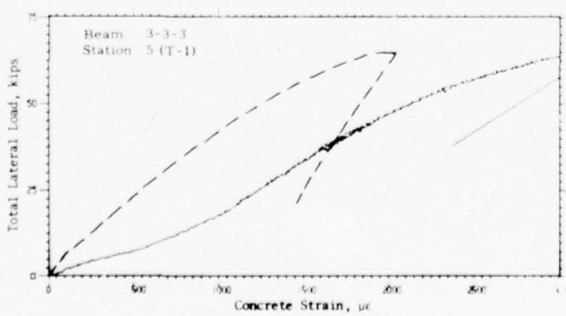
Beam 3-3-3
Station 5 (T-1)
Total Lateral Load, kips
Concrete Strain, με

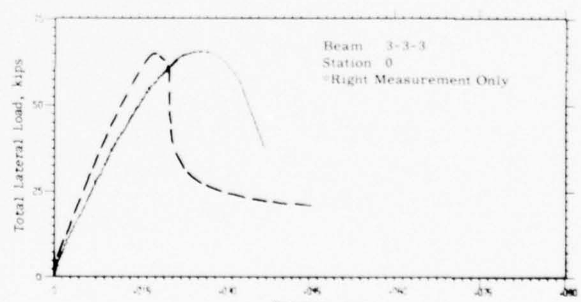
Beam 3-3-3
Station 0
*Right Measurement Only
Total Lateral Load, kips
Rotation, rad

APPENDIX B

PROGRAM BEAM

A listing of the computer code used to calculate the beam behavior from the analytical model is presented.

```
      PROGRAM BEAM(INPUT,OUTPUT,TAPE6,TAPE7,TAPE8,TAPE9,FILMPL)
C
C     PROGRAM BEAM COMPUTES THE BEHAVIOR OF A SYMMETRICALLY LOADED
C     REINFORCED CONCRETE BEAM UNDER COMBINED LATERAL AND AXIALS LOADS.
C
C          UPDATED DECEMBER 13,1973
C     TAPE6=CALCOMP,TAPE7=MICROFILM,TAPE8=GOULD
      COMMON/A/AK3,EO,EU,ECR,FPC,EMS,FY,FYP,FYV,ESH,ASH,BSH,ESHP,ASHP,
     1BSHP,P,D,PP,EMCON,AK6,AK8,XPC
      COMMON/B/ERR,ER1
      COMMON/C/RM(20),ES(20),AK4(20),AK10(20),PHI(20),CCON(20),FS(20),
     1FS1(20),ES1(20),EB(20),AK10X(20),ESP(20),ECT1(20),ECT2(20)
      COMMON/D/EMAX(20),AK1MAX(20),AK2MAX(20)
      COMMON/E/AK1(20),AK2(20)
      COMMON/G/ AL(20),AP(20),V(20),AM(20),DELTA(20),THETA(20),DTHETA(20
     1),EC(20),SA(20),SRC(20),SRT(20),DELTB(20)
      FSCON(CCON,AAK4)=FDT*SQRT(1.0+CCON/(FDT*AAK4))*AAK4
    1 FORMAT(I5)
    2 FORMAT(8F10.5)
      ICL=1
C
C     READ INPUT DATA
C
C     N = NUMBER OF NODE POINTS
      READ 1,N
C     AL(I) = LENGTH OF BEAM SEGMENTS BETWEEN NODES
      READ 2,(AL(I),I=1,N)
C     READ MATERIAL PROPERTIES
      READ 2,AK3,EO,EU,ECR,FFF,EMS,FY,FYP
      READ 2,FYV,ESH,ASH,BSH,ESHP,ASHP,BSHP
C     READ GEOMETRICAL PROPERTIES
      READ 2,T,P,D,B,PP,DP,PV
C     READ LOAD PARAMETERS
  800 READ 2,(AP(I),I = 1,N)
      DO 606 I=1,N
      IF(AP(I).GT.0.)GO TO 607
  606 CONTINUE
  607 IAP=I
C     READ TOTAL BEAM LENGTH, LOAD RATIO, CONCRETE STRENGTH
  801 READ 2,TL,AK,XXX,FPC
C
C     INITIALIZE DATA
C
      DO 1000 I=1,6
      DELTB(I)=0.0
      SA(I)=0.0
      EC(I)=0.0
      ES(I)=0.0
      ESP(I)=0.
      THETA(I)=0.0
 1000 PHI(I)=0.0
    3 FORMAT(I4,11E12.3)
    5 FORMAT(///35X*AXIALLY LOADED BEAM BEHAVIOR*///)
    6 FORMAT(//35X*SPAN AND LOAD PARAMETERS*//)
    7 FORMAT(//35X*SECTION PROPERTIES*//)
    8 FORMAT(//35X*MATERIAL PROPERTIES*//)
```

```
    9 FORMAT(//35X*BEHAVIOR CHARACTERISTICS*//)
   12 FORMAT(* SPAN LENGTH RATIO-AXIAL*/3X*(INCHES)  /LATERAL*/13X*LOAD*
     1/)
   13 FORMAT(11E12.3)
   14 FORMAT(I4,12X, 2E12.3)
   15 FORMAT(//* NODE/*11X*SEGMENT*5X*FRACTION OF*/* SEGMENT*9X*LENGTH*6
     2X*HALF SPAN*/17X*(INCHES)*4X*LOAD*/)
   16 FORMAT(* TOTAL DEPTH EFFECTIVE*7X*WIDTH  COMPRESSION*5X*STEEL*5X*C
     1OMP STEEL  SHEAR STL*/5X*(T)*5X*DEPTH (D)*8X*(B)    STL DEPTH-DP  P
     2ERCENTAGE  PERCENTAGE  PERCENTAGE*/)
   17 FORMAT(6X*K3*8X*EO*11X*EU*10X*ECR*9X*FPC*6X*STL-MOD*8X*FY*9X*FYP*
     110X*FYV*8X*ESH*9X*ASH*//)
   18 FORMAT(*  NODE RESISTING*5X*AXIAL    CENTERLINE   ROTATION    CONC
     1RETE*5X*STEEL*7X*APPLIED*6X*TOTAL    CONCRETE*8X*K4*9X*CRACK*/8X
     2*MOMENT*7X*LOAD*5X*DEFLECTION*16X*STRAIN*6X*STRAIN*7X*SHEAR*6X*SHE
     AAR*6X,*SHEAR*
     320X*HEIGHT*/81X*FORCE*5X*CAPACITY   CAPACITY*/)
   19 FORMAT(1H1)
C
C      PRINT INPUT DATA
C
      PRINT 19
      PRINT 5
      PRINT 6
      PRINT 12
      PRINT 13,TL,AK
      PRINT 15
      PRINT 14,(I,AL(I),AP(I),I=1,N)
      PRINT 7
      PRINT 16
      PRINT 13,T,D,B,DP,P,PP,PV
      PRINT 8
      PRINT 17
      PRINT 13,AK3,EO,EU,ECR,FPC,EMS,FY,FYP,FYV,ESH,ASH
      PRINT 9
      PRINT 18
C
C      COMPUTE CONSTANTS
C
      EMCON=55400./SQRT(FPC*1000.)
      AK6=T/D
      AK8=DP/D
      FDT=5./SQRT(FPC*1000.)
      CP=FPC*B*D
      CM=CP*D
      AB=FY/FPC-AK3
      AC=FYP/FPC-AK3
      XPC=((AK3*AK6**2.)/2.+PP*AC*(AK6-AK8)+P*AB*(AK6-1.))/(AK6*AK3+PP*
     1AC+P*AB)
      ERR = 0.0001
      ER1=.001
      ERD = 0.01
      SRS=PV*FYV/FPC
C
C      COMPUTE LOADING COEFFICIENTS
```

```
      V(1)=1.0/AK
      AM(1)=V(1)*AL(1)/D
      DO 10 I=2,N
      V(I)=V(I-1)-AP(I-1)/AK
   10 AM(I)=AM(I-1)+V(I)*AL(I)/D
C
C     INITIALIZE DEFLECTIONS
C
      DO 11 I=1,N
      FS1(I) = 0.0
      FS1(I) = 0.0
      AK2MAX(I)=0.0
      EMAX(I)=0.0
      AK1MAX(I)=0.0
      AK1oX(I)=0.0
      DELTB(I) = 0.0
   11 DELTA(I)=0.0
      PA1 = 0.0
      ECMAX = 0.0
      KDELTA = 0
      DELTAN=0.0
      EC(N) = 0.00
      DEC=0.0001
   20 IF(EC(N).GE.EU+.001) DEC=.001
      EC(N)=EC(N)+DEC
   23 DEB = .001
      EB(N) = DEB-EC(N)
C
C     CALCULATE AXIAL FORCE AND MOMENT AT BEAM CENTERLINE
C
   21 CALL FORCE(N,EC(N),EB(N),PA)
      AEM=PA*(AM(N)+DELTA(N))
C
C     COMPARE APPLIED MOMENT TO RESISTING MOMENT
C
      IF(ABS((RM(N)-AEM)/RM(N)).LE.ERR) GO TO 30
      IF(RM(N).GT.AEM) GO TO 22
      EB(N) = EB(N)+DEB
      GO TO 21
   22 EB(N) = EB(N)-.75*DEB
      DEB=DEB/4.
      GO TO 21
   30 CONTINUE
C
C     NOW HAVE PA AT CENTERLINE -- FIND PARAMETERS AT OTHER NODES
C
      M=N-1
      DO 500 I=1,M
      J=N-I
      AEM=PA*(AM(J)+DELTA(J))
      EC2=EC(J+1)
      IF(AK.GT.1.0)GO TO 490
      IF(I.EQ.1.AND.PA1.GT.PA) EC2 = ECMAX
  490 CALL ECANDK(J,EC2,PA,AEM,EC(J),EC(N))
  500 CONTINUE
C     COMPUTE DEFLECTIONS FROM NEW PHIS
```

```
      KDELTA = KDELTA+1
      DTHETA(1)=AL(1)*PHI(1)/(3.*D)+AL(2)*(2.*PHI(1)+PHI(2))/(6.*D)
      THETA(1)=DTHETA(1)
      DO 40 I=2,N
      DTHETA(I)=(AL(I)*(2.*PHI(I)+PHI(I-1))+AL(I+1)*(2.*PHI(I)+PHI(I+1))
     1)/(6.*D)
   40 THETA(1)=THETA(1)+DTHETA(I)
      IF(EC(N).GT.EU)THETA(1)=THETA(1)+(PHI(N)-PHI(N-1))/4.0
      DELTA(1)=THETA(1)*AL(1)/D
      DO 41 I=2,N
      THETA(I)=THETA(I-1)-DTHETA(I-1)
   41 DELTA(I)=DELTA(I-1)+THETA(I)*AL(I)/D
C
C     COMPARE NEW DELTA TO PREVIOUS DELTA
C
      IF(ABS((DELTA(N)-DELTAN)/DELTA(N)).LE.ERD) GO TO 600
      IF(KDELTA.GE.6) GO TO 502
      DO 501 I = 1,N
  501 DELTB(I) = DELTA(I)
      DELTAN = DELTA(N)
      GO TO 23
  502 DO 503 I = 1,N
      DELTA(I) = (DELTA(I)+DELTB(I))/2.
  503 DELTB(I) = DELTA(I)
      DELTAN = DELTA(N)
      KDELTA = 0
      GO TO 23
  600 DELTAN=DELTA(N)
      DO 611 I=1,N
      IF(EC(I).LE.EMAX(I)) GO TO 611
      EMAX(I)=EC(I)
      AK1MAX(I)=AK1(I)
      AK2MAX(I)=AK2(I)
  611 CONTINUE
      PA=PA*CP
      DO 601 I=1,N
      FS1(I) = AMAX1(FS1(I),FS(I))
      ES1(I) = AMAX1(ES1(I),ES(I))
      AK10X(I)=AMAX1(AK10(I),AK10X(I))
      RM(I)=RM(I)*CM
      ECT1(I)=(EC(I)*(AK4(I)-0.08))/AK4(I)
      ECT2(I)=(EC(I)*(AK4(I)-0.20))/AK4(I)
      DELTB(I)=DELTA(I)*D
      SA(I)=V(I)*PA
      SRC(I)=FSCON(CCON(I),AK4(I))*CP
  601 SRT(I)=SRC(I)+SRS*CP
C             DELETED OUT PRINT STATEMENT DEC 13,1973
C
C     PRINT CALCULATED BEAM RESPONSE
C
      WRITE(9,3)(I,RM(I),PA,DELTB(I),THETA(I),EC(I),ES(I),SA(I),SRT(I),
     1SRC(I),AK4(I),AK10(I),I=1,N)
      PRINT 602
  602 FORMAT(1H ,/)
```

```
      PA=PA/CP
      IF(PA1-PA) 604,604,605
  604 ECMAX = EC(N)
      PA1 = PA
  605 IF(EC(N).GE..005) GO TO 603
      GO TO 20
  603 CALL PLTS(JK,IAP,AK,FPC)
      CALL PLOT(0.,0.,-3)
      IF(XXX) 800,801,802
  802 CALL PLOT(0.,0.,40)
      STOP 101
      END
      SUBROUTINE ECANDK(I,EC1,PA,AEM,EC,XXX)
C
C     SUBROUTINE ECANDK CALCULATES A CONCRETE STRAIN AND DISTANCE TO
C     THE NEUTRAL AXIS THAT SATISFIED THE APPLIED LOADS
C
      COMMON/B/ER1,ERR
      DEC=AMIN1(EC1/2.,.001)
      EC=EC1
      K=1
    1 CALL FK4P(EC,PA,I,RM,XXX)
      K=K+1
      IF(ABS((AEM-RM)/AEM).LE.ERR)GO TO 10
      IF(K.GT.50)GO TO 10
      IF(RM.LT.AEM)GO TO 9
      EC=EC-DEC
      IF(EC.GT.0.0) GO TO 1
      DEC = DEC/2.0
      EC = DEC
      GO TO 1
    9 EC=EC+.75*DEC
      IF(EC.GT.XXX) GO TO 11
      DEC = DEC/4.
      GO TO 1
   11 DEC = .0001
      EC = EC1 + .75*DEC
      DEC = DEC/4.
      GO TO 1
   10 RETURN
      END
      SUBROUTINE FORCE(I,EC,EB,PA)
C
C     SUBROUTINE FORCE CALCULATES CONCRETE AND REBAR FORCES GIVEN A
C     STRAIN DISTRIBUTION
C
      COMMON/A/AK3,EO,EU,ECR,FPC,EMS,FY,FYP,FYV,ESH,ASH,BSH,ESHP,ASHP,
     1BSHP,P,D,PP,EMCON,AK6,AK8,XPC
      COMMON/C/RM(20),ES(20),AK4(20),AK10(20),PHI(20),CCON(20),FS(20),
     1FS1(20),ES1(20),BLANK(20),AK10X(20),ESPP(20)
      COMMON/F/AKK1(20),AKK2(20)
      IF(EC+EB.EQ.0.0)GO TO 30
      AK4(I)=AK6*EC/(EC+EB)
      ECRR=ECR
      PHI(I)=EC/AK4(I)
      ESP=EC*(AK4(I)-AK8)/AK4(I)
```

```
      ES(I)=EC*(1.-AK4(I))/AK4(I)
      GO TO 36
   30 ESP=EC
      ES(I)=-EC
      AK4(I)=100.
   36 CALL CONCRT(EC,AK4(I),AK1,AK2,I)
      FS(I) = STEEL(ES(I),FY,ESH,ASH,BSH,EMS,ES1(I),FS1(I))
      AK7 = FS(I)*P/FPC
      AK7P = STEEL(ESP,FYP,ESHP,ASHP,BSHP,EMS,0.0,0.0)*PP/FPC
      IF(ESP.GE.EU)AK7P=AK7P*EXP((EU-ESP)/.0001)
      IF(EB.LE.0.0) GO TO 10
      IF(EB.LT.ECR) GO TO 11
      AK9=ECR*AK4(I)/EC
      AK10(I)=(AK6-AK4(I)-AK9)*D
      IF(AK10(I).GE.AK10X(I))GO TO 20
      AK99=AK9-(AK10X(I)-AK10(I))/D
      ECRR=ECR*AK99/AK9
      AK9=AK99
      IF(AK9.LE.0.0)AK9=0.0
      GO TO 20
   10 AK9=0.0
      AK10(I)=0.0
      GO TO 20
   11 AK9=AK6-AK4(I)
      AK10(I)=0.0
   20 E=ECRR
      IF(EB.LE.ECR) E=EB
      CCON(I)=AK1*AK3*AK4(I)
      TCON=E*EMCON*AK9/2.
      PA=CCON(I)+AK7P-AK7-TCON
      RM(I)=CCON(I)*(AK6-XPC-AK2*AK4(I))+AK7P*(AK6-XPC-AK8)+AK7*(XPC-AK6
     1+1.)+TCON*(XPC-AK6+AK4(I)+2.*AK9/3.)
      AKK1(I)=AK1
      AKK2(I)=AK2
      ESPP(I)=ESP
      RETURN
      END
      SUBROUTINE FK4P(EC,PA,I,RMI,XXX)
C
C     SUBROUTINE FK4P CALCULATES THE DISTANCE TO THE NEUTRAL AXIS FOR
C     A GIVEN CONCRETE STRAIN TO SATISFY APPLIED LOADS
C
      COMMON/B/ERR,ICL
      COMMON/C/RM(20),ES(20),AK4(20),AK10(20),PHI(20),CCON(20),FS(20),
     1FS1(20),ES1(20),EBB(20)
      CALL FORCE(I,EC,-EC,PMAX)
      IF(PA.GE.PMAX) GO TO 2
      ICOUNT = -1
      DEB = .001
      EB = EBB(I+1)
    1 CALL FORCE(I,EC,EB,PA1)
      IF(ABS((PA-PA1)/PA).LE.ERR) GO TO 10
      IF(PA.LT.PA1) GO TO 9
      ICOUNT = 1
      EB = EB-DEB
      IF(EC+EB.GT.0.0) GO TO 1
```

```
      DEB=DEB/2.
      EB =DEB-EC
      GO TO 1
    9 IF(ICOUNT)11,11,12
   11 EB = EB + DEB
      GO TO 1
   12 EB = EB + 0.75*DEB
      DEB=DEB/4.
      GO TO 1
    2 RMI = 0.0
      RETURN
   10 RMI = RM(I)
      EBB(I)=EB
      RETURN
      END
      FUNCTION STEEL(ES,FY,ESH,ASH,BSH,EMS,ESO,FSO)
C
C     FUNCTION STEEL CALCULATES A STEEL STRESS GIVEN A STEEL STRAIN
C
      EY=FY/EMS
      ESA=ABS(ES)
      IF(FSO.EQ.0.0) GO TO 2
      IF(ES.GE.ESO) GO TO 2
      STEEL = FSO-(ESO-ES)*EMS
      RETURN
    2 IF(ESA.LE.EY) GO TO 10
      IF(ESA.LE.ESH)GO TO 11
      STELA=FY+ASH*(ESA-ESH)-BSH*(ESA-ESH)**2
      GO TO 12
   10 STEEL=ES*EMS
      RETURN
   11 STELA=FY
   12 IF(ES.LT.0.0) GO TO 13
   14 STEEL = STELA
      RETURN
   13 STEEL=-STELA
      RETURN
      END
      FUNCTION FVALUE(E,EO,EU,I)
C
C     FUNCTION VALUE CALCULATES A VALUE OF CONCRETE STRESS GIVEN A
C     CONCRETE STRAIN
C
      FM(EO,EU)=2.*EO/(3.*(EU**2-EO**2))
      E20=(0.8+EO*FM(EO,EU))/FM(EO,EU)
      IF(E.GT.E20)GO TO 3
      IF(E.GT.EO)GO TO 2
      FVALUE=2*E/EO-(E/EO)**2
      GO TO 10
    2 FVALUE=1.0-(E-EO)*FM(EO,EU)
      GO TO 10
    3 FVALUE=0.2
   10 RETURN
      END
      SUBROUTINE CONCRT(A,AK4,AK1,AK2,I)
```

```
C     SUBROUTINE CONCRT CALCULATES CONCRETE STRESS BLOCK PARAMETERS
C     GIVEN A CONCRETE STRAIN AND DISTANCE  TO THE NEUTRAL AXIS
C
      COMMON/A/AK3,EO,EU,ECR,FPC,EMS,FY,FYP,FYV,ESH,ASH,BSH,ESHP,ASHP,
     1BSHP,P,D,PP,EMCON,AK6,AK8,XPC
      COMMON/D/EMAX(20),AK1MAX(20),AK2MAX(20)
      FM(EO,EU)=2.*EO/(3.*(EU**2-EO**2))
      FA1(E)=(3.*EO*E**2-E**3)/(3.*EO**2)
      FEB1(E)=(8.*E*EO-3.*E**2)/(12.*EO-4.*E)
      FA2(E)=E-0.5*FM(EO,EU)*E**2
      FEB2(E)=(3.*E-2.*FM(EO,EU)*E**2)/(6.-3.*FM(EO,EU)*E)
      FA3(E)=0.2*E
      FEB3(E)=0.5*E
      FAREA2(E)=FA1(EO)+FA2(E-EO)
      FEBT2(E)=(FA1(EO)*FEB1(EO)+FA2(E-EO)*(EO+FEB2(E-EO)))/FAREA2(E)
      FAREA3(E)=FA1(EO)+FA2(E20-EO)+FA3(E-E20)
      FEBT3(E)=(FA1(EO)*FEB1(EO)+FA2(E20-EO)*(EO+FEB2(E20-EO))+FA3(E-E20
     1)*(E20+FEB3(E-E20)))/FAREA3(E)
      EUNLOD=2.0/EO
      E20=(0.8+EO*FM(EO,EU))/FM(EO,EU)
      RFACT = 1.0
      E = A
      IF(E.GT.EMAX(I)) GO TO 1
      FCMAX=FVALUE(EMAX(I),EO,EU,I)
      FC=FCMAX-(EMAX(I)-E)*EUNLOD
      IF(FC.LE.0.0)GO TO 22
      RFACT = FC/FCMAX
      E = EMAX(I)
      IF(AK4.GT.AK6) GO TO 20
      AK1 = RFACT*AK1MAX(I)
      AK2=AK2MAX(I)
      RETURN
   22 AK1=0.0
      AK2=0.33
      RETURN
    1 IF(AK6/AK4.LT.1.0)GO TO 20
      IF(E.GT.E20) GO TO 3
      IF(E.GT.EO)GO TO 2
      AK1=FA1(E)/E
      AK2=1.0-FEB1(E)/E
      RETURN
    2 AK1=FAREA2(E)/E
      AK2=1.0-FEBT2(E)/E
      RETURN
    3 AK1=FAREA3(E)/E
      AK2=1.0-FEBT3(E)/E
      RETURN
   20 ALPHA=1.0-AK6/AK4
      EP=E*ALPHA
      IF(E.GT.E20)GO TO 5
      IF(E.GT.EO) GO TO 4
      AK1=(FA1(E)-FA1(EP))/E
      AK2=1.0-(FA1(E)*FEB1(E)-FA1(EP)*FEB1(EP))/((FA1(E)-FA1(EP))*E)
      GO TO 100
    4 IF(EP.GT.EO) GO TO 6
      AK1=(FAREA2(E)-FA1(EP))/E
```

```
      AK2=1.0-(FAREA2(E)*FEBT2(E)-FA1(EP)*FEB1(EP))/((FAREA2(E)-FA1(EP))
     1*E)
      GO TO 100
    6  IF(EP.GT.E20) GO TO 7
      AK1=(FAREA2(E)-FAREA2(EP))/E
      APAR2=((FAREA2(E)-FAREA2(EP))*E)
      APAA2=FAREA2(E)*FEBT2(E)
      APAB2=FAREA2(EP)*FEBT2(EP)
      AK2=1.0-(APAA2-APAB2)/APAR2
      GO TO 100
    5 IF(EP.GT.E20)GO TO 77
      IF(EP.GT.E0)GO TO 8
      AK1=(FAREA3(E)-FA1(EP))/E
      APAR3=((FAREA3(E)-FA1(EP))*E)
      AK2=1.0-(FAREA3(E)*FEBT3(E)-FA1(EP)*FEB1(EP))/APAR3
      GO TO 100
    8 AK1=(FAREA3(E)-FAREA2(EP))/E
      APAR=((FAREA3(E)-FAREA2(EP))*E)
      APAAB2=FAREA3(E)*FEBT3(E)
      APABB2=FAREA2(EP)*FEBT2(EP)
      AK2=1.0-(APAAB2-APABB2)/APAR
      GO TO 100
   77 AK1=(FAREA3(E)-FAREA3(EP))/E
      APAR1=((FAREA3(E)-FAREA3(EP))*E)
      APAAC2=FAREA3(E)*FEBT3(E)
      APABC2=FAREA3(EP)*FEBT3(EP)
      AK2=1.0-(APAAC2-APABC2)/APAR1
      GO TO 100
    7 PRINT 25
   25 FORMAT(///10X*EP EXCEEDS E20*)
      STOP
  100 AK1 = AK1*RFACT
      RETURN
      END
```

ABBREVIATIONS, ACRONYMS, AND SYMBOLS

A	area
A_i	factors relating to lateral load distribution in beams
A_s	area of tensile reinforcement
A'_s	area of compression reinforcement
A_{sh}, B_{sh}	constants relating to steel stress-strain curve
C_c	compressive concrete force
C_s	compressive reinforcement force
E_{conc}	modulus of elasticity of concrete
E_s	modulus of elasticity of steel
E_{unload}	unloading modulus of elasticity of concrete
F	lateral load
K	axial-to-lateral-load ratio (P/F)
L	length of beam
M	moment capacity of section
M_i	moment coefficient at node i
M_R	resisting moment
M_{Ri}	resisting moment at node i
N	factor used in expression for moment capacity of beams; number of nodes
P	axial load
T_c	tensile force in concrete
T_s	tensile force in reinforcement
V_i	shear coefficient in segment i
X_c	depth of concrete tension stress-block
X_{PC}	distance from bottom of beam to plastic centroid
a	depth of rectangular concrete stress-block
a_s	shear span
a_s/d	shear-span-to-beam-depth ratio
b	width of cross section
c	distance from compressive face of member to neutral axis
d	distance from compressive face of member to centroid of reinforcing steel
f_c	compressive stress in concrete

ABBREVIATIONS, ACRONYMS, AND SYMBOLS (Cont'd)

f'_c	compressive strength of concrete test cylinder
f''_c	flexural strength of concrete in compression
f'_{cu}	cube strength
f_i	forces at node i
f_s	stress in tensile reinforcement
f'_s	stress in compression reinforcement
f_{su}	ultimate steel stress
f_y	yield strength of reinforcement
k	ratio of distance from compression face to neutral axis to effective depth (d)
k_1, k_2	stress-block constants
k_3	factor relating strength of concrete in beam to concrete cylinder strength
m	slope of descending portion of concrete stress-strain curve used for analytical model
m_i	bending moment at node i
n	modular ratio
p	reinforcement ratio
p_{cr}	critical reinforcement
t	beam depth
v_i	shear force in segment i
δ_i	deflection of node i
ε	strain
ε_b	strain at bottom of beam
ε_c	concrete strain
ε_{ci}	concrete strain at node i
ε_{cr}	concrete strain at cracking; limiting concrete tensile strain
ε_o	concrete strain at maximum concrete stress
ε_s	strain in tension reinforcement
ε'_s	strain in compression reinforcement
ε_{sh}	strain at commencement of strain hardening in steel
ε_{su}	steel strain at maximum stress
ε_u	ultimate concrete strain; strain at maximum k_1
ε_{20}	concrete strain at stress of 20 percent of maximum

ABBREVIATIONS, ACRONYMS, AND SYMBOLS (Concl'd)

η	plasticity ratio ($\varepsilon_u/\varepsilon_o$)
θ_i	rotation of node i
μ	ductility ratio
μ'	collapse ductility ratio
ϕ_i	curvature at node i

DISTRIBUTION LIST

No. Cys.	DEPARTMENT OF DEFENSE
	Director, ARPA
1	Dr. Stan Ruby (WMRO-RM, 3D170)
	Director, DNA
2	SPSS
3	STTL, Technical Library
1	STSI, Archives
	DDR&E
1	Asst. Dir., Strat. Wpns.
1	Dir., DIA
1	Dir., OSD, ARPA (NMR)
1	Cdr., FCDNA (FCPR)
1	Ch., LVLO (FCTCL)
1	JSTPS (JLTW)
2	DDC (TCA), Cameron Station
	DEPARTMENT OF THE ARMY
1	CO, USACDC, Inst. Nuc. Stud.
	CO, BRL
1	AMXBR-TB
1	Ch. Eng. (DAEN-RDM), Dept. Army
3	Dir., USA Eng. WWES
	Director, US Army Construction Engineering Research Lab.
1	Dr. J. Preudergast
	DEPARTMENT OF THE NAVY
1	Dir. NRL (2027)
1	Cdr., NSWC (730)
3	NCEL

No. Cys.	DEPARTMENT OF THE AIR FORCE
	Hq. USAF
1	SA
1	SAMI
1	PREE
1	PREPB
1	RDPQ, 1C370
1	RDQPN, 1D425
1	RDQS
1	Hq. USAF, AFTAC (TAP)
1	AFCEC (PREC)
1	Dir. Nuc. Surety (SN)
1	AFSC (DOB)
	TAC
1	DEE
1	LGMD
	CINCSAC
1	DEE
1	DOXS
1	XPFC
1	AFLC, WPAFB (DEMG), Mr. Edward Fink
1	ADC, Ent AFB (XPQY)
1	AUL (LDE)
1	AU (ED, Dir. Civ. Eng.)
	AFIT, WPAFB
1	Tech. Lib., Bldg. 640, Area B
1	CES
1	USAF, SCLO (Maj Pierson, Chief, LO)
	USAFA
1	DFSLB
1	FJSRL, CC

No. Cys.	DEPARTMENT OF THE AIR FORCE (Continued)
1	AFML, WPAFB, Tech. Lib.
1	AFFDL, WPAFB, DOO/Lib.
1	RADC, Doc. Lib.
	AFWL
1	HO, Dr. Minge
2	SUL
1	DE
20	DES
1	AFOSR

No. Cys.	ENERGY RESEARCH & DEVELOPMENT ADMINISTRATION
1	Sandia Lab., Tech. Library
	Dir. Ofc., LLL
1	Tech. Info. Dept.
1	LLL (Lib.), Bldg. 50, Rm. 134
1	Dir., LASL

No. Cys.	OTHER GOVERNMENT AGENCIES
1	Robert Crist National Bureau of Standards Building Research Division II A7

No. Cys.	DEPARTMENT OF DEFENSE CONTRACTORS
1	Prof. James H. Smith Texas Tech. University Civil Engineering
	Teledyne Brown Engineering
1	Dr. M. C. Patel
	Bechtel Corporation
1	P. L. Williams
	Physics International Co.
1	Mr. Fred Sauer & Dr. C. Godfrey
	TRW Systems, Inc.
1	Dr. P. Dai

No. Cys.	DEPARTMENT OF DEFENSE CONTRACTORS (Continued)
	Holmes & Narver, Inc.
1	R. Kennedy
	The Boeing Company
1	Mr. Ron Carlson
	IIT Research Institute
1	Library
	Aerospace Corporation
1	Library
	TRW Systems Group
1	Mr. Greg Hulcher
	Agbabian Asso.
1	M. Agbabian
	Applied Theory, Inc.
1	Dr. J. G. Trulio
1	Consulting & Special Engineering Services, Inc.
	The Rand Corporation
1	Library
	R & D Associates
1	Dr. H. Cooper
	Systems, Sciences & Software
1	Library
	Weidlinger Asso.
1	Dr. M. Baron
	McDonald Douglas Astro. Co.
1	K. McClymonds & K. Narasimham
1	University of Illinois Dr. N. M. Newmark, Dr. W. Hall, Dr. J. Haltiwanger
	Science Applications, Inc.
1	Ray Sheenk
25	Civil Engineering Research Facility, Dr. G. Lane
1	Mechanics Research, Inc.

No. Cys.	DEPARTMENT OF DEFENSE CONTRACTORS (Continued)
1	Civil Nuclear Systems Corp.
	R. M. Parsons Co.
1	Mr. Herb Saffell
1	Utah State University Dept. of Civil & Environmental Engineering, Vance T. Christiansen
	VPI & SU Dept. of Civil Engineering
1	Siegfrid M. Holzer

No. Cys.	DEPARTMENT OF DEFENSE CONTRACTORS (Continued)
1	Prof. A. C. Scordelis Dept. of Civil Engineering - SESM Davis Hall University of California
	Science Applications, Inc.
1	John E. Reaugh
	Official Record Copy
1	Lieutenant R. Galloway AFWL/DES